University of Illinois at Urbana-Champaign

ACRC

Air Conditioning and Refrigeration Center A National Science Foundation/University Cooperative Research Center

Experimental Investigation of Two-Phase Refrigerant Distribution in a Microchannel Manifold

C. D. Bowers, T. A. Newell, and P. S. Hrnjak

ACRC TR-245 July 2006

For additional information:

Air Conditioning and Refrigeration Center
University of Illinois
Mechanical & Industrial Engineering Dept.
1206 West Green Street
Urbana, IL 61801

(217) 333-3115

Prepared as part of ACRC Project #154
Experimental Investigation of Two-Phase Fluid Distribution in Microchannel Manifolds
T. A. Newell and P. S. Hrnjak, Principal Investigators

The Air Conditioning and Refrigeration Center was founded in 1988 with a grant from the estate of Richard W. Kritzer, the founder of Peerless of America Inc. A State of Illinois Technology Challenge Grant helped build the laboratory facilities. The ACRC receives continuing support from the Richard W. Kritzer Endowment and the National Science Foundation. The following organizations have also become sponsors of the Center.

Arçelik A. S.
Behr GmbH and Co.
Carrier Corporation
Cerro Flow Products, Inc.
Copeland Corporation
Daikin Industries, Ltd.
Danfoss A/S
Delphi Thermal and Interior
Embraco S. A.
General Motors Corporation
Hill PHOENIX
Honeywell
Hydro Aluminum Precision Tubing
Ingersoll-Rand/Climate Control
Lennox International, Inc.
LG Electronics, Inc.
Manitowoc Ice, Inc.
Matsushita Electric Industrial Co., Ltd.
Modine Manufacturing Co.
Novelis Global Technology Centre
Parker Hannifin Corporation
Peerless of America, Inc.
Samsung Electronics Co., Ltd.
Sanden Corporation
Sanyo Electric Co., Ltd.
Tecumseh Products Company
Trane
Visteon Automotive Systems
Wieland-Werke, AG

For additional information:

Air Conditioning & Refrigeration Center
Mechanical & Industrial Engineering Dept.
University of Illinois
1206 West Green Street
Urbana, IL 61801

217 333 3115

Abstract

The affects of microchannel protrusion, mass flux, quality and inlet distance on the distribution of two phase refrigerant R-134a was studied through a series of experiments conducted in two different horizontally oriented microchannel manifolds. One manifold was constructed in such a manner that the cross sectional area was rectangular in nature, with dimensions of 12.7 x 18.5 mm. The second manifold was constructed using a transparent PVC tube in order to achieve a circular cross-section; the inner diameter of this manifold was 20.4 mm. Both manifolds fed a linear array of 15 microchannels with hydraulic diameter of 1.54 mm. In the rectangular manifold, three different uniform microchannel protrusion schemes were studied; the microchannels protruded one-quarter, one-half, and three-quarters of the flow field depth. While in the circular manifold the same three uniform schemes were studied, two staggered schemes were studied as well. In each manifold the expansion device was put at two different lengths from the microchannel array. In the case of the rectangular manifold, these lengths were 50 mm and 250 mm, and in the case of the circular manifold 89 mm and 267 mm. Flow parameters were also varied in this study. The inlet quality of the refrigerant was varied from 0-0.35, and the mass flow rate from 15-35g/s. Liquid refrigerant distribution was measured through the use of a series of a collection tanks, in which a time averaged mass flow rate could be obtained.

Table of Contents

List of Figures

Page

List of Tables

Page

List of Symbols

A	Cross-sectional area [m^2]
CV	Coefficient of Variation
G	Mass flux [kg/m^2-s]
G_{eff}	Effective mass flux [kg/m^2-s]
$G_{eff,liq}$	Liquid mass fraction scaled effective mass flux [kg/m^2-s]
$G_{eff,vap}$	Vapor mass fraction scaled effective mass flux [kg/m^2-s]
$\dot{m}$	Liquid mass flow rate [g/s]
$\overline{\dot{m}}$	Average liquid mass flow rate per collection tank [g/s]
n_{tanks}	Number of collection tanks
σ	Standard deviation
x	Quality

Chapter 1. Introduction

The efficiency of microchannel heat exchangers is directly influenced by the distribution of the refrigerant within the manifold of the heat exchanger. In the case of microchannel evaporators, the maldistribution of the liquid refrigerant can cause hot or cold spots in the heat exchanger. These maldistributions affect both the performance of the heat exchanger and the life span. Figure 1-1 shows a real microchannel heat exchanger with part of the manifold cut away in order to show the structure of actual manifolds.

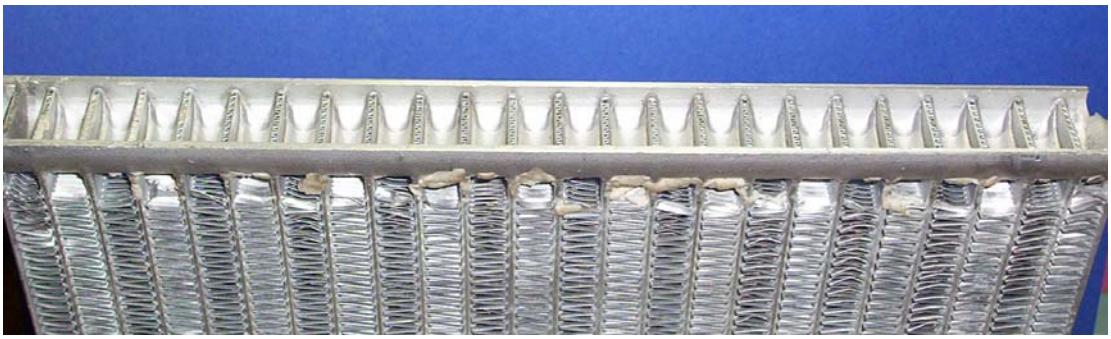

Figure 1-1: Cutaway of Actual Microchannel Heat Exchanger Manifold

The primary objective of this project is to gain a better understanding of the parameters governing the distribution of two-phase refrigerant flow in a generic microchannel manifold. This project aims to do this through experiments run in generic manifold distributing refrigerant to fifteen microchannels set in a linear array. This generic manifold is similar in scale to a small capacity automotive heat exchanger. A working fluid of R134a is used. Test parameters of quality, mass flux, and microchannel protrusion are varied in order to garner their effect on distribution. Microchannel protrusion depth is one of the key parameters in this study due to the fact that in the manufacturing process of real microchannel heat exchangers the microchannels are protruded into the manifold, as seen in Figure 1-1. Similar projects investigating distribution characteristics of air/water and R134a have been conducted. Air/water investigations using a similar manifold with flush mounted microchannels were conducted by Thompkins (2002) and Yoo (2002). Another air/water investigation of manifolds was done by Lee and Lee (2004), in which tube intrusion effects were studied in a vertically oriented manifold. A previous R134a investigation using one of the manifolds used in this project, with the microchannels mounted flush in the manifold was conducted by Zhang (2004). Vist and Petersen (2004) studied two phase flow distribution in a horizontally oriented circular manifold feeding 10 parallel 4mm tubes with R-134a. All of these projects have in common the goal of a better understanding of the very physically complex phenomena involved in refrigerant distribution.

Chapter 2. Experimental Facilities and Techniques

2. 1. Manifold Design

For this investigation, there were two different manifold designs used; a manifold with a rectangular cross section, and one with a circular cross section. The rectangular manifold was used in order to dovetail with a previous study using the same manifold without microchannel protrusion and the cylindrical manifold was used in order to better represent manifolds seen in industry designed heat exchangers. These manifolds were implemented into the investigation in the same manner, but the design was unique to each.

2. 1. 1. Rectangular Manifold

The rectangular microchannel manifold design used for this investigation consists of three components: microchannel mounting plate, view plate, and spacer plate. The exterior dimensions of all three plates are 101.6 cm by 558.8 cm (4" x 22"). The view plate, shown in Figure 2-1, is made from clear polyvinyl chloride (PVC) to allow for the flow within the manifold to be observed. This plate has two 6.35 mm (1/4") ports that are used as refrigerant inlet ports. The microchannel mounting plate, shown in Figure 2-2, is made of aluminum. Machined into the mounting plate are fifteen equally spaced mounts used to mount fifteen separate microchannels. The spacer plate between the view plate and the microchannel mounting plate is also made of aluminum. The spacer plate is 12.7mm (1/2") thick, with an 18.5mm (0.73") wide center cut. This center cut makes up the flow path area (234.95mm2) for the refrigerant.

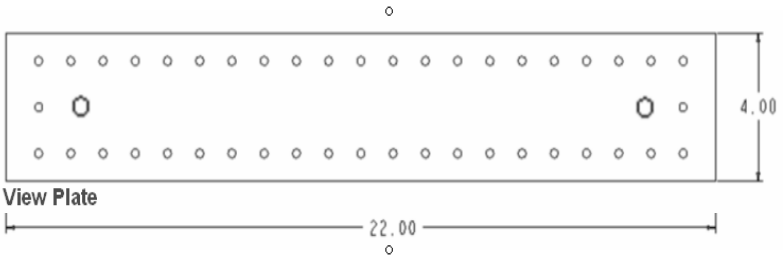

Figure 2-1: Manifold View Plate (dimensions are in inches)

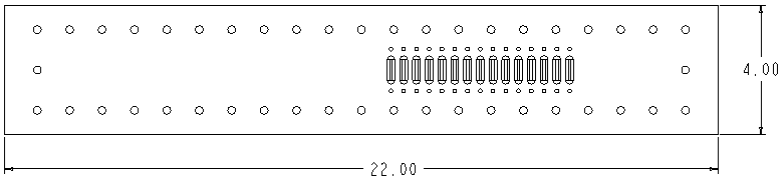

Figure 2-2: Microchannel Mounting Plate (dimensions are in inches)

The array of microchannels is mounted at three different depths into the flow path, ¼, ½, and ¾ depths. These depths are measured by the fraction of the flow path into which the microchannel is protruded (i.e. when the microchannels are protruded 3.175mm (.125") into the 12.7mm (1/2") flow path they are considered to be ¼ depth protruded). The previous study by Zhang investigated many of the same parameters as this investigation with the microchannels mounted flush in the same rectangular microchannel manifold. The microchannel mounting array is offset on the mounting plate as can be seen in Figure 2-2. This offset in the mounting of the microchannel array

allows for two different lengths between the refrigerant inlet ports and the microchannels. These "entrance" lengths are 50mm (2") for the shorter length and 250mm (10") for the longer. Figure 2-3 shows a schematic of the assembled rectangular microchannel manifold, while Figure 2-4 is a picture of the manifold in the test facility.

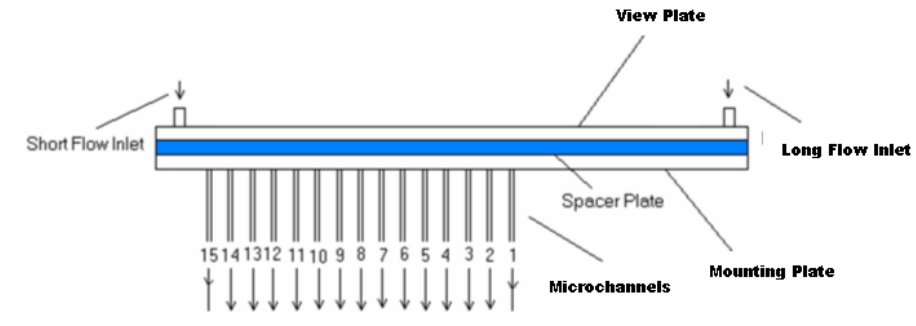

Figure 2-3: Assembled Rectangular Microchannel Manifold

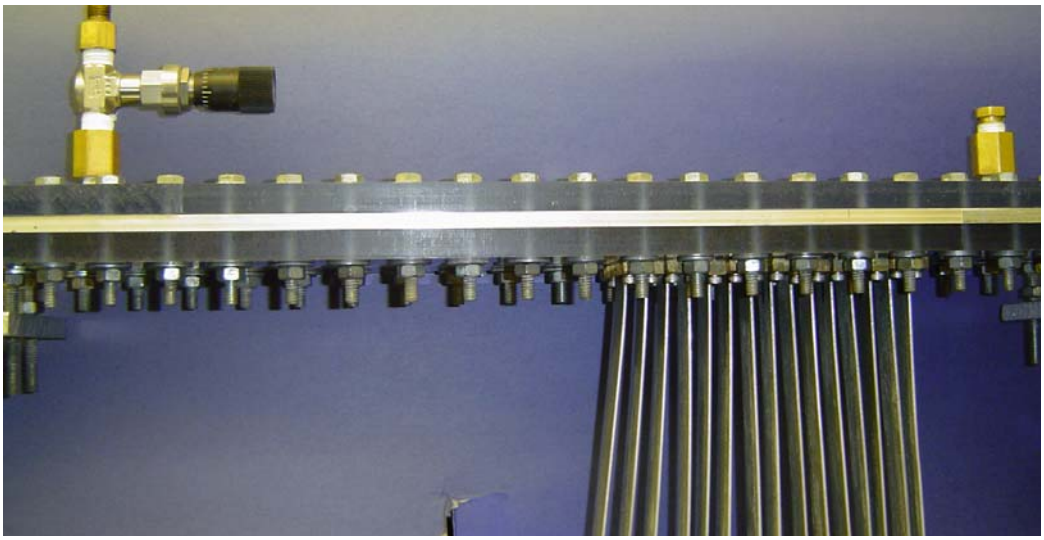

Figure 2-4: Test Manifold in Test Facility

2. 1. 2. Circular Manifold

In order to represent more realistically the manifold of a real microchannel heat exchanger, a circular microchannel manifold was designed and constructed. This manifold was designed and constructed to work in a very similar manner to the rectangular microchannel manifold. Again, the manifold consists of three main components: a view plate, a microchannel mounting plate, and the manifold tube. The view plate and the mounting plate both have exterior dimensions of 101.6mm by 165.1mm (4"x 6.5"). The view plate, shown in figure 2-5, is made of clear polycarbonate; while the mounting plate, shown in figure 2-6, is made of aluminum. The mounting array for the microchannels is the same design as that in the rectangular microchannel manifold, except that the array is not offset on the plate. A manifold tube makes up the flow field of the manifold; this tube has an inner diameter of 20.42mm (.804") and a length of 482.6mm (19"). The manifold tube, shown in Figure 2-7, is made of clear PVC and sealed between the view plate and the mounting plate. An array of slots for the microchannels is machined into the tube so that the microchannels can be protruded into the tube. This array is offset on the tube so

that there are two different lengths between the inlet and the microchannels, in the same manner as the rectangular manifold. The two “entrance” lengths for the circular manifold are 267mm (10.5”) and 89mm (3.5”) from the microchannel array respectively.

Again, the array of microchannels is protruded into the flow field to the desired protrusion depth. In order to seal properly, the microchannels must be protruded to the point that the microchannel entirely fills the machined slots in the manifold tube. This results in the microchannels being protruded nearly one quarter of the diameter of the tube, or 5.6mm (.22”). This particular protrusion scheme is very similar to the protrusion of microchannels in a real heat exchanger. The two other uniform protrusion depths studied have the microchannels protruded half the diameter of the tube and to the point where the microchannels hit the upper wall of the tube; this is nearly three-quarters of the diameter. These depths are 10.2mm (.40”) and 14.7mm (.58”) respectively. Two additional microchannel protrusion cases were studied for the circular manifold. These cases consisted of two separate methods of the staggering the depth of the microchannel protrusion as they progressed through the manifold. The array was staggered from 5.6mm into the manifold to 14.7mm into the manifold (or from “1/4” depth to “3/4” depth), for one case and in the reverse direction for the other. Figure 2-8 is a photograph of the circular manifold test section installed in the test facility.

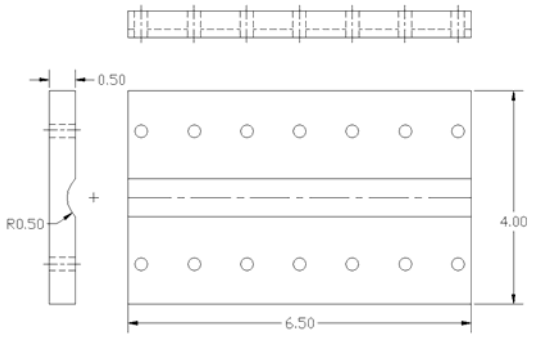

Figure 2-5: Circular Manifold View Plate (dimensions are in inches)

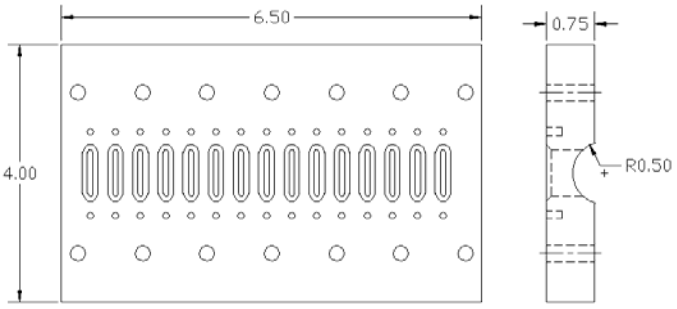

Figure 2-6: Circular Manifold Mounting Plate (dimensions are in inches)

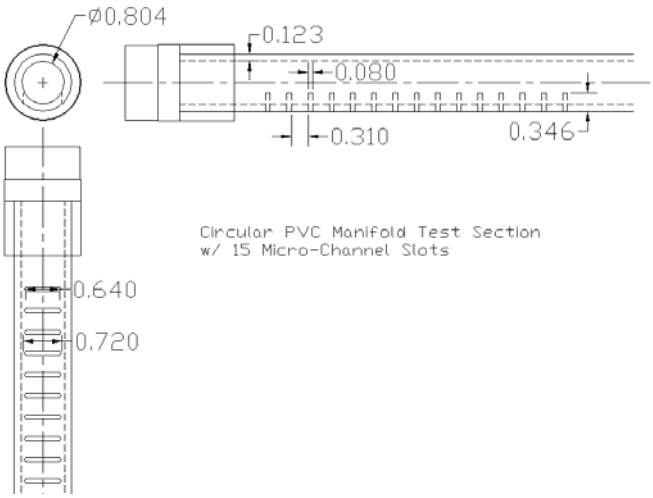

Figure 2-7: Manifold Tube (dimensions are in inches)

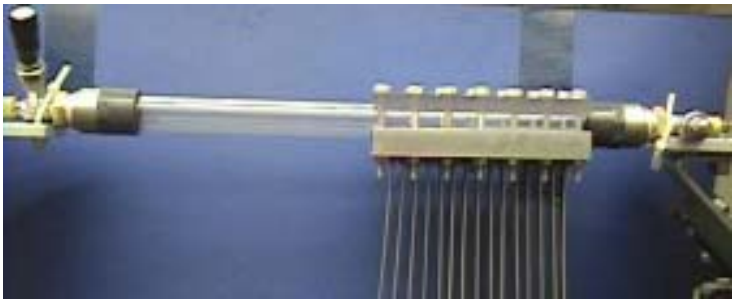

Figure 2-8: Circular Manifold in Test Facility

2. 2. Expansion Device

While there are several different devices and methods used in expanding high pressure, single phase refrigerant flow into lower pressure two-phase flow , for simplicity of control the expansion device used for both the rectangular and circular manifold tests was a manually controllable Swagelok needle valve. A photograph and a cutaway drawing of the valve can be seen in Figure 2-9. It should be noted that the orientation of the valve and thus the flow exiting the valve and entering the manifold is different for the two types of manifolds. In the case of the rectangular manifold the, as seen in Figure 2-4 the exit of the valve into the manifold is at a 90° angle to the orientation of the flow in the manifold itself. This is not the case in the circular manifold. As can be seen in Figure 2-8 the flow exiting the expansion valve is flowing in the same direction as the flow in the manifold.

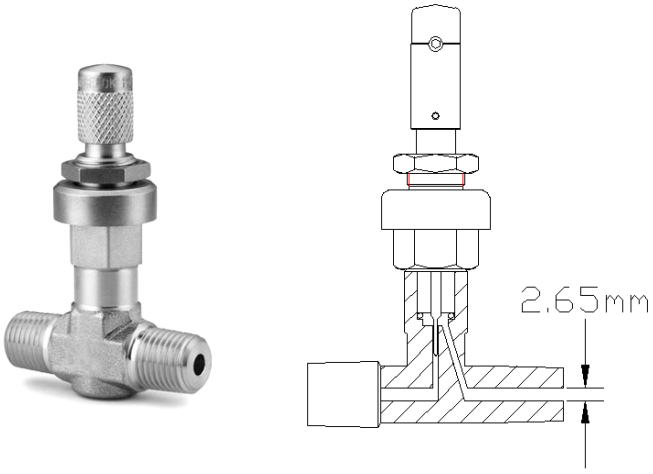

Figure 2-9: Expansion Valve

2. 3. Microchannel Tube Description

One of the microchannel tubes used in these experiments can be seen in Figure 2-10. These microchannel tubes are 6-port tubes manufactured by Brazeway Corp, with a hydraulic diameter of 1.54mm (0.06”). The length of the tubes is 317.5 mm (12.5”). Sealing of the tubes, in both manifolds, is achieved by a rubber o-rings placed in the chamfered grooves on the microchannel mounting plate kept in place by brass brackets. The tubes are grouped into sets of three with each set of three feeding an individual collection tank.

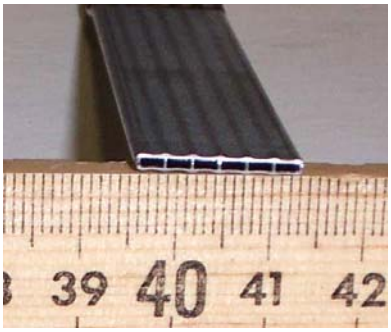

Figure 2-10: Typical Microchannel Tube Used in Manifold

2. 4. Experimental Parameters

There were several geometric parameters considered in this experiment. These parameters included the geometric shape of the manifold (rectangular vs. circular), the protrusion of the microchannels to varying depths and the length from the expansion device to the first microchannel. In addition to varying geometric parameters, inlet flow parameters were varied. The inlet flow parameters that were varied were the mass flow rate and the inlet quality. For both the rectangular and the circular test sections, the inlet quality was varied from 0% to 35% , and the mass flow rate was varied from 15g/s to 35 g/s. For the rectangular manifold these mass flow rates yield inlet mass fluxes of 63.84 to 149 kg/m^2-s and 45.79 to 106.86 kg/m^2-s for the circular manifold. Where mass flux in defined as the mass flow rate divided by the cross-sectional area of the manifold, as seen in Equation 2-1.

Equation 2-1 $$G = \frac{\dot{m}}{A}$$

2. 5. Test Matrix

Based upon the parameters mentioned above there are many possible test conditions. The geometric constraints allow for 20 non-dynamic test conditions: 2 (cross-section types) x 5 (protrusion schemes) x 2 (inlet lengths). The inlet flow parameters allow for 35 different dynamic test conditions: 7 (qualities of 0%, 10%, 15%, 20%, 25%, 30%, and 35%) x 5 (mass flow rates of 15, 20, 25, 30, and 35 g/s). This yields 700 total possible test conditions, however due to limitations imposed by the equipment used and other constraints this was reduced to 496 possible test cases, with 489 conditions actually being tested.

2. 6. Experimental Facility

The manifold test sections used in this experiment were installed in the refrigerant loop shown in Figure 2-11. Most of the design and construction of this loop was done by Fei (2004) with later modifications being made by Zhang (2004); for a more detailed analysis of the facility refer to Fei (2004). A single-phase pump is used to obtain the desired mass flow rate through the loop. The mass flow rate and density is measured by a Micro-Motion mass flow meter (±0.10%). The inlet pressure of the manifold is controlled by an expansion valve placed near the inlet of the manifold. Inlet quality is controlled by an electric heater and is calculated using system pressures and temperatures and checked by measurement of liquid flow rates. The two system pressures measured were the inlet pressure (before the expansion device) and outlet pressure (after the manifold). These pressures varied from .8 MPa to 2.9 MPa (120 psi – 420 psi) and 600 kPa to 760 kPa (88 psi – 110 psi), respectively. Pressure transducers (±0.1 psi) placed before and after the test section measured these pressures. System temperatures were measured in a similar manner using thermocouples (the greater of ±0.5°C or ±0.4%) placed before and after the test section. Inlet temperatures varied from 22°C to 65°C, while outlet temperatures were maintained at room temperature (22°C). Liquid flow rates through the microchannels were measured using a series of five cylinders in which liquid and vapor are separated with the mass of liquid gathered during a given amount of time being measured, thus yielding a time averaged liquid mass flow rate for five groups of three microchannels. The grouping of the microchannels along with the collection cylinders can be seen schematically in Figure 2-11. This allowed for a secondary determination of the vapor quality of the flow. This determination was made by summing the liquid mass flow into the 5 tanks and comparing it to the total mass flow to see if it corresponded to the desired quality for any given test condition.

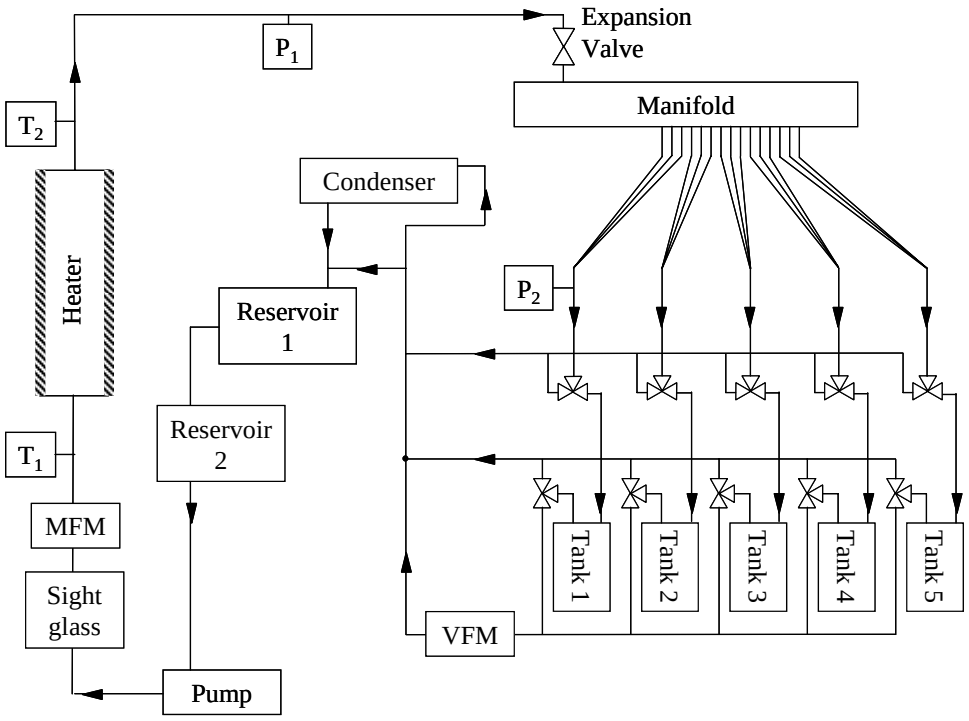

Figure 2-11: Refrigerant Loop

Chapter 3. R134a Liquid Distribution Results for Rectangular Manifold

3. 1. Data Matrix

As mentioned in Chapter 2, various parameters determined each test condition. For the rectangular manifold design the dynamic parameters varied were the inlet quality and the mass flow rate, which affects the inlet mass flux. The other parameters that were varied were the geometrical parameters of the flow field, namely the microchannel protrusion depth and the distance between the inlet port and the microchannels. The three protrusion schemes examined are presented in Figure 3-1, while the lengths between the inlet port and the microchannels are shown in Figure 3-2. These parameters and the facility capabilities allowed for a total of 186 possible test conditions using the rectangular manifold, Table 3-1 shows all the experimental cases that were tested, a total of 183. All liquid distribution results for the rectangular manifold are presented in graphical form for all test cases in Appendix B.

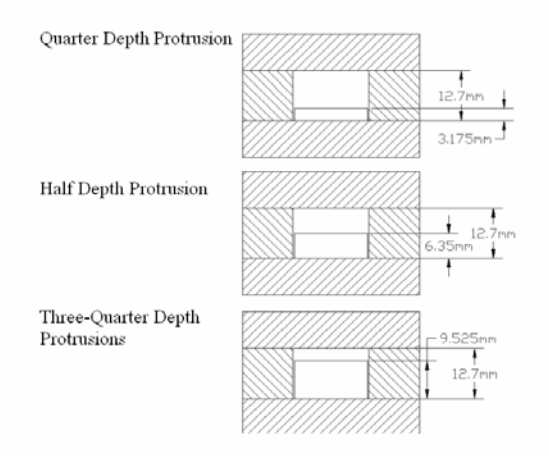

Figure 3-1: Microchannel Protrusion Depths for Rectangular Manifold (drawings not to scale)

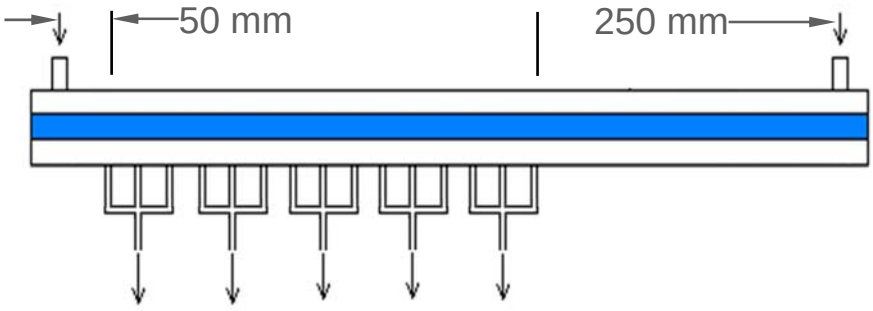

Figure 3-2: Lengths from Entrance Port to Microchannels

Table 3-1: Test Cases for Rectangular Manifold

1/4 Depth Protrusion				1/2 Depth Protrusion				3/4 Depth Protrusion			
Short		Long		Short		Long		Short		Long	
m(g/s)	x (%)	m (g/s)	x (%)	m(g/s)	x (%)	m (g/s)	x (%)	m (g/s)	x (%)	m (g/s)	x (%)
15	0	15	0	15	0	15	0	15	0	15	0

15	10	15	10	15	10	15	10	15	10	15	10
15	15	15	15	15	15	15	15	15	15	15	15
15	20	15	20	15	20	15	20	15	20	15	20
15	25	15	25	15	25	15	25	15	25	15	25
15	30	15	30	15	30	15	30	15	30	15	30
15	35	15	35	15	35	15	35	15	35	15	35
20	0	20	0	20	0	20	0	20	0	20	0
20	10	20	10	20	10	20	10	20	10	20	10
20	15	20	15	20	15	20	15	20	15	20	15
20	20	20	20	20	20	20	20	20	20	20	20
20	25	20	25	20	25	20	25	20	25	20	25
20	30	20	30	20	30	20	30	20	30	20	30
20	35	20	35	20	35	20	35	20	35	20	35
25	0	25	0	25	0	25	0	25	0	25	0
25	10	25	10	25	10	25	10	25	10	25	10
25	15	25	15	25	15	25	15	25	15	25	15
25	20	25	20	25	20	25	20	25	20	25	20
25	25	25	25	25	25	25	25	25	25	25	25
25	30	25	30	25	30	25	30	25	30	25	30
25	35	25	35	25	35	25	35	25	35		
30	0	30	0	30	0	30	0	30	0	30	0
30	10	30	10	30	10	30	10	30	10	30	10
30	15	30	15	30	15	30	15	30	15	30	15
30	20	30	20	30	20	30	20	30	20	30	20
30	25	30	25	30	25	30	25	30	25	30	25
35	0	35	0	35	0	35	0	35	0	35	0
35	10	35	10	35	10	35	10	35	10	35	10
35	15	35	15	35	15	35	15	35	15	35	15
35	20	35	20	35	20	35	20	35	20	35	20
35	25			35	25	35	25	35	25		

3. 2. Quarter Depth Protrusion

This section will discuss the set of experiments performed with the microchannel array protruded a quarter of the way into the flow field, or 3.175mm (.125”). The liquid distribution trends are presented against varying inlet mass flux and quality. There is a noticeable difference in the data of the short and the long entrance lengths, therefore discussion will be divided into so-called short entrance length results and long entrance length results.

3. 2. 1. Short Entrance Results

The refrigerant flow enters from the port located 50mm from the microchannels for this set of experiments, and the microchannels are mounted so that they protrude one quarter of the flow field height. Flow direction is from left to right within the manifold. The inlet cross-sectional area is 235mm^2, with an inlet mass flux range of 64 to 149 kg/m^2-s, corresponding to a mass flow rate range of 15 to 35 g/s. All test conditions for this geometric configuration show large liquid flow rates’ feeding the first two tanks decreasing to dry out or near dry out in the last two collection tanks. Figure 3-3 illustrates the effects of increasing inlet quality while holding inlet mass flux constant. Increasing inlet quality at a specific inlet mass flux provides a slight improvement in distribution. However, this

slight improvement is not enough to reverse the dry out conditions in the last tank. Figure 3-4 illustrates the effect of increasing inlet mass flux while holding inlet quality constant. This shows that an increase in inlet mass flux has a similar effect as an increase in quality at constant mass flux, which is that the uniformity of the distribution is slightly improved by this increase. Again, this improvement in uniformity is not enough to remove the large disparity in liquid flow rates seen between the first and the last tank.

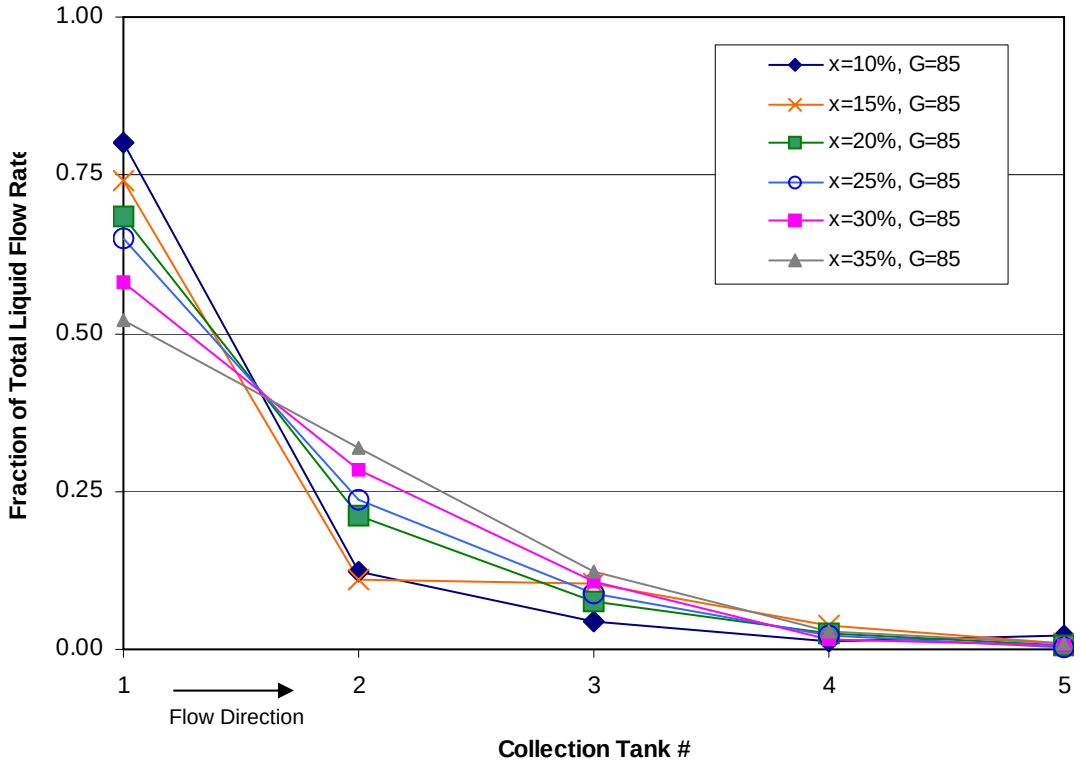

Figure 3-3: Inlet Quality Effects, Quarter Depth Protrusion, Short Entrance

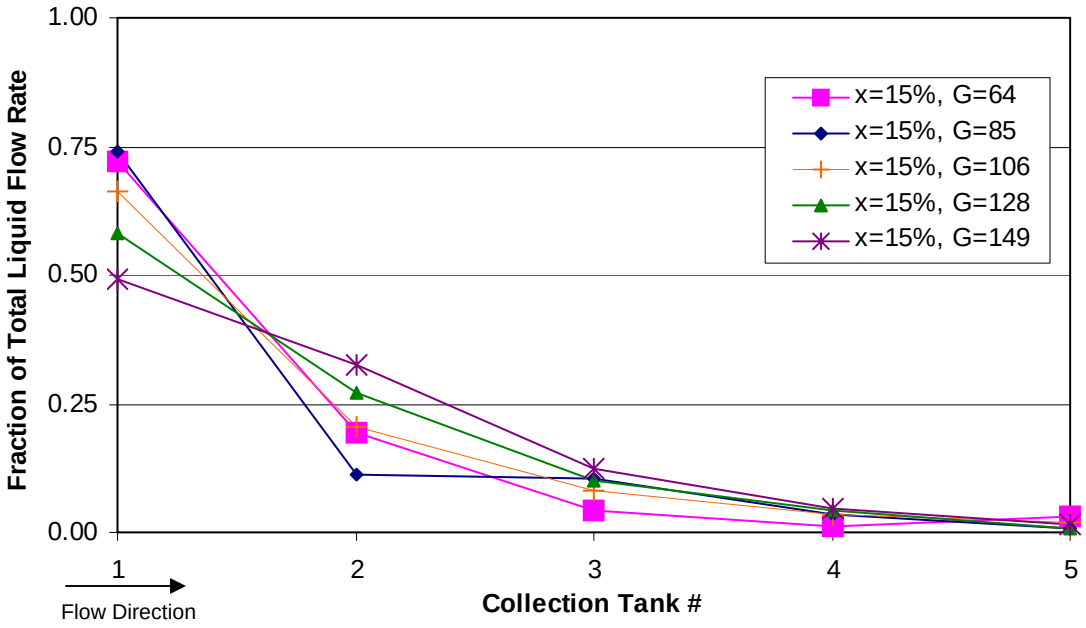

Figure 3-4: Inlet Mass Flux Effect, Quarter Depth Protrusion, Short Entrance

3. 2. 2. Long Entrance Results

For this set of experiments the refrigerant entered through the port located 250mm from the microchannel array, with the microchannels protruded one quarter of the flow field depth. Again, the flow direction is from left to right within the manifold. The inlet flow area and mass flux range is the same as for the short inlet case. The results for all test conditions in this configuration show large liquid flow rates entering the first tank with small flow rates in the second tank and the last three tanks seeing either dry out or near dry out conditions. Figure 3-5 illustrates the effect of increasing inlet quality on the liquid flow distribution for a constant inlet mass flux. This shows that increasing inlet quality provides very little help in improving liquid distribution. Figure 3-6 illustrates the effect of increasing inlet mass flux while holding the inlet quality constant. While, Figure 3-6 shows that increasing inlet mass flux for a given inlet quality produces a slight improvement in liquid distribution the improvement provides very little shift toward uniformity. Both Figures 3-5 and 3-6 illustrate the dry out or near dry out experienced in the last three tanks and in some cases the second tank as well, a very undesirable condition in a real heat exchanger.

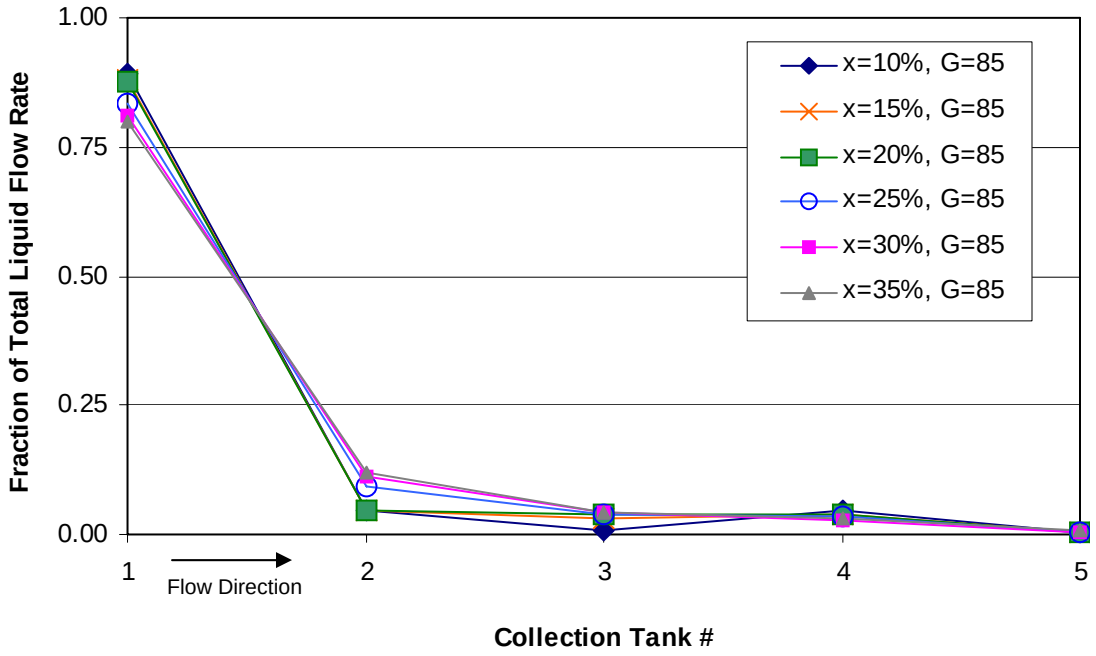

Figure 3-5: Inlet Quality Effects, Quarter Depth Protrusion, Long Entrance

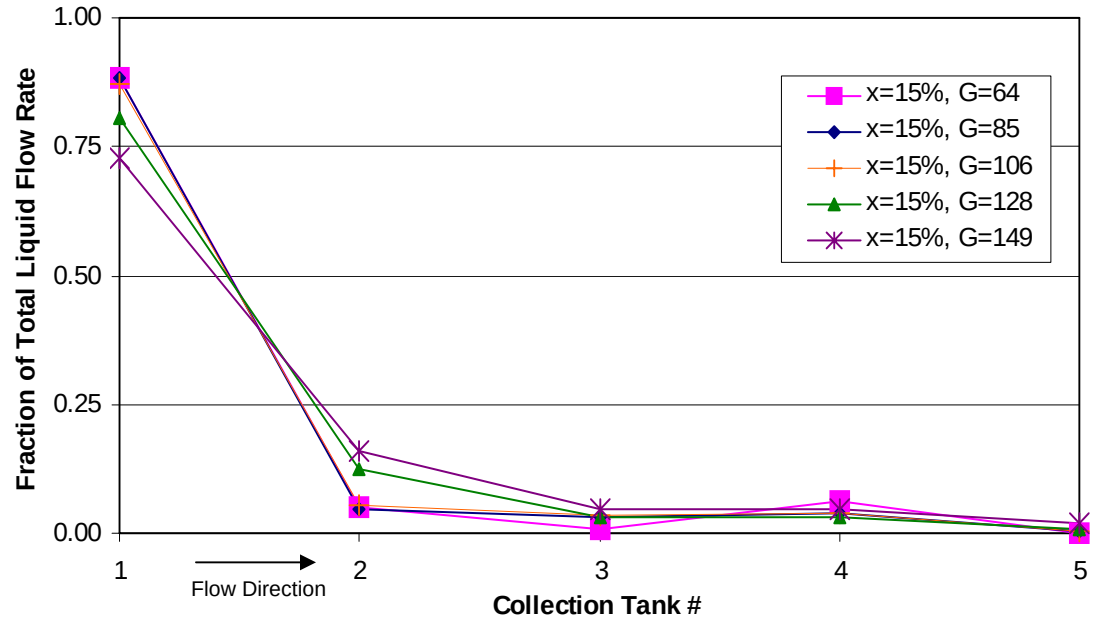

Figure 3-6: Inlet Mass Flux Effects, Quarter Depth Protrusion, Long Entrance

3. 3. Half Depth Protrusion

The next set of experiments to be discussed was performed with the microchannels protruded to a depth of one half of the flow field, or 6.35mm (.25”). All test cases were performed so that all of the inlet parameters were the same as the inlet parameters for the case where the microchannels were protruded to one quarter depth. Again,

the two inlet lengths, long and short, yielded noticeably different results. Thus discussion will once again be divided into short and long entrance cases.

3. 3. 1. Short Entrance Results

For this set of results the refrigerant entered through the port located 50 mm from the microchannel array, with the microchannel protruded to one half of the flow field depth. The flow was from left to right within the flow field. The results for all of these cases show marked improvement in distribution over the results for the same conditions with the microchannels only protruded to one quarter depth. Dry out, or near dry out, conditions are not as common in the third and fourth tanks as in the previous short entrance cases. Also, the effect of increasing inlet mass flux and inlet quality on improving liquid distribution seems to be more noticeable. However, dry out still occurs in the fifth tank under many inlet conditions. Figure 3-7 illustrates the effect on liquid distribution by increasing inlet quality for a constant inlet mass flux. It can be seen from Figure 3-7 that an increase in inlet quality provides improvement in liquid distribution similar to that seen in the one quarter depth microchannel insertion cases (see Fig 3-3). However, the liquid refrigerant distribution is slightly more uniform for the half depth case than for the quarter depth. Figure 3-8 illustrates the effect of varying inlet mass flux on liquid distribution for a constant inlet quality. It can be seen from Figure 3-8 that, again, increasing the inlet mass flux improves distribution for a given inlet quality. For the cases with higher inlet mass flux, the dry out conditions in the third and fourth collection tank disappear and now the fifth collection tank is the only one that experiences dry out or near dry out conditions. This distribution is far more desirable, with respect to uniformity, than all the previous cases discussed, yet still far from completely uniform.

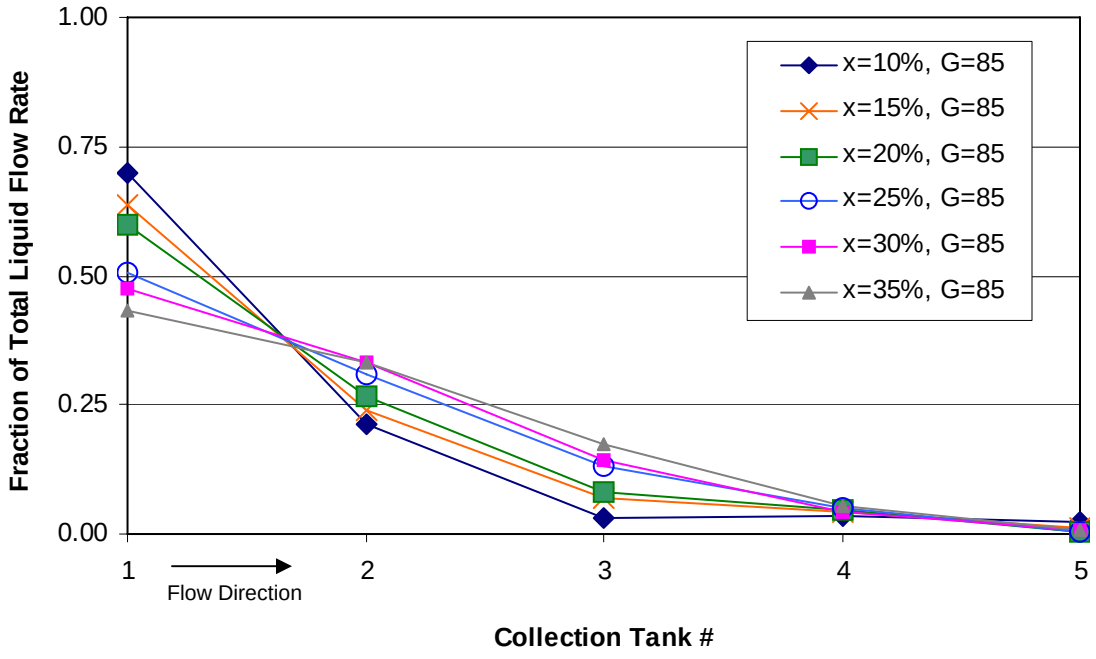

Figure 3-7: Inlet Quality Effects, Half Depth Protrusion, Short Entrance

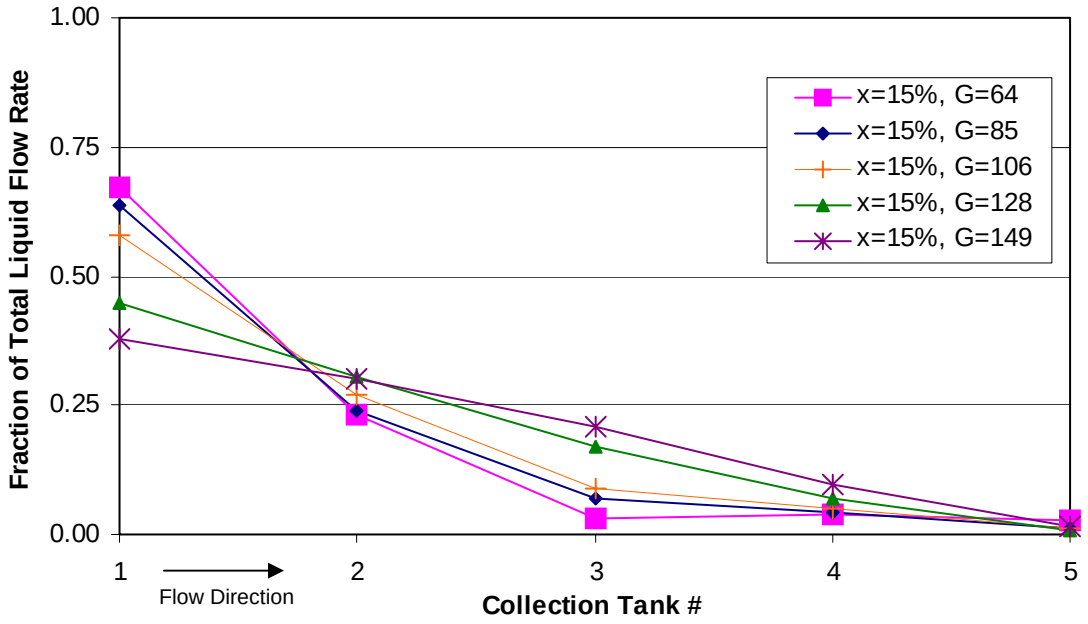

Figure 3-8: Inlet Mass Flux Effects, Half Depth Protrusion, Short Entrance

3. 3. 2. Long Entrance Results

The following test cases were performed with the refrigerant entering through the inlet port located 250mm from the microchannels. The microchannel array was protruded to half of the flow field depth and the inlet parameters were the same as the short entrance cases for one half depth protrusion. Flow direction was from left to right within the manifold. Figure 3-9 illustrates the effects of varying inlet quality while holding inlet mass flux constant. Again, as is seen, from Figure 3-9, increasing the inlet quality in the manifold leads to improved uniformity of the liquid distribution. It should be noted that flow entering through the short inlet port is more uniform than that coming from the long with the same inlet quality and mass flow rate (Figures 3-7 and 3-9). Figure 3-10 illustrates the effect of varying inlet mass flux while holding the inlet quality constant. This shows that increasing the inlet mass flux for a given inlet quality improves the uniformity of the liquid distribution only slightly, as seen in all the other long entrance cases so far. While some steps towards complete uniformity in the liquid distribution are seen, mainly through increasing inlet mass flux, liquid distribution for all inlet conditions, for this geometrical configuration, are far from complete uniformity.

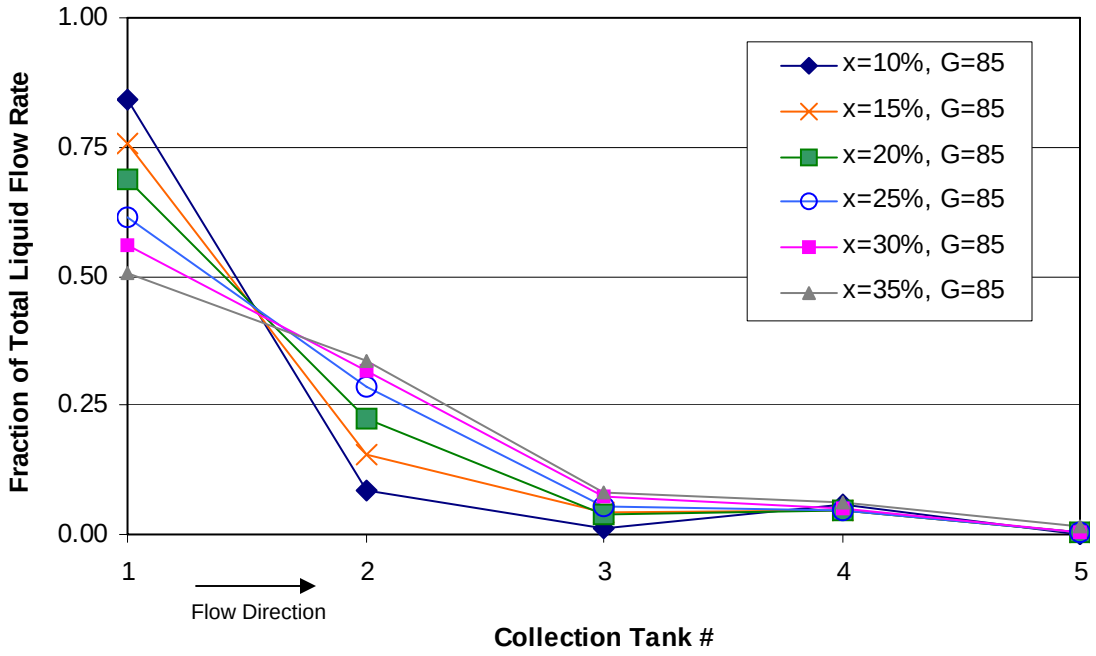

Figure 3-9: Inlet Quality Effects, Half Depth Protrusion, Long Entrance

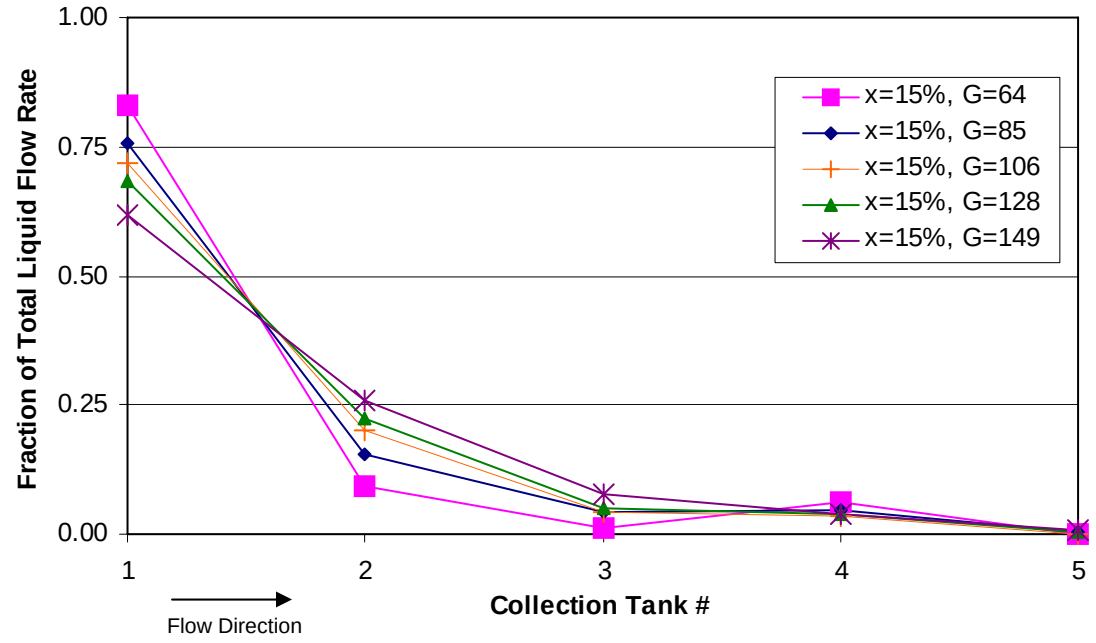

Figure 3-10: Inlet Mass Flux Effect, Half Depth Protrusion, Long Entrance

3. 4. Three-Quarter Depth Protrusion

The following set of experiments was performed using the same inlet parameters as all the other previous experiments, however, the microchannel protrusion depth was increased to three-quarters of the flow field depth, 9.525mm (.375”). Again, the two different inlet ports produced results different enough to warrant separate

discussion, thus dividing the results between the short entrance length case and the long entrance length case. Flow direction is from left to right within the manifold in both cases.

3. 4. 1. Short Entrance Results

The following results were obtained from tests performed with the refrigerant entering 50mm form the microchannel array. For many of the cases, liquid flow was relatively well distributed among the first three to four collection tanks with only the fifth tank experiencing dry out or near dry out conditions. Figure 3-11 illustrates the effect of varying inlet quality while holding inlet mass flux constant. It is easily seen from Figure 3-11 that increasing inlet quality has the effect of improving liquid distribution slightly; however, the improvement in liquid distribution is never enough to make the liquid distribution completely uniform. Figure 3-12 illustrates the effect of increasing inlet mass flux while holding inlet quality constant. Figure 3-12 shows how increasing inlet mass flux helps to improve the liquid distribution, with the highest inlet mass flux for a fixed quality yielding the most uniformly distributed flow rates of the test cases presented thus far.

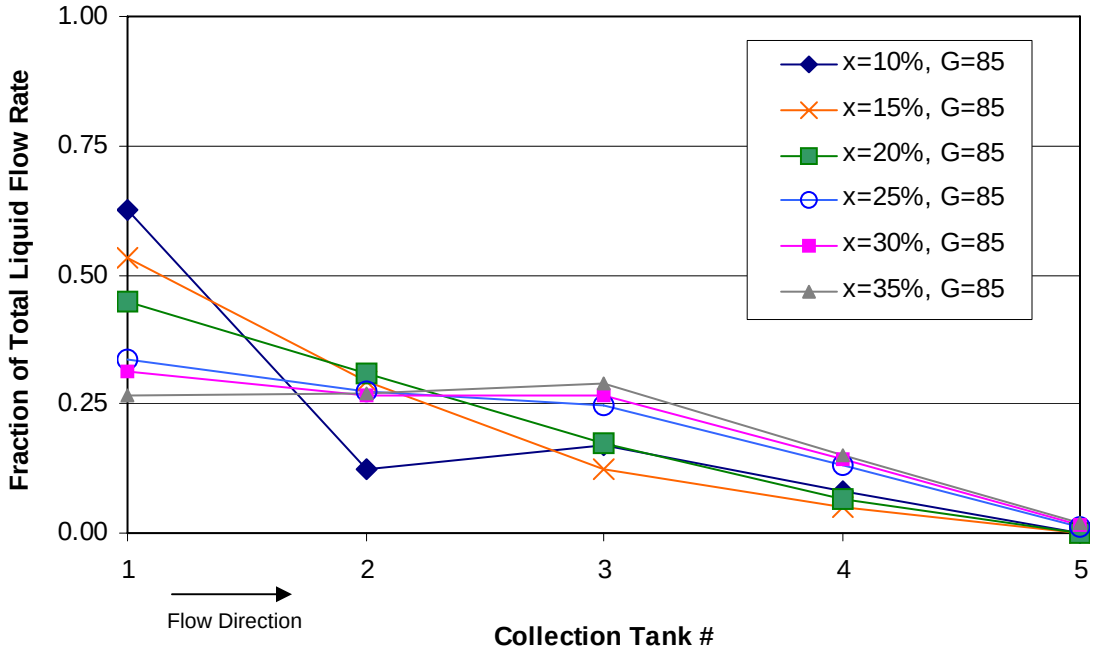

Figure 3-11: Inlet Quality Effects, Three-Quarter Depth Protrusion, Short Entrance

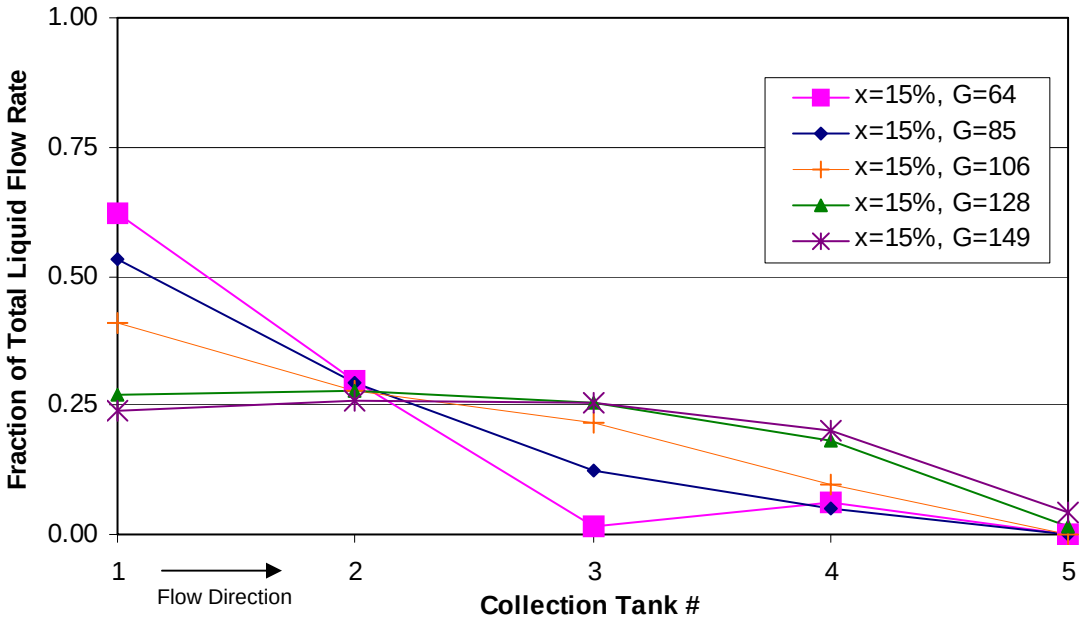

Figure 3-12: Inlet Mass Flux Effect, Three-Quarter Depth Protrusion, Short Entrance

3. 4. 2. Long Entrance Results

The following test cases were performed with the refrigerant entering the inlet port located 250mm from the microchannels. The microchannel array was protruded to three quarters of the flow field depth and the inlet parameters were the same as the short entrance cases for one three quarter depth protrusion. Flow direction was from left to right within the manifold. The effect of varying the inlet quality while holding the inlet mass flux constant is seen in Figure 3-13. It is easily seen from this figure that there is some slight improvement in the uniformity of liquid flow distribution for increasing quality, however this effect is not as noticeable as the same effect in the short entrance cases for the same protrusion depth (compare Figure 3-11 to Figure 3-13). Figure 3-14 illustrates the effect of varying inlet mass flux while holding the inlet quality constant. From Figure 3-14 it is easily seen that there is very little change in liquid flow distribution associated with a change in inlet mass flux. This is drastically different from the improved distribution caused by increased inlet mass flux experienced by the short inlet cases for the three quarter depth protrusion cases, as seen in Figure 3-12.

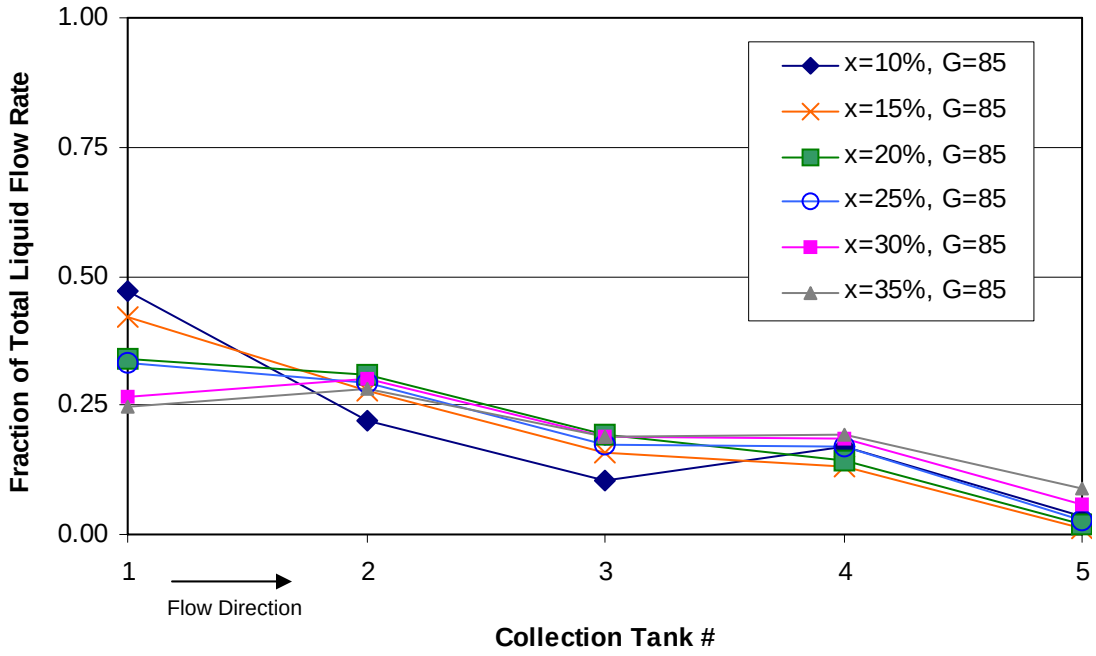

Figure 3-13: Inlet Quality Effects, Three-Quarter Depth Protrusion, Long Entrance

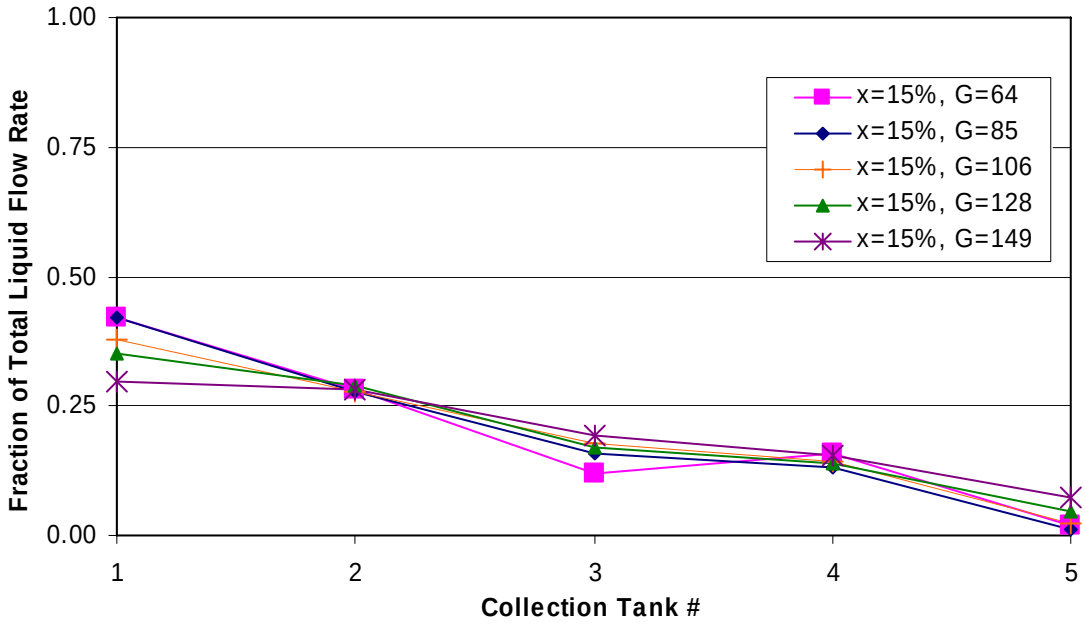

Figure 3-14: Inlet Mass Flux Effect, Three-Quarter Depth Protrusion, Long Entrance

3. 5. Effect of Microchannel Protrusion

Previous discussions noted the effects of inlet mass flux and quality on liquid refrigerant distribution within the rectangular microchannel manifold for a given protrusion scheme and inlet. The following discussion will focus on the effects of microchannel protrusion depth on liquid refrigerant flow distribution in the rectangular

microchannel manifold. In general, it seems that increasing the microchannel protrusion depth has the affect of improving liquid flow distribution for a given test case. This holds true for both the short and long entrance cases. Figure 3-15 illustrates this effect for the short entrance case at a given inlet mass flux and quality, while Figure 3-16 illustrates it for the same conditions in the long entrance case. Figures 3-15 and 3-16 both show that increasing the depth of the microchannel protrusion improves liquid distribution for a given set of inlet parameters. To see how this compared to the results obtained for the flush mounted microchannel cases the data for those cases was included both in these Figures and in the complete accounting of the Appendices. It should be noted that the improvement in distribution made by increasing the protrusion of the microchannels is more noticeable for the long entrance results. For all cases with an inlet quality above 0% the three quarter depth microchannel protrusion provided the best liquid flow rate distribution. Still, no case presents a completely uniform liquid distribution.

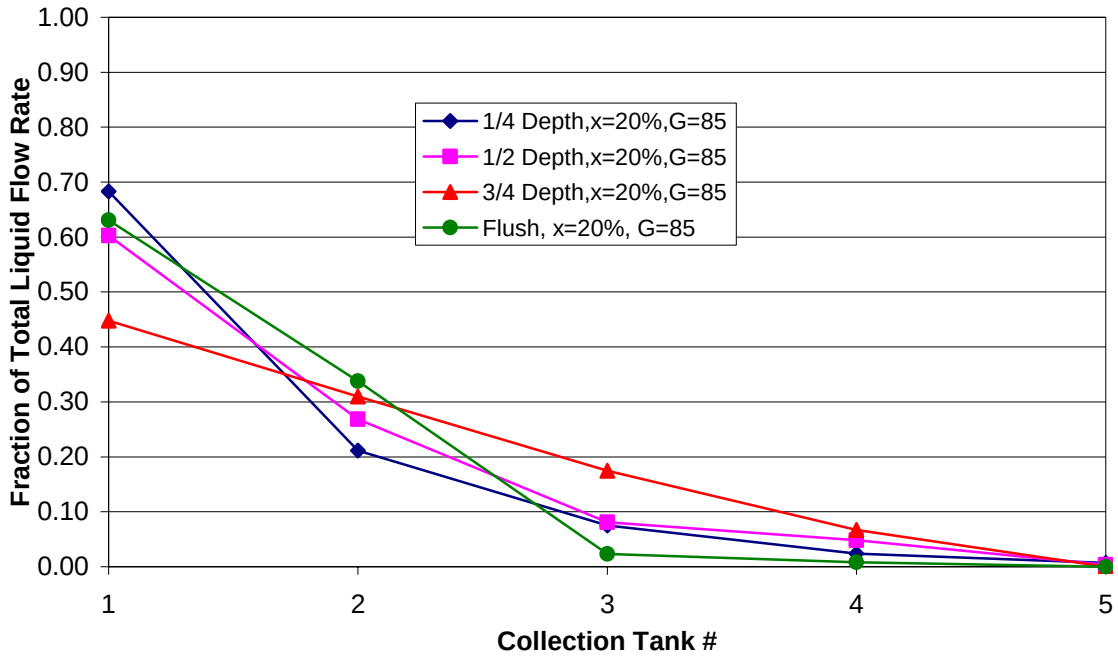

Figure 3-15: Microchannel Protrusion Effects, Short Entrance

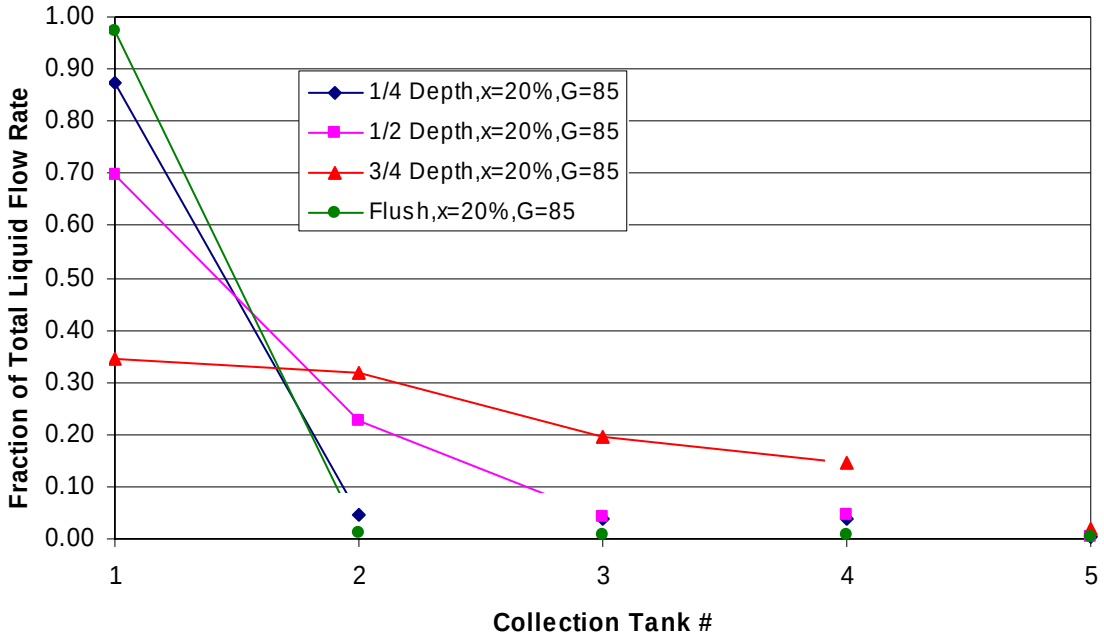

Figure 3-16: Microchannel Protrusion Effects, Long Entrance

3. 6. Reduced Rectangular Results

Although the raw distribution results present some discernable trends regarding varying inlet mass flux, inlet quality, entrance length, and microchannel protrusion depth reducing the results in some fashion may lead to a better understanding of these trends. Several representative cases of each reduced measure will be discussed below. For some cases results are compared to flush data which was obtained in the study done by Zhang, in order to obtain a more complete picture of the trends. A more detailed account of all reduced results is presented in graphical form in Appendix B.

3. 6. 1. Coefficient of Variation

The coefficient of variation (CV) is a measure of relative scatter with respect to a mean. To better quantify maldistribution within the manifold the mean is considered to be exactly uniform liquid distribution (i.e. all the collection tanks receive the same liquid flow rate). Thus, for present concerns the CV measures how far the liquid flow distribution deviates from completely uniform distribution. The use of the coefficient of variation allows the five points relating to liquid flow in each collection tank to be reduced to one point that tells how uniformly the flow is distributed. This allows for a more compact analysis of the effect of varying test parameters. Equation 3-1 shows the equation used to obtain the CV. Where the standard deviation is gained from Equation 3-2 and the mean liquid mass flow rate is defined as shown in Equation 3-3. For this study the CV is bounded by 0 and 2. The boundary value of 0 represents completely uniform distribution while the boundary value of 2 represents the entire liquid flow rate entering only 1 collection tank. It should be noted that the simplicity gained by using the CV as a measure of the uniformity of the distribution leads to a loss of information regarding where the maldistribution occurs within the manifold. In other words, the flow could be distributed to one side of the manifold and yield a specific value of CV that could also be obtained from an equally maldistributed flow on the opposite side of the manifold. In order to

gain perspective on what a particular value of CV means with respect to flow distribution, Figure 3-17 shows the distribution chart for two different inlet conditions and the corresponding values of CV for these conditions. The first condition with inlet quality of 15% and inlet mass flux of 64 kg/m^2-s sees most of the flow going into the first two tanks with the last three seeing dry out or near dry out conditions, the value of CV for this condition is 1.19. While the second point, with inlet quality of 15% and inlet mass flux of 149 kg/m^2-s, is much more evenly distributed and has a CV value of 0.40. Now that the distribution has been reduced and quantified in the form of a CV value it is much more compact and easier to meter with respect to other parameters.

Equation 3-1 $$CV = \frac{\sigma}{\dot{m}}$$

Equation 3-2 $$\sigma = \sqrt{\sum_{i=1}^{n_{tanks}} (\dot{m}_i - \overline{\dot{m}})^2 / n_{tanks}}$$

Equation 3-3 $$\overline{\dot{m}} = \frac{\sum_{i=1}^{n} \dot{m}_i}{n_{tanks}}$$

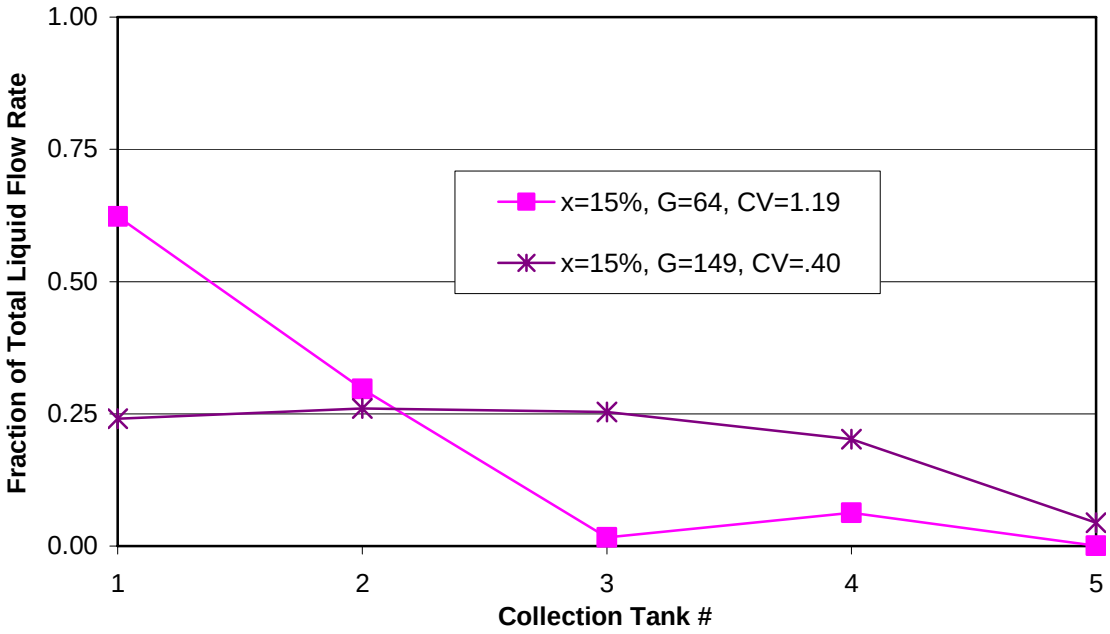

Figure 3-17: Liquid Flow Distributions and Their Respective CV Values

3. 6. 2. Effective Mass Flux

The effects of the microchannel protrusion and inlet mass flux on liquid flow distribution were presented previously in separate discussions. Figure 3-18 combines these effects for a constant inlet quality of 20% with the flow entering from the long entrance. It can be seen from Figure 3-18 that as inlet mass flux increases there is slight improvement in flow distribution. More importantly, it shows that increasing the protrusion depth has a dramatic

effect on improving distribution. Figure 3-19 serves to illustrate similar trends when the mass flux is held constant and the inlet quality is varied. Again, the dramatic effect of changing the protrusion depth is very obvious. Similar graphs could be constructed in an analysis of the rest of the distribution data, however, it would be advantageous to have a parameter that combined the effects of both protrusion depth and inlet mass flux so that these four "lines" can be collapsed down to one. This will be done by using a parameter which will be referred to as the effective mass flux (G_{eff}). The determination of an effective mass flux is simple. The only difference between the calculation of the effective mass flux and the inlet mass flux is the area, instead of the entire flow field area, only the area above the microchannel is considered, as illustrated by the red shading in Figure 3-20. The effective mass flux range, for all protrusion depths, was 64-596 (kg/m^2s). Figure 3-21 shows how inlet mass flux and protrusion depth relate to the effective mass flux that has been defined above.

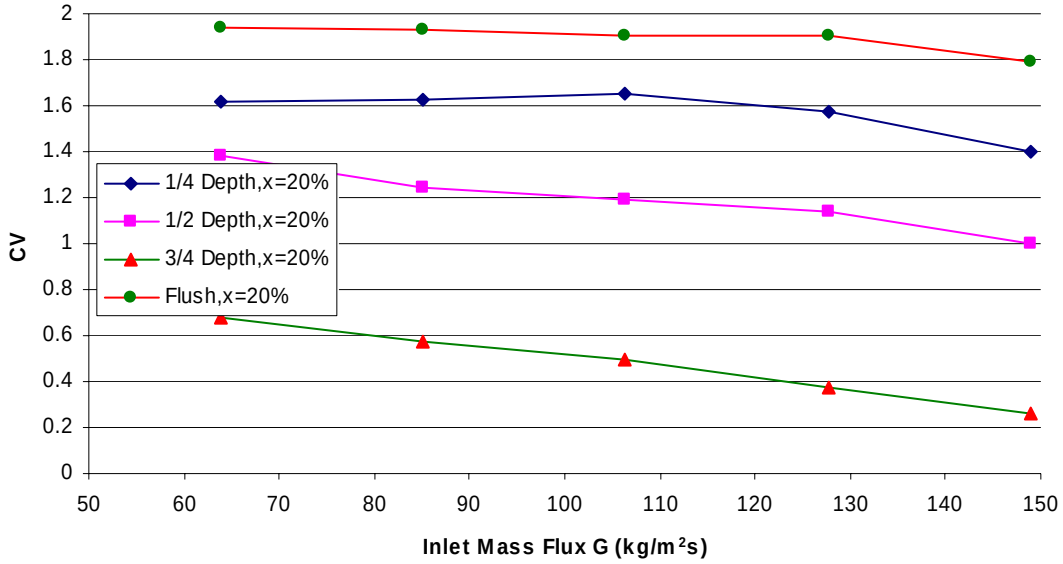

Figure 3-18: CV vs. Inlet Mass Flux for Varying Protrusion Depths, Long Entrance

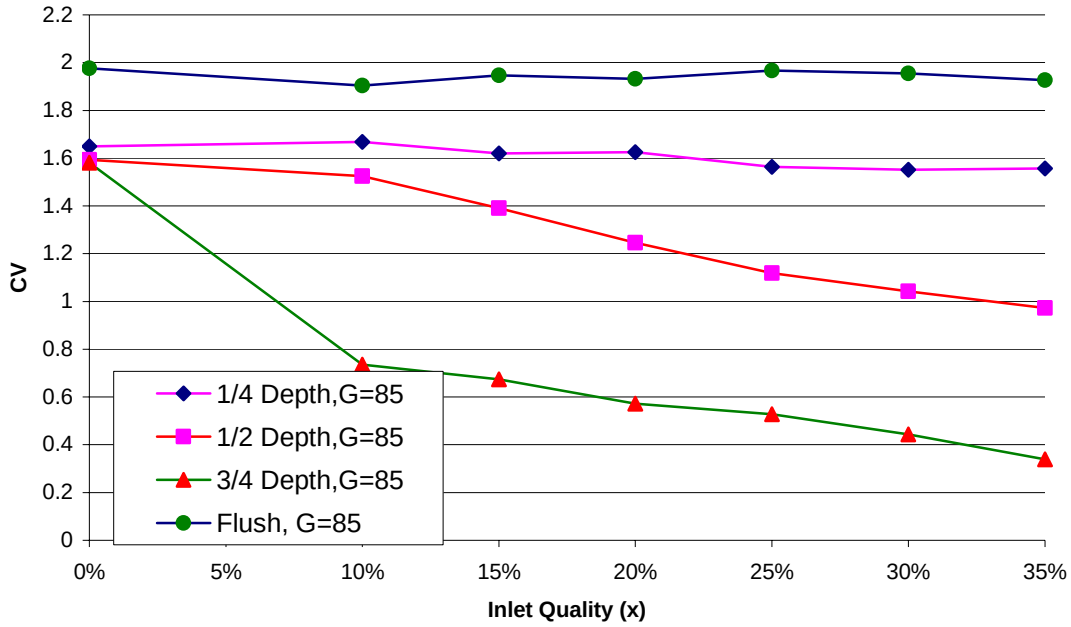

Figure 3-19: CV vs. Inlet Quality for Varying Protrusion Depths, Long Entrance

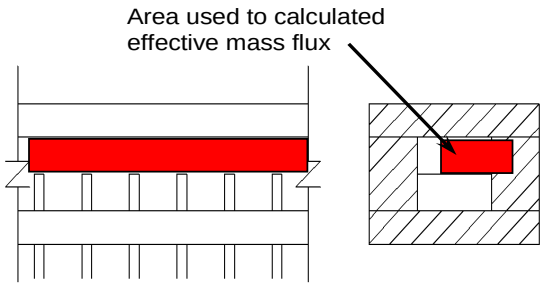

Figure 3-20: Area Used in Calculation Effective Mass Flux

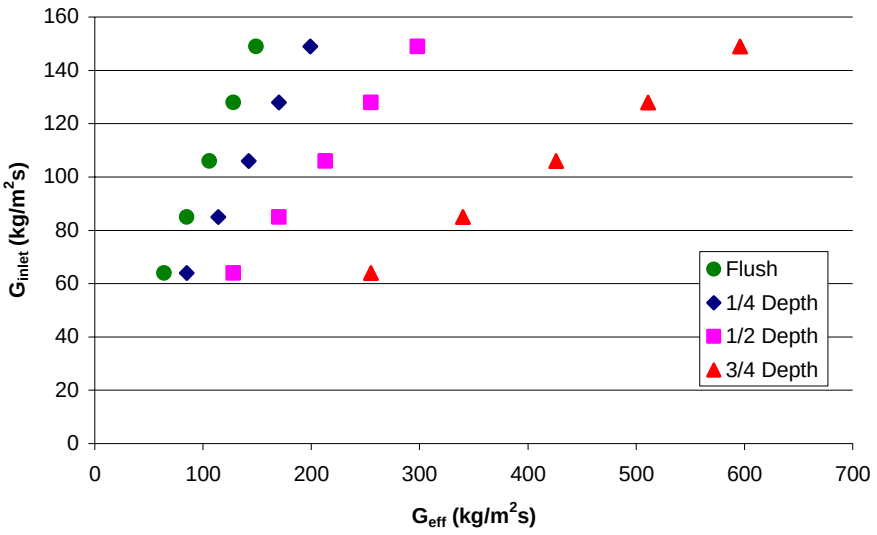

Figure 3-21: Inlet Mass Flux vs. Effective Mass Flux

Now, CV can be compared to the effective mass flux as is done in Figure 3-22. Figure 3-22 presents all the data represented in Figure 3-18, while Figure 3-23 shows the results for the same inlet quality (20%) in the short entrance case. Both of these figures show that increasing the effective mass flux dramatically improves the uniformity of liquid distribution for both the long and short entrance cases.

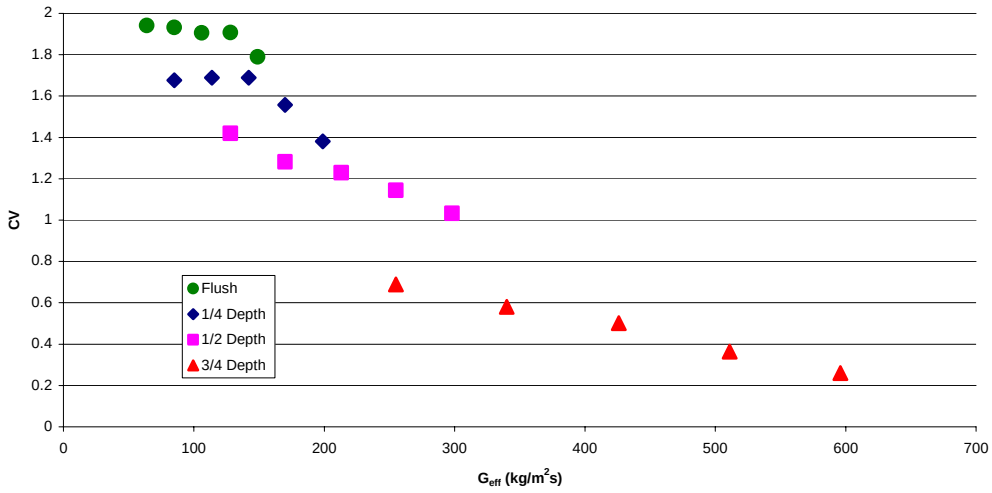

Figure 3-22: Effective Mass Flux Effects, Long Entrance, 20% Inlet Quality

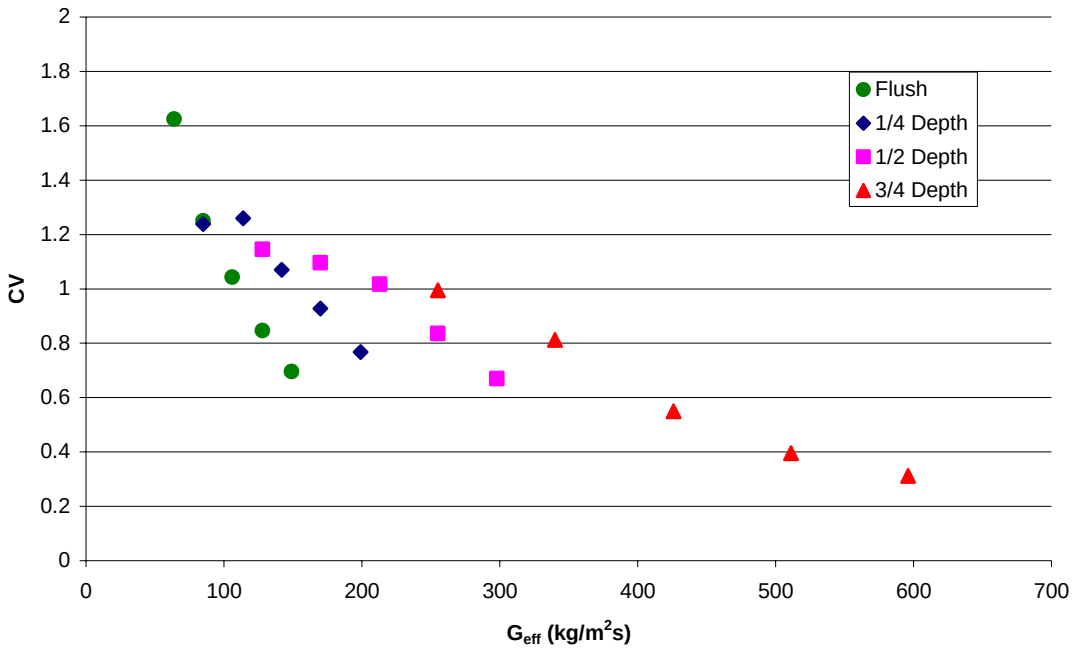

Figure 3-23: Effective Mass Flux Effects, Short Entrance, 20% Inlet Quality

This trend holds generally for all inlet qualities, except 0% where distribution is poor for all effective mass fluxes. Obviously, with this particular study in mind, there are two ways in which the effective mass flux can be changed, either by changing the mass flow rate or microchannel protrusion depth. In the case of the longer entrance, increasing the effective mass flux by increasing the protrusion depth of the microchannels is more effective in regards to improving distribution, as seen in Figure 3-24. In Figure 3-24 changing the effective mass flux by changing the protrusion is represented by the dashed lines and changing it by changing mass flow rate is represented by the solid lines. While the line representations remain the same he opposite trend seems to be true for flow entering through the short entrance, as seen in Figure 3-25. It is still fair to say that in both cases an increase in effective mass flux provides marked improvement in distribution. It seems that once the microchannels are protruded to three-quarters of the flow field, the long entrance cases seem to have better distribution than the short for the same inlet conditions. In line with this, is the fact that while the effect of microchannel protrusion is positive, with respect to uniformity of distribution, for both long and short entrances it is more dramatic in the cases in which the flow is expanded further from the manifold. Another note that should be made is that while microchannel protrusion improves distribution it will also have an effect on pressure drop within the manifold, this effect was neither quantified nor qualified for the rectangular manifold; however, this effect was studied briefly for the circular manifold, and will be discussed in the chapter pertaining to those experiments. A complete record of reduced results such as those in Figure 3-22 and 3-23 is provided in Appendix B

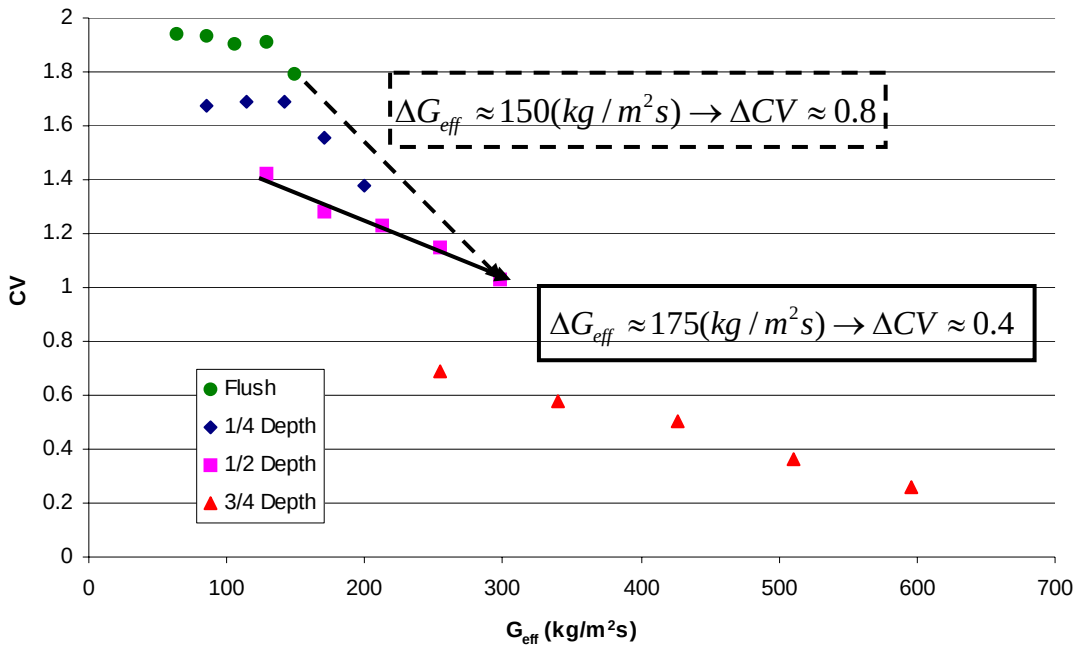

Figure 3-24: Effective Mass Flux Effects, Long Entrance, 20% Inlet Quality

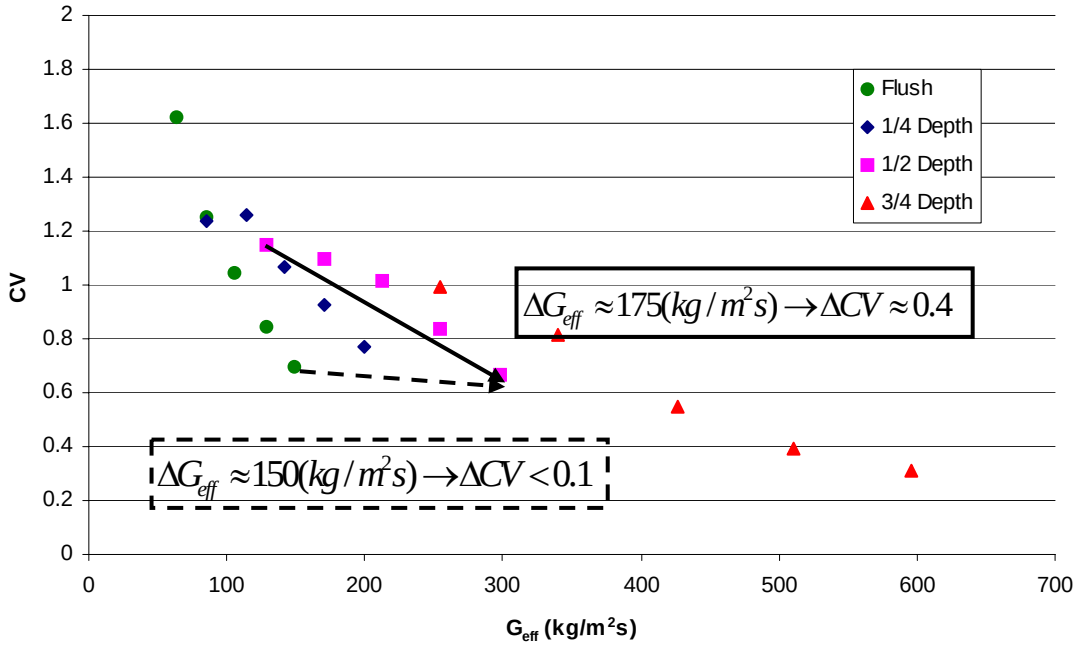

Figure 3-25: Effective Mass Flux Effects, Long Entrance, 20% Inlet Quality

3. 6. 3. Comparison to Flush Results

To see if the effective mass flux is an accurate quantification of how the microchannel protrusion effects distribution within the manifold, the effective mass flux will be compared to similar values of inlet mass flux obtained from Zhang's study with the microchannels mounted flush to the manifold. This can be done due to the

fact that the entire flow area was changed in Zhang's study to yield inlet mass fluxes similar to the effective mass fluxes seen in this study. Comparing these results will show whether decreasing the flow field area by protruding the microchannels or by simply making the entire manifold cross sectional area smaller has the more desired effect. Figure 3-26 presents the case in which the inlet quality is fixed at 20% and the flow enters through the short entrance. It is easily seen from Figure 3-26 that the results from the protrusion cases and the flush cases match up very well when the refrigerant enters the manifold closer to the microchannel array. This seems to imply that, for the short entrance length, protruding the microchannels has the same effect as reducing the entire manifold cross-section. This also implies that for flows that do not have enough time to and distance to separate or develop the area for the flow is an important factor in determining distribution. While this particular point will be discussed more in depth when the flow visualization experiments in the circular manifold are examined, it should be mentioned that others, Kulkarni *et al* (2004)., have noted the importance of avoiding phase separation when distribution in a manifold is of concern.

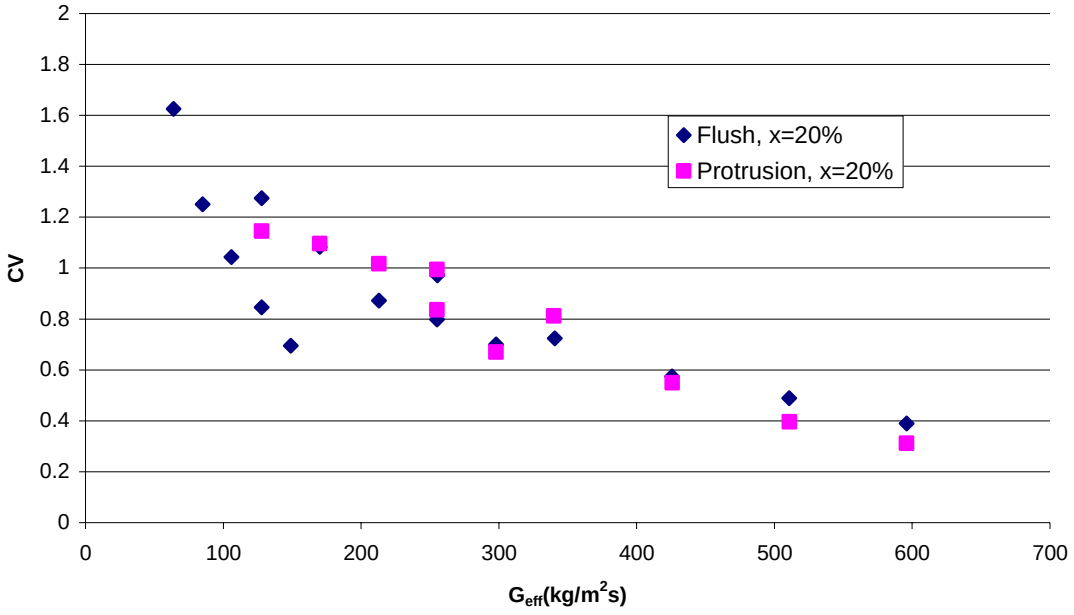

Figure 3-26: Flush and Protrusion Comparison, Short Entrance, 20% Inlet Quality

Figure 3-27 presents the same results except that now the flow enters through the longer inlet. This figure shows that the flush cases and the protruded cases follow the same trends, except that now there is an offset between the two. Here, the offset favors the cases in which the flow area is decreased by protruding the microchannels rather than by decreasing the entire area of the manifold. This may imply that disturbing a relatively separated flow by protruding the microchannels is more beneficial, with respect to distribution, than merely increasing the mass flux or effective mass flux. This also agrees with ideas put forward in both Fei(2004) and Zhang(2004), namely that development length of the flow plays a very important role in distribution. Again, this notion of flow development and protrusion depth playing coupled roles in liquid distribution will be discussed at length in a later chapter. All results for these comparisons for all conditions are presented completely in graphical form in Appendix B.

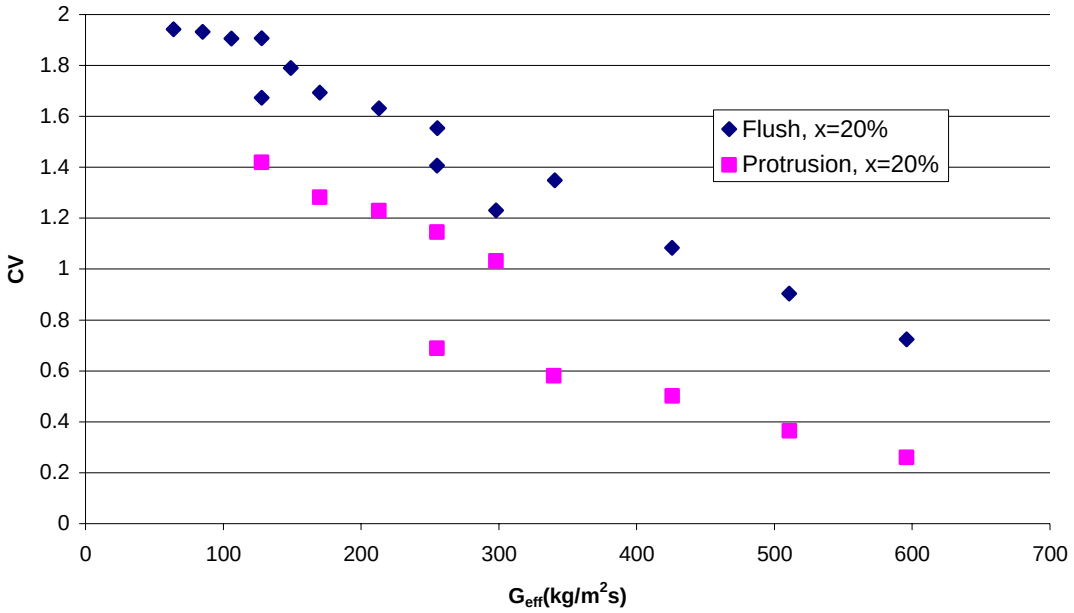

Figure 3-27: Flush and Protrusion Comparison, Longs Entrance, 20% Inlet Quality

3. 6. 4. Quality Scaled Effective Mass Flux

While the effective mass flux helps to show the effects of both microchannel protrusion and mass flow rate on distribution, it would be helpful to be able to combine this with the effect of inlet quality as well. This would allow all of the inlet parameters to be lumped into one value. To do this the effective mass flux was multiplied by one minus the inlet quality, as seen in Equation 3-4. This value, the

Equation 3-4 $$G_{eff,liq} = (1-x) \times G_{eff}$$

liquid scaled effective mass flux ($G_{eff,liq}$), weights the mass flux that is seen at the first microchannel by the mass fraction of liquid refrigerant. This allows comparison of distribution for all inlet conditions for a given inlet length. The results for the rectangular manifold experiments presented in this manner can be seen in Figures 3-28 and 3-29 for the short inlet and long inlet cases respectively. There is a somewhat general trend that appears in these figures, mainly that as this value is increased the liquid distribution improves, but there is also a more subtle trend that appears as well. This subtlety is most noticeable in the three-quarter cases for each inlet length. While the trend is generally that distribution improves with increased $G_{eff,liq}$, the trend reverses itself for the five distinct mass flow rates and distribution actually becomes slightly less uniform with increases in $G_{eff,liq}$ due to an increase in quality. There are even large differences in the CV values for cases in which the values of $G_{eff,liq}$ are similar. This suggests that the liquid scaled effective mass flux is not key in governing liquid distribution.

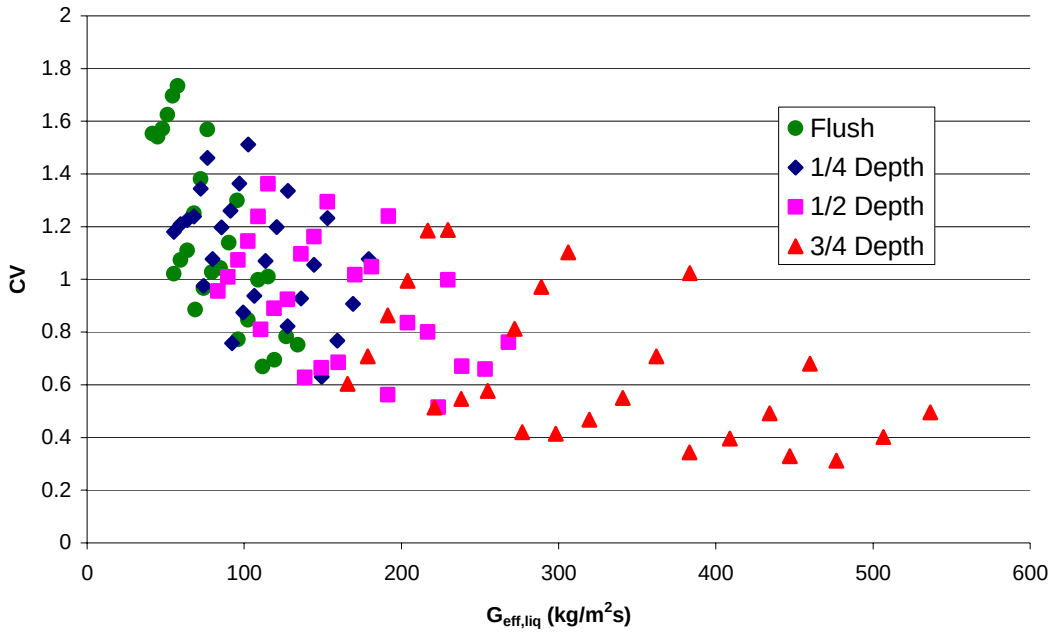

Figure 3-28: Liquid Mass Fraction Scaled Effective Mass Flux Effects, Short Entrance

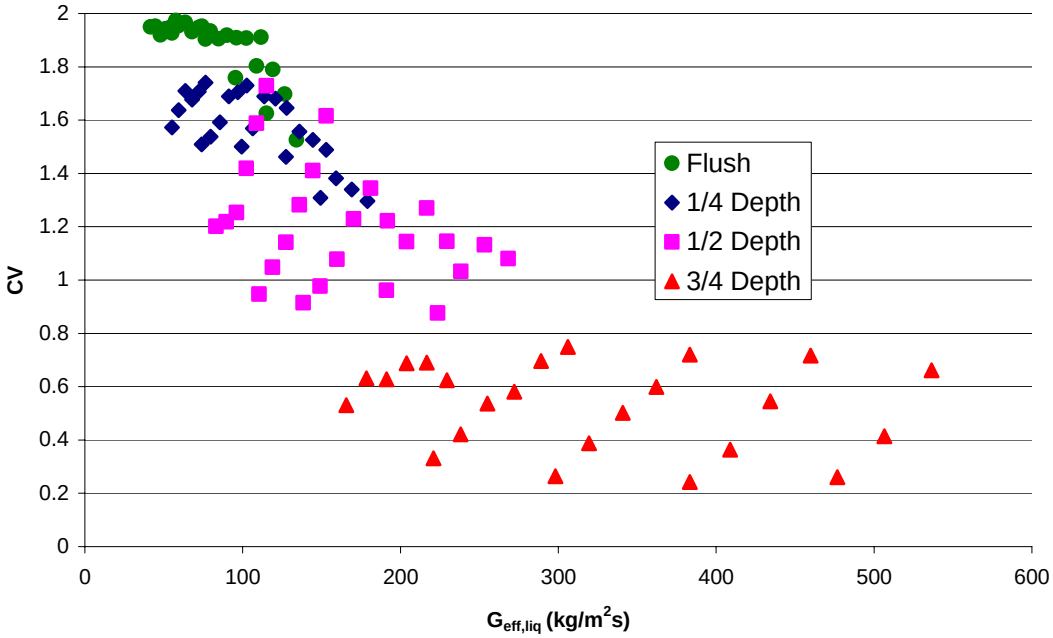

Figure 3-29: Liquid Mass Fraction Scaled Effective Mass Flux Effects, Long Entrance

With the suggestion that a liquid scaled effective mass flux may not be the strongest factor in determining the liquid distribution a similar parameter to the one above was calculated with the effective mass flux weighted by the vapor mass fraction ($G_{eff,vap}$) as seen in Equation 3-4, instead of the liquid mass fraction. The distribution results are plotted against the inlet conditions reduced in this fashion in Figures 3-30 and 3-31. These figures show a much

clearer trend than the one seen in Figures 3-28 and 3-29. For the short inlet cases the distribution consistently becomes more uniform as $G_{eff,vap}$ increases, without showing large changes due only to an increase in protrusion depth. The cases in which the fluid entered through the long entrance show a similar trend, but with a more of a stepwise type of improvement associated with increases in protrusion depth.

Equation 3-5 $$G_{eff,vap} = x \times G_{eff}$$

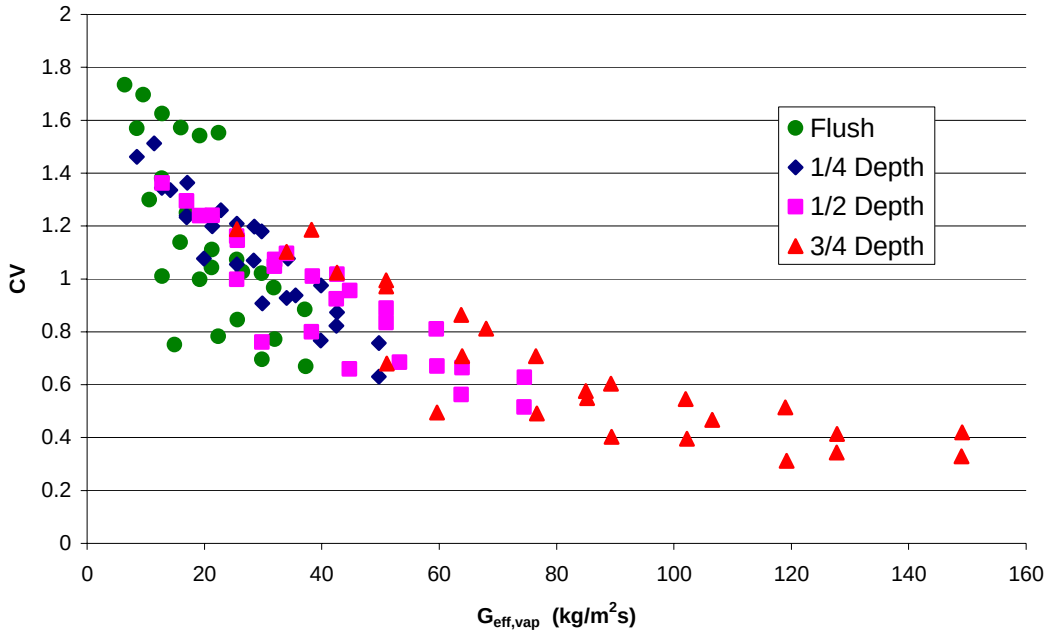

Figure 3-30: Vapor Quality Scaled Effective Mass Flux Effects, Short Entrance

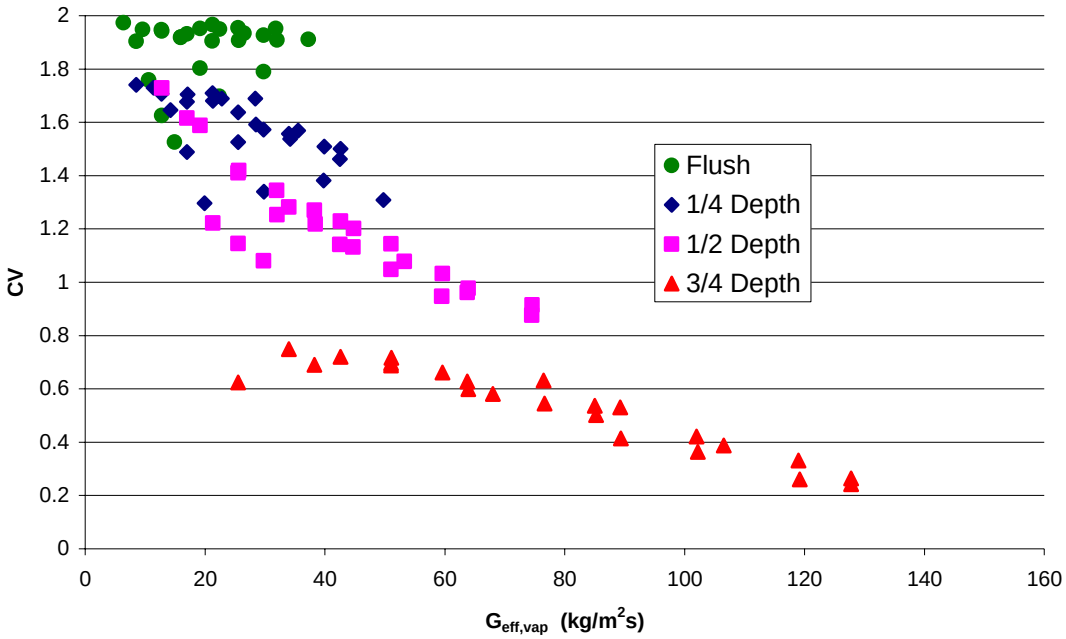

Figure 3-31: Vapor Quality Scaled Effective Mass Flux Effects, Long Entrance

3. 7. Conclusions

Several different parameters were considered in studying the distribution of R-134a in this microchannel manifold with a rectangular cross sectional area. The flow conditions that were altered in order to study their affect on the flow were quality and mass flow rate the quality being varied from 0 to 35% and the mass flow rate being varied from 15 to 35 grams per second. The geometric parameters that were considered were the entrance length and the uniform protrusion of the microchannels into the manifold. Two different entrance lengths were used the short, located 50mm from the microchannel array and the long, 250mm from the array.

The liquid distribution results showed some very clear trends with respect to the influence of the various parameters used in testing. The first and most marginal, with respect to improvement in liquid distribution uniformity, of these trends is how the distribution changes with changing inlet quality. When the inlet quality was increased slight gains toward uniformity were seen; but for the cases in which the last tanks received no liquid flow at lower inlet qualities, increasing the quality usually did not provide enough improvement in distribution for the last tanks to receive flow. The next trend to note is that as the inlet mass flux increases, the uniformity of the liquid distribution generally improves. This trend, while it occurs in the cases in which the flow enters through the inlet port closer to the array seems to be more pronounced, and thus more beneficial in terms of more uniform distribution, when the flow enters from the port further from the array. The most noticeably effective means of improving distribution uniformity was by increasing the depth of the microchannel protrusion, or in other words decreasing the area of the manifold. Again, this effect was more noticeable in the cases in which the flow was expanded further from the microchannel array, suggesting that the development of the flow in this length somehow plays an integral role in distribution as well.

With all of these trends in mind a reduction of the parameters of microchannel protrusion and inlet mass flux into one value was performed by considering the area change presented by the microchannel protrusion as an effective change in the total mass flux of the fluid before distribution to the microchannels begins. Comparing this so-called effective mass flux to distribution results in the form of a CV value showed that indeed the two separate trends collapsed somewhat into the general trend of improving uniformity in liquid distribution with increases in the effective mass flux, for both the long and short inlet cases over the entirety of inlet qualities tested. This led to a further scaling of the effective mass flux by the inlet vapor quality to see how the liquid distribution behaved when all of the inlet conditions and the microchannel protrusion depth were considered simultaneously. When the results of this reduction were compared to the corresponding distribution results it was seen that as this value was increased the liquid distribution within the manifold became more uniform in an obvious manner. For the short inlet case the uniformity improved smoothly, while for the long entrance case there was a somewhat stepwise improvement in uniformity based upon microchannel protrusion depth.

The trends observed in this study lead to a few general statements important to the distribution of liquid in a microchannel manifold distributing two-phase R-134a. First, and not necessarily that surprising, expanding the fluid closer to the manifold leads to more a uniformly distributed liquid phase than when the flow is expanded further from the manifold. Next, increases in inlet mass flow rates and inlet qualities also provide a modest amount of improvement in distribution uniformity. This is also not that surprising due to that fact that increasing both the quality and the mass flow rate increases the energy of the flow allowing it to be carried further down the length of the manifold to the microchannels that under less energetic conditions see little or no liquid flow. The most noticeable improvement was made by increasing the depth of the microchannel protrusion. As the microchannels protrude further into the flow the uniformity of the liquid distribution improves for both entrance cases, with the largest protrusion depths producing the most uniform liquid distribution. For the short cases this was essentially the same effect as decreasing the area of the manifold. However, for the long entrance the uniformity was improved more than when just the area of the manifold was decreased, suggesting that the microchannels actually act in a way that counteracts the phase separation that occurs over the longer distance.

Chapter 4. R134a Liquid Distribution Results for Circular Manifold

4. 1. Data Matrix

The dynamic parameters varied for the cases involving the circular manifold were the same as the ones for the rectangular manifold. That is, the inlet quality and mass flow rate ranges were exactly the same for both cases. However, the geometrical parameters were obviously different. This geometrical difference led to a difference in flow field area, inlet mass flux, microchannel protrusion schemes, and length from the inlet port. Five different protrusion schemes were used for testing with the circular manifold. The three uniform microchannel protrusion schemes examined are presented in Figure 4-1 and given nominal designations of “Quarter Depth”, “Half Depth”, and “Three Quarter Depth”. While the two staggered arrangements tested are presented in Figure 4-2, and given designations of “stagger up” and “stagger down”. The depths for these staggered schemes vary from “quarter depth” to “three quarter depth”, and from “three quarter depth” to “quarter depth” respectively. The two lengths between the inlet port and the microchannel array are presented in Figure 4-3 and are 65mm and 250mm respectively. All of these parameters, along with the limitations of the system led to a 310 possible test cases for the circular manifold; however only 306 were tested. Table 4-1 shows all of the test cases performed using the cylindrical manifold. All liquid distribution results for the circular manifold are presented in graphical form for all test cases in Appendix C.

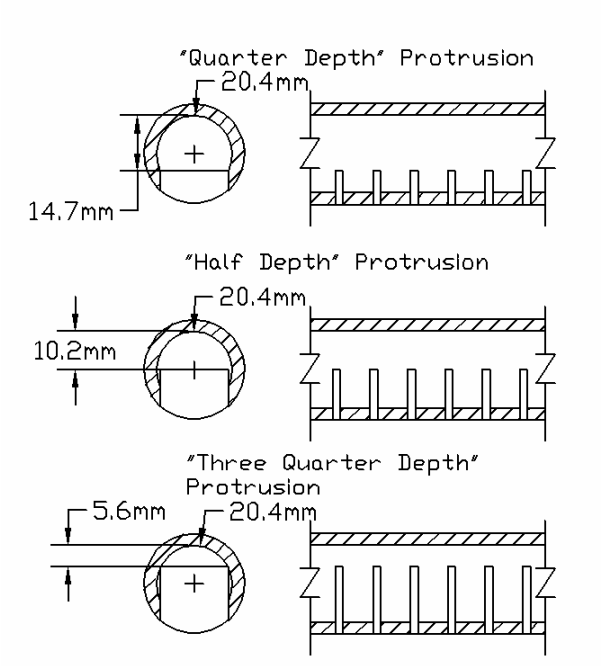

Figure 4-1: Uniform Microchannel Protrusion Depths for Circular Manifold

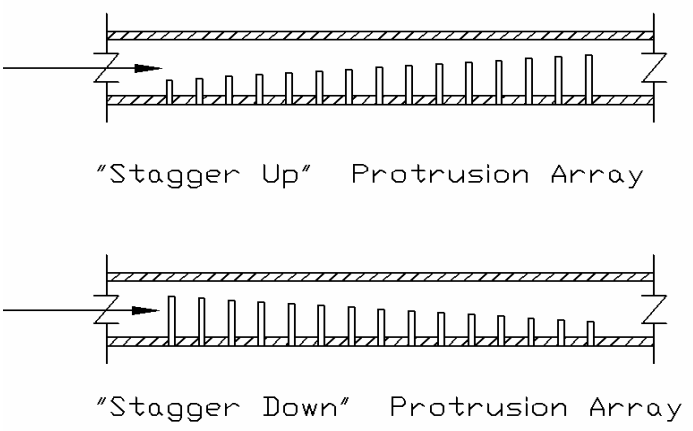

Figure 4-2: Staggered Microchannel Protrusion Depths for Cylindrical Manifold

Table 4-1: Test Cases for Cylindrical Manifold

1/4 Depth Protrusion				1/2 Depth Protrusion				3/4 Depth Protrusion				Stagger Up Protrusion				Stagger Down Protrusion			
Short		Long		Short		Long		Short		Long		Short		Long		Short		Long	
m (g/s)	x (%)	m (g/s)	x (%)	m (g/s)	x (%)	m (g/s)	x (%)	m (g/s)	x (%)	m (g/s)	x (%)	m (g/s)	x (%)	m (g/s)	x (%)	m (g/s)	x (%)	m (g/s)	x (%)
15	0	15	0	15	0	15	0	15	0	15	0	15	0	15	0	15	0	15	0
15	10	15	10	15	10	15	10	15	10	15	10	15	10	15	10	15	10	15	10
15	15	15	15	15	15	15	15	15	15	15	15	15	15	15	15	15	15	15	15
15	20	15	20	15	20	15	20	15	20	15	20	15	20	15	20	15	20	15	20
15	25	15	25	15	25	15	25	15	25	15	25	15	25	15	25	15	25	15	25
15	30	15	30	15	30	15	30	15	30	15	30	15	30	15	30	15	30	15	30
15	35	15	35	15	35	15	35	15	35	15	35	15	35	15	35	15	35	15	35
20	0	20	0	20	0	20	0	20	0	20	0	20	0	20	0	20	0	20	0
20	10	20	10	20	10	20	10	20	10	20	10	20	10	20	10	20	10	20	10
20	15	20	15	20	15	20	15	20	15	20	15	20	15	20	15	20	15	20	15
20	20	20	20	20	20	20	20	20	20	20	20	20	20	20	20	20	20	20	20
20	25	20	25	20	25	20	25	20	25	20	25	20	25	20	25	20	25	20	25
20	30	20	30	20	30	20	30	20	30	20	30	20	30	20	30	20	30	20	30
20	35	20	35	20	35	20	35	20	35	20	35	20	35	20	35	20	35	20	35
25	0	25	0	25	0	25	0	25	0	25	0	25	0	25	0	25	0	25	0
25	10	25	10	25	10	25	10	25	10	25	10	25	10	25	10	25	10	25	10
25	15	25	15	25	15	25	15	25	15	25	15	25	15	25	15	25	15	25	15
25	20	25	20	25	20	25	20	25	20	25	20	25	20	25	20	25	20	25	20
25	25	25	25	25	25	25	25	25	25	25	25	25	25	25	25	25	25	25	25
25	30	25	30	25	30	25	30	25	30	25	30	25	30	25	30	25	30	25	30
25	35	25	35	25	35	25	35	25	35			25	35	25	35	25	35	25	35
30	0	30	0	30	0	30	0	30	0	30	0	30	0	30	0	30	0	30	0
30	10	30	10	30	10	30	10	30	10	30	10	30	10	30	10	30	10	30	10
30	15	30	15	30	15	30	15	30	15	30	15	30	15	30	15	30	15	30	15
30	20	30	20	30	20	30	20	30	20	30	20	30	20	30	20	30	20	30	20
30	25	30	25	30	25	30	25	30	25	30	25	30	25	30	25	30	25	30	25
35	0	35	0	35	0	35	0	35	0	35	0	35	0	35	0	35	0	35	0
35	10	35	10	35	10	35	10	35	10	35	10	35	10	35	10	35	10	35	10
35	15	35	15	35	15	35	15	35	15	35	15	35	15			35	15	35	15
35	20	35	20	35	20	35	20	35	20	35	20	35	20	35	20	35	20	35	20
35	25			35	25	35	25	35	25			35	25	35	25	35	25	35	25

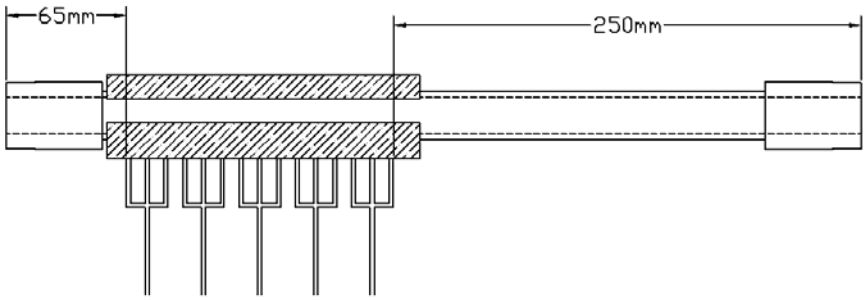

Figure 4-3: Lengths from Inlet Port to Microchannel Array

4. 2. Quarter Depth Protrusion

This section will discuss the set of experiments performed with the microchannels protruded into the circular manifold only enough to create a seal. As seen in Figure 4-1 this protrusion depth is 14.7mm or nominally one quarter of the flow field depth. As with the rectangular manifold, the liquid distribution trends are presented against varying inlet mass flux and quality. Again, there is a noticeable difference between the results for the experiments done with the short entrance length and the long entrance length. Thus, the discussion will once again be divided into the short entrance length results and the long entrance length results.

4. 2. 1. Short Entrance Results

The following test cases were performed with the refrigerant entering the port located 65mm from the microchannel array. The flow was from left to right within the manifold. Figure 4-4 illustrates the effect of varying inlet quality for a given inlet mass flux on liquid distribution. This figure shows that varying the inlet quality has little effect in improving the liquid distribution. It should be noted however, that the liquid distribution for these test cases presents relatively uniform liquid distribution, when compared to similar cases for the rectangular manifold data. Figure 4-5 illustrates the effect of varying the inlet mass flux for a given inlet quality on liquid distribution. Again, it is easily seen from Figure 4-5 that varying the inlet mass flux for a given quality has little effect on the liquid distribution within the manifold. The following general trend holds for both Figures 4-4 and 4-5; that the first tank has a slightly smaller liquid flow rate, while the liquid flow rate in the last four tanks stays fairly constant and uniform even with the varying parameters. While these cases do not represent perfectly uniform liquid distribution, they are very close.

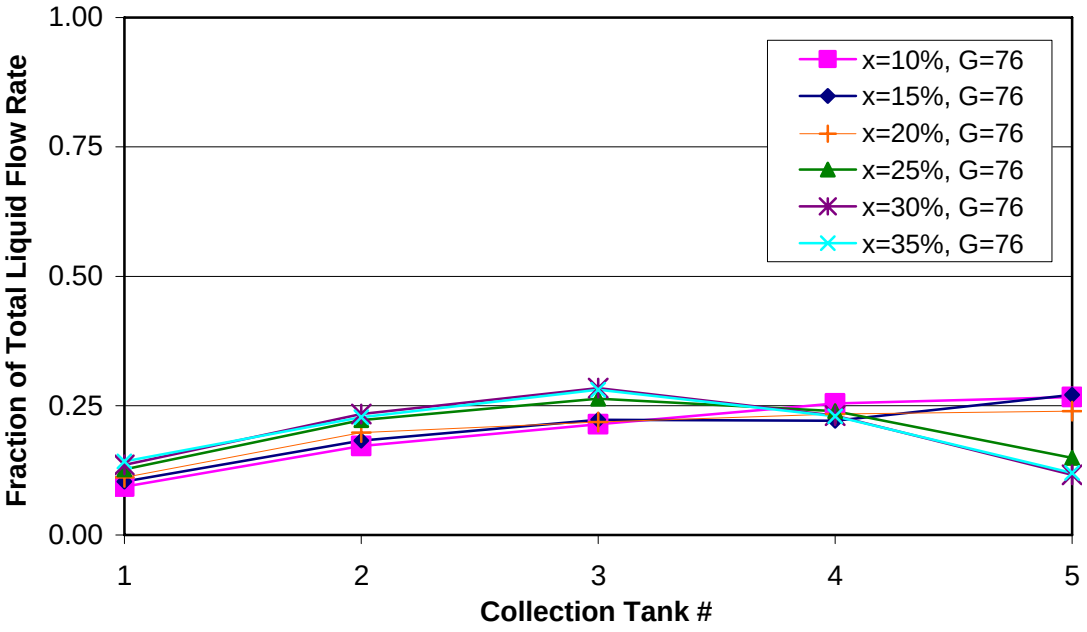

Figure 4-4: Inlet Quality Effect. Quarter Depth Protrusion, Short Entrance

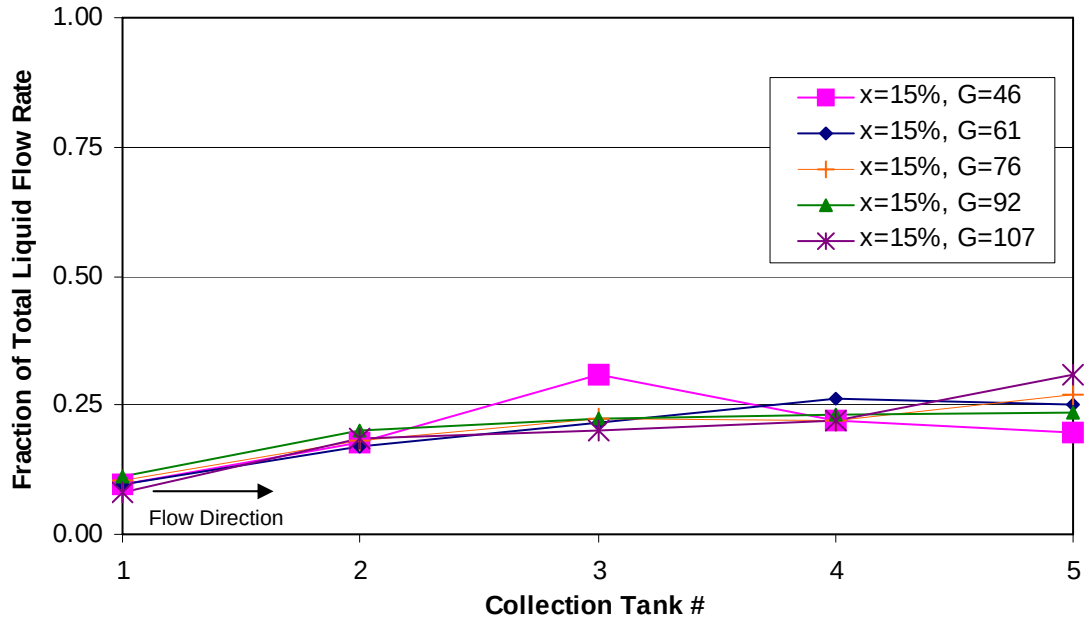

Figure 4-5: Inlet Mass Flux Effect, Quarter Depth Protrusion, Short Entrance

4. 2. 2. Long Entrance Results

The following results are from the test cases in which the flow entered through 250mm inlet length with the microchannel array protruded to the one quarter depth specification. Again, the flow direction is from left to right within the manifold. For the long entrance case a significantly more maldistributed flow is seen than that which

was seen when the flow entered from the inlet port closest to the array. For these test conditions the first two collection tanks see the majority of the liquid flow while the third, fourth, and fifth collection tank see little or no liquid flow. Figure 4-6 illustrates the effect that varying inlet quality, for a given inlet mass flux, has on liquid distribution within the manifold. This figure shows that there is no significant improvement in liquid distribution with increasing inlet quality. Figure 4-7 illustrates the effects of varying inlet mass flux for a given inlet quality. Unlike Figure 4-6, Figure 4-7 shows that increasing the inlet mass flux parameter yields a noticeable improvement, with respect to uniformity, in liquid distribution within the manifold, although the last two collection tanks see little or no liquid flow for this particular case. It should be noted that while steps toward uniformity can be made by increasing the inlet mass flux, all of the cases for this particular geometric configuration have a rather high degree of non-uniformity in liquid flow distribution.

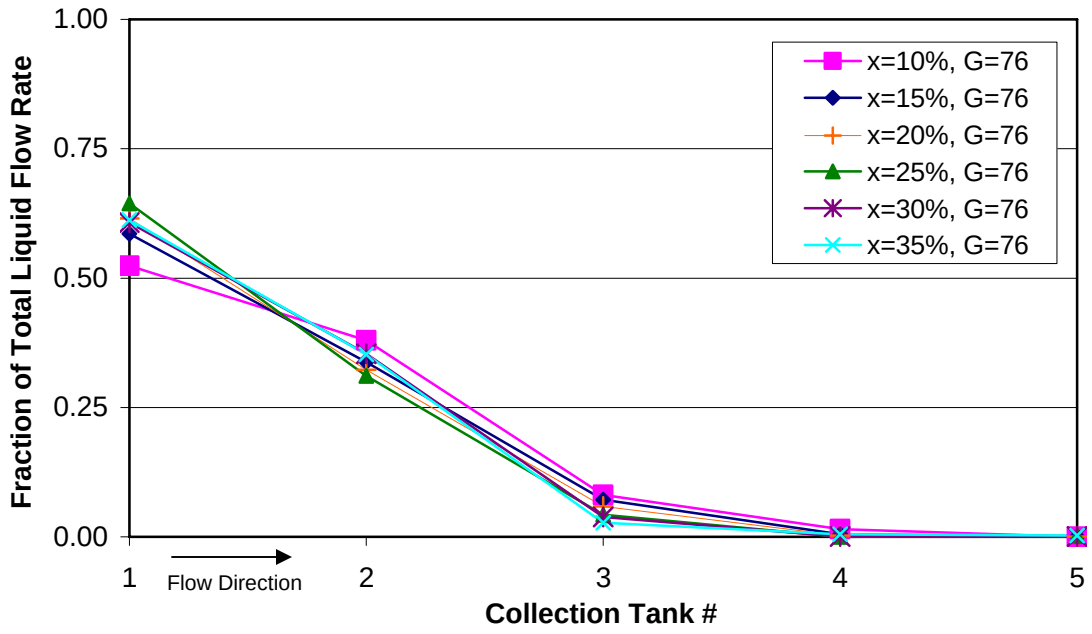

Figure 4-6: Inlet Quality Effect, “Quarter Depth” Protrusion, Long Entrance

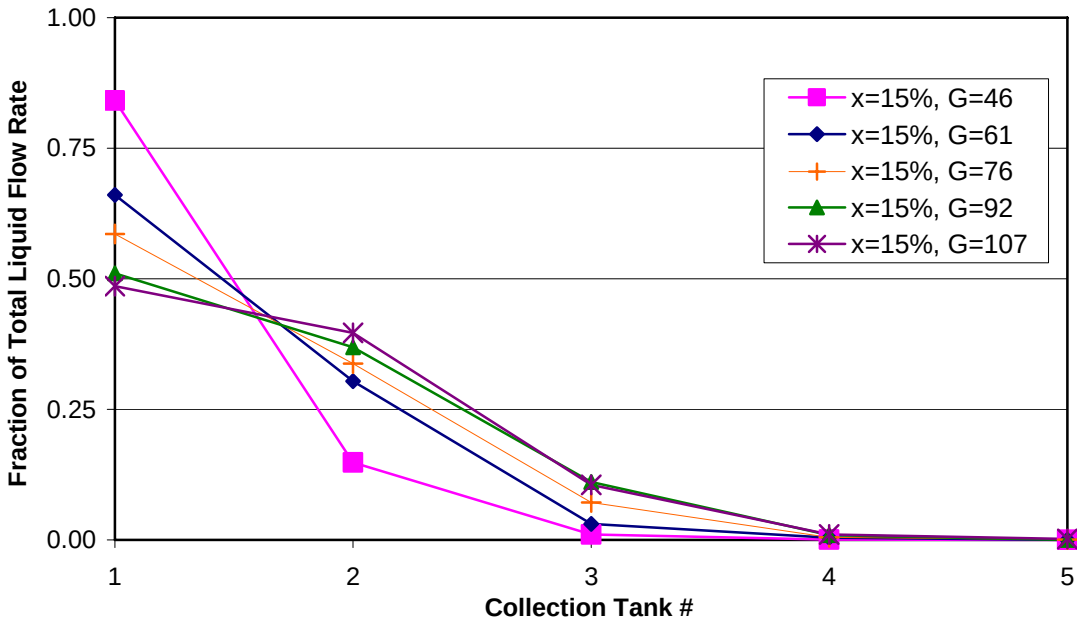

Figure 4-7: Inlet Mass Flux Effect, "Quarter Depth" Protrusion, Long Entrance

4. 3. Half Depth Protrusion

The discussion of this section focuses on the test cases for which the microchannels are protruded to half of the diameter of the manifold or 10.2mm (.40"). Results for both the short and long entrance conditions with this protrusion scheme will be discussed separately.

4. 3. 1. Short Entrance Results

The following cases represent the results for the cases in which the microchannel array is protruded uniformly to half of the manifold diameter with the flow entering from the shorter inlet port. Figures 4-8 and 4-9 illustrate the trends observed for these cases in the same manner as previous results have been illustrated. Figure 4-8 shows that increasing inlet quality, for a given inlet mass flux, slightly improves the uniformity of liquid flow distribution. Although not shown in this figure, it was seen (and can be seen from figures in Appendix C) that as the inlet quality increases this effect becomes less pronounced. Figure 4-9 shows that increasing inlet mass flux for a given inlet quality has an almost negligible effect on liquid flow distribution. These trends hold true for all the data pertaining to the half depth, short entrance cases. The whole set of data presented in graphical form can be found in Appendix C.

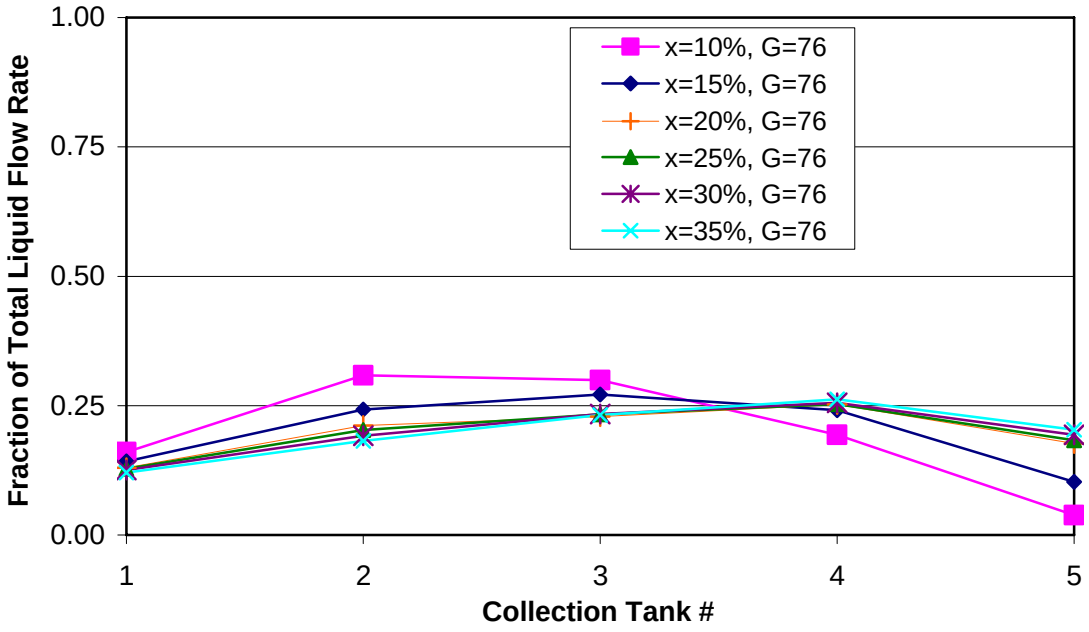

Figure 4-8: Inlet Quality Effect, Half Depth Protrusion, Short Entrance

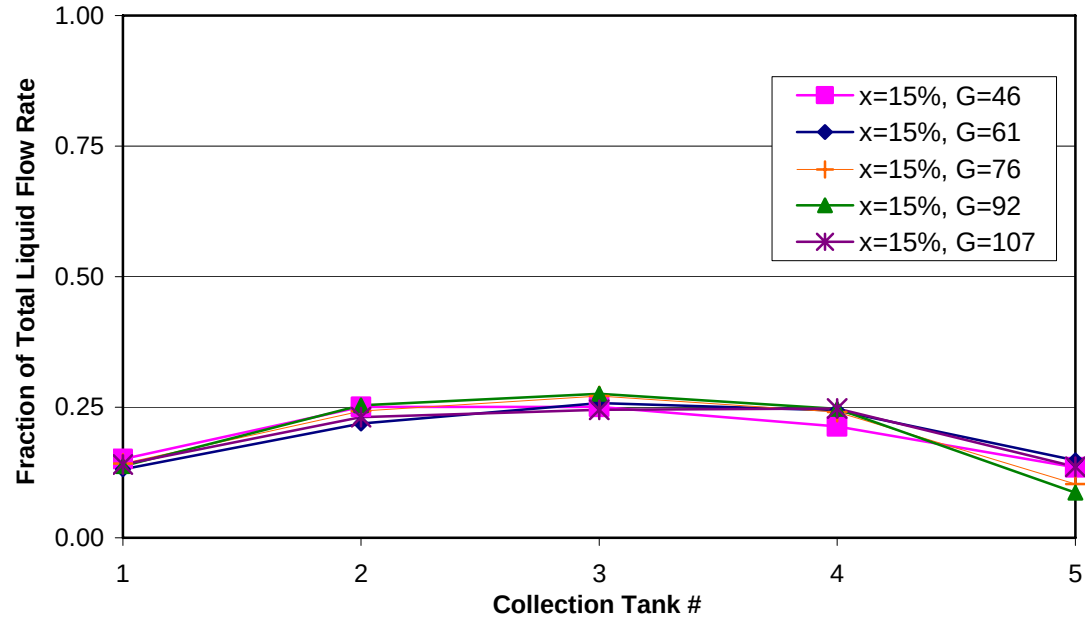

Figure 4-9: Inlet Mass Flux Effect, Half Depth Protrusion, Short Entrance

4. 3. 2. Long Entrance Results

The results presented below are from the test cases in which the two-phase refrigerant entered through the inlet port located 250mm from the microchannel array, with the array protruded uniformly to half of the flow field diameter. The flow direction within the manifold is from left to right. Again, the liquid flow distribution is much

more maldistributed for the test cases using the longer entrance length with this microchannel protrusion scheme, than the cases with fluid entering through the short entrance length. For all of these cases the first three collection tanks see the majority of the flow with the last two tanks seeing little or no liquid refrigerant flow. Figure 4-10 illustrates the effects of varying inlet quality while holding the inlet mass flux constant. It is easily seen from Figure 4-10 that changing the inlet quality has very little effect on the liquid flow distribution. While Figure 4-10 only shows the effect of inlet quality for one inlet mass flux, the trend can be seen to be consistent for every other inlet mass flux tested in Figures C, in Appendix C. Figure 4-11 illustrates the effect of varying the inlet mass flux while holding the inlet quality constant. Again, a dramatic change in liquid flow distribution is seen with increasing inlet mass flux. While this change moves the liquid distribution toward uniformity, the last microchannels still see little or no liquid flow.

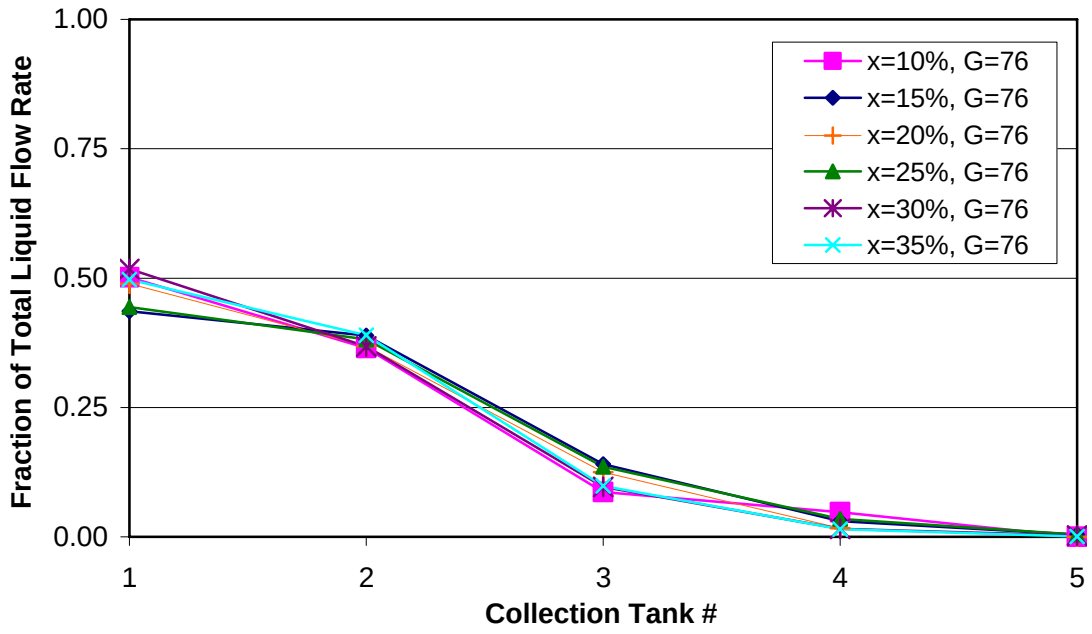

Figure 4-10: Inlet Quality Effect, Half Depth Protrusion, Long Entrance

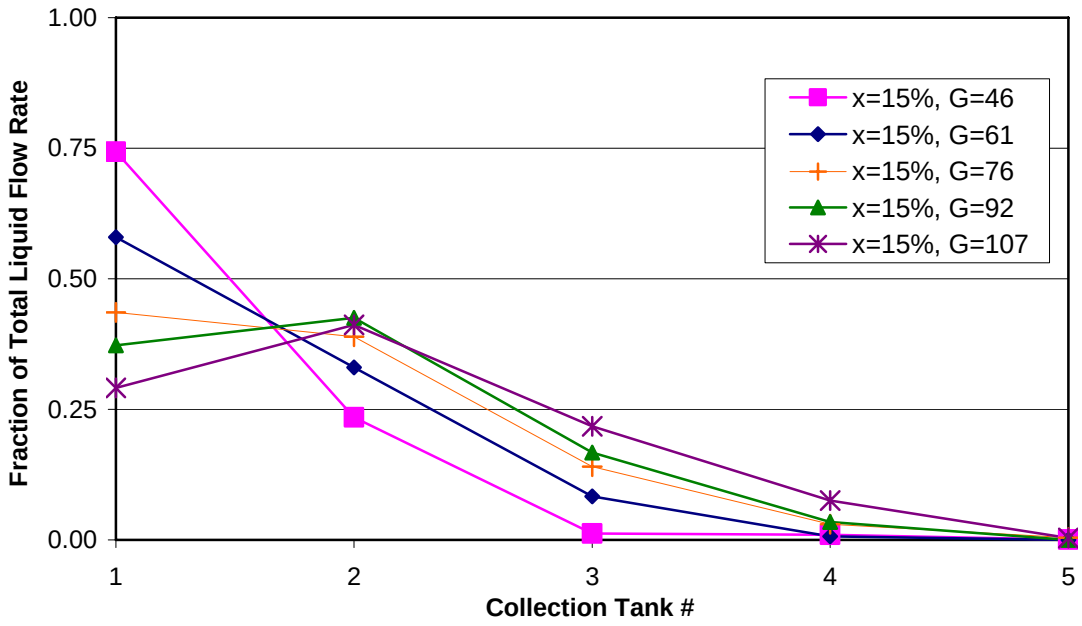

Figure 4-11: Inlet Mass Flux Effect, Half Depth Protrusion, Long Entrance

4. 4. Three Quarter Depth Protrusion

The following discussion will focus on the results from the conditions in which the microchannel array was protruded uniformly as far as possible into the microchannel manifold. In other words, the microchannels were inserted until they actually butted up against the top of the manifold. This was very close to three-quarters of the inner diameter of the manifold and will be referred to as the "three-quarter depth" protrusion scheme.

4. 4. 1. Short Entrance Results

The following discussion will focus on the results for the cases in which the fluid entered the manifold from the entrance 65mm from the microchannel array. The graphs presented in Figures 4-12 and 4-13 serve to illustrate the general trends observed in these test cases. Figure 4-12 shows the effect of changing inlet quality on liquid flow distribution, for a given inlet mass flux. There is some change in liquid flow distribution seen with changing quality, but the general trend of the distribution remains the same. That is, the middle three tanks see a similar amount of liquid flow, while the first and last tanks see flows that are slightly less than those seen in the middle three tanks. Figure 4-13 illustrates the same kind of trend being seen when inlet quality is held constant. By combining the trends seen in Figures 4-12 and 4-13, it can be seen that, for a wide variety of inlet flow conditions, the liquid flow stays relatively uniformly distributed throughout the manifold.

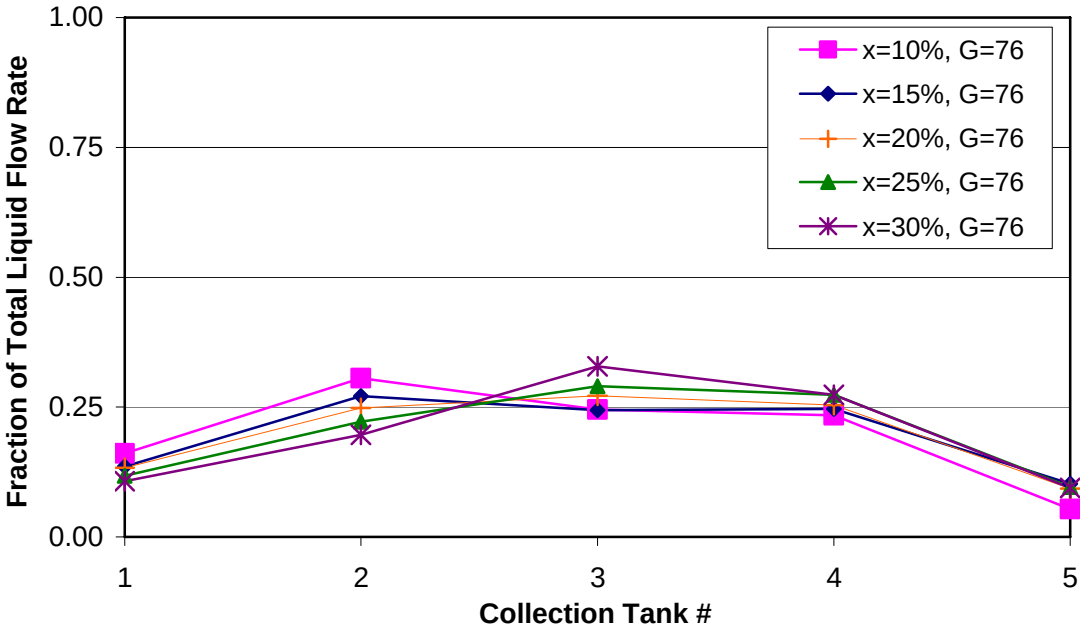

Figure 4-12: Inlet Quality Effect, Three-Quarter Depth Protrusion, Short Entrance

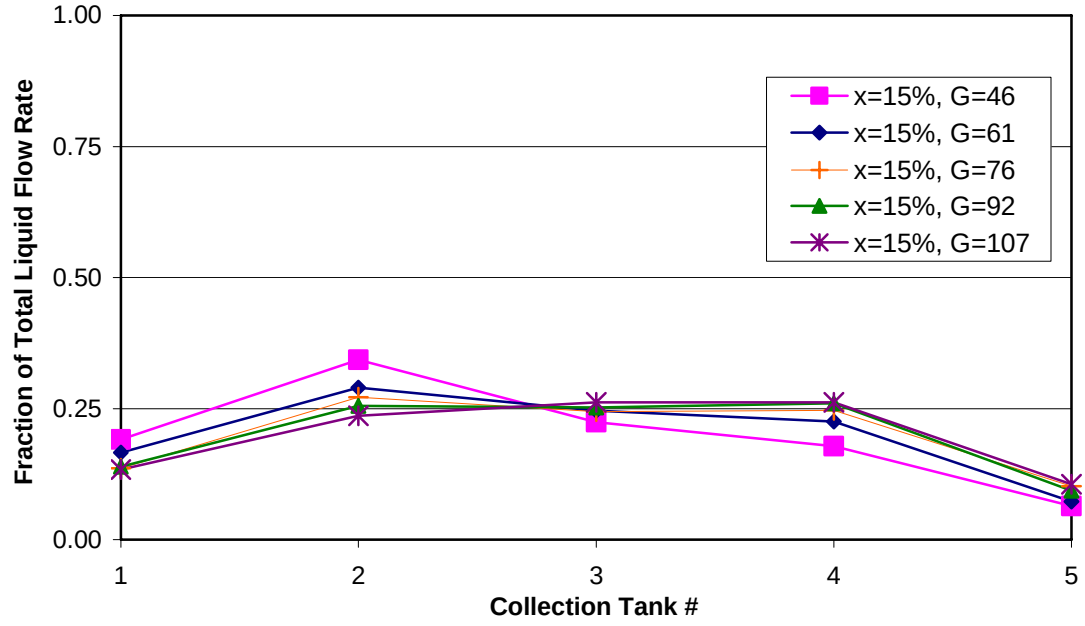

Figure 4-13: Inlet Mass Flux Effect, Three-Quarter Depth Protrusion, Short Entrance

4. 4. 2. Long Entrance Results

Here, the results of the test cases in which the microchannel array is uniformly protruded to the "three quarter" protrusion depth, and the fluid enters through the entrance 250mm from the microchannel array will be discussed. Again, representative data is shown in graphical form to show trends regarding the effects of changing

inlet conditions. Figure 4-14 illustrates the effect of changing inlet quality for a constant inlet mass flux; while Figure 4-15 illustrates the effect of changes in inlet mass flux, for a given inlet quality. These both show a drastic departure from the same dynamic inlet conditions with the "half depth" protrusion scheme (compare Figure 4-10 with Figure 4-14). Figures 4-14 and 4-15 both show a liquid flow distribution that, while not completely uniform, is much more uniform than any of the cases in which the fluid entered through the longer entrance seen thus far. This seems to support an idea hinted at several times in earlier discussions. That is, that a separated flow (a result of the longer entrance) that can somehow be "disturbed" or re-homogenized will be more uniformly distributed, at least in the liquid phase, than one that remains developed and separated. As stated in the earlier discussion, this idea will be explored more fully, in a later discussion focusing on flow visualization experiments carried out in conjuction with the distribution experiments.

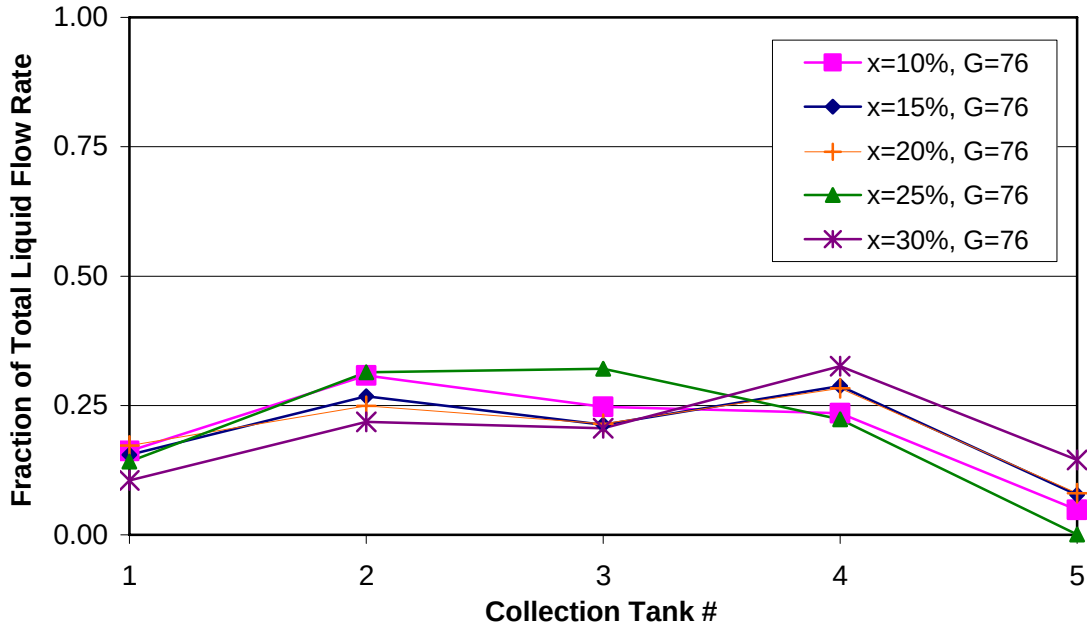

Figure 4-14: Inlet Quality Effect, Three-Quarter Depth Protrusion, Long Entrance

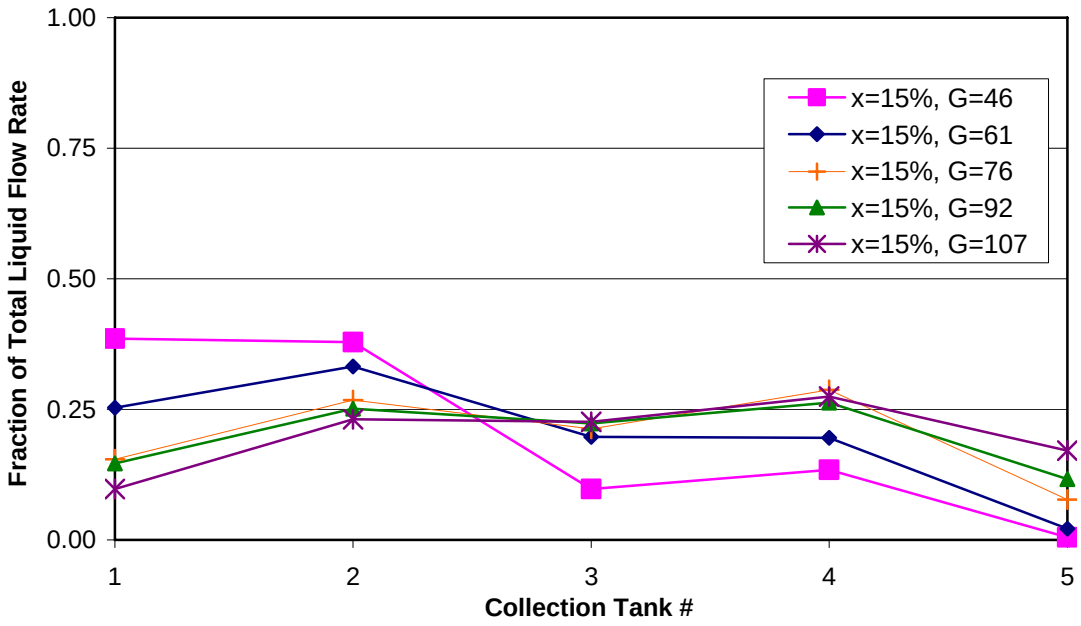

Figure 4-15: Inlet Mass Flux Effect, Three-Quarter Depth Protrusion, Long Entrance

4. 5. Stagger Up Protrusion

To see if staggering the protrusion depth of the microchannel array had any significant effect on distribution, experiments were carried out in which the microchannel protrusion depth was staggered from the minimum depth required to seal to the three-quarter depth and vice versa. The former has been designated as the stagger up protrusion scheme, while the later has been designated as the stagger down protrusion scheme. The following discussion will focus on the condition in which the microchannels were staggered up; again, focusing separately on the two different entrance length conditions.

4. 5. 1. Short Entrance Results

Figures 4-16 and 4-17 illustrate the liquid flow distribution trends that are seen when the fluid enters through the inlet closest to the microchannel array and the inlet quality and inlet mass flux are changed respectively. Both of these figures show that distribution is nearly impervious to changes in inlet quality or mass flux. For any of the given inlet conditions the first four tanks receive nearly the same amount of liquid flow with the flow rate in the fifth trailing off. As can be seen from these figures, liquid flow is very uniform, when compared to earlier results, over a wide range of inlet conditions. While these figures only represent a fraction of the data obtained for this particle microchannel protrusion scheme and entrance length, the rest of the results are very similar, as can be seen in Appendix C.

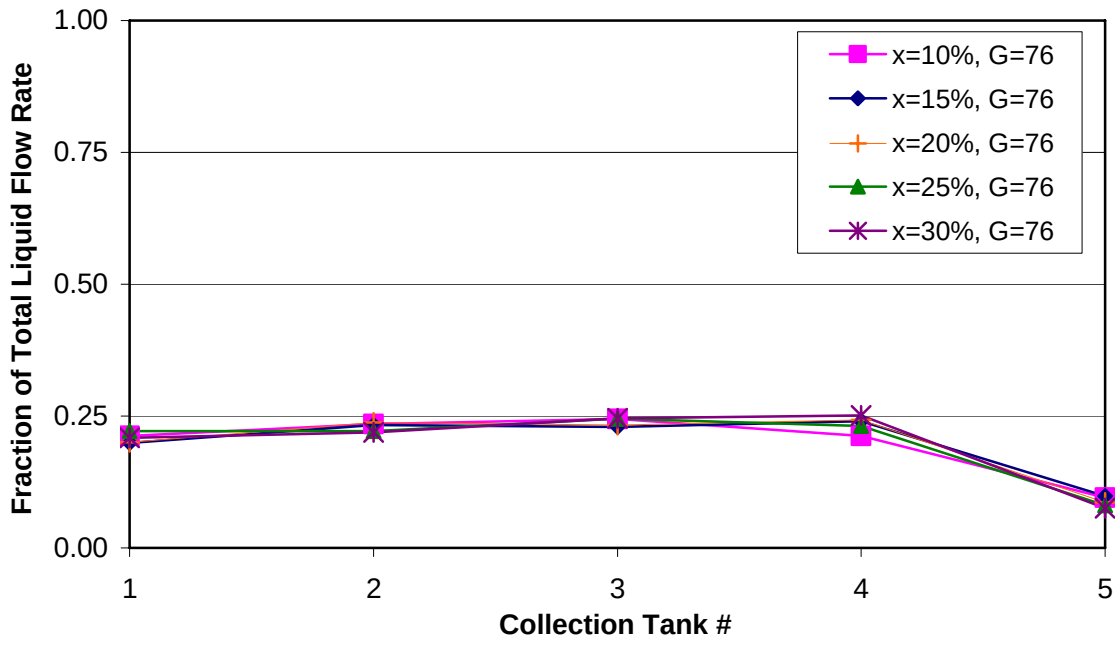

Figure 4-16: Inlet Quality Effect, Stagger Up Protrusion, Short Entrance

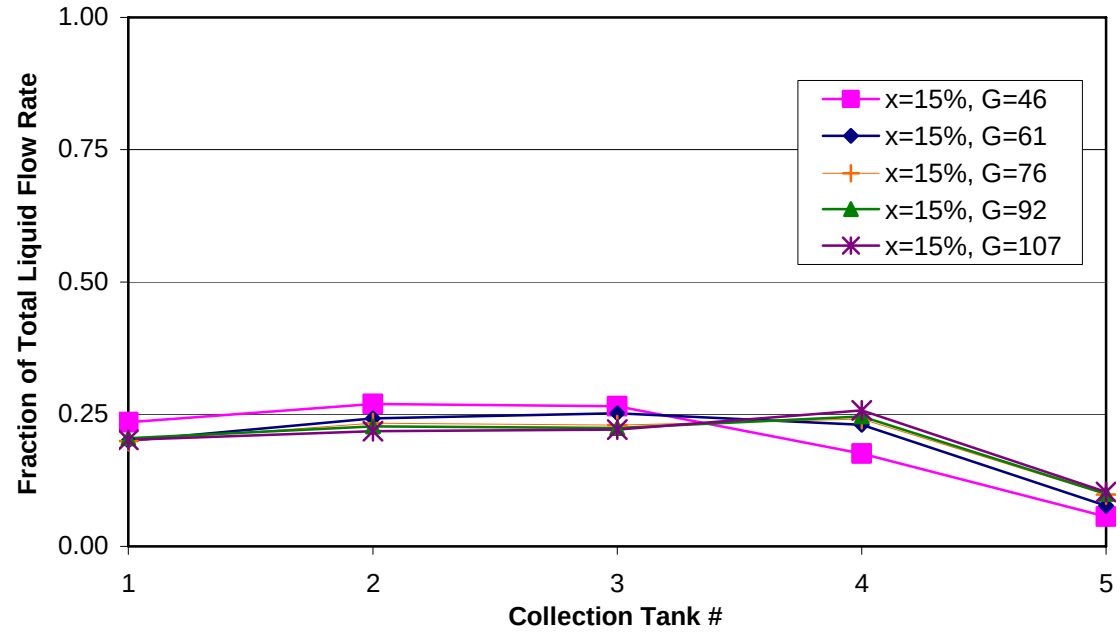

Figure 4-17: Inlet Mass Flux Effect, Stagger Up Protrusion, Short Entrance

4. 5. 2. Long Entrance Results

Figures 4-18 and 4-19 show representative results for the long entrance cases in which the micro- channel protrusion depth was staggered up. Figure 4-18 shows the effect of increasing inlet quality while holding inlet mass flux constant. It can be seen from this figure that, with the exception of an inlet quality of 20%, changing the inlet

quality has little effect on the distribution of the liquid flow. The first two collection tanks receive most of the liquid flow, with the third trailing off and the fourth and fifth being at or near dry out conditions. The case with an inlet quality of 20% proved to be drastically different, for unknown reasons. Figure 4-19 shows the effect of changing inlet mass flux while holding inlet quality constant. Again, there seems to be little difference between the conditions, with exception of the lowest inlet mass flux. It seems that once the inlet mass flux is increased to more than the lowest value there is little or no more effect of increasing inlet mass flux on liquid flow distribution. This general trend holds for all inlet qualities, as can be seen by the graphs in Appendix C.

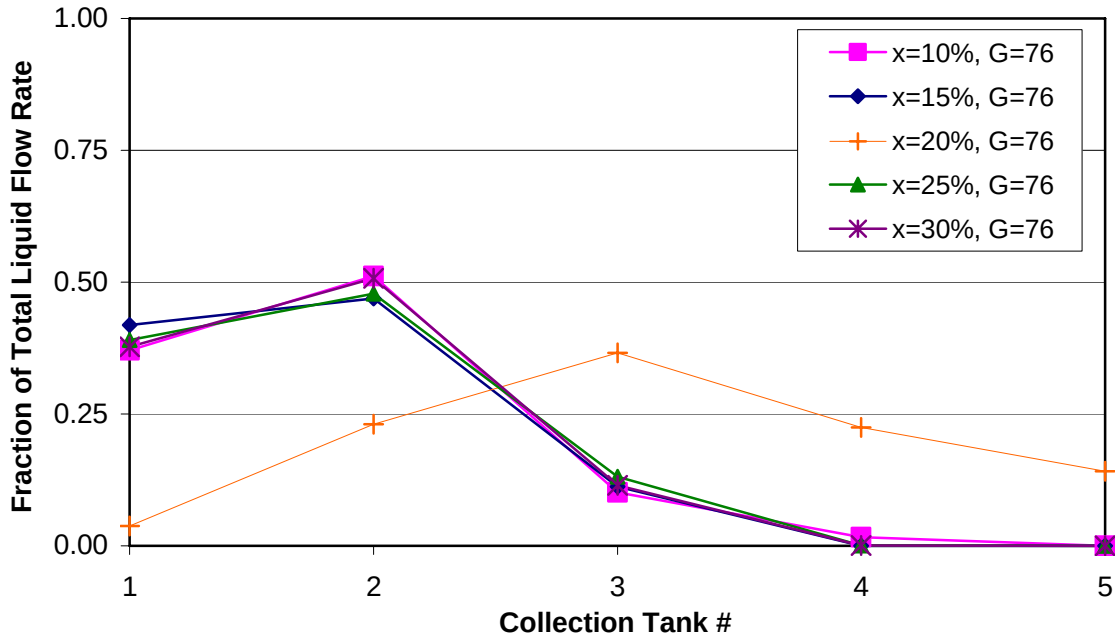

Figure 4-18: Inlet Quality Effect, Stagger Up Protrusion, Long Entrance

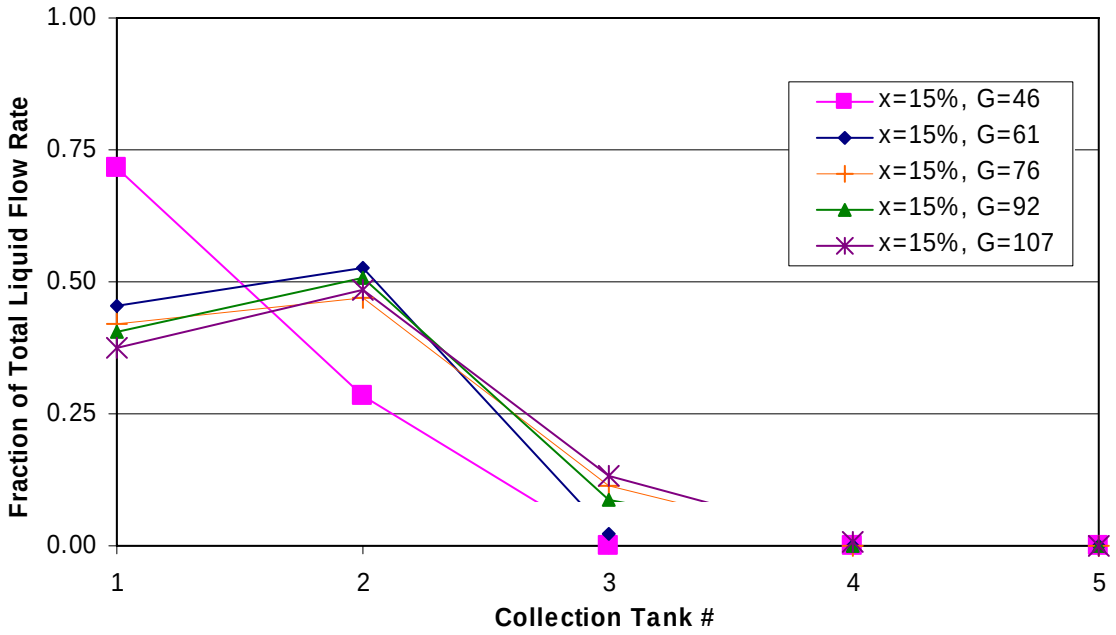

Figure 4-19: Inlet Mass Flux Effect, Stagger Up Protrusion, Long Entrance

4. 6. Stagger Down Protrusion

The above discussion focused on the case in which the microchannels protrusion scheme was such that the array was staggered up as it progressed through the manifold in the direction of the flow. The following discussion will focus on the opposite cases; that is, with the array protrusion depths staggered downward. As done previously, the two different entrances will be discussed separately.

4. 6. 1. Short Entrance Results

Much like the previous short entrance results the effect of changing inlet parameters such as inlet quality and inlet mass flux is minimal for the cases in which the microchannel protrusion depths are staggered down. These general effects are illustrated in Figures 4-20 and 4-21, and are representative of all the data for this particular protrusion and entrance setup. Figure 4-20 shows that as inlet quality is changed for a given inlet mass flux there is little change to the relatively uniform distribution. While Figure 4-21 shows that increasing inlet mass flux for a given inlet quality slightly improves the uniformity of the distribution. It is worth while to note that, while not perfectly uniform, both of these figures show distribution that is fairly symmetrical. That is, the middle tank receives the most liquid flow while the second and fourth receive slightly less, but nearly the same amount, with this continuing out to the first and fifth tanks.

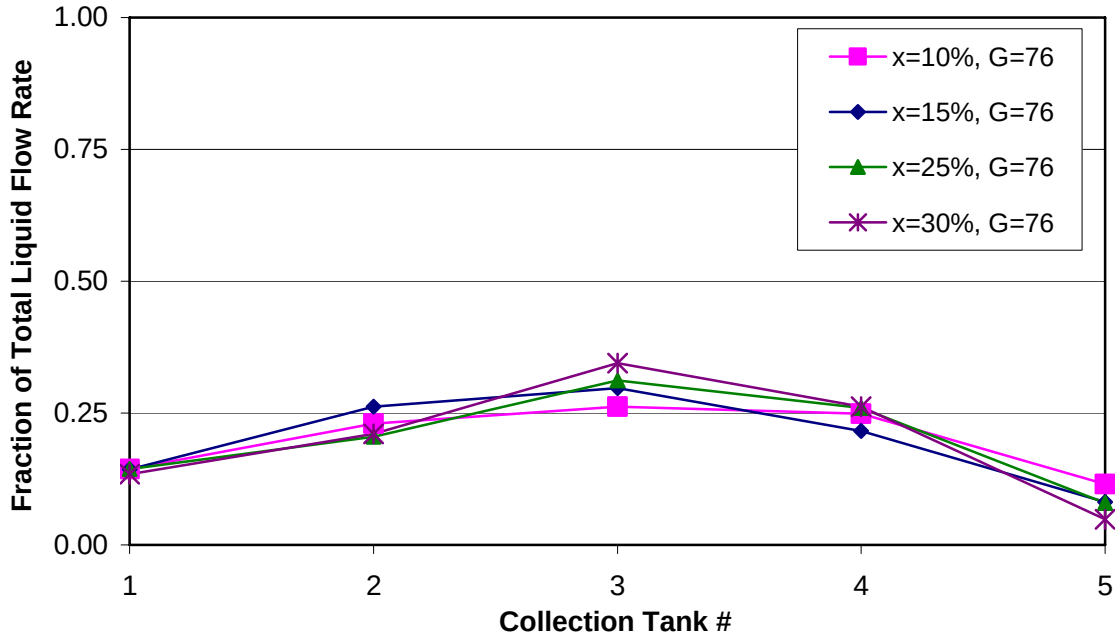

Figure 4-20: Inlet Quality Effect, Stagger Down Protrusion, Short Entrance

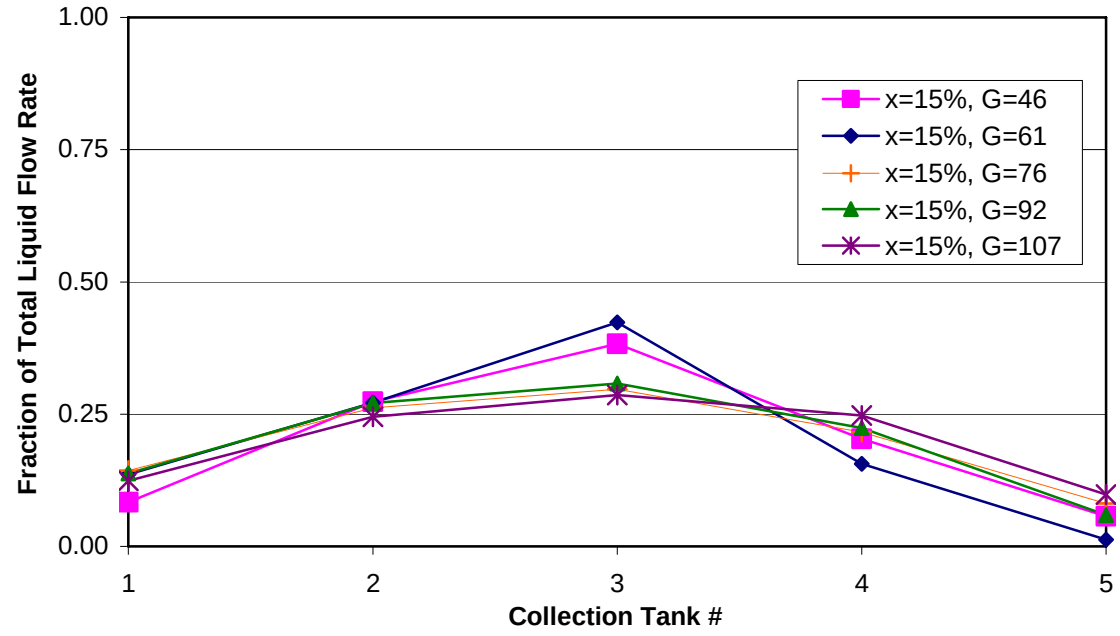

Figure 4-21: Inlet Mass Flux Effect, Stagger Down Protrusion, Short Entrance

4. 6. 2. Long Entrance Results

Figures 4-22 and 4-23 illustrate the results obtained for the cases in which the microchannel protrusions were staggered down and the flow entered through the longer entrance. Figure 4-22 shows that changing the inlet quality for a given inlet mass flux has little effect on the distribution of the flow. It can be seen form Figure 4-23

that increasing the inlet mass flux for a given inlet quality actually provides slight improvements in flow distribution. Both of the trends presented in Figures 4-22 and 4-23 are representative of the rest of the data collected for these cases. The rest of the data is presented in the same graphical form in Appendix C.

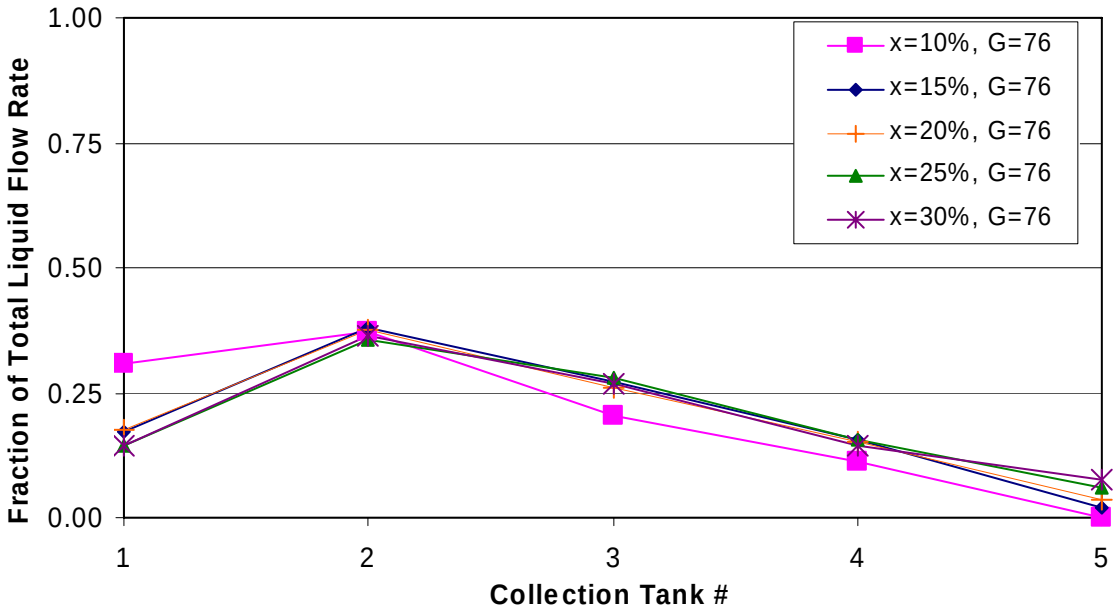

Figure 4-22: Inlet Quality Effect, Stagger Down Protrusion, Long Entrance

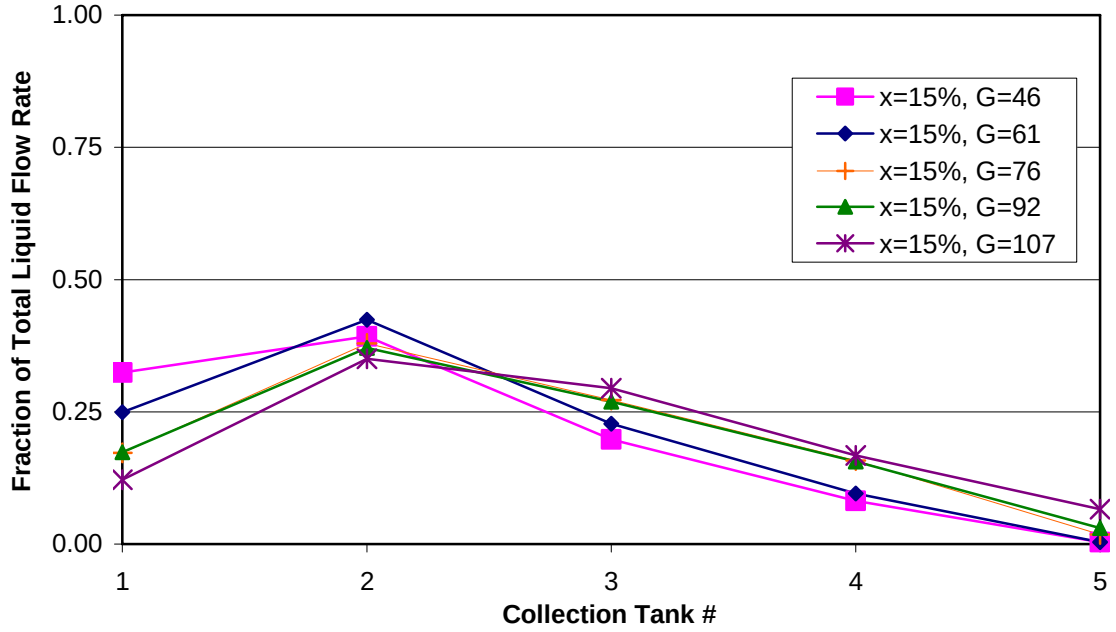

Figure 4-23: Inlet Mass Flux Effect, Stagger Down Protrusion, Long Entrance

4. 7. Effect of Microchannel Protrusion

While the above discussion focused on the effect of changing inlet mass flux and inlet quality for a given protrusion scheme and entrance length, Figures 4-24 and 4-25 illustrate the general effect of microchannel protrusion for a given set of inlet conditions (quality and mass flux). Figure 4-24 shows how little varying the protrusion depth or scheme affects the distribution trends, when the fluid is expanded close to the microchannel array. For all cases, except the one-quarter depth protrusion scheme, the first and the last collection tank receive the least amount of flow while the middle tank receives the most. However, the distribution is relatively uniform, especially when compared to the results for the cases in which the fluid is expanded further from the microchannel array. Figure 4-25 illustrates this; showing how protrusion depth and scheme effects the distribution within the manifold. It can be seen from Figure 4-25, that changing the protrusion depth and scheme has a significant effect on distribution. The 1/4 depth, 1/2 depth, and stagger up protrusion schemes all produce rather maldistributed flow, with the first two tanks receiving most of the flow and flow in the last three tanks trailing off to dry out or near dry out. However, the 3/4 depth and stagger down protrusion schemes have vastly different and much more uniform distribution of the flow. Both Figures 4-24 and 4-25 are illustrative of general trends seen in the results; a presentation of all results in this graphical form can be found in Appendix C.

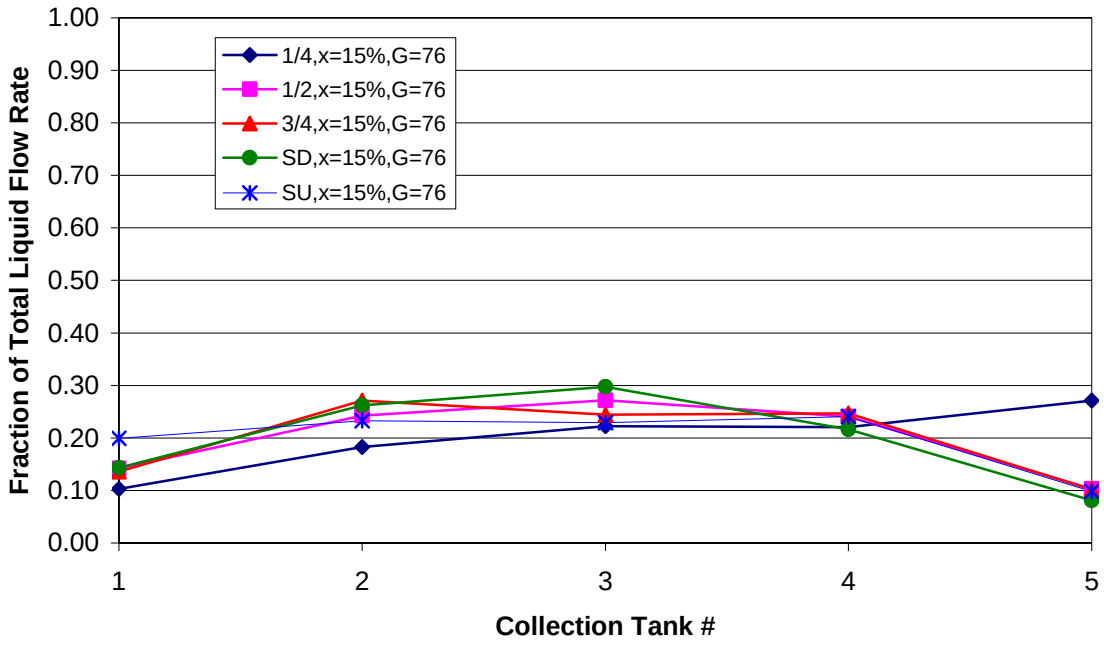

Figure 4-24: Microchannel Protrusion Effects, Short Entrance

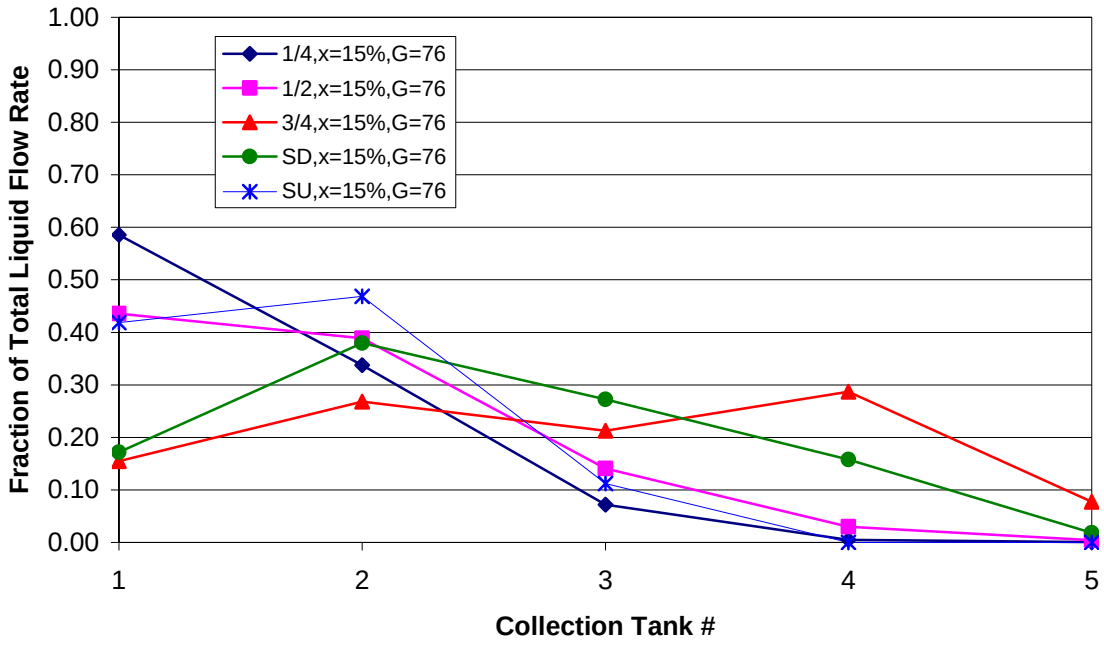

Figure 4-25: Microchannel Protrusion Effects, Long Entrance

4. 8. Reduced Results for Circular Manifold

As with rectangular manifold test cases there are discernable trends visible in the data for the circular manifold. However, it is desirable to condense these results into a more compact and possibly more meaningful form through data reduction. The same parameters that were used in the case of the rectangular manifold will be used in the following discussion for the sake of cohesiveness and to see if similar trends are observed here. The coefficient of variation is again defined in the same manner as it was when applied to the rectangular manifold results (Equations 3-1 through 3-3). The defined method of calculating the effective mass flux is along the same lines as used for the rectangular manifold; however, due to the drastic difference in geometry, a short discussion of this calculation follows.

4. 8. 1. Effective Mass Flux

When the effective mass flux was calculated for the rectangular manifold, the calculation was rather straightforward because only the area above the microchannel was considered (see Figure 3-20). Due to the cross section shape of the circular manifold, the area on the sides of the microchannels also needed to be considered for the calculation of the effective mass flux. The area used for the calculation of the effective mass flux is shown in red in Figure 4-26, the particular case represented in this figure is the microchannel being protruded to one half of the manifold diameter. The area could be determined by performing an integral of the arc cut by the circle on the microchannel over the width of the microchannel; however, for simplicity the area was found by making a drawing of the desired protrusion and cross-section in a CAD program and retrieving the area from the program. Performing these calculations led to an effective mass flux range, for all protrusion depths, of 59-397 (kg/m^2s). It should be noted that for the staggered schemes, both up and down, the effective mass flux was considered to be the effective mass flux that would result if the calculation was performed based upon the protrusion of the first microchannel that

the flow sees. That is, the effective mass flux for the stagger up schemes is the same as that of the one quarter depth uniform protrusion scheme, and the effective mass flux for the stagger down scheme is the same as calculated for the three quarter depth protrusion scheme. This is appropriate because, for all cases, the mass flux begins to change as soon as flow begins to flow into the microchannels, but at the first microchannel, before flowing into it, should be based upon the area that the fluid sees. Figure 4-27 shows how inlet mass flux translates to effective mass flux for the three different uniform protrusions.

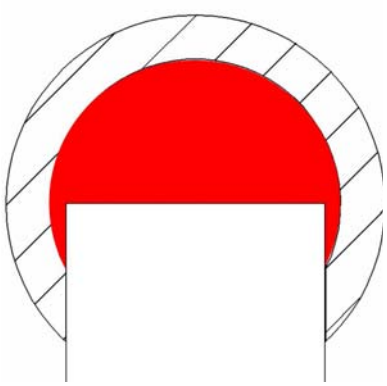

Figure 4-26: Area Used in Calculation of Effective Mass Flux

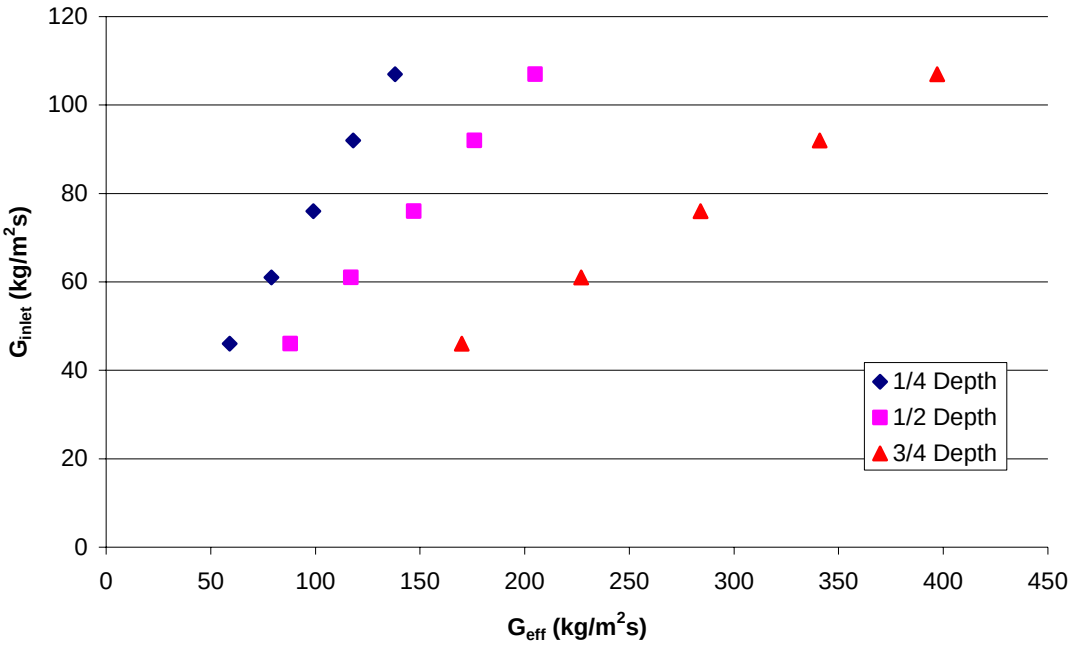

Figure 4-27: Effective Mass Fluxes For Given Inlet Mass Fluxes and Protrusion Schemes

As was done with the rectangular manifold, the measure of the liquid distribution will be quantified in the form of the CV value as define in Chapter 3. For a review of representative results, Figures 4-28 and 4-29 present the effect of increasing the effect mass flux, for a given inlet quality, on liquid flow distribution for the long and short entrances respectively. Figure 4-28 shows that increasing the effective mass flux improves the distribution up to a point, and then the effect on distribution levels off. The most uniform liquid distribution is seen in the case of

the 3/4 quarter dept protrusion. Figure 4-29 shows the same data for the short entrance case. From this figure, it is seen that changing only the distance which the expansion device is located from the microchannels has a drastic effect on the liquid distribution trends. Figure 4-29 shows that changing the effective mass flux within the manifold has very little effect on the liquid flow distribution. While not shown in this figure, this is generally true for all inlet qualities as well (with a very obvious exception at an inlet quality of 0%) as can be seen by the rest of these results presented in Appendix C. The obvious advantage that the short entrance results present over the long, is the ability to have relatively uniform liquid distribution over a wide range of operating conditions (inlet mass flux and quality); while the long entrance case shows a means of improvement of uniformity in liquid distribution for cases in which the fluid cannot be expanded very close to the manifold.

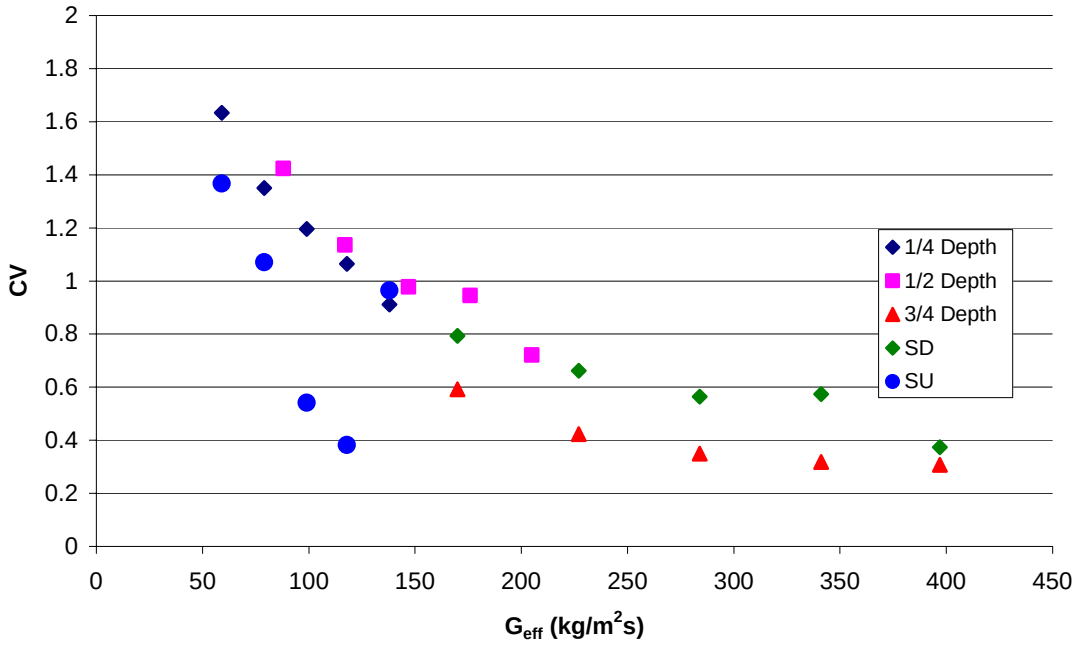

Figure 4-28: Effective Mass Flux Effects, Long Entrance, 20% Inlet Quality

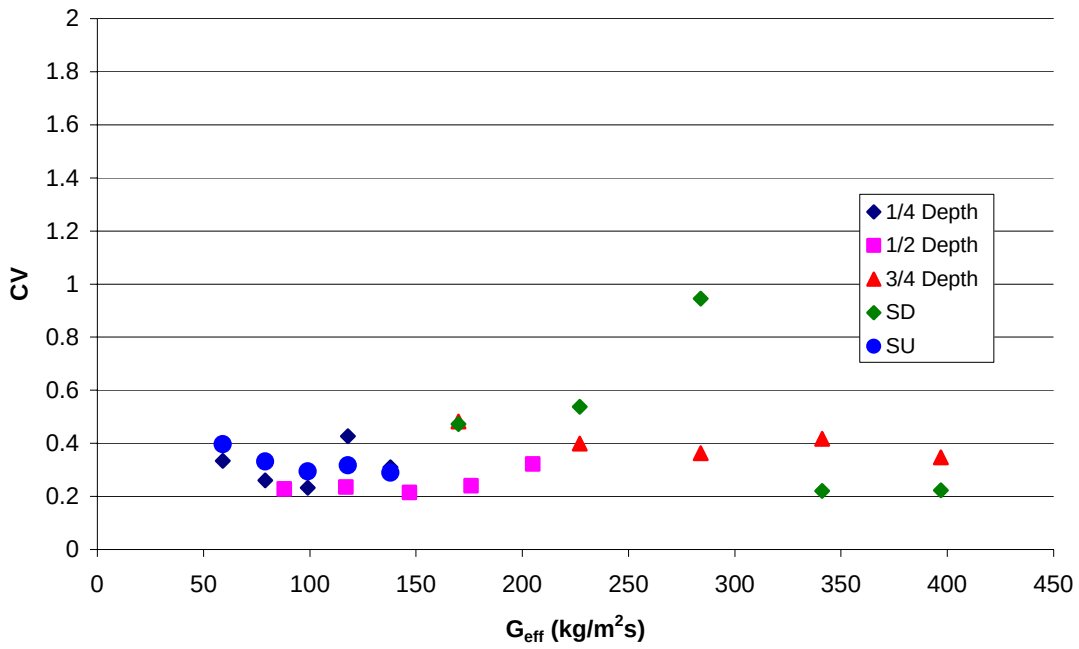

Figure 4-29: Effective Mass Flux Effects, Short Entrance, 20% Inlet Quality

4. 8. 2. Quality Scaled Effective Mass Flux

In discussion of the rectangular manifold results it was seen that scaling the effective mass flux somehow by the inlet quality helped to clarify some of the trends seen in the distribution results. With that in mind, a similar attempt at scaling the effective mass flux of the circular manifold by inlet quality was attempted. For the rectangular manifold, it was shown that when the effective mass flux was scaled by multiplying by the vapor quality, distribution trends became very clear. Mainly, that as the so-called vapor effective mass flux increased, the distribution showed marked improvement for both the long and short inlet cases (see Figures 30-30 and 30-31). Figures 4-30 and 4-31 compare the same vapor effective mass flux to distribution results in the form of the CV for the short and long entrance cases respectively. For both Figures 4-30 and 4-31 the distinction of the trends does not seem to be very clear. This suggests that, unlike in the case of the rectangular manifold, it might be better to investigate the trends when the effective mass flux is scaled by multiplying it by one minus the inlet quality, or by the liquid mass fraction.

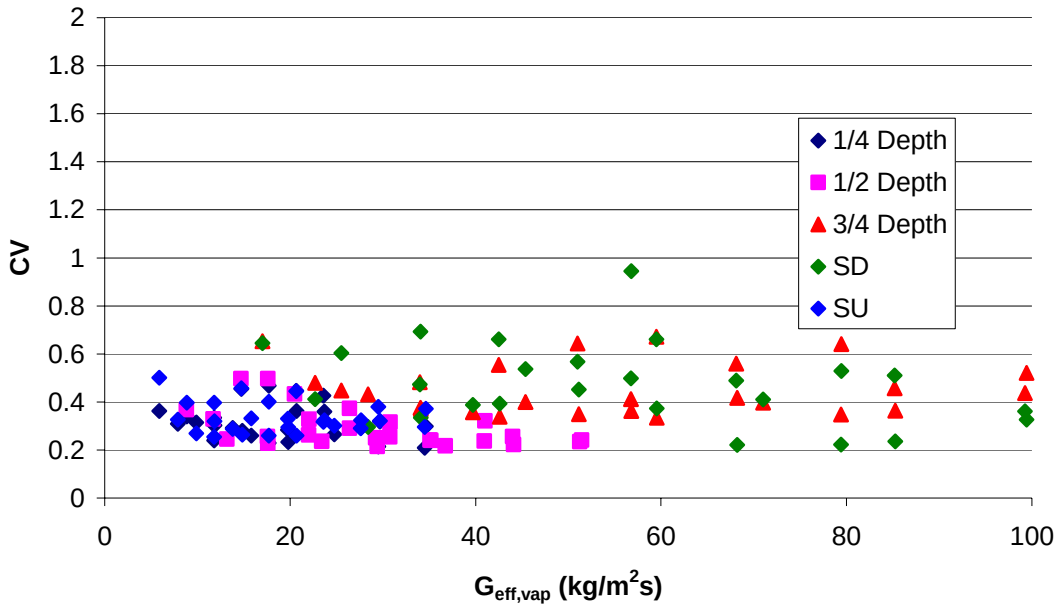

Figure 4-30: Vapor Effective Mass Flux Effects, Short Entrance

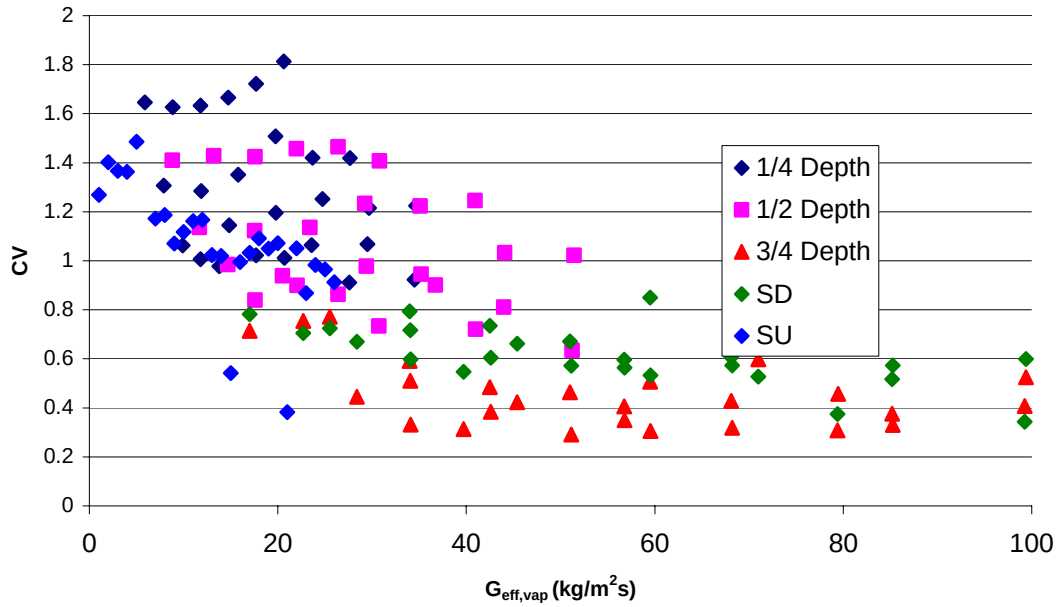

Figure 4-31: Vapor Effective Mass Flux Effects, Long Entrance

Comparison of the liquid scaled effective mass flux and the distribution results is presented in Figures 4-32 and 4-33 for the short and long entrance cases respectively. These figures both show trends that are much easier to discern than those in Figures 4-30 and 4-31. For the short entrance case, presented in Figure 4-32, there are two distinct, yet similar patterns that appear. The first is seen in the results of the

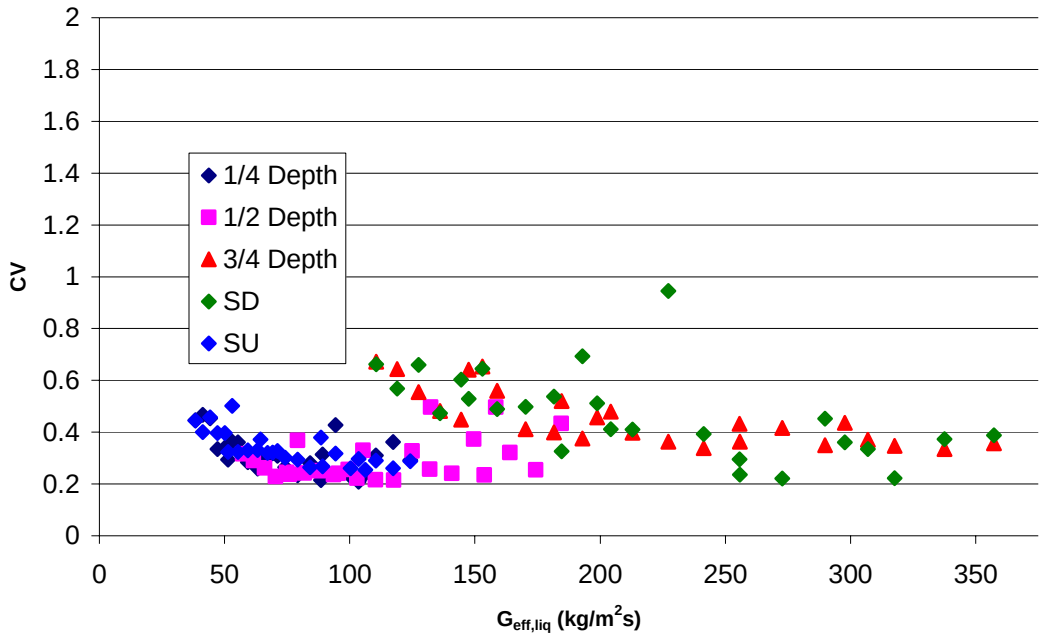

Figure 4-32: Liquid Effective Mass Flux Effects, Short Entrance

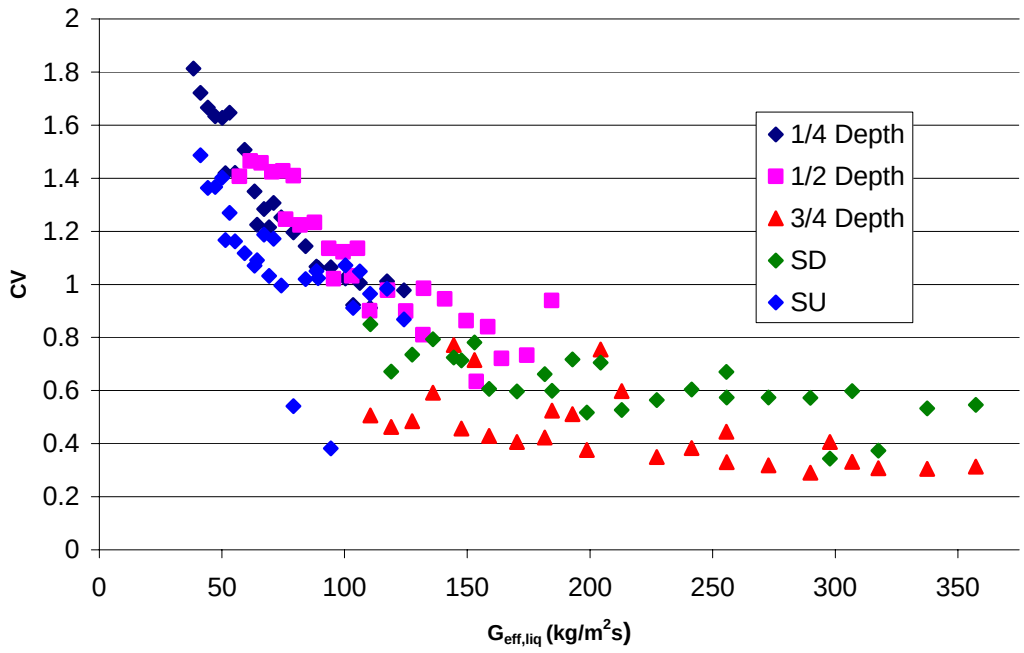

Figure 4-33: Liquid Effective Mass Flux Effects, Long Entrance

4. 9. Pressure Drop Considerations

For both the circular and the rectangular manifold the most uniform liquid distribution was found to occur when the microchannels were protruded the deepest into the manifold. Since these protrusions would have some effect on the pressure drop in the manifold, the pressure drop associated with the microchannel protrusion was

investigated briefly in the circular manifold. This was by no means an exhaustive study of pressure drop and its mechanism, but merely a look to see if the protrusion of the microchannels presented a huge disadvantage in terms of pressure drop. Pressure drop measurements were carried out using pressure transducers (±0.1 psi) placed before the microchannel array, but after the expansion device, and at the opposite end of the manifold.

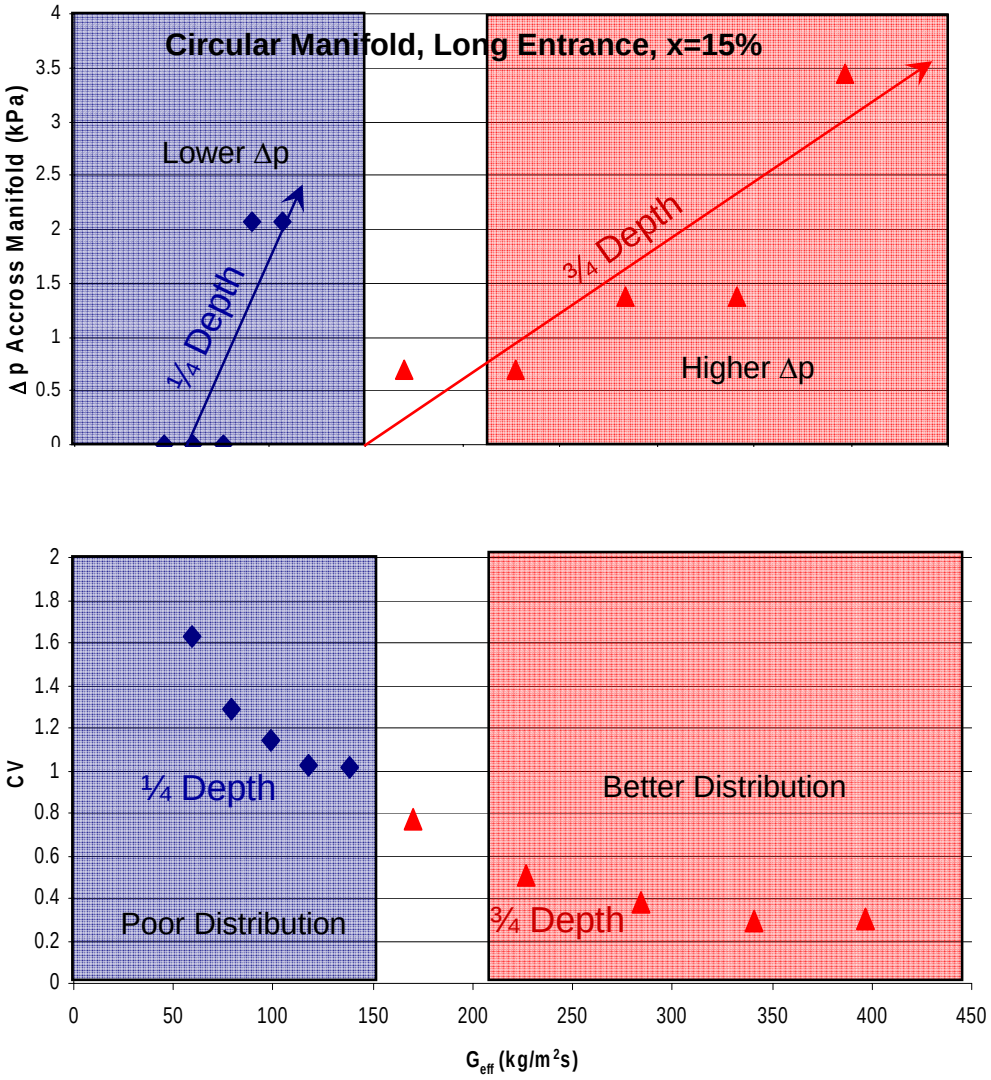

Figure 4-34: Pressure Drop and Distribution Results for Long Entrance, 15% Inlet Quality

Figure 4-34 presents some of the pressure drop data plotted against the effective mass flux for both the one quarter depth and the three quarter depth protrusion cases with an inlet quality of 15% and the flow entering from the long entrance, as well as the distribution results for the corresponding pressure drop data. From this figure it is seen that the cases in which the microchannels were protruded further produced slightly higher pressure drop; however, the magnitude of this pressure drop was not large at all (~3.5 kPa). The relatively low magnitude of the pressure drop and the much improved distribution in the case of the three quarter depth protrusion seem to lead to

the conclusion that the benefits of increased protrusion depth, with respect to distribution, outweigh the slight increase in pressure drop.

4. 10. Flow Visualization for Circular Manifold

To better understand the phenomena that are described by the distribution results, flow visualization experiments were performed in concert with the distribution measurement experiments. The following qualitative discussion will center on these results and how they help to explain the quantitative results described thus far. . Flow visualization was achieved through the use of transparent material in parts of the test section. In the case of the circular manifold the cylinder itself was made of clear PVC in order to allow for flow visualization. The same conditions that were investigated in the distribution experiments were studied in the flow visualization experiments. Typically flow visualization results are discussed in terms of different flow regimes or patterns, however in the case of these tests many of the images show flow that has not fully developed into a constant regime. This makes discussing visualizations in terms of defined flow regimes difficult and thus typical flow regime mapping and qualification will not be heavily relied on. The discussion that follows will focus on setup of the visualization apparatus, and results from the experiments with an emphasis on how they pertain to corresponding results obtained from the distribution experiments.

4. 10. 1. Flow Visualization Setup

In order to gain both still images and video images a digital camcorder was used. The camera used to capture these images was a Sony DCR-TVR19 camcorder. This camera was used for its small size, digital format and entry level pricing with reasonably good quality images. The DCR-TVR19 has 10X zoom with auto focus and records in digital format so that conversion from analog to digital is not necessary. While the camcorder had the capability to capture still images, to preserve quality and allow for best image selection all still images presented were extracted from the video images on a frame by frame basis. An image of the DCR-TVR19 is shown in Figure 4-35.

Figure 4-35: Sony Camcorder Used for Flow Visualization

It was found while conducting flow visualization tests that using a stroboscope while capturing the images helped to clear up the images and make focus on smaller more individual characteristics of the flow such as bubbles and droplets clearer. The stroboscope used was variable frequency so that the best frequency for taking video could be “dialed in”. An image of a stroboscope very similar to the one used in theses experiments is shown in Figure 4-36.

Figure 4-36: Omega Stroboscope used for Flow Visualization

The diagram shown n Figure 4-37 illustrates the experimental setup for flow visualization using the circular manifold. A white backdrop was placed behind the test section to diffuse and reflect the light from the stroboscope. The flow entered either from the left or from the right depending upon the entrance port being used. With this in mind, the camcorder and the stroboscope were attached to a rail in order to allow translation from left to right or vice versa depending upon the entrance port used. The camcorder and stroboscope are then translated along the test section for the whole length of the test section for any given test condition, yielding a video image of the entire test section under that particular condition. The circular manifold was designed with sufficient space between the two plates to allow for flow visualization along the entire length of the test section this can be seen from Figure 2-8 and Figure 4-3.

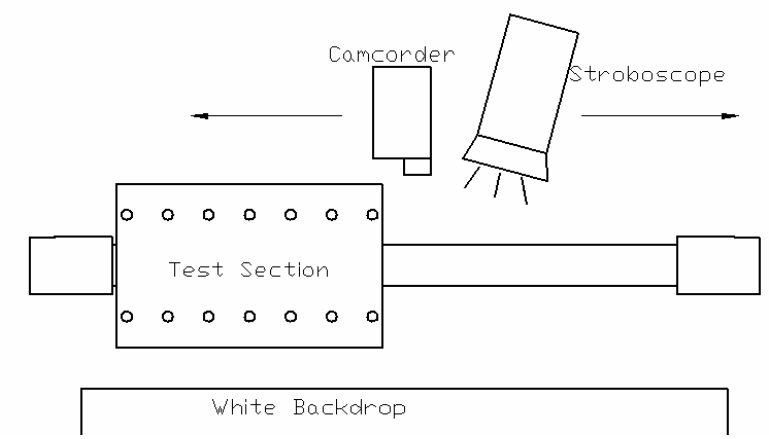

Figure 4-37: Flow Visualization Diagram

4. 10. 2. Flow Visualization Results for Long Entrance

In earlier discussions it was noted that the distribution may be affected by the ability of the flow to develop and the two phases to separate, in which the microchannel protrusion may play some role. Figure 4-38 is a compilation taken from the frames of the video shot for the long entrance case with the microchannels protruded to the one half depth. In this figure flow is from right to left, with the distance from the expansion device shown above the pictures. This Figure illustrates very well the separation of the two refrigerant phases. At about seven inches from the expansion device significant separation becomes apparent, with separation becoming complete by nine inches. Interestingly, the flow makes a jump at about 10 1/2 inches and the two phases recombine slightly. The flow stays somewhat combined and turbulent over the first four or five microchannels and then becomes stratified again, with little or no disturbances being seen in the flow at the end of the manifold near the last microchannels. These characteristics of the flow seem to correspond to the distribution results as can be seen in Figure C-64 of

Appendix C. For all of the long entrance length tests it seemed that the length was sufficient for the flow to either see significant or complete phase separation.

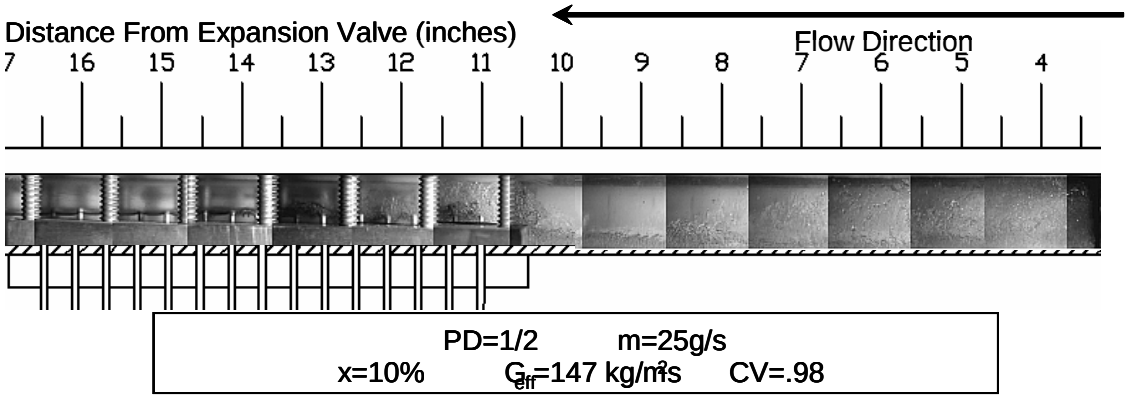

Figure 4-38: Flow Visualization of Entire Manifold Using Long Entrance

Due to the fact that the flow seems to separate, to some degree, in the manifold before it reaches the microchannel array in the long entrance cases it may be beneficial to look closer at the area right before the array to see exactly how the separation looks and how that is changed by the protrusion of the microchannels. Figure 4-39 concentrates on this area for the test cases in which the microchannels were protruded to the one quarter depth specification at inlet qualities of 10 and 20 percent. To the right of each picture in Figure 4-39 the protrusion depth, mass flow rate, effective mass flux, and coefficient of variation value are listed. Flow in the pictures is from left to right, also the location of the first microchannel in the array is marked by the black ellipse. The first interesting point to note about Figure 4-39 is how the void fraction in the manifold increases as the mass flow rate increases. This can be seen by going down in the sequences of photographs on both left and right side of the figure. At lower mass flow rates there is a large liquid layer on the bottom with a small film of bubbles and then the vapor layer on top with very little turbulent/chaotic type features to the flow. As the mass flow rate increases the liquid layer on the bottom decreases in thickness, as does the bubble film that separates the liquid and vapor flows. The interesting point to notice in this trend is how the structure of the flow changes once it reaches the microchannel array. For the lower mass flow rates there is very little change in the nature of the flow once it reaches the microchannels; there is still noticeable liquid and vapor layer separated by a film of bubbles (See the top two pictures in Figure 4-39). This changes however when the mass flow rate is increased, now the once separated flow seems to "jump" and somewhat rehomogenizes the two phases forming more bubbles and adding turbulent features to the flow. Notice also that as the mass flow rate is increased the value of CV decreases as well, or more uniform liquid distribution is seen. This lends to the idea discussed previously, namely that if the flow can somehow be kept or made somewhat homogenous with respect to the two phases more uniform liquid distribution will result.

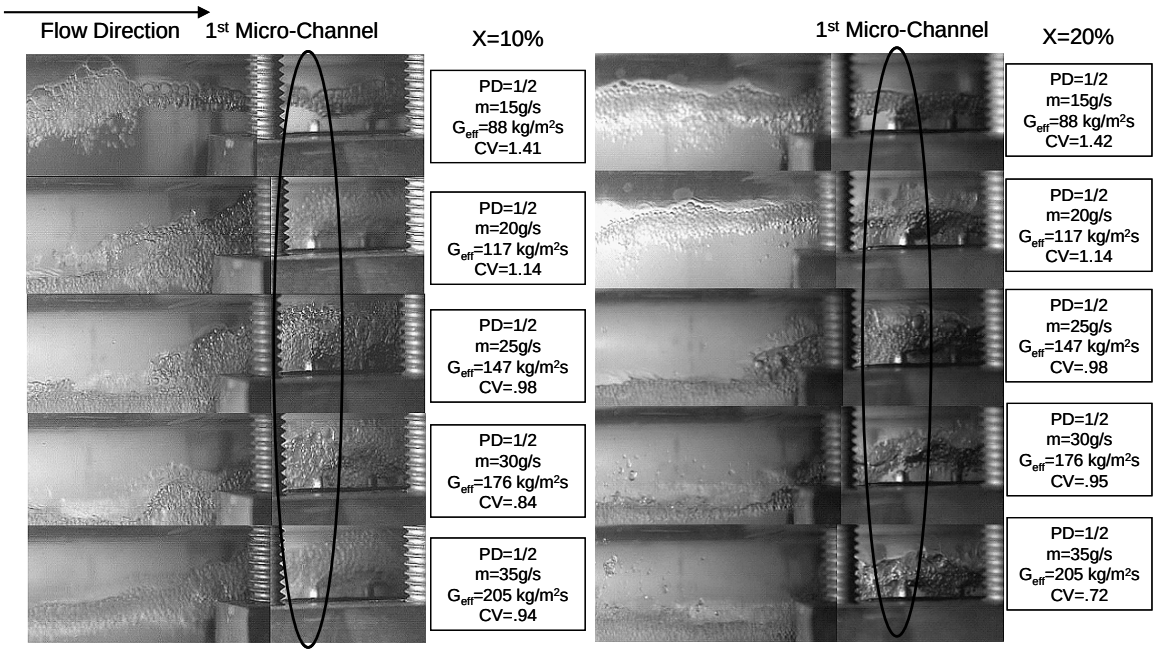

Figure 4-39: Flow Visualization for Long Entrance, One Quarter Depth Protrusion, 10 & 20% Inlet Quality

Another interesting thing to note about Figure 4-39 is the effect of changing quality. There is a noticeable, but not extreme change in the flow when the quality is increased from 10% to 20% (The left hand side of Figure 4-39 versus the right hand side.) For both the lower and higher mass flow rates it looks as though the amount of bubbles decreases while at the higher mass flow rates a few droplets actually begin to become entrained in the vapor flow (the two bottom photographs on the right hand side). However, these small changes in flow structure do not seem to translate into a large change in the liquid distribution results, as can be seen in the presented CV values.

While some information has been gained examining the pictures obtained in the flow visualization experiments conducted with the microchannels protruded to the one quarter depth specification it would also be of interest to look at similar flow visualization results for another protrusion scheme. To that end, Figure 4-40 presents flow visualization similar to those in Figure 4-39, with the microchannels being protruded uniformly to the three quarter depth specification. Again, the flow is from left to right in the photographs, with the flow conditions and distribution results in the box to the right of each picture. The two columns represent two different inlet qualities with 10% on the left and 20% on the right.

While these photographs represent the same inlet flow conditions, i.e. inlet quality and mass flow rate, as those in Figure 4-39, there are some major differences in the images as well as the distribution results. For the top two photographs images similar to the top two of Figure 4-39, mainly that there is an obvious separation of the two phase by a layer of bubbles with very little change in the structure of the flow being seen as it approaches the microchannel array. Again, the photographs show an increase in void fraction before the array as the mass flow rate is increased, that is as the sequence of photos goes down the page. One of the major differences in the Figures 4-39 and 4-40 is how the flow structure does begin to change upon "seeing" the first microchannel in the array, for the higher mass flow rates. Whereas the flow seemed to slightly rehomogenize in Figure 4-39, in Figure 4-40 it seems that the flow almost reverts back to an entirely homogenous flow regime. This is most evident in photographs for

the 10% -25 & 30g./s and 20%-30 g/s. Combining these flow visualization results with a comparison of the distribution results between Figures 4-39 and 4-40 helps to show that there may be a link between changes in the flow and the uniformity of distribution. This idea lends toward what was alluded to in Chapter 2, namely that while for the most part protruding the microchannels acts the same as merely reducing the cross sectional area of the manifold, but in cases where the flow has sufficient time to separate, the protruded microchannels help to recombine the separated flow. This recombined or homogenous flow allows the kinetically energetic vapor phase to impart some energy to the lower energy liquid phase. This "more energetic" liquid phase can now be carried further down the manifold than the "less energetic" liquid phase seen in the separated flows, resulting in more uniform distribution.

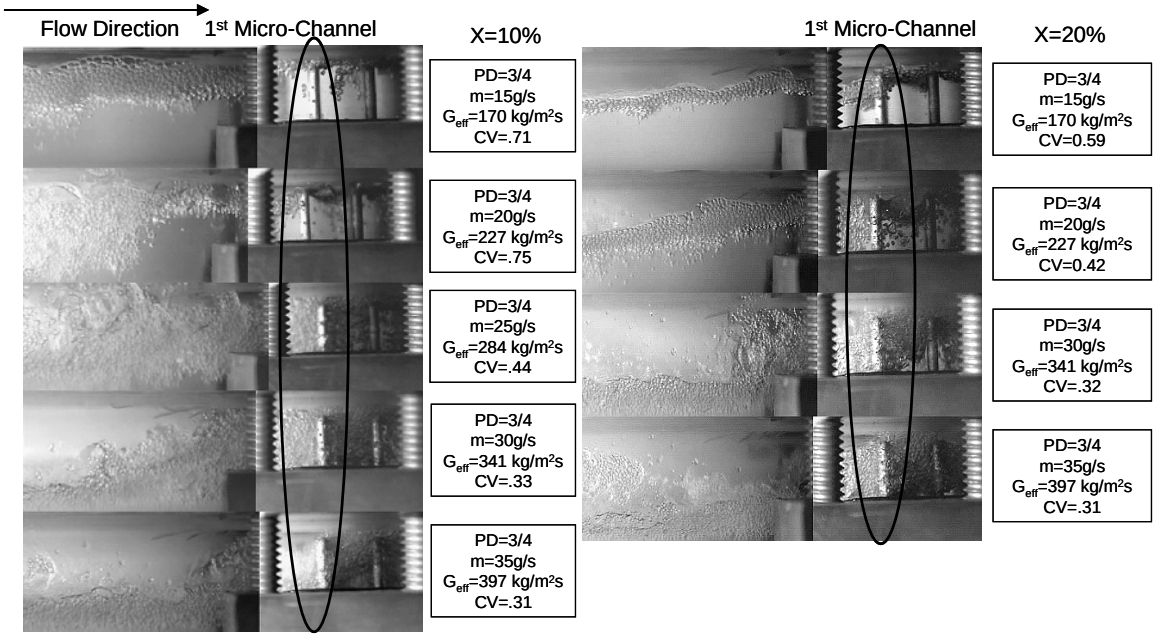

Figure 4-40: Flow Visualization for Long Entrance, Three Quarter Depth Protrusion, 10 & 20% Inlet Quality

4. 10. 3. Flow Visualization Results for Short Entrance

Similar flow visualization test were conducted with the two phase refrigerant entering through the shorter entrance, these results help to offer some insight into the distribution trends seen earlier, and help to solidify the idea that more uniform liquid distribution results, on average, from homogenous type flow. The first illustration of this point is Figure 4-41. Figure 4-41 presents images obtained for the case in which the microchannels were protruded to the one half depth specification, with the flow entering through the short entrance, having an inlet quality of 15% and inlet mass flow rate of 25 g/s. Flow is from left to right within the manifold. This figure shows a very homogenous flow entering the manifold on the left hand side and staying rather homogenous until approximately half way down the length of the manifold. The flow then begins to separate, at which point a small layer of bubbles is visible at the interface between the two phases. The distribution in this case is one of the better with regards to uniformity, having a CV value of 0.33. The actual distribution results of this case can be seen in graphical form in Figure C-20 of Appendix C.

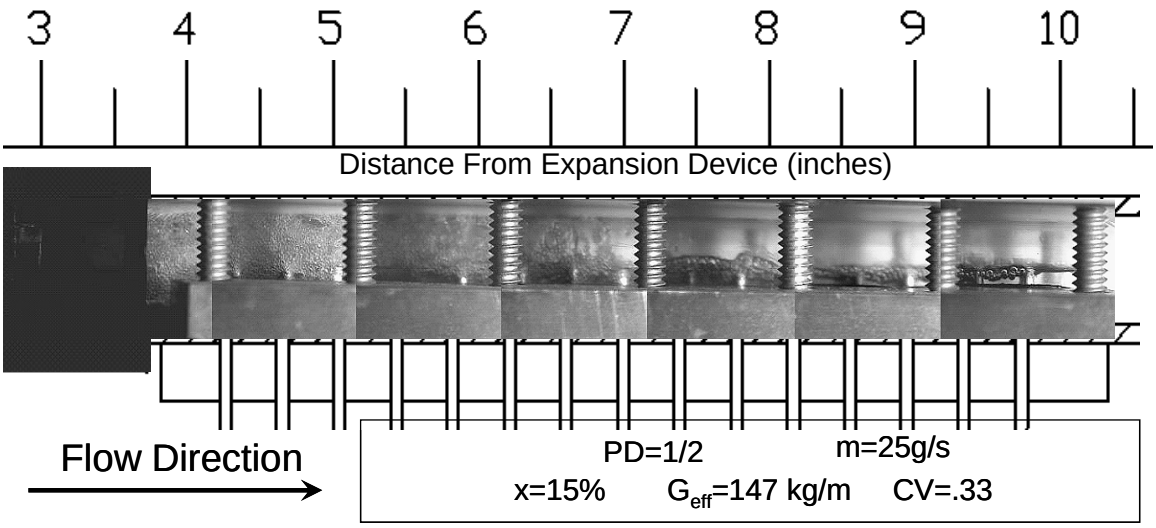

Figure 4-41: Flow Visualization of Short Manifold, One Half Depth

While the inlet conditions are not the same as those presented in Figure 4-38, since there is little change in flow structure between the 10 and 20% quality cases of the 25 g/s test in Figure 3-39 some general comparisons between Figures 4-41 and 4-38 can justifiably be made. It has already been noted that in Figure 4-38 there is a very noticeable separation that occurs well before the flow enters the area of the microchannel array. It was also seen, that while the flow is disturbed somewhat by the microchannels it separates again soon after it enters the array part of the manifold, where this is not the case in Figure 4-41. These differences in flow correspond to an already noted difference in liquid distribution. This lends strength to the idea that liquid distribution is more uniform for flows expanded close to the manifold because the flow does not have time to separate, or develop from the homogenous flow that exits the expansion valve.

Figure 4-42 presents flow visualization results for the same inlet conditions as Figure 4-41, quality of 15% and mass flow rate of 25g/s, with the microchannels protruded to the three quarter depth protrusion specification. Comparing the CV values for the conditions in Figures 4-41 and 4-42, shows that there is little change in the uniformity of the liquid distribution for these cases. This is interesting seeing the differences that appear in examination of the flow visualization. Both Figures show that the flow enters the manifold in a homogenous regime and stays that way through the first several microchannels in the array. The interesting difference between the two is that there does not appear to be any significant separation of the phases in Figure 4-42, this may be due to the very small area that the flow actually has to flow through when the microchannels are protruded to three quarter depth. Another interesting characteristic of the flow that occurs near the last five microchannels is the small fingers of bubbles the move down the face of the microchannels. These “fingers” may be caused by a recirculation formed by the high velocity flow going across the top of what essentially appears to be a relatively static volume of liquid refrigerant, with the bubbles being formed at the top edge of the previous microchannel .

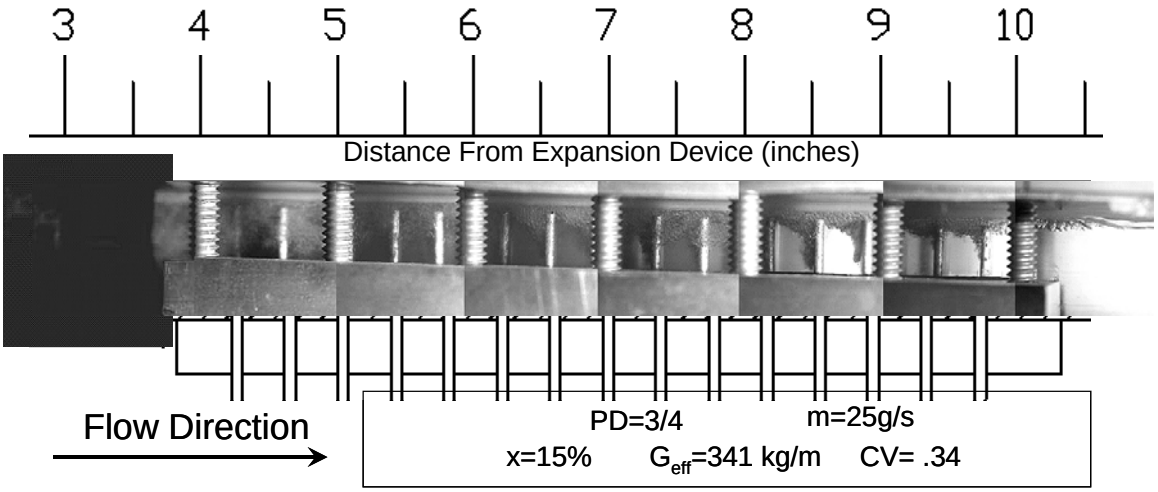

Figure 4-42: Flow Visualization of Short Manifold, Three Quarter Depth

It was stated earlier in this chapter that for the short entrance cases of the manifold tests at higher qualities the uniformity of the liquid distribution actually saw a small reversal in trend, namely that the liquid distribution became less uniform. It is of interest to see if there is a significant change in the visual appearance of the flow that may explain this interesting trend. Figure 4-43 presents a series of pictures compiled from the flow visualization tests conducted under the same conditions of Figure 4-42 with the exception of the inlet quality being increased to 30%. For the first half of the manifold there is little or no discernable difference between Figures 4-42 and 4-43. Again, the "fingers" of bubbles that reach down the front of several of the microchannels are observed between 8 and 9 inches from the expansion valve. After this, however, is where a subtle difference can be seen between Figures 4-42 and 4-43. In Figure 4-42 it is still apparent that between 9 and 10 inches from the expansion valve there is still a significant amount of bubbly flow appearing, but in Figure 4-43 between 9 and 10 inches there seems to be more of a separated flow with a thin layer of bubbles. With that observed, it still seems very difficult to connect, in any meaningful way, this trend of slightly decreased uniformity directly to some sort of flow structure using the results from the flow visualization. The actual distribution results of both Figures 4-42 and 4-43 can be seen in graphical form in Figure C-27 of Appendix C.

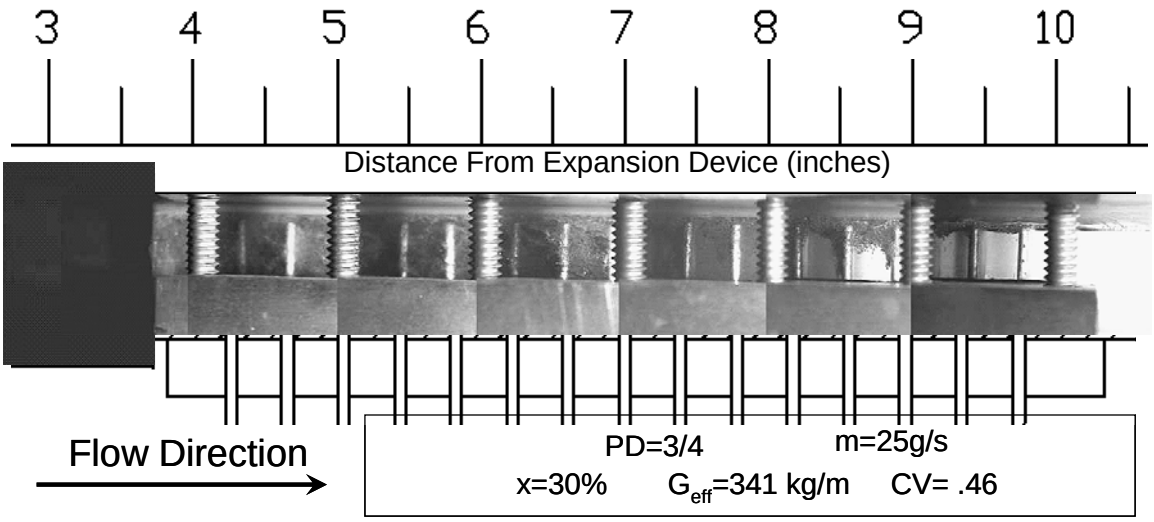

Figure 4-43: Flow Visualization of Short Manifold, Three Quarter Depth

4. 11. Conclusions

Several different parameters were considered in studying the distribution of R-134a in a circular microchannel manifold. The flow conditions that were altered in order to study their affect on the liquid flow distribution were quality and mass flow rate; the quality being varied from 0 to 35% and the mass flow rate being varied from 15 to 35 grams per second. The geometric parameters that were considered were the entrance length and the protrusion scheme of the microchannels being fed by the manifold, as well as two different entrance lengths. Two different entrance lengths used were the short, located 65mm from the microchannel array and the long, 250mm from the array.

Liquid distribution within the microchannel manifold shows dependence to some degree on all of the above conditions, to varying degrees. Generally, as the mass flux and protrusion depth increase the distribution becomes more uniform. The shorter inlet length provides the most consistently uniform distribution with an optimum protrusion depth near one half. The longer entrance length seems to see more improvement from increasing the above stated parameters, most notably from microchannel protrusion. The best uniformity of distribution occurred in the long entrance case when the microchannels were protruded three-quarters into the manifold. These results show that for the best consistently uniform liquid distribution in a manifold of this sort it is desirable to expand the fluid as close to the manifold as possible. However, when this is not possible, there are ways that the uniformity of the liquid distribution can be improved, mainly by decreasing the area which the flow sees by microchannel protrusion.

In conjunction with the distribution tests, flow visualization experiments were also carried out in order to see the effect of changing the different parameters on the appearance of the flow. These experiments provided insight into some of the trends observed in the distribution experiments. In line with the conclusion that expanding the fluid close to the manifold is desirable for uniform liquid distribution, the flow visualization results suggest that the liquid phase of the refrigerant will be more uniformly distributed when the flow is not separated and in a homogenous type regime. This conclusion also offered some insight into why the uniformity of the distribution saw more improvement for the long entrances cases as the microchannel protrusion depth was increased. The short

entrance length cases saw slight improvement in uniformity of distribution from protrusion of the microchannels due to the decrease in cross sectional area, and thus an increase of average flow velocity. It seems that there is an added effect in the long entrance cases where the microchannels act in a manner that actually "rehomogenizes" the flow after it has already separated. While Fei (2004) studied, to some degree, the characteristic of developing adiabatic two phase refrigerant flow, this particular observation begs for further study on the subject.

Bibliography

Fei, P. and P. S. Hrnjak, “Adiabatic Developing Two-phase Refrigerant Flow in Manifolds of Heat Exchangers”, Air Conditioning and Refrigeration Center, University of Illinois at Urbana-Champaign, 2004.

Kulkarni, T., Bullard, C., Keumnam, C., 2004, Header Design Tradeoff in Micro-channel Evaporators, *Applied Thermal Engineering.*, 24 p. 759-776

Lee, J. K., Lee, S. Y., 2004, Distribution of Two-Phase Annular Flow at Header-Channel Junctions, *Experimental Thermal and Fluid Science.*, 28 p. 217-222

Tompkins, D. M., P. S. Hrnjak, and T. A. Newell, “Single Phase, Two-Phase Modeling: X-Ray Visualization for a Microchannel Manifold Distribution System”, Air Conditioning and Refrigeration Center, University of Illinois at Urbana-Champaign, 2002.

Vist, S., Pettersen, J., Two-Phase Flow Distribution in Compact Heat Exchanger Manifolds, *Experimental Thermal and Fluid Science.*, 28 p. 209-215

Yoo, T., P. S. Hrnjak, and T. A Newell, “An Experimental Investigation of Two-Phase Flow Distribution in Microchannel Manifolds”, Air Conditioning and Refrigeration Center, University of Illinois at Urbana-Champaign, 2002.

Zhang, Q. M., Hrnjak, P.S., Newell, T.A., *An Experimental Investigation of R134a Flow Distribution in Horizontal Micro-channel Manifolds,*. Technical Report TR-223. Air Conditioning and Refrigeration Center, Univ. Illinois at Urbana-Champaign, 2004

Appendix A. Equations Used

Equation 2-1 $$G = \frac{\dot{m}}{A}$$

Equation 3-1 $$CV = \frac{\sigma}{\overline{\dot{m}}}$$

Equation 3-2 $$\sigma = \sqrt{\sum_{i=1}^{n_{\text{tanks}}} (\dot{m}_i - \overline{\dot{m}})^2 / n_{\text{tanks}}}$$

Equation 3-3 $$\overline{\dot{m}} = \frac{\sum_{i=1}^{n} \dot{m}_i}{n_{\text{tanks}}}$$

Equation 3-4 $$G_{eff,liq} = (1 - x) \times G_{eff}$$

Equation 3-5 $$G_{eff,vap} = x \times G_{eff}$$

Appendix B. R134a Liquid Distribution Results for Rectangular Manifold

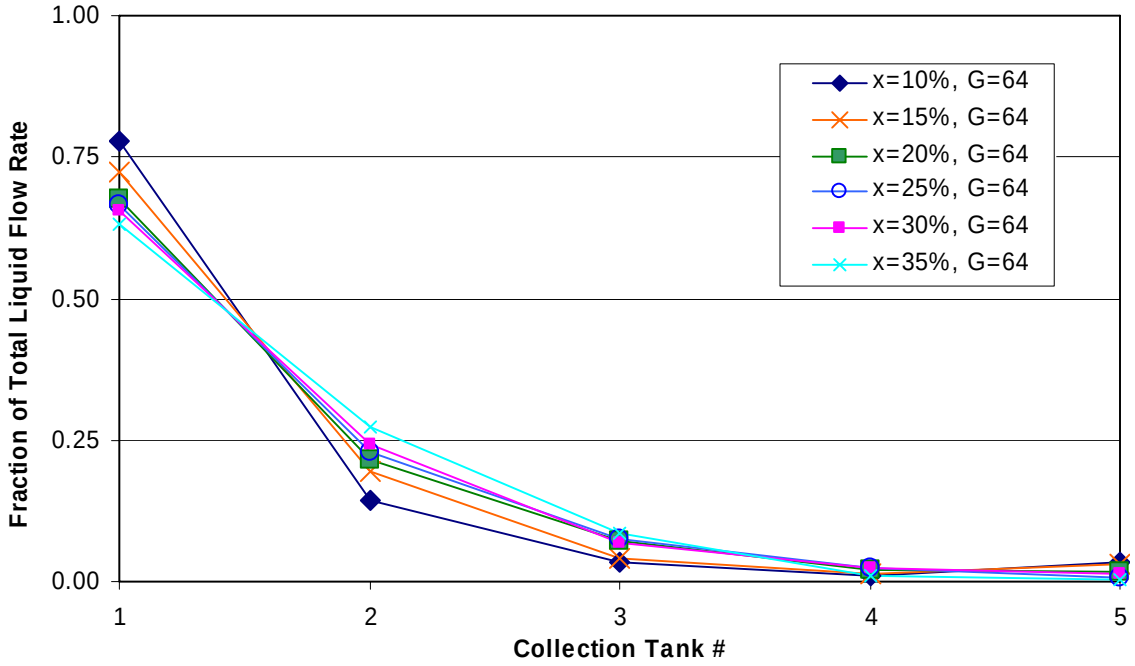

Figure B-1: 1/4 Depth Protrusion, Short Inlet, G=64 kg/m^{2}s

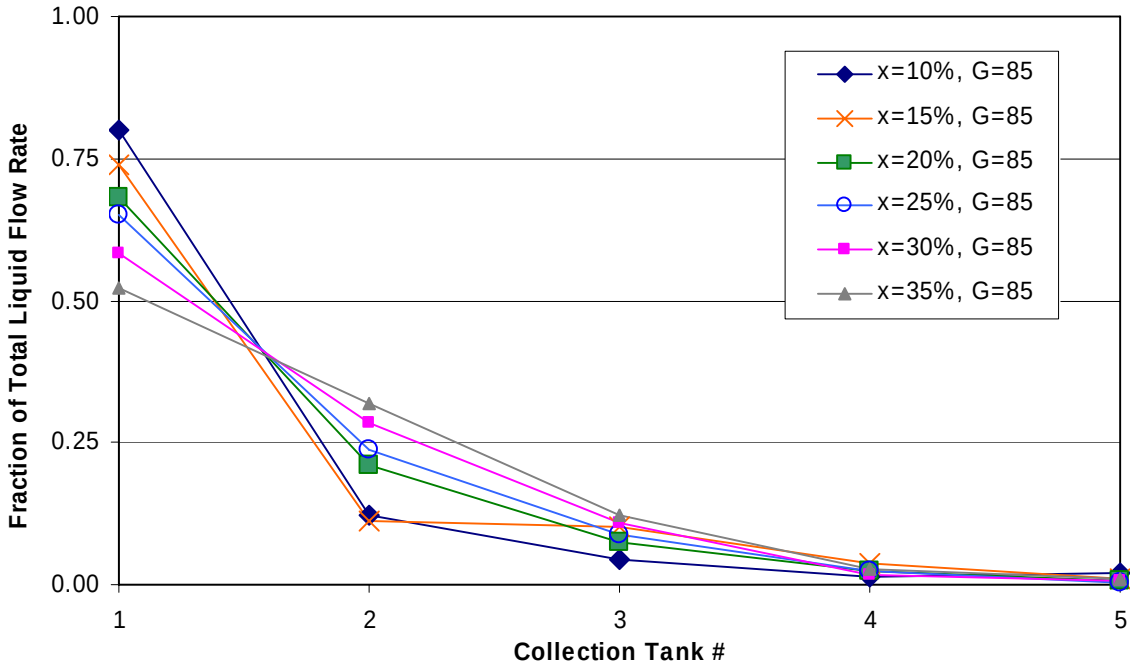

Figure B-2: 1/4 Depth Protrusion, Short Inlet, G=85 kg/m^{2}s

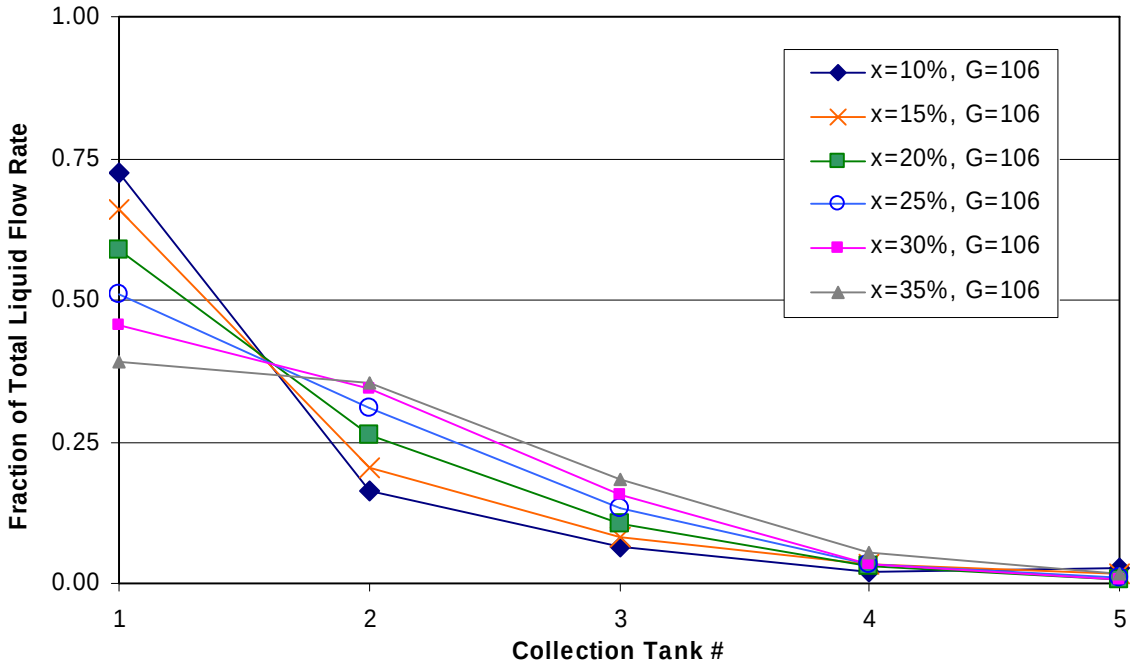

Figure B-3: 1/4 Depth Protrusion, Short Inlet, G=106 kg/m^{2}s

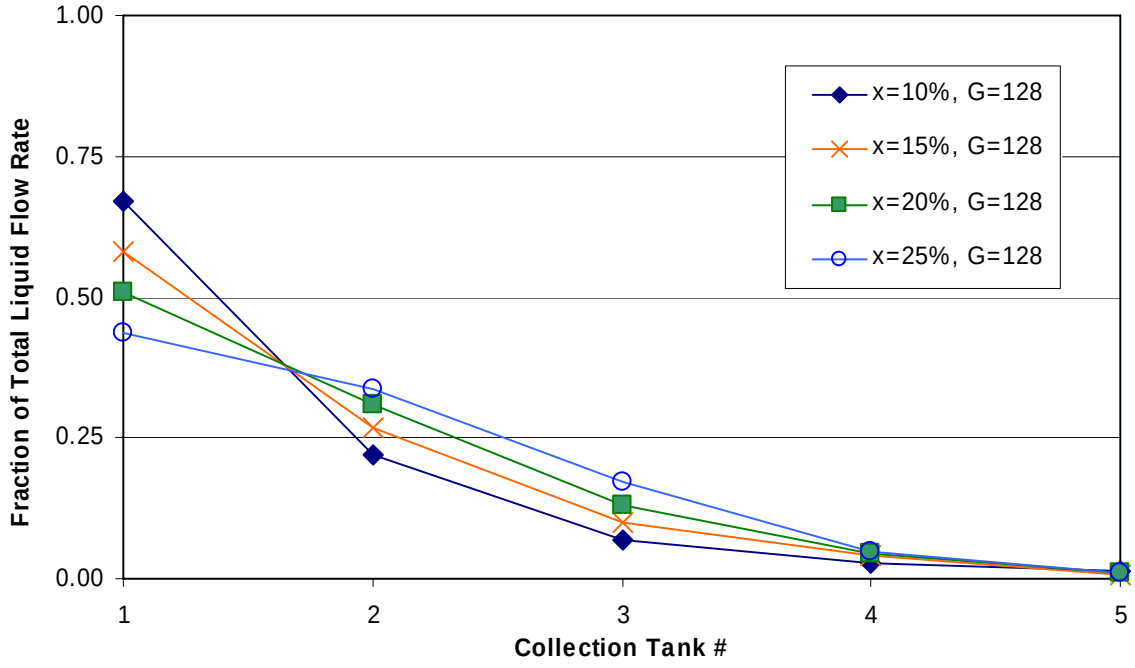

Figure B-4: 1/4 Depth Protrusion, Short Inlet, G=128 kg/m^{2}s

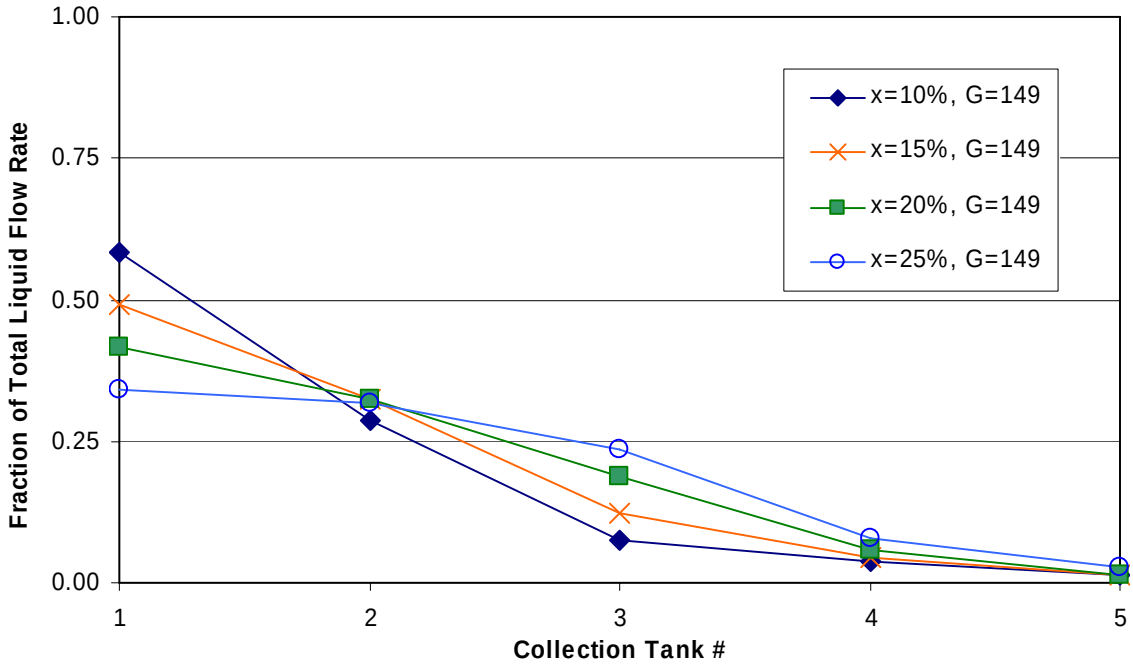

Figure B-5: 1/4 Depth Protrusion, Short Inlet, G=149 kg/m^{2}s

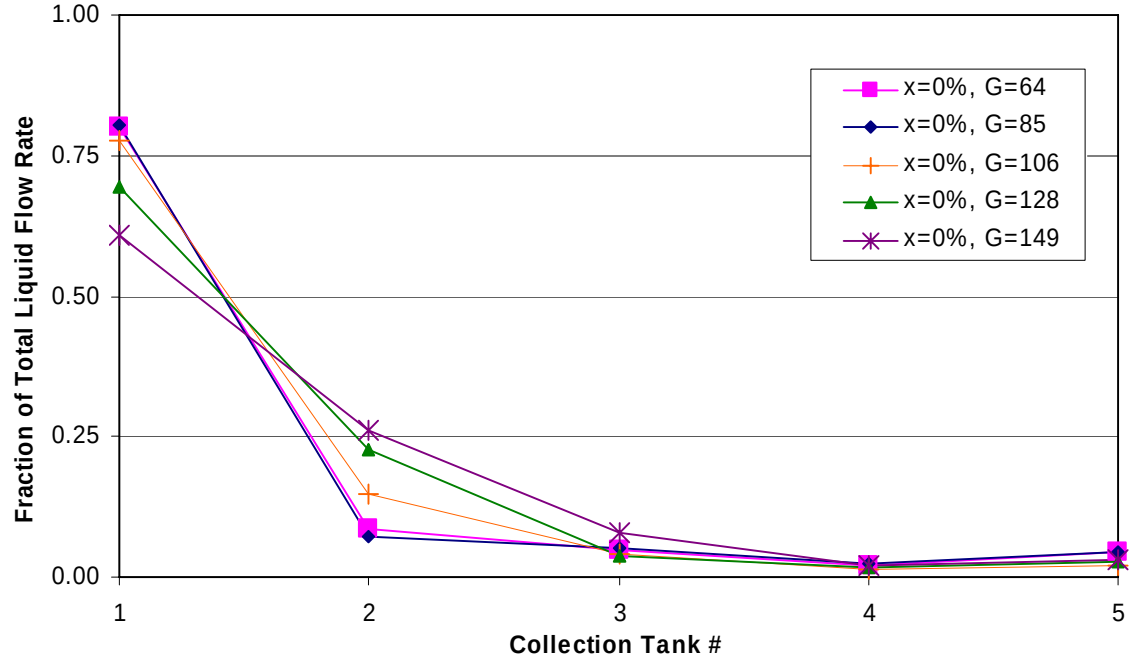

Figure B-6: 1/4 Depth Protrusion, Short Inlet, x=0%

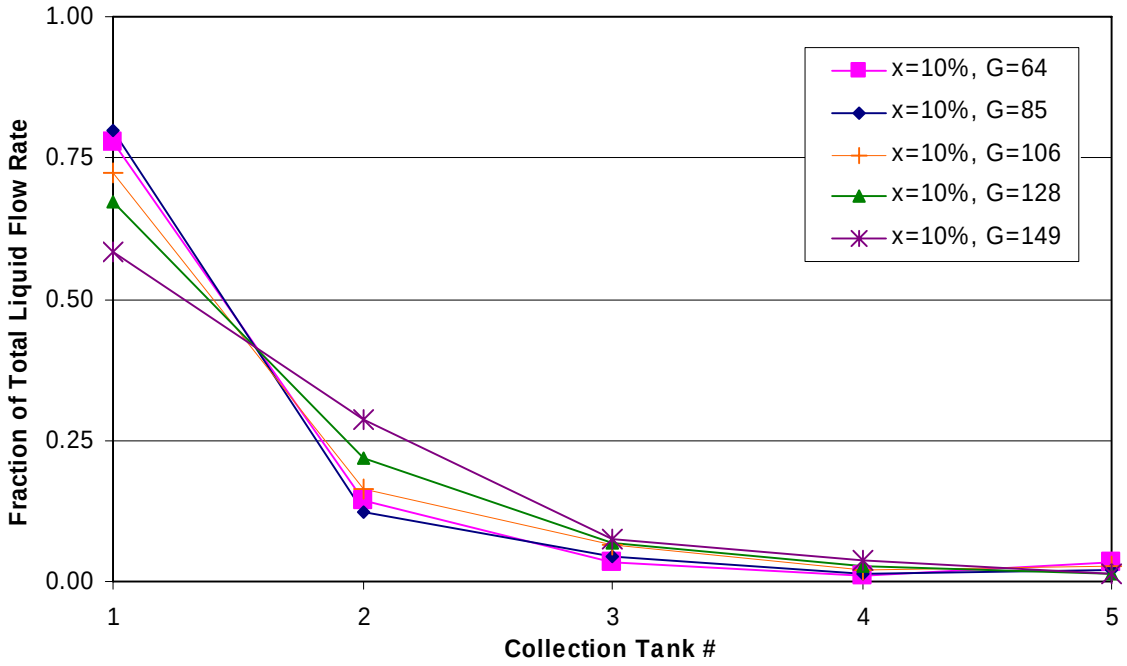

Figure B-7: 1/4 Depth Protrusion, Short Inlet, x=10%

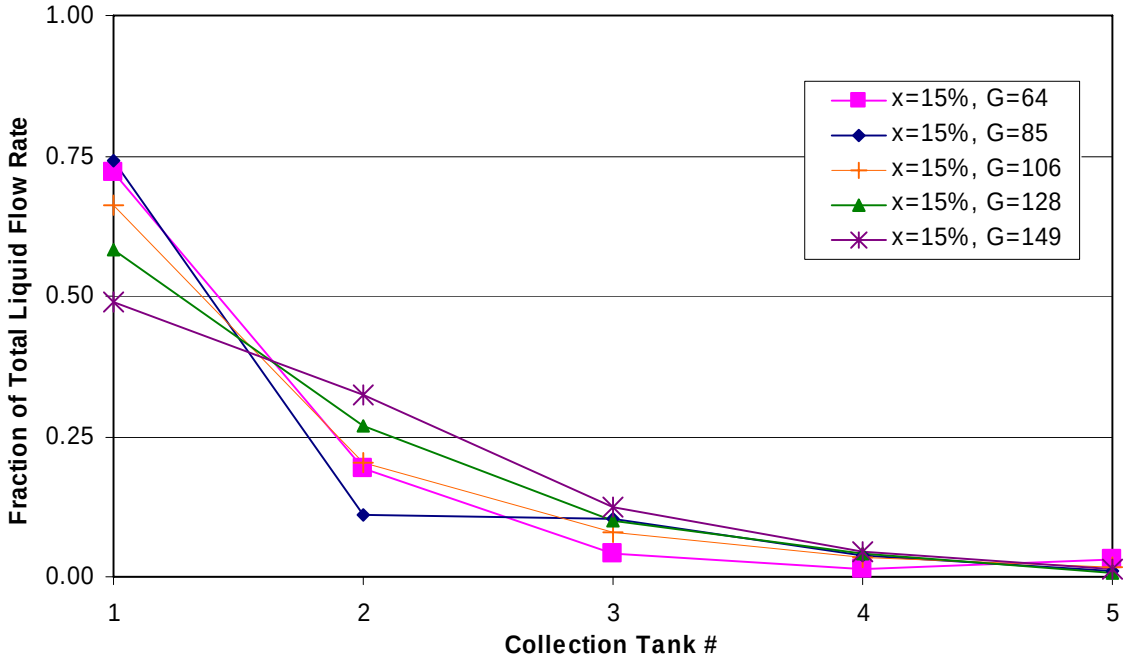

Figure B-8: 1/4 Depth Protrusion, Short Inlet, x=15%

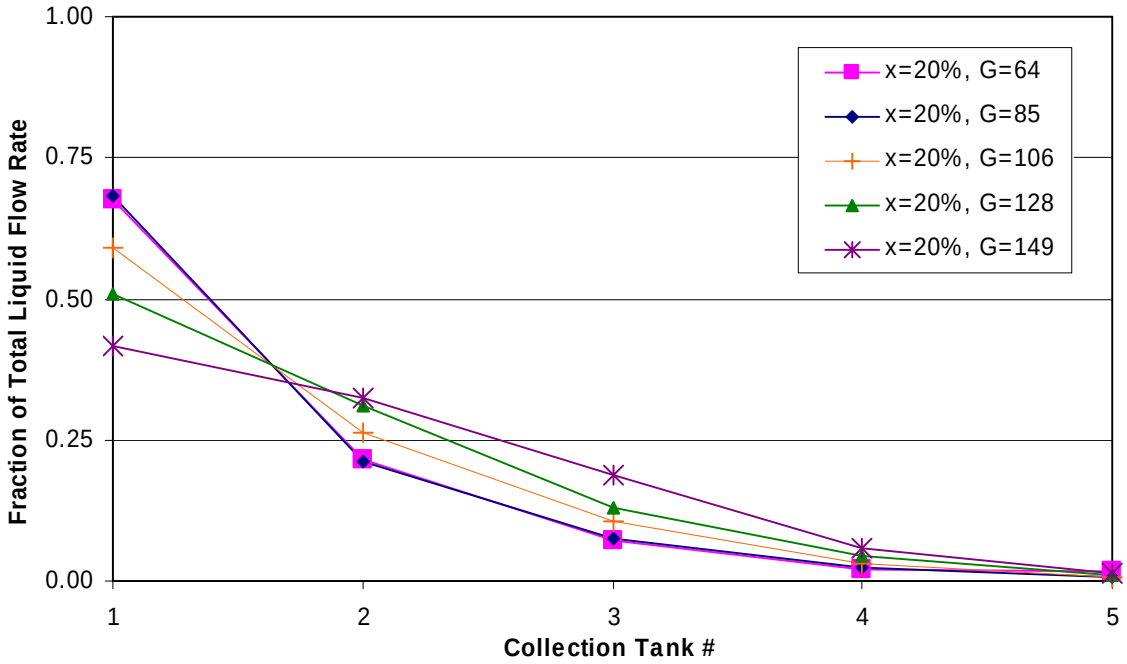

Figure B-9: 1/4 Depth Protrusion, Short Inlet, x=20%

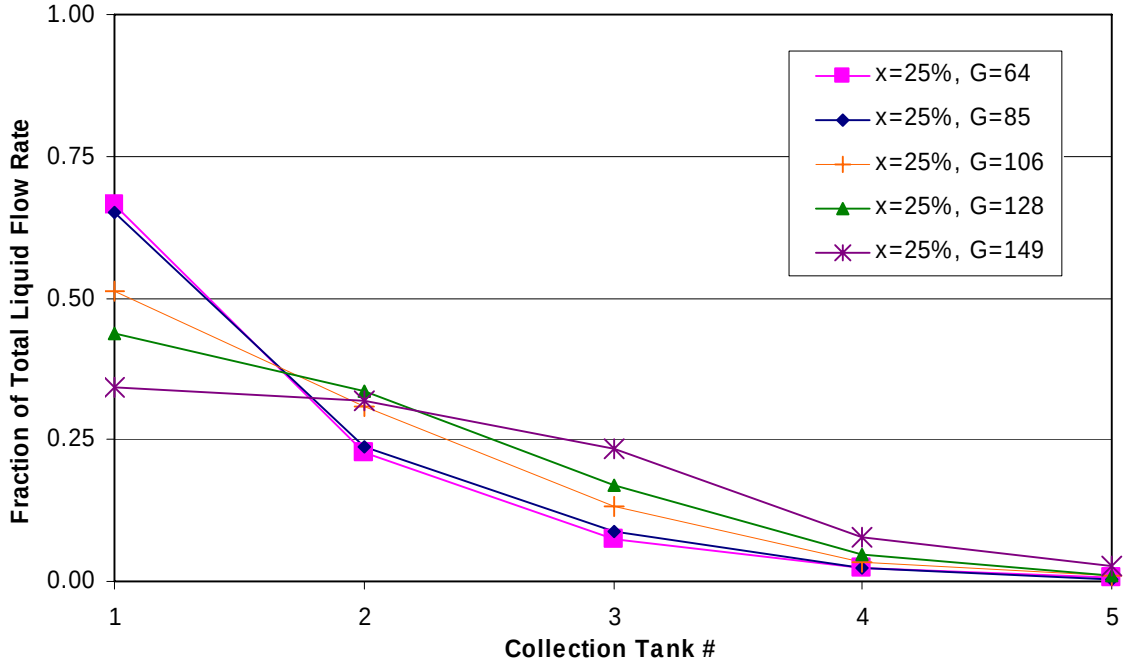

Figure B-10: 1/4 Depth Protrusion, Short Inlet, x=25%

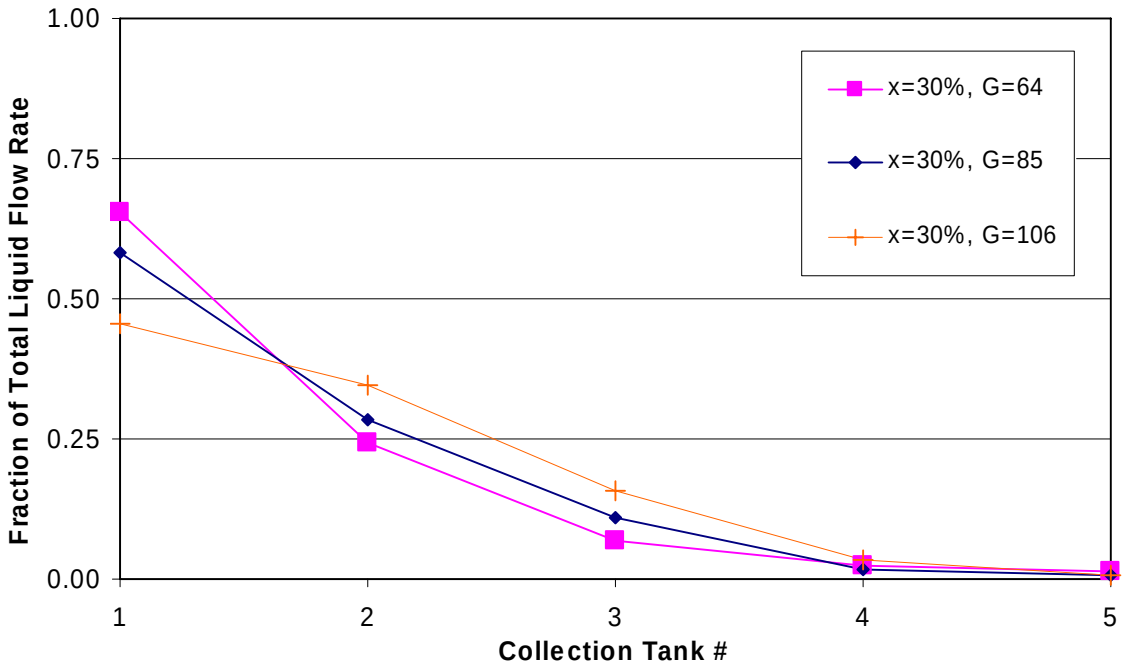

Figure B-11: 1/4 Depth Protrusion, Short Inlet, x=30%

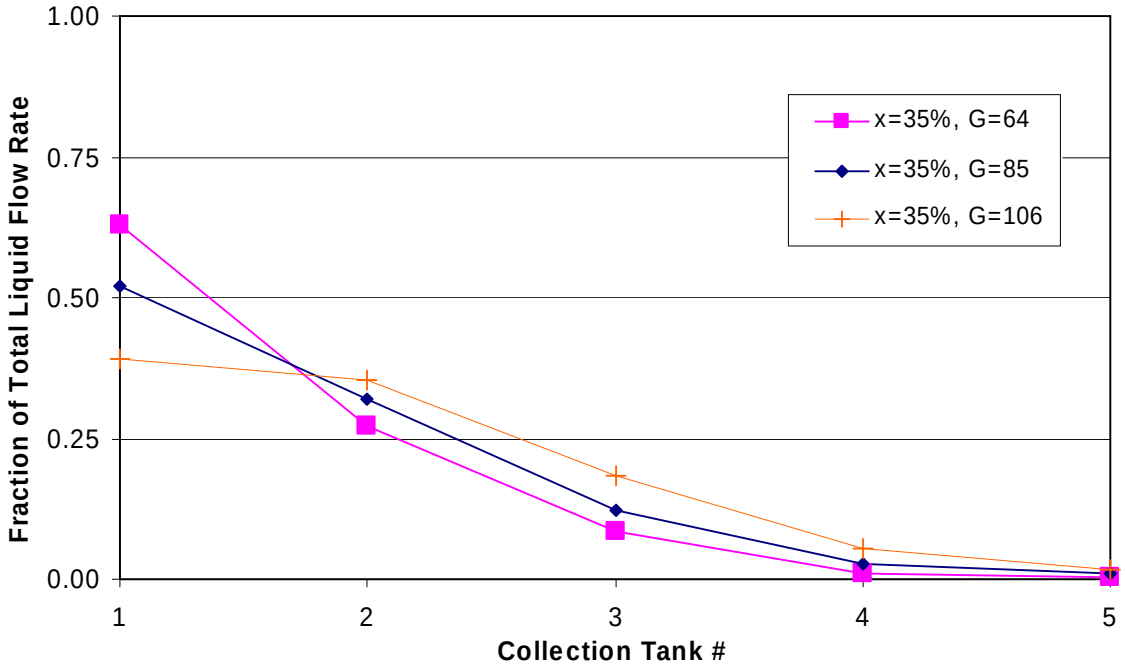

Figure B-12: 1/4 Depth Protrusion, Short Inlet, x=35%

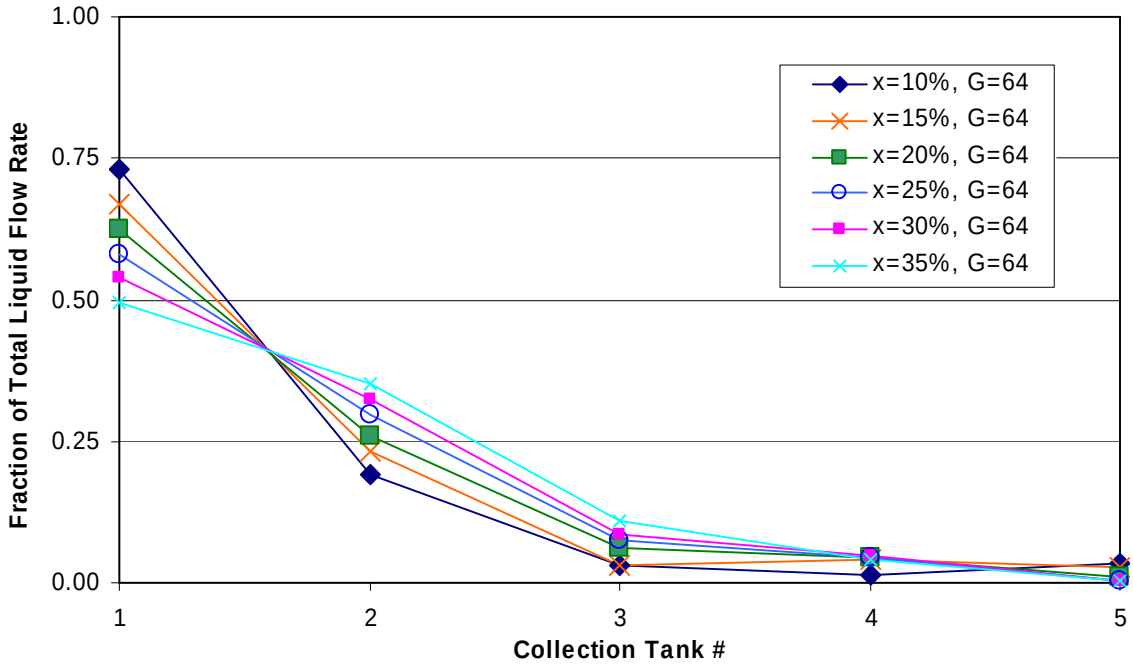

Figure B-13: 1/2 Depth Protrusion, Short Inlet, G=64 kg/m^{2}s

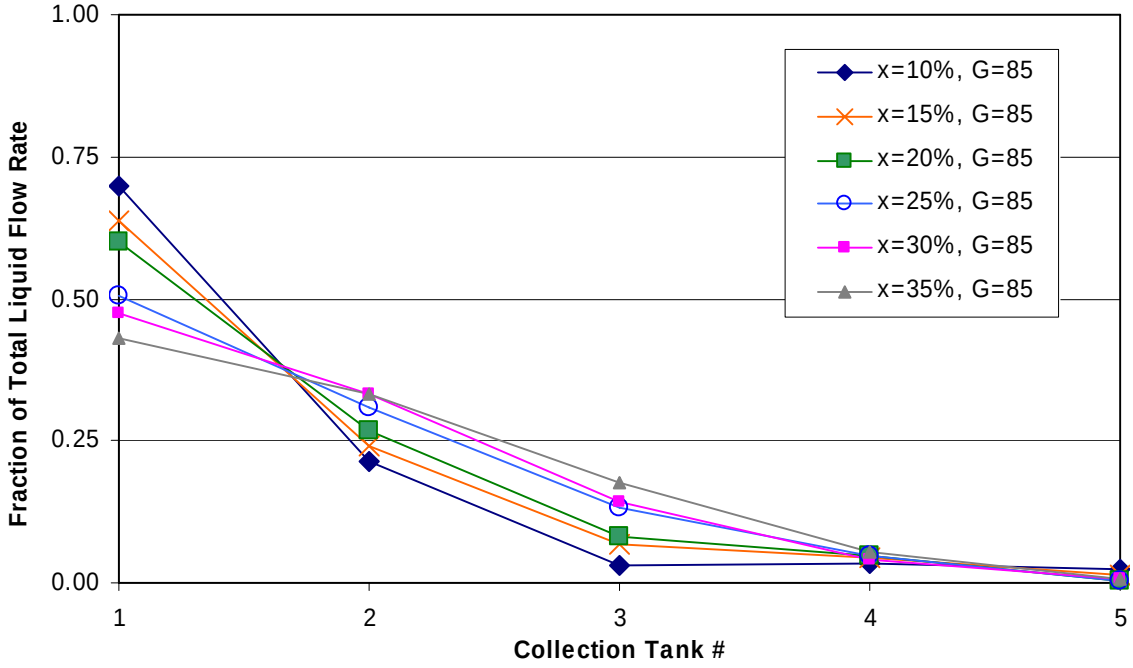

Figure B-14: 1/2 Depth Protrusion, Short Inlet, G=85kg/m^{2}s

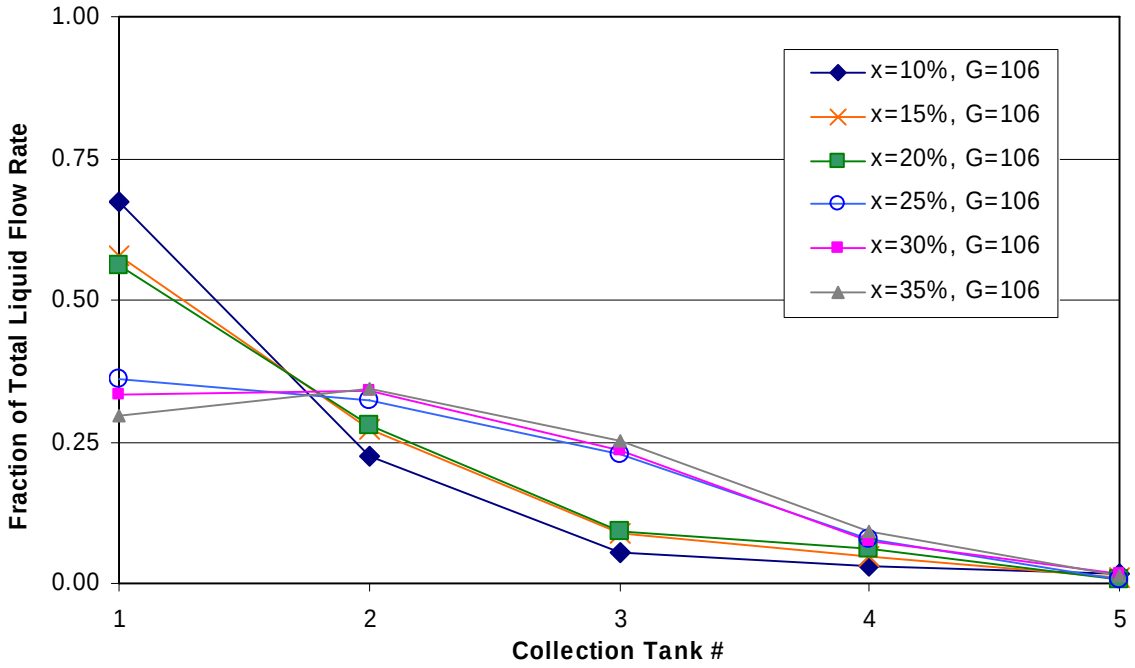

Figure B-15: 1/2 Depth Protrusion, Short Inlet, G=106 kg/m^{2}s

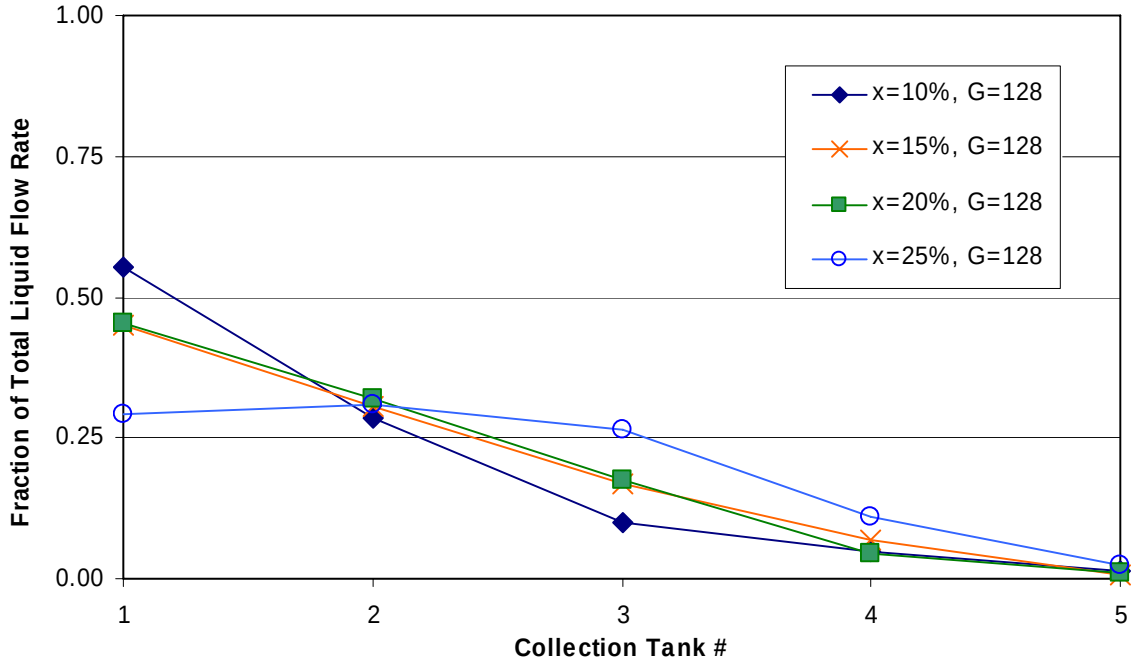

Figure B-16: 1/2 Depth Protrusion, Short Inlet, G=128 kg/m^{2}s

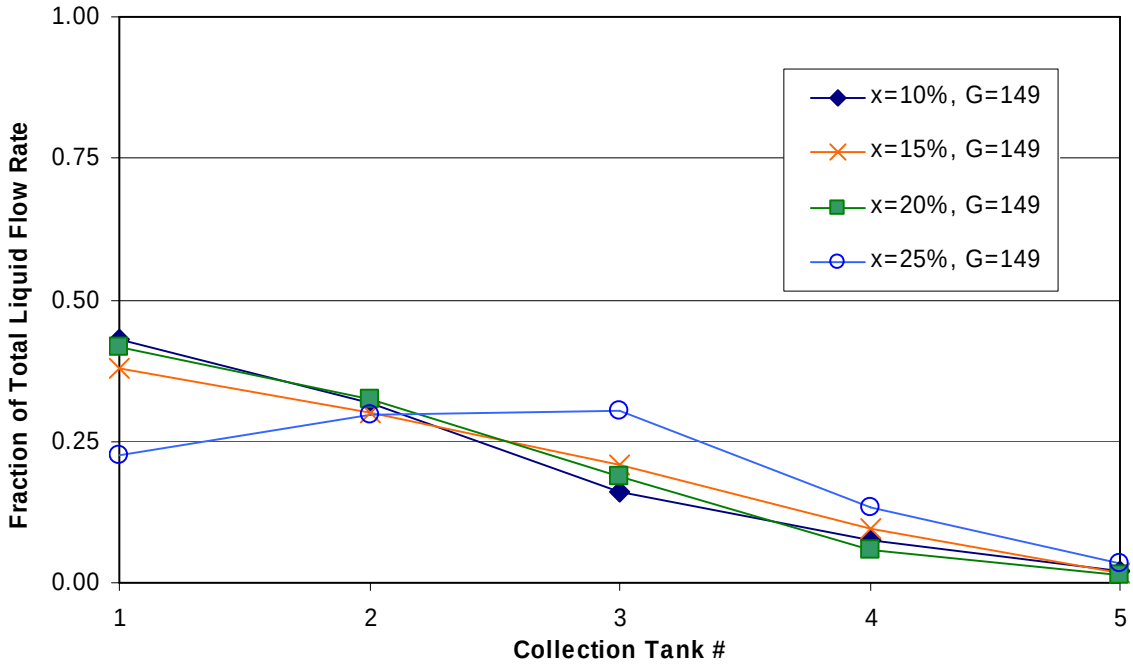

Figure B-17: 1/2 Depth Protrusion, Short Inlet, G=149 kg/m^{2}s

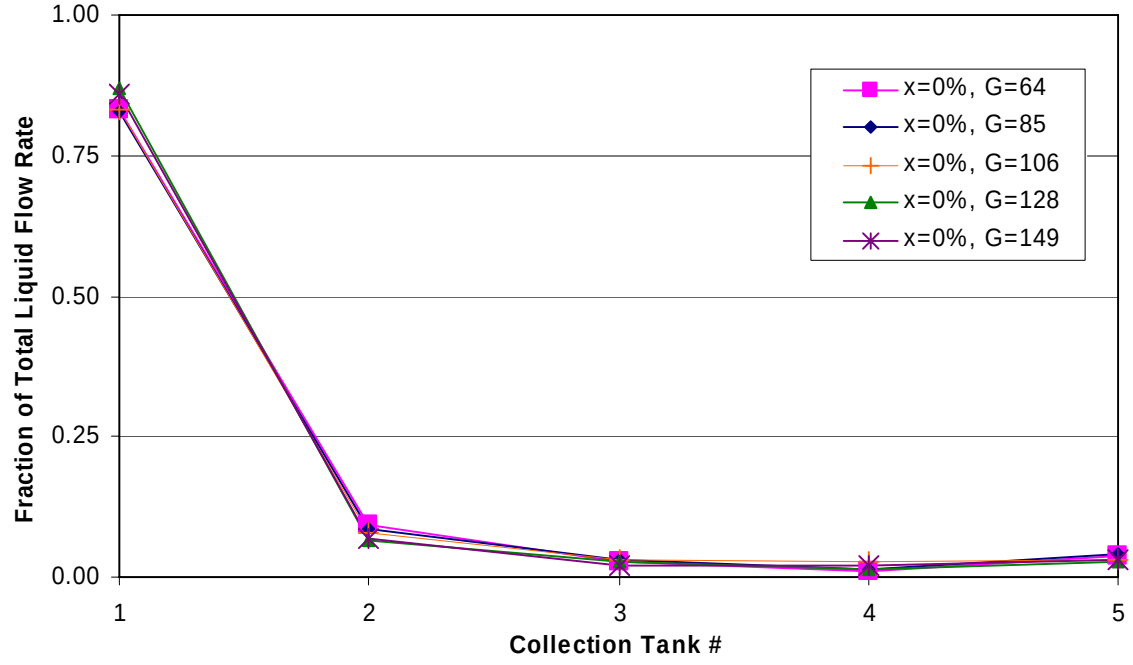

Figure B-18: 1/2 Depth Protrusion, Short Inlet, x=0%

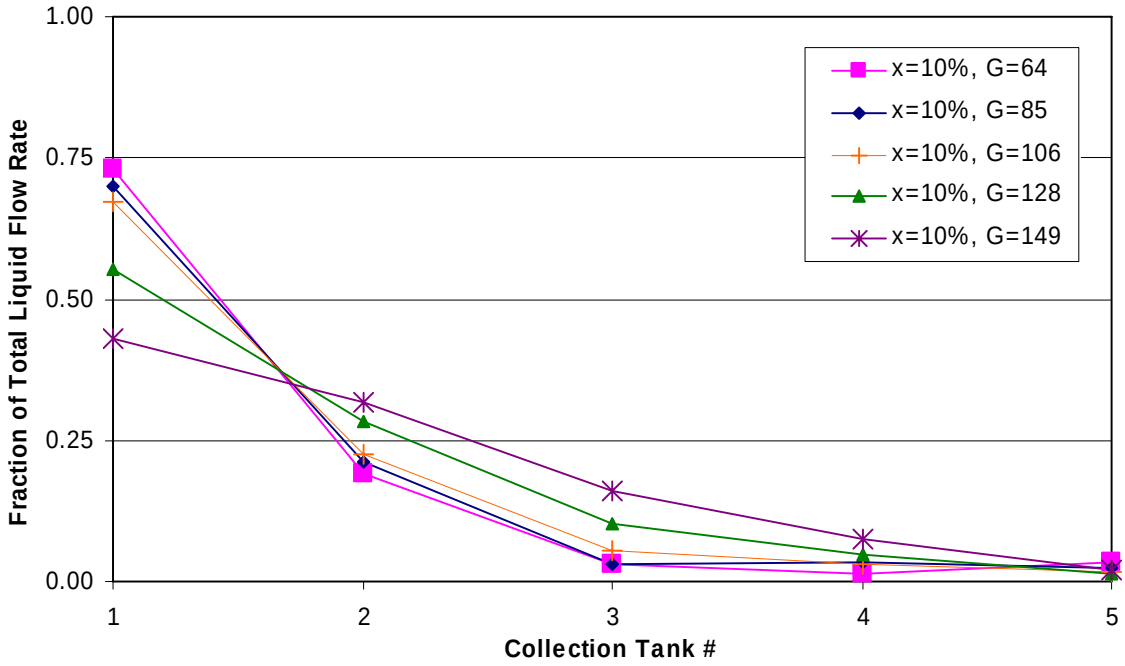

Figure B-19: 1/2 Depth Protrusion, Short Inlet, x=10%

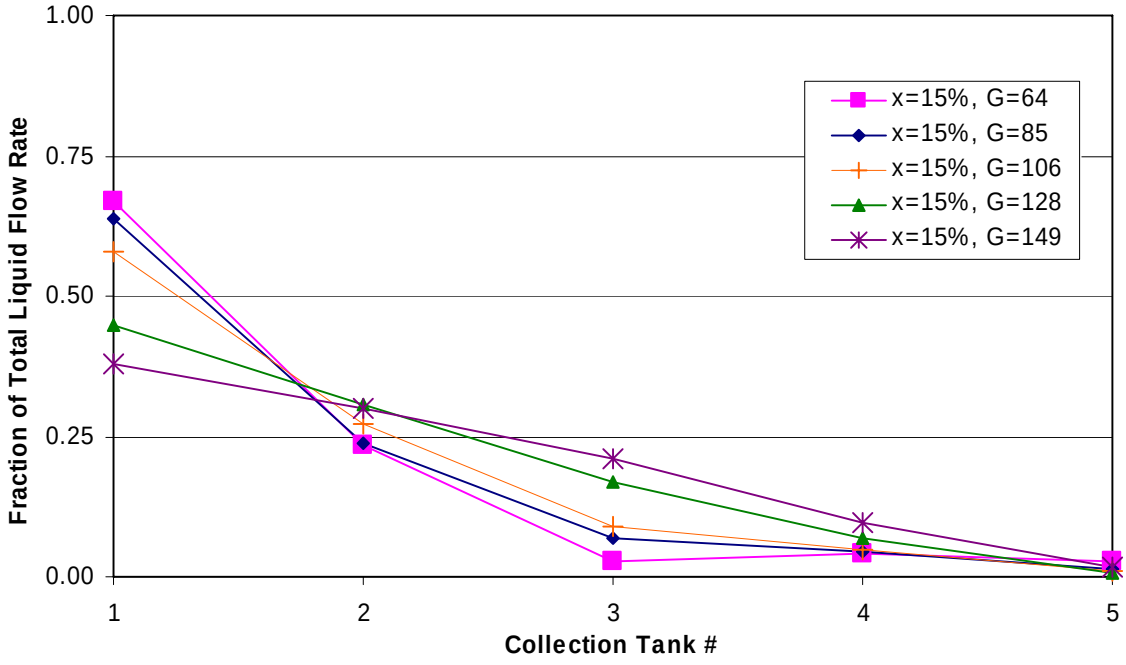

Figure B-20: 1/2 Depth Protrusion, Short Inlet, x=15%

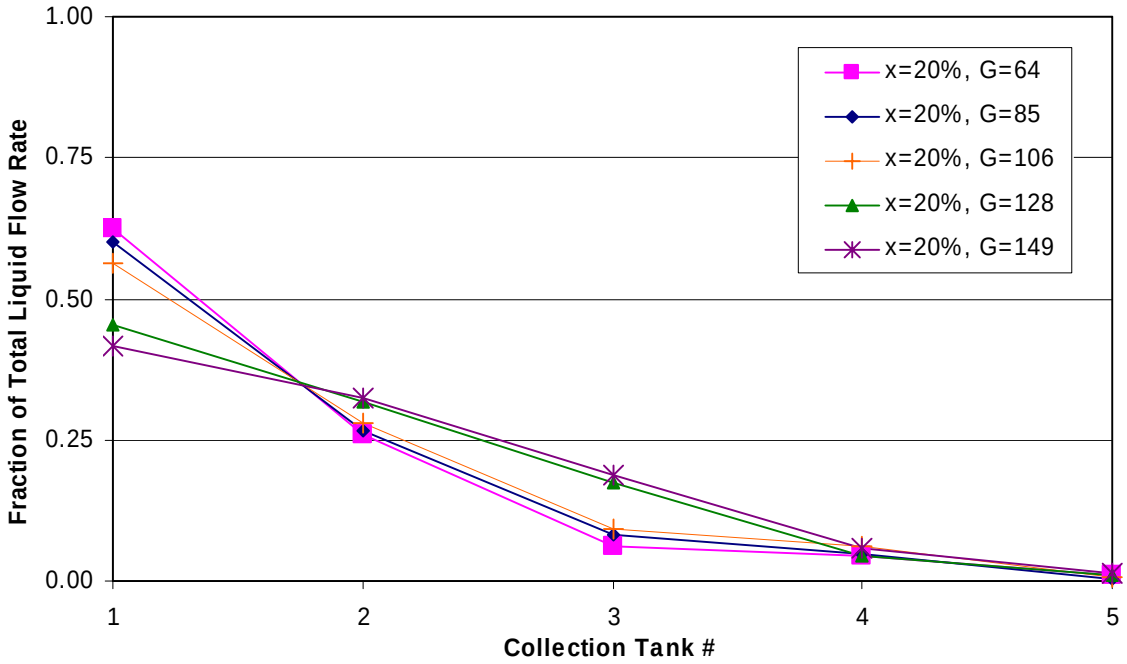

Figure B-21: 1/2 Depth Protrusion, Short Inlet, x=20%

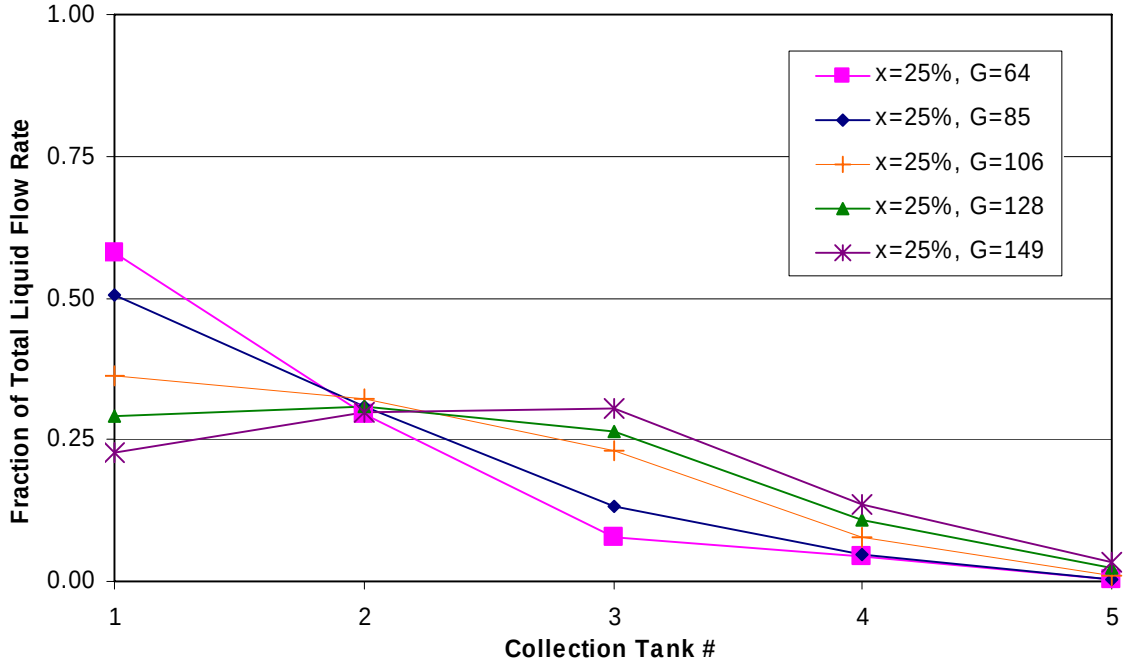

Figure B-22: 1/2 Depth Protrusion, Short Inlet, x=25%

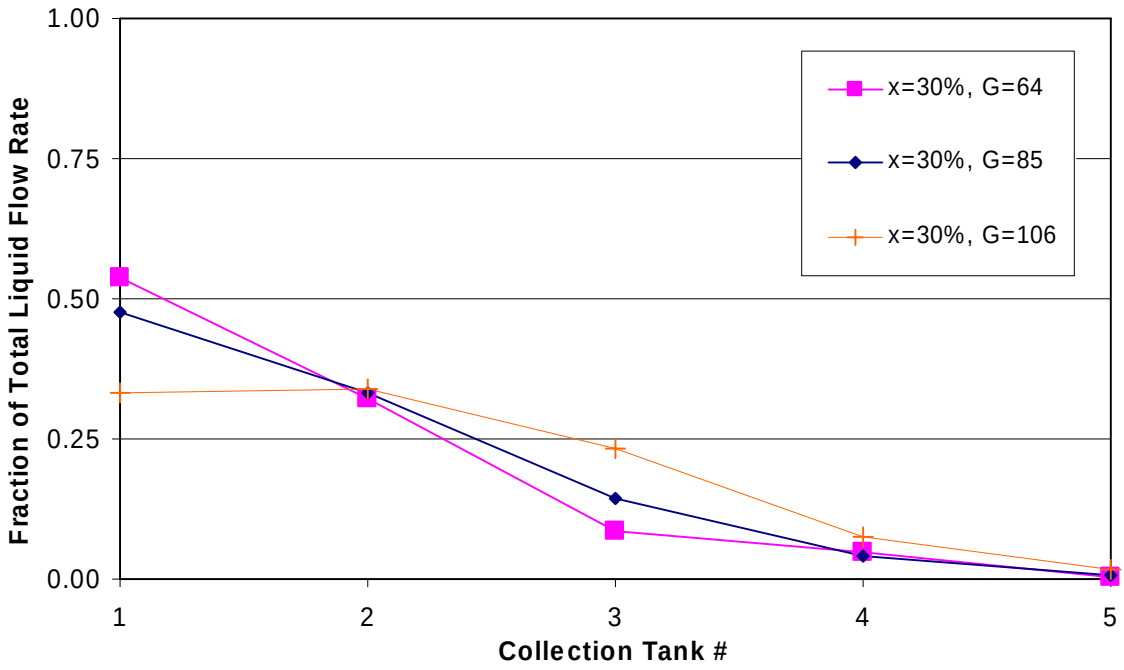

Figure B-23: 1/2 Depth Protrusion, Short Inlet, x=30%

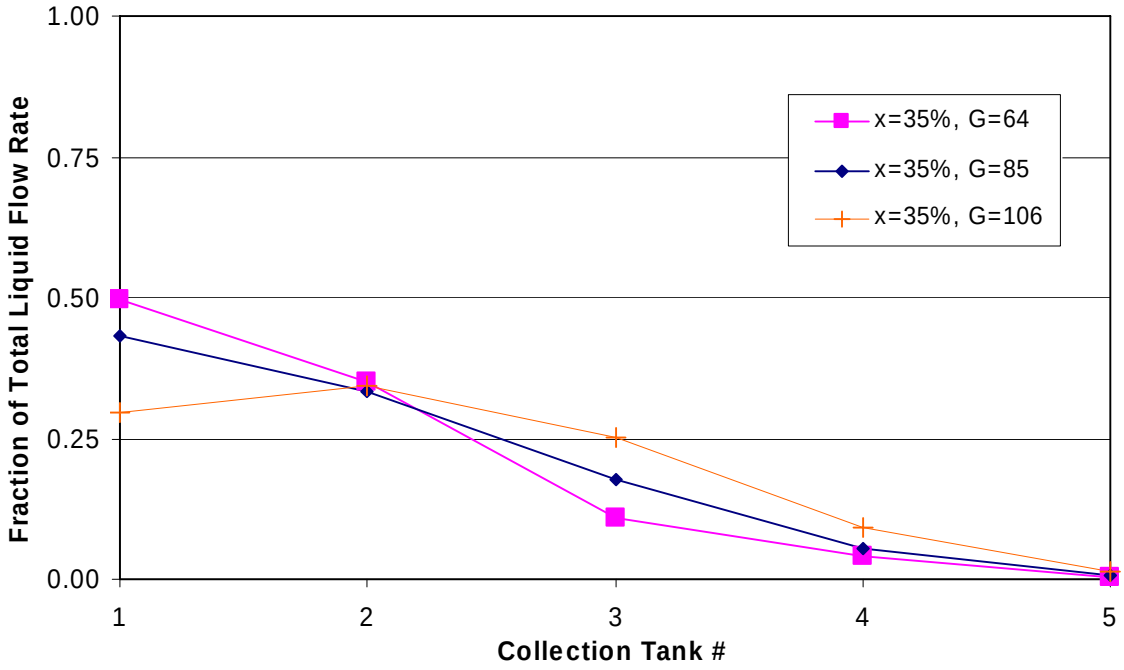

Figure B-24: 1/2 Depth Protrusion, Short Inlet, x=35%

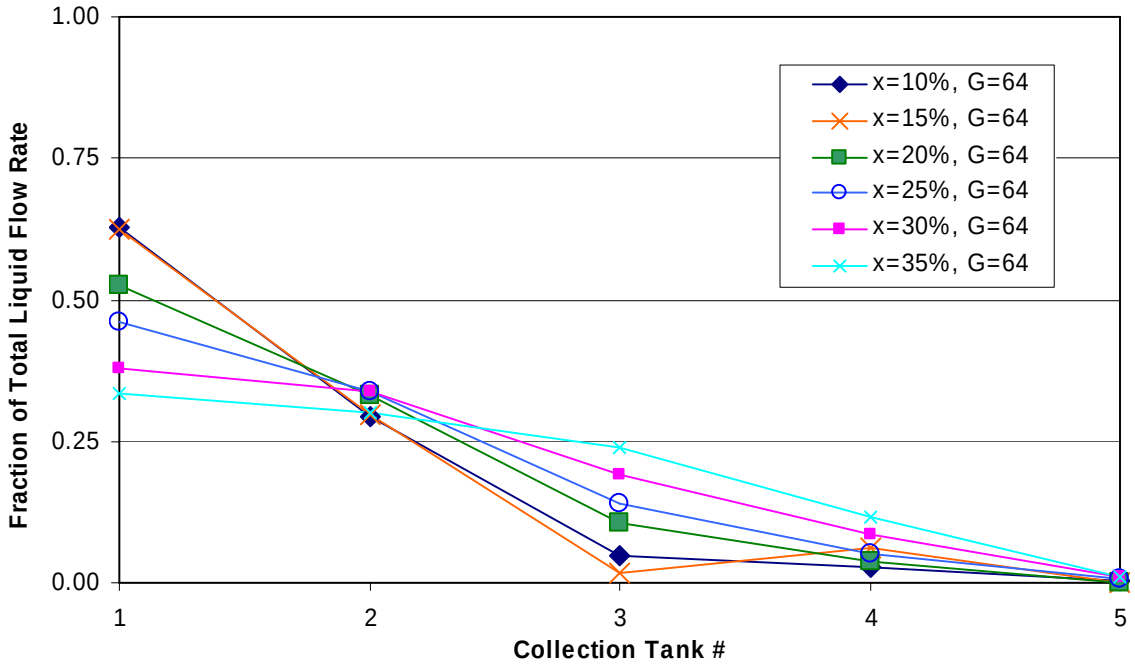

Figure B-25: 3/4 Depth Protrusion, Short Inlet, G=64 kg/m^{2}s

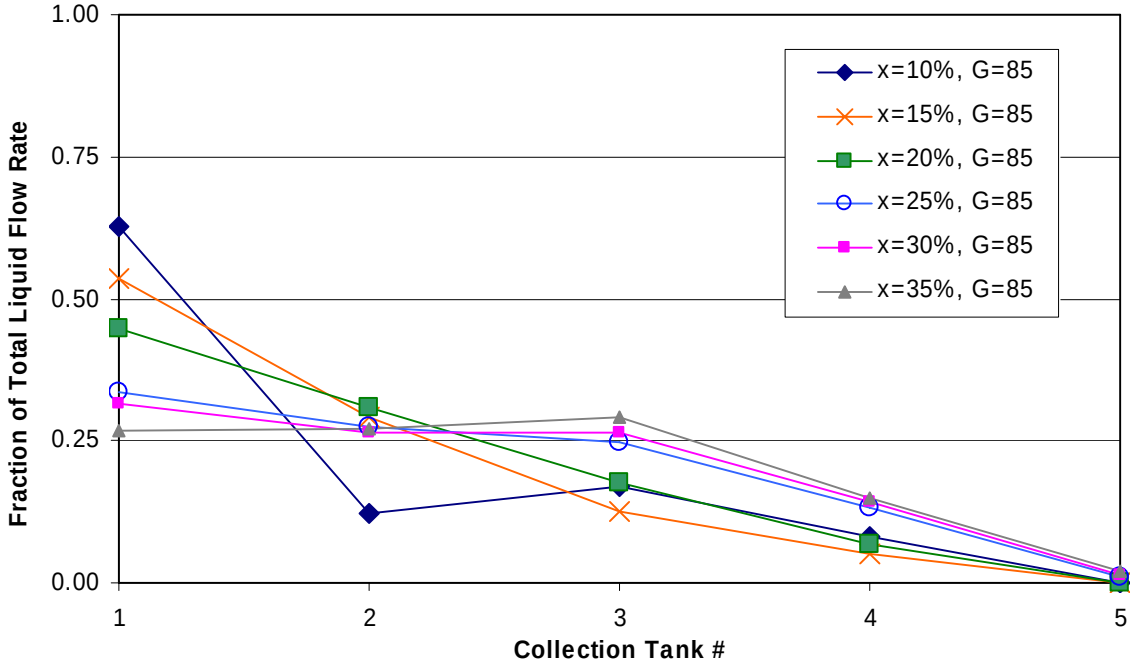

Figure B-26: 3/4 Depth Protrusion, Short Inlet, G=85 kg/m^{2}s

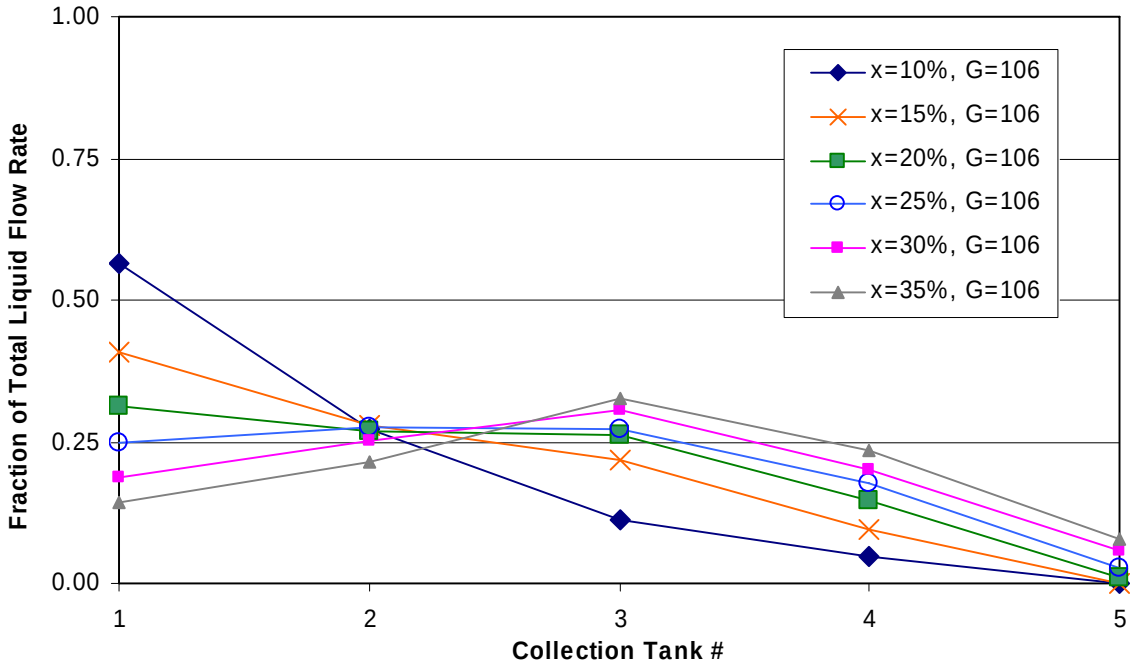

Figure B-27: 3/4 Depth Protrusion, Short Inlet, G=106 kg/m^{2}s

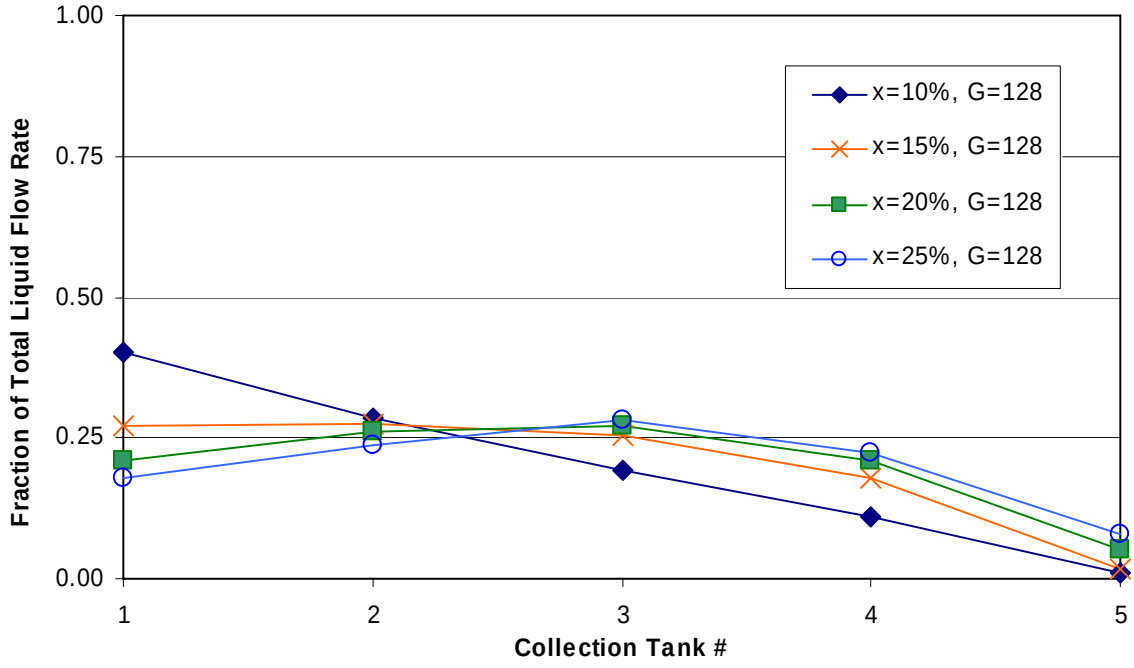

Figure B-28: 3/4 Depth Protrusion, Short Inlet, G=128 kg/m^{2}s

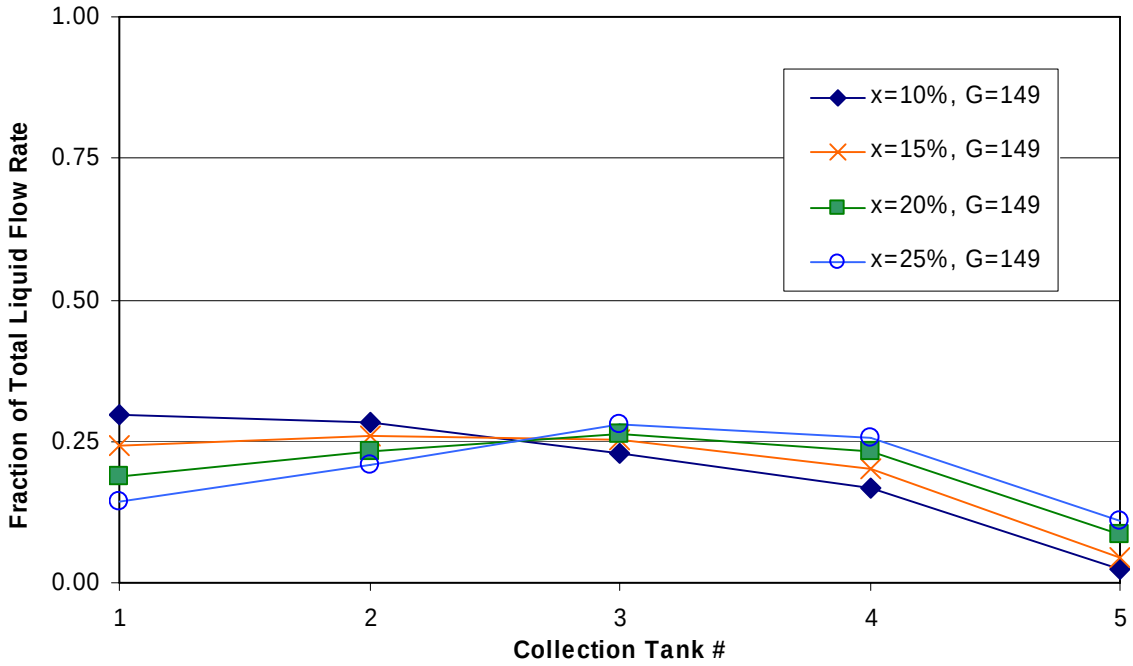

Figure B-29: 3/4 Depth Protrusion, Short Inlet, G=149 kg/m^{2}s

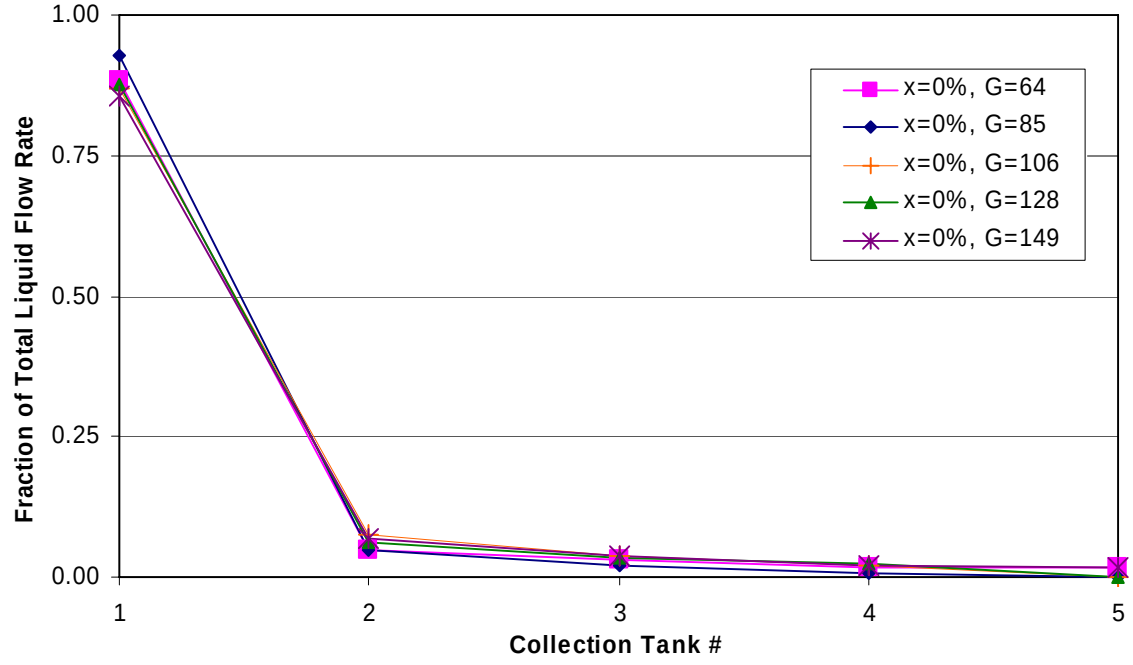

Figure B-30: 3/4 Depth Protrusion, Short Inlet, x=0%

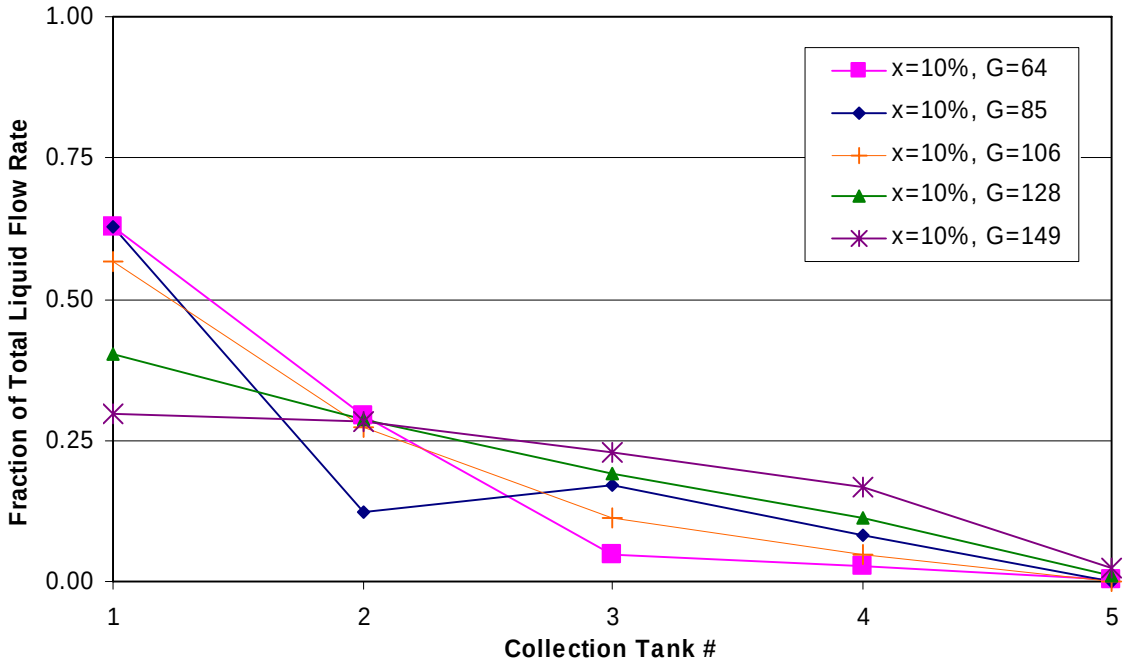

Figure B-31: 3/4 Depth Protrusion, Short Inlet, x=10%

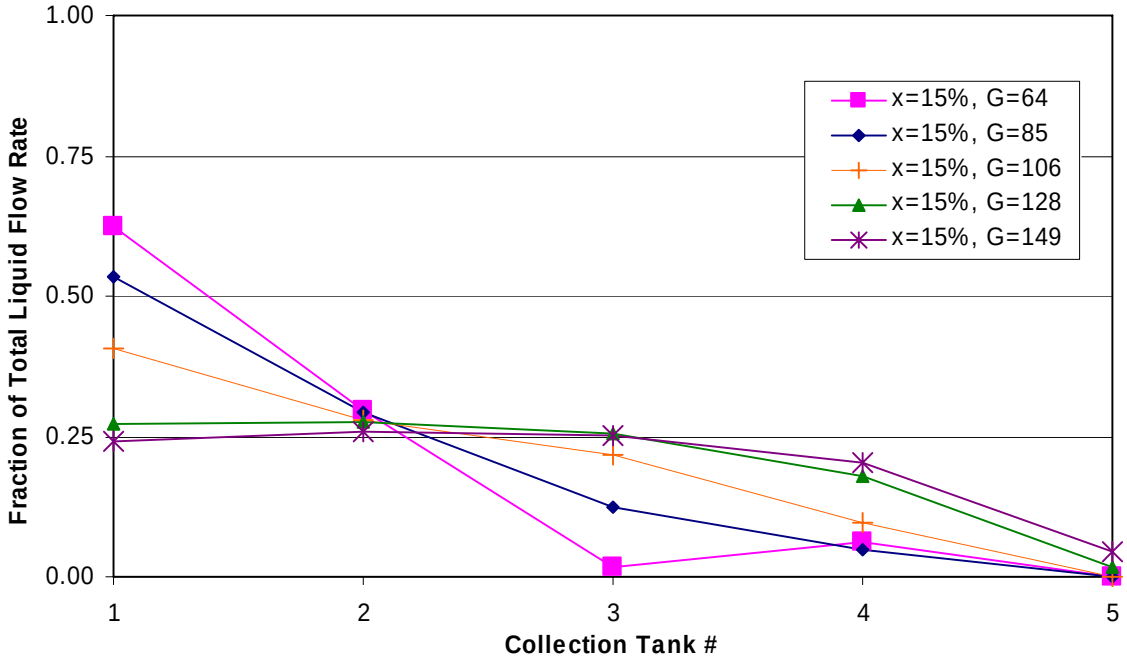

Figure B-32: 3/4 Depth Protrusion, Short Inlet, x=15%

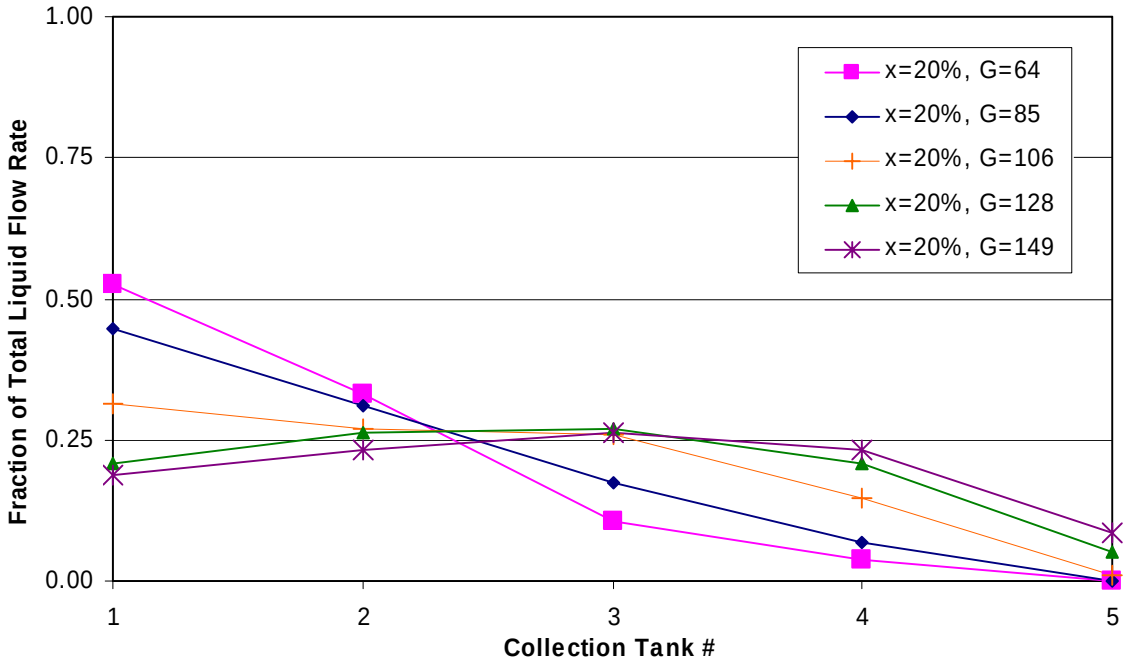

Figure B-33: 3/4 Depth Protrusion, Short Inlet, x=20%

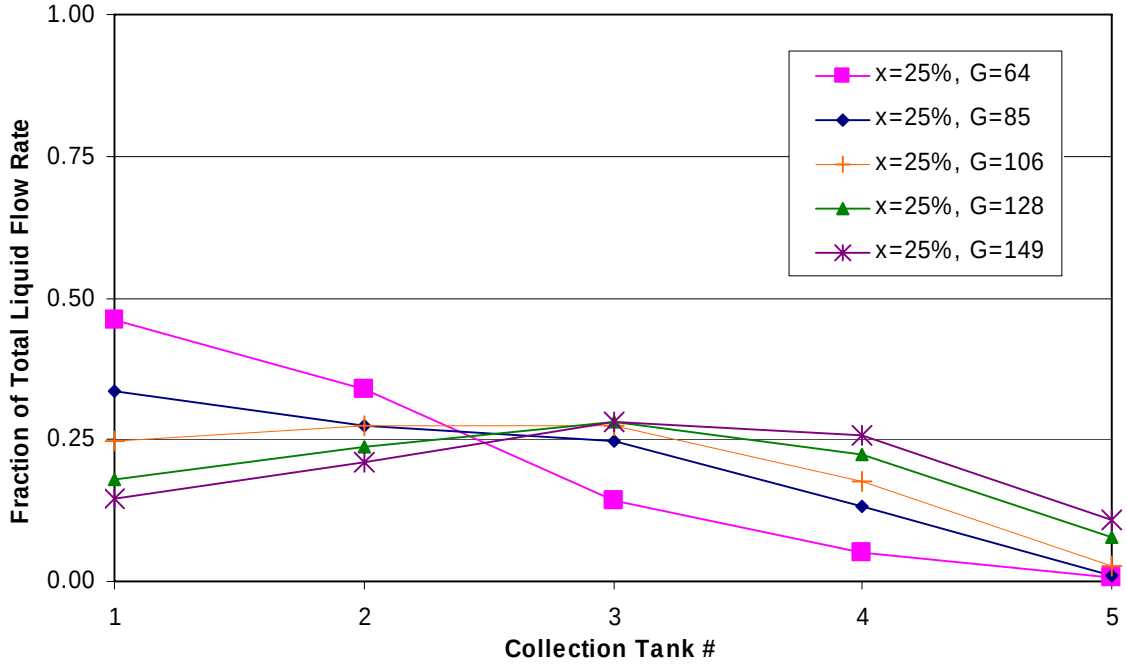

Figure B-34: 3/4 Depth Protrusion, Short Inlet, x=25%

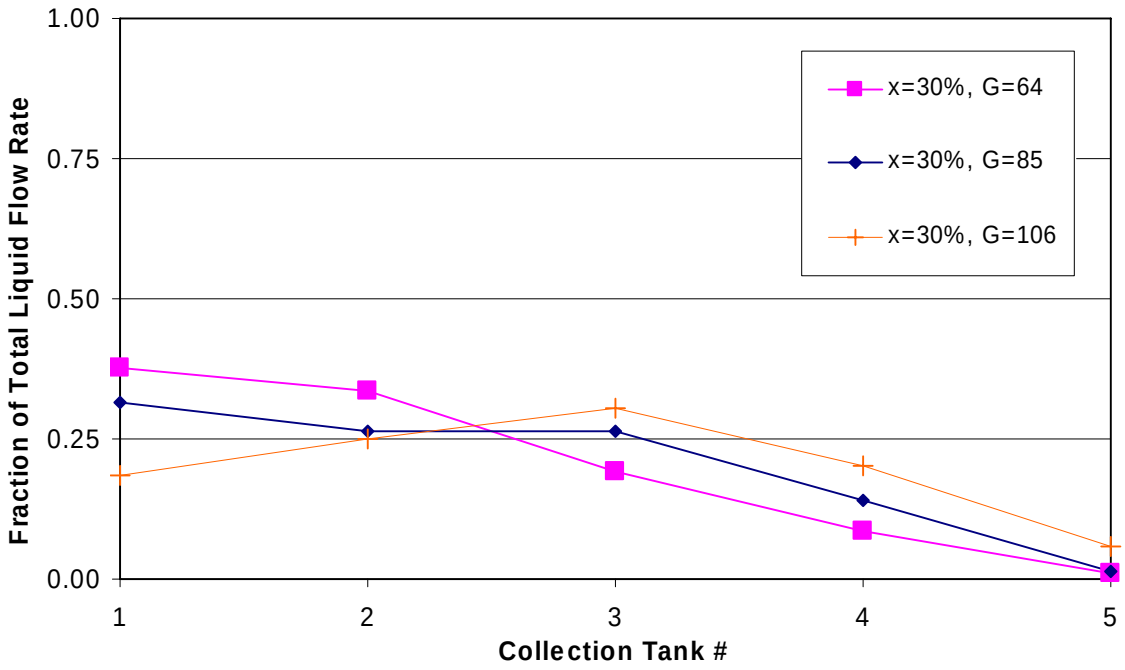

Figure B-35: 3/4 Depth Protrusion, Short Inlet, x=30%

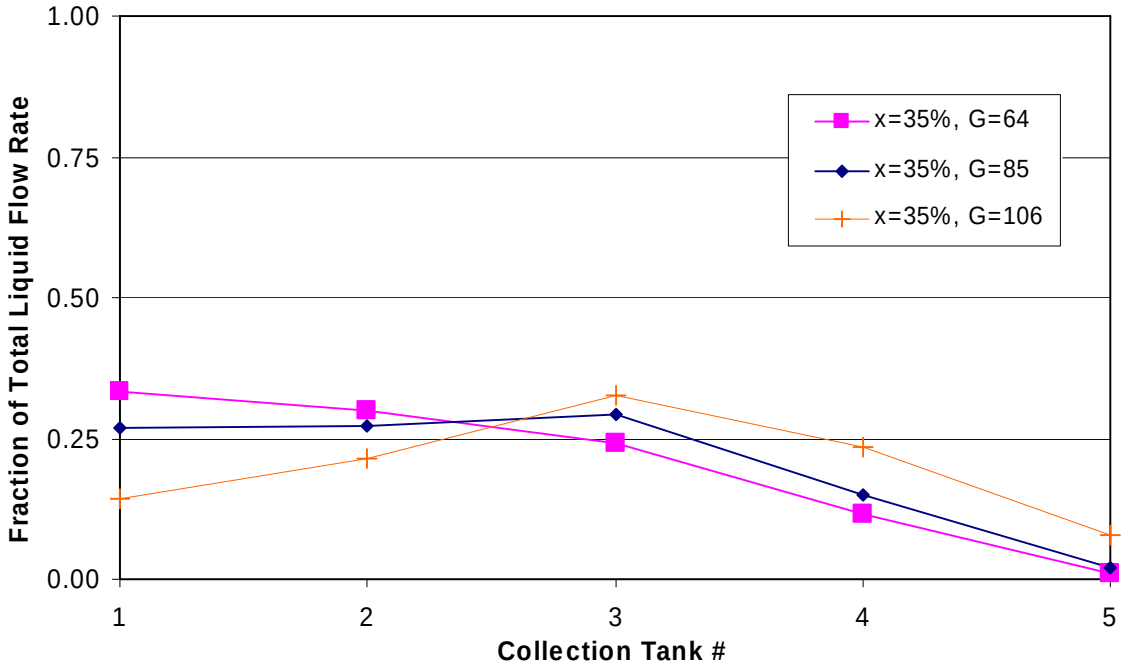

Figure B-36: 3/4 Depth Protrusion, Short Inlet, x=35%

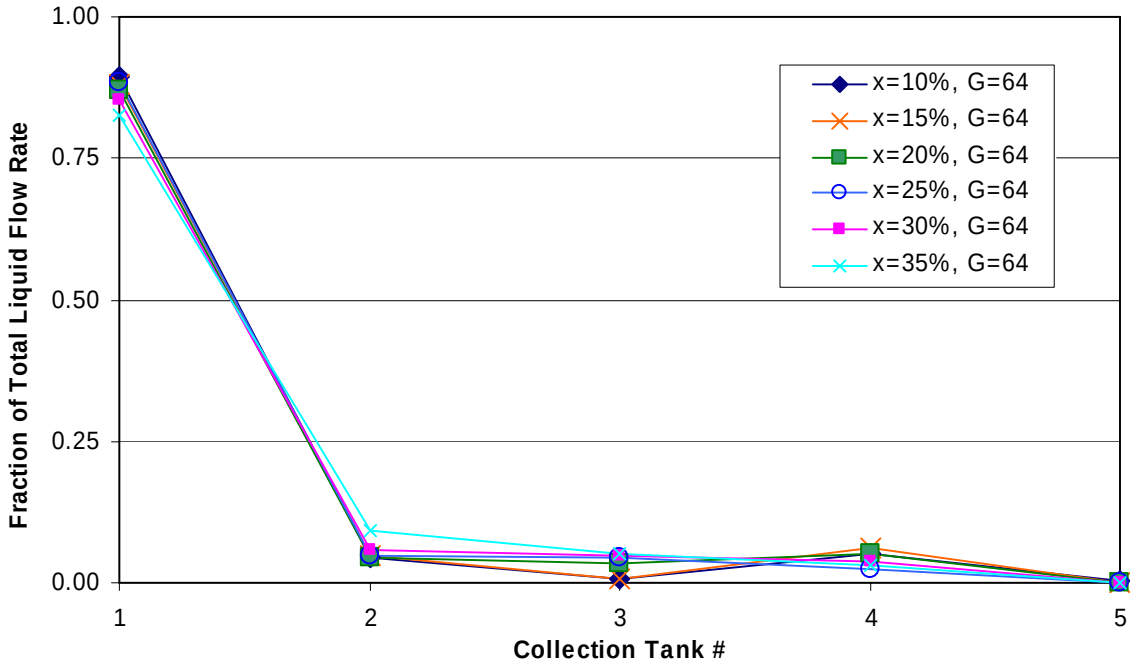

Figure B-37: 1/4 Depth Protrusion, Long Inlet, G=64 kg/m^{2}s

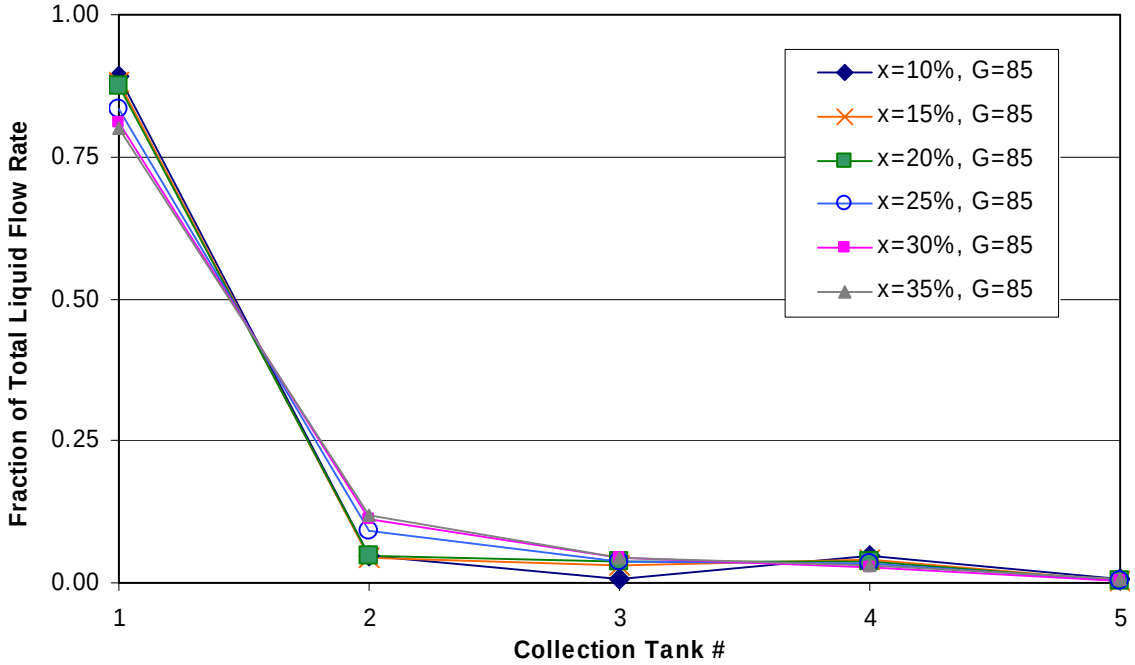

Figure B-38: 1/4 Depth Protrusion, Long Inlet, G=85 kg/m^{2}s

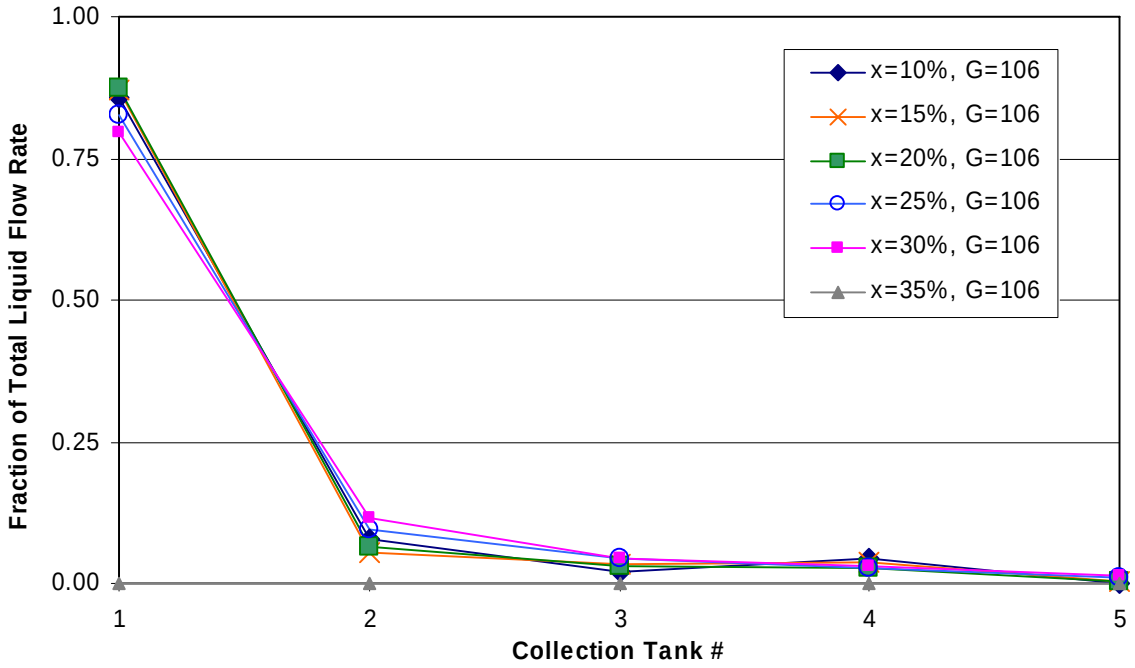

Figure B-39: 1/4 Depth Protrusion, Long Inlet, G=106 kg/m^{2}s

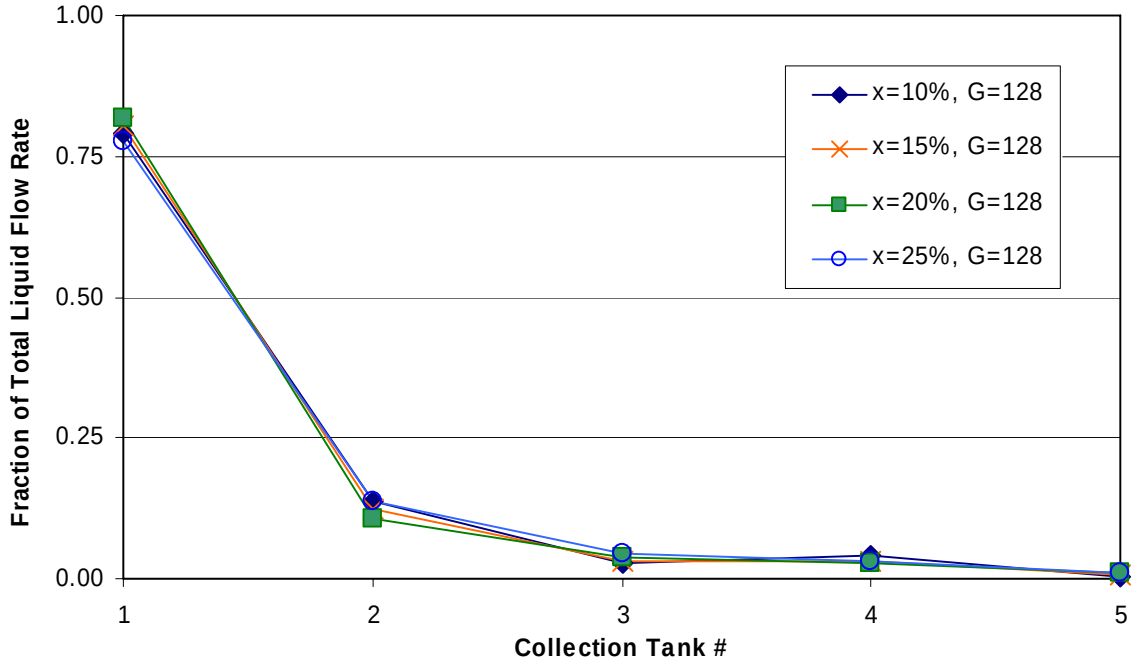

Figure B-40: 1/4 Depth Protrusion, Long Inlet, G=128 kg/m^{2}s

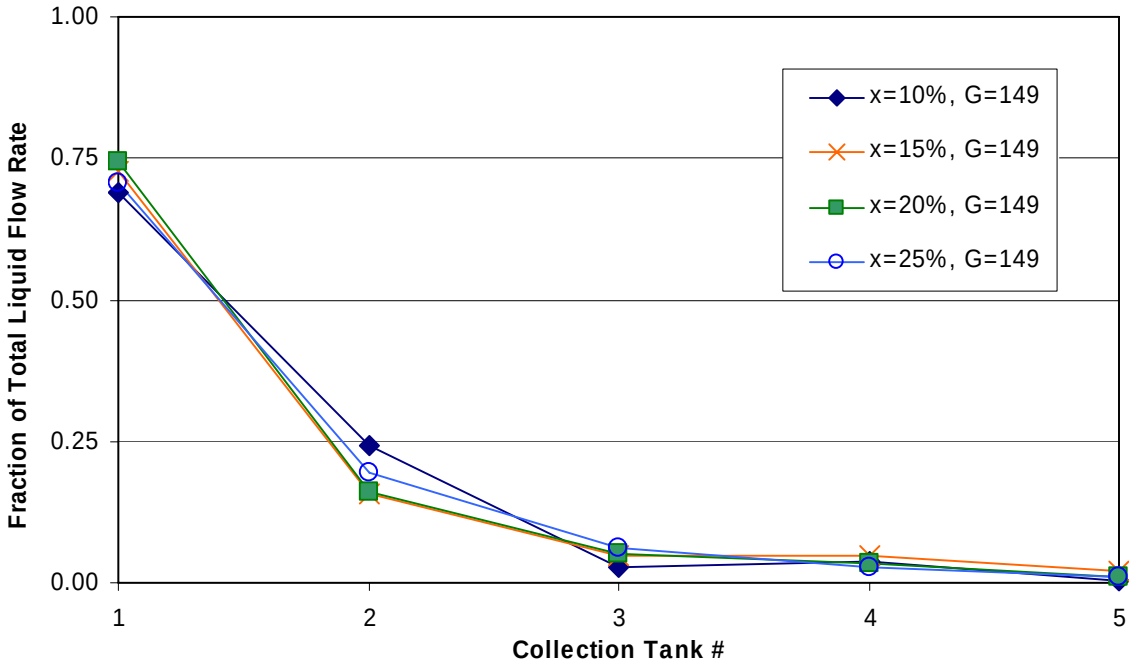

Figure B-41: 1/4 Depth Protrusion, Long Inlet, G=149 kg/m^{2}s

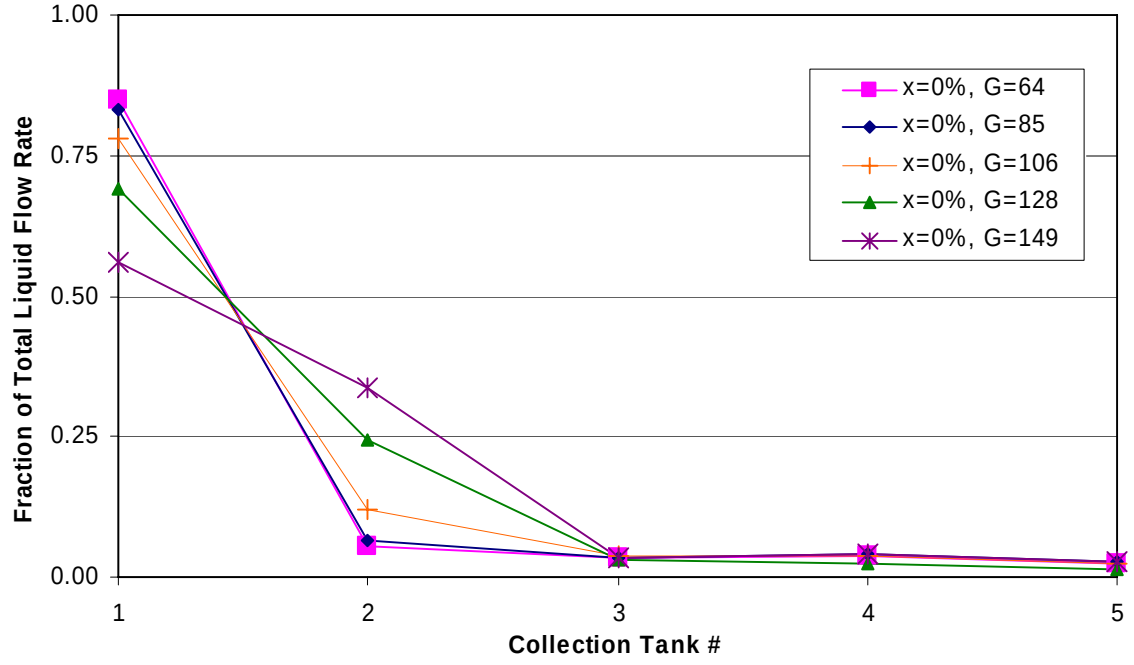

Figure B-42: 1/4 Depth Protrusion, Long Inlet, x=0%

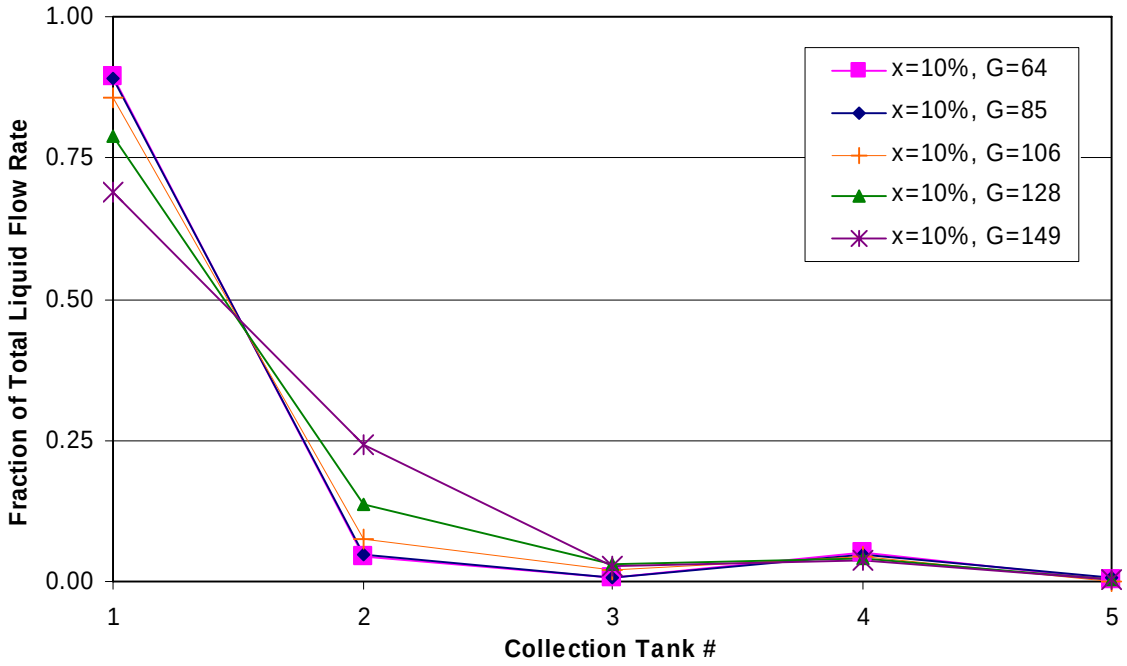

Figure B-43: 1/4 Depth Protrusion, Long Inlet, x=10%

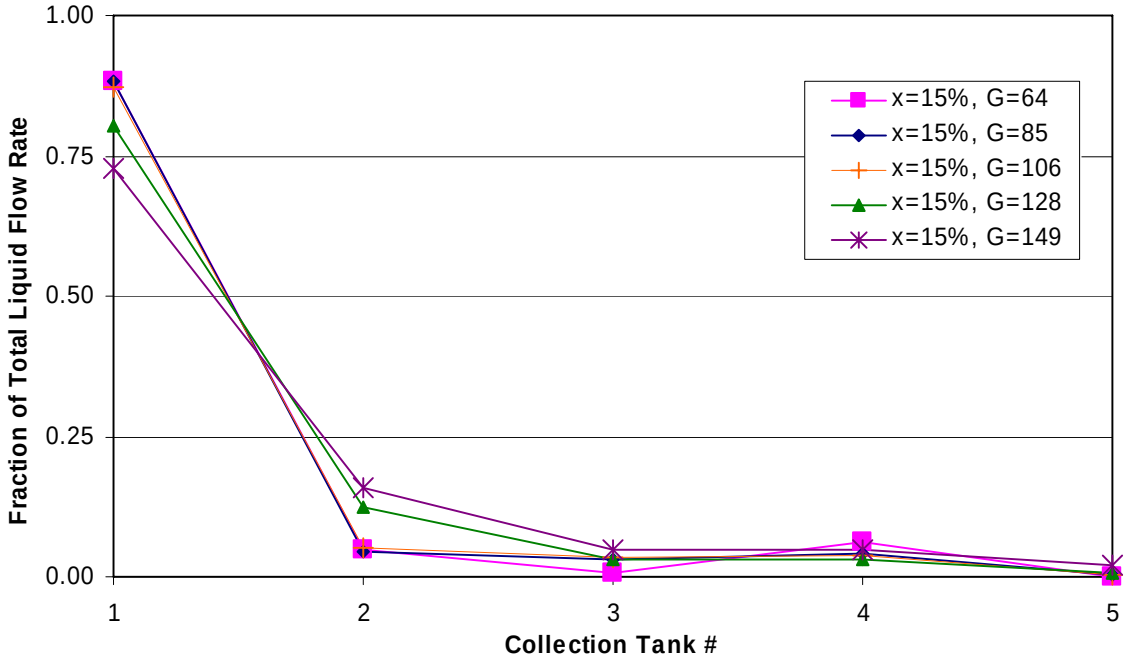

Figure B-44: 1/4 Depth Protrusion, Long Inlet, x=15%

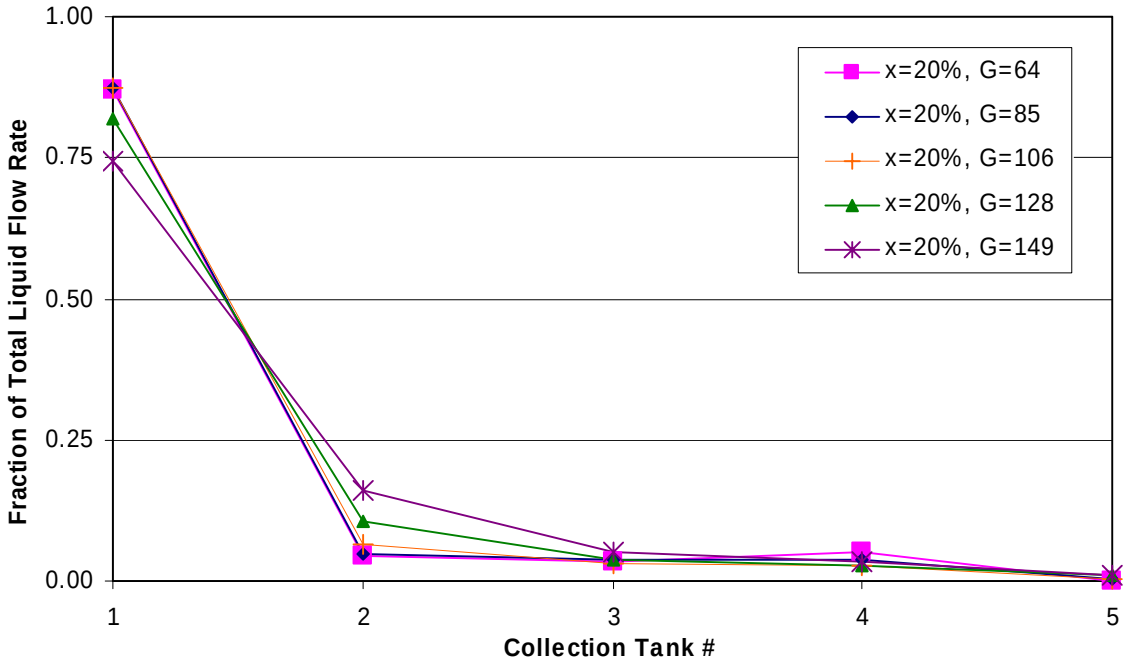

Figure B-45: 1/4 Depth Protrusion, Long Inlet, x=20%

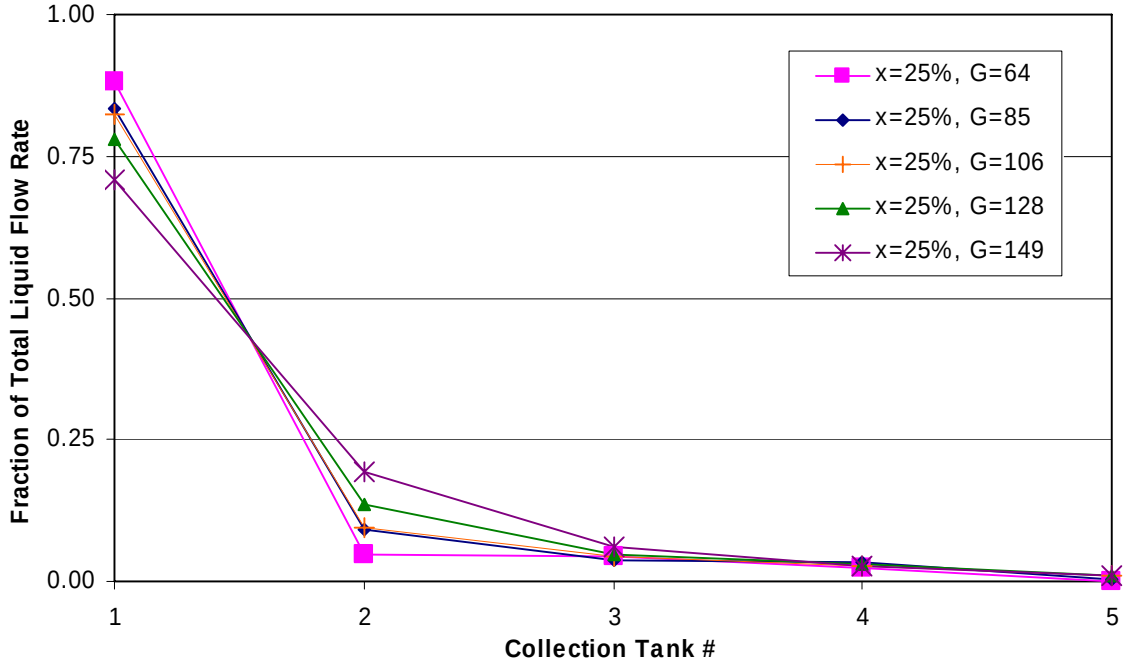

Figure B-46: 1/4 Depth Protrusion, Long Inlet, x=25%

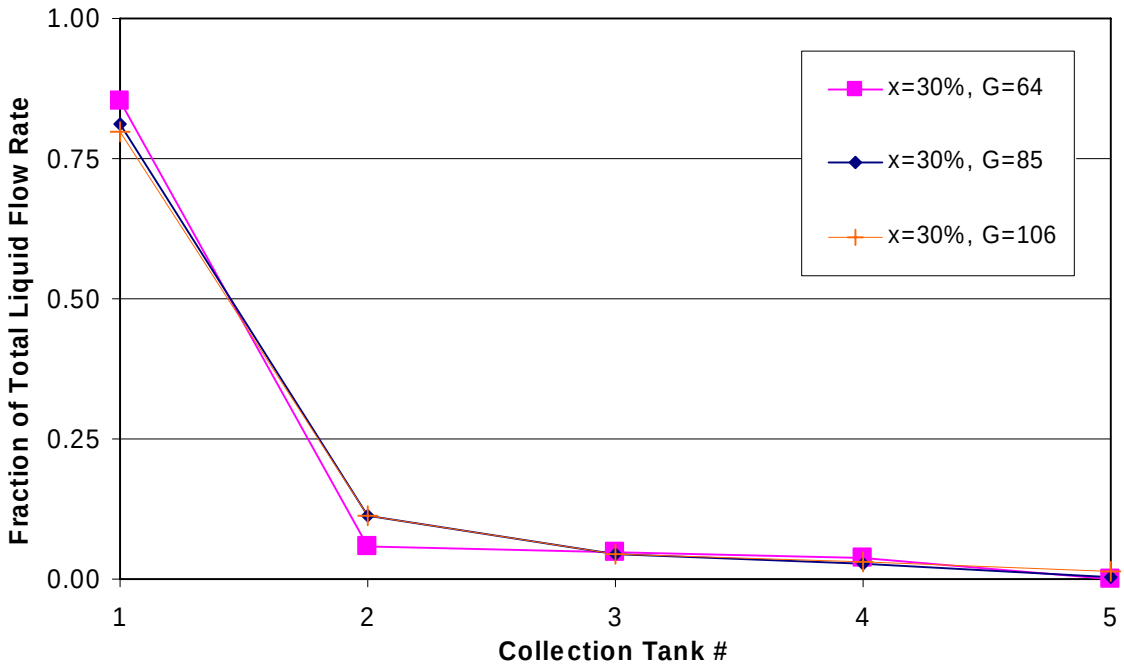

Figure B-47: 1/4 Depth Protrusion, Long Inlet, x=30%

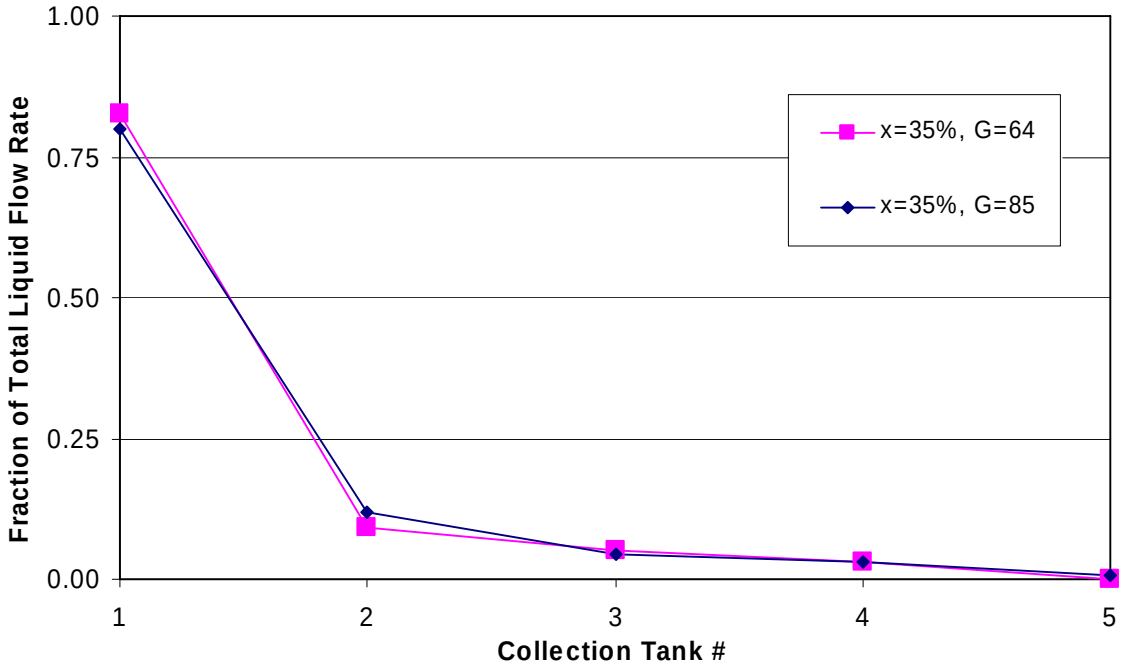

Figure B-48: 1/4 Depth Protrusion, Long Inlet, x=35%

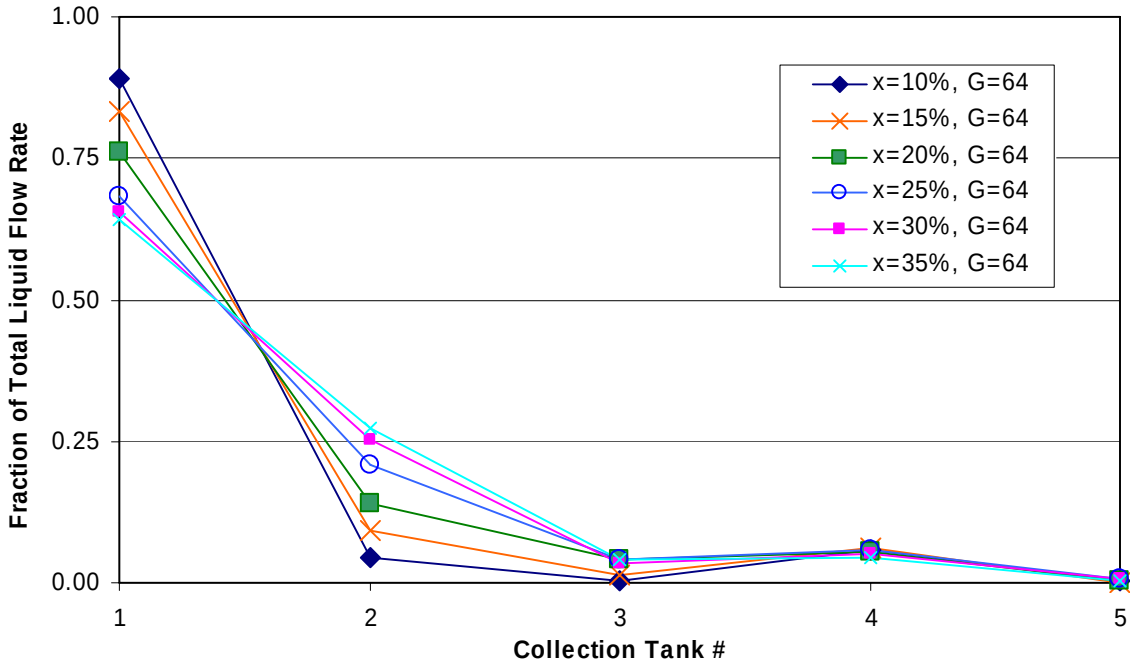

Figure B-49: 1/2 Depth Protrusion, Long Inlet, G=64 kg/m^{2}s

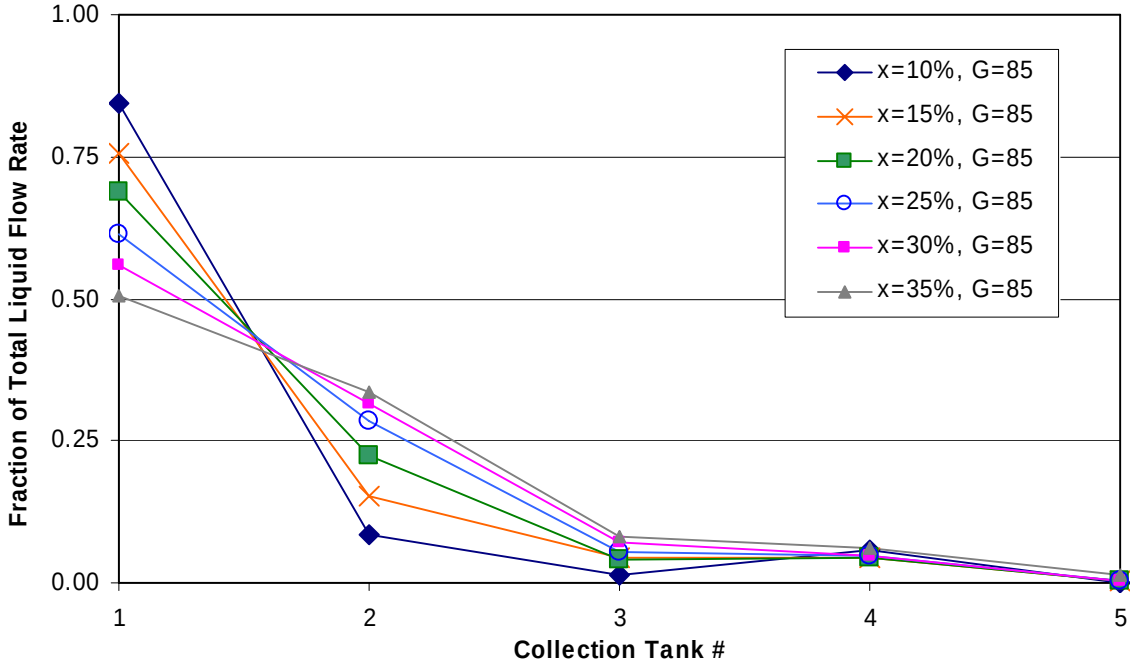

Figure B-50: 1/2 Depth Protrusion, Long Inlet, G=85 kg/m^{2}s

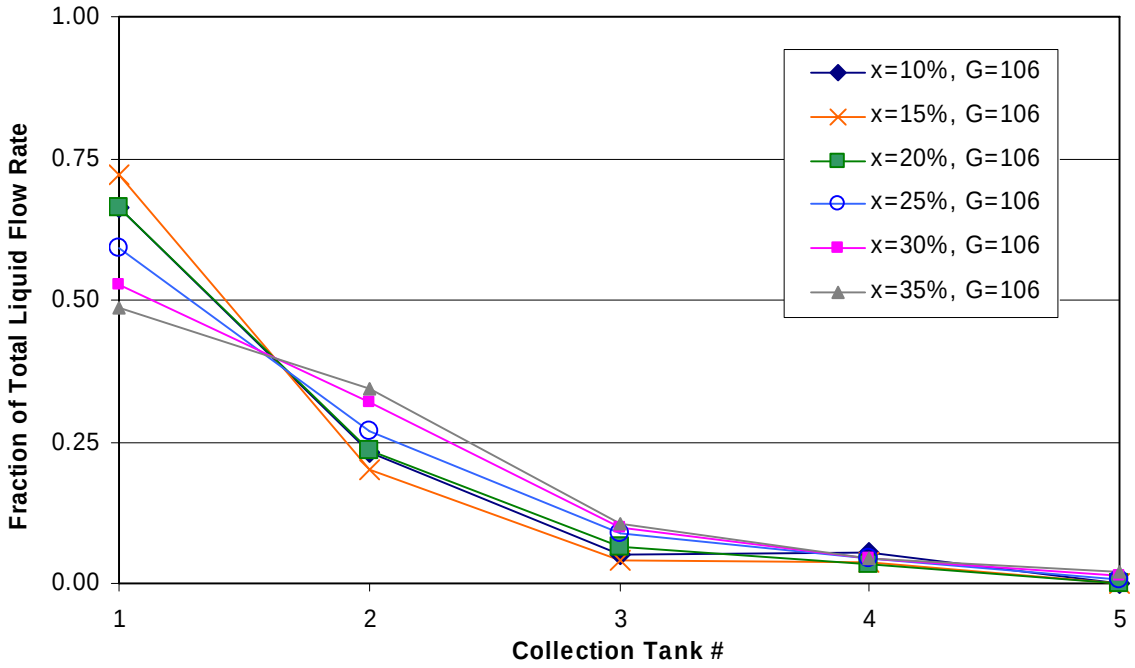

Figure B-51: 1/2 Depth Protrusion, Long Inlet, G=106 kg/m^{2}s

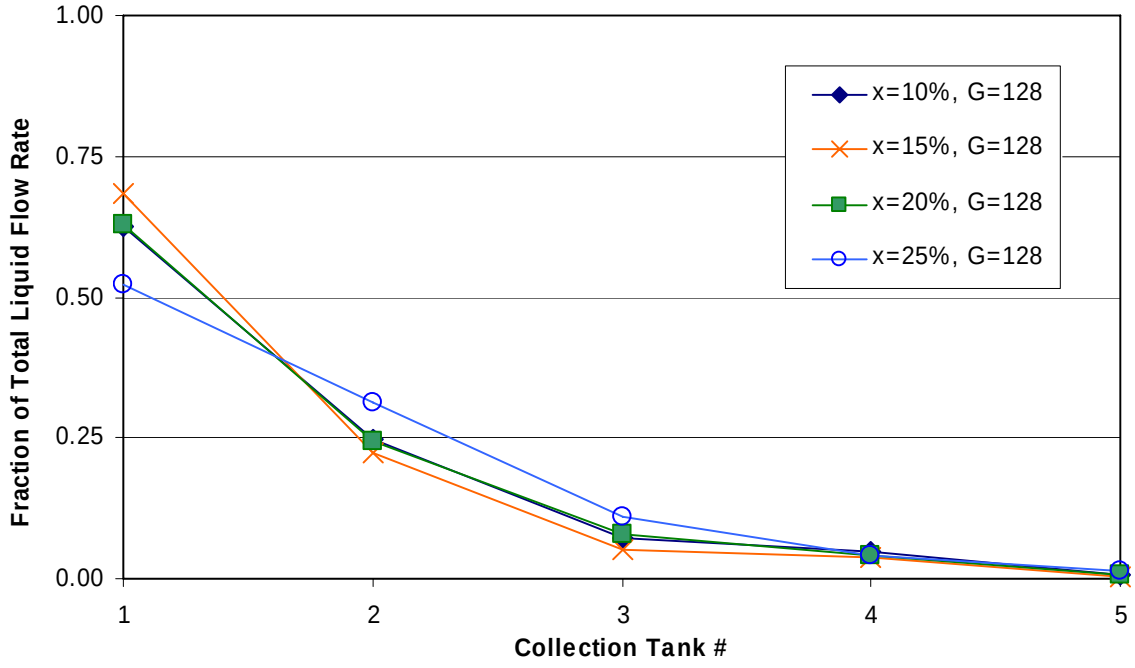

Figure B-52: 1/2 Depth Protrusion, Long Inlet, G=128 kg/m^{2}s

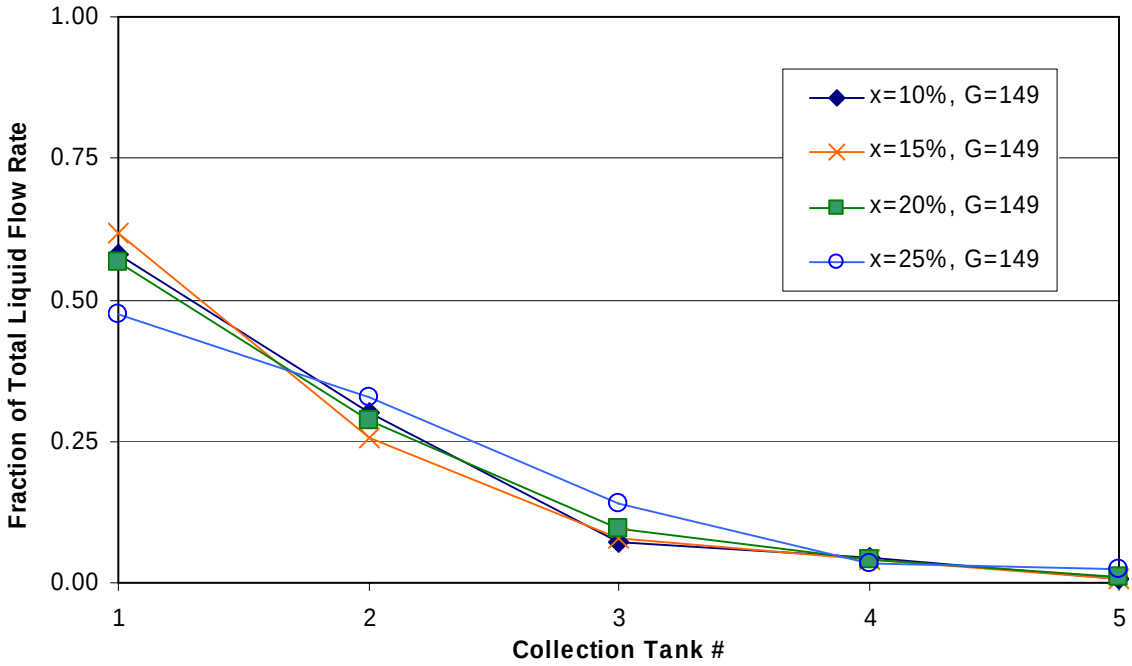

Figure B-53: 1/2 Depth Protrusion, Long Inlet, G=149 kg/m^{2}s

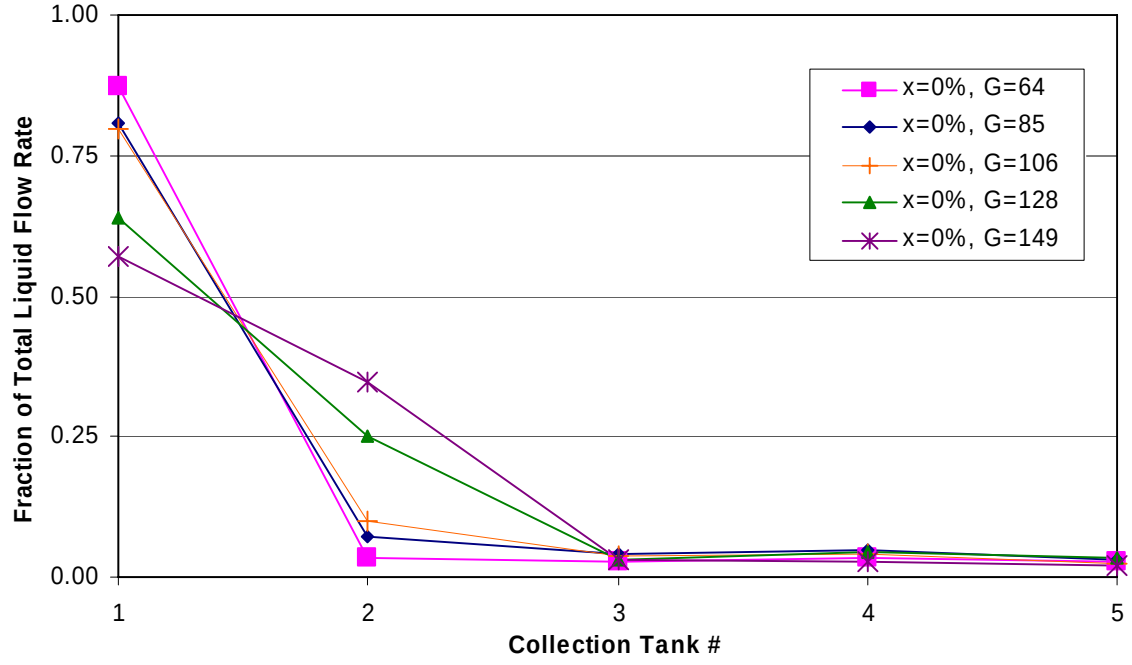

Figure B-54: 1/2 Depth Protrusion, Long Inlet, x=0%

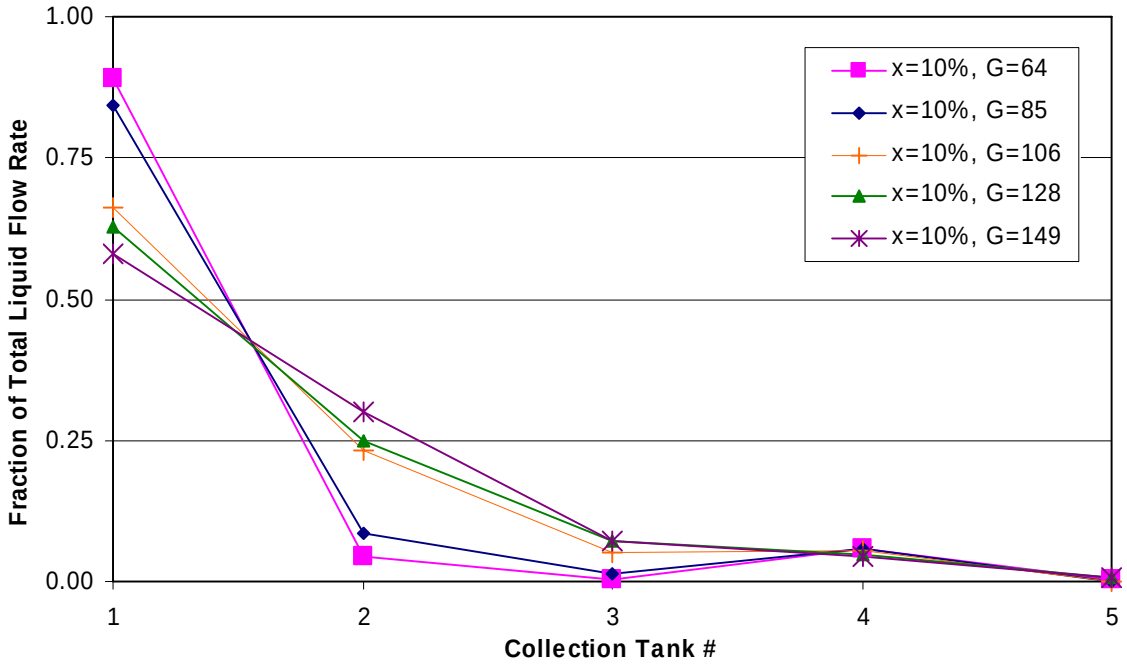

Figure B-55: 1/2 Depth Protrusion, Long Inlet, x=10%

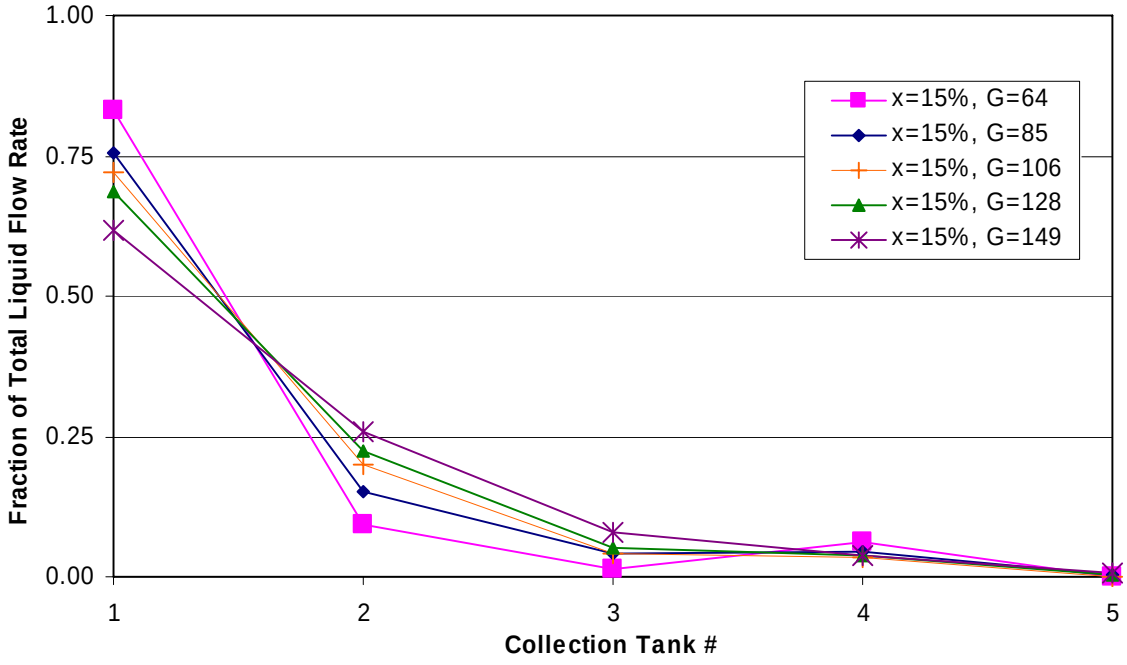

Figure B-56: 1/2 Depth Protrusion, Long Inlet, x=15%

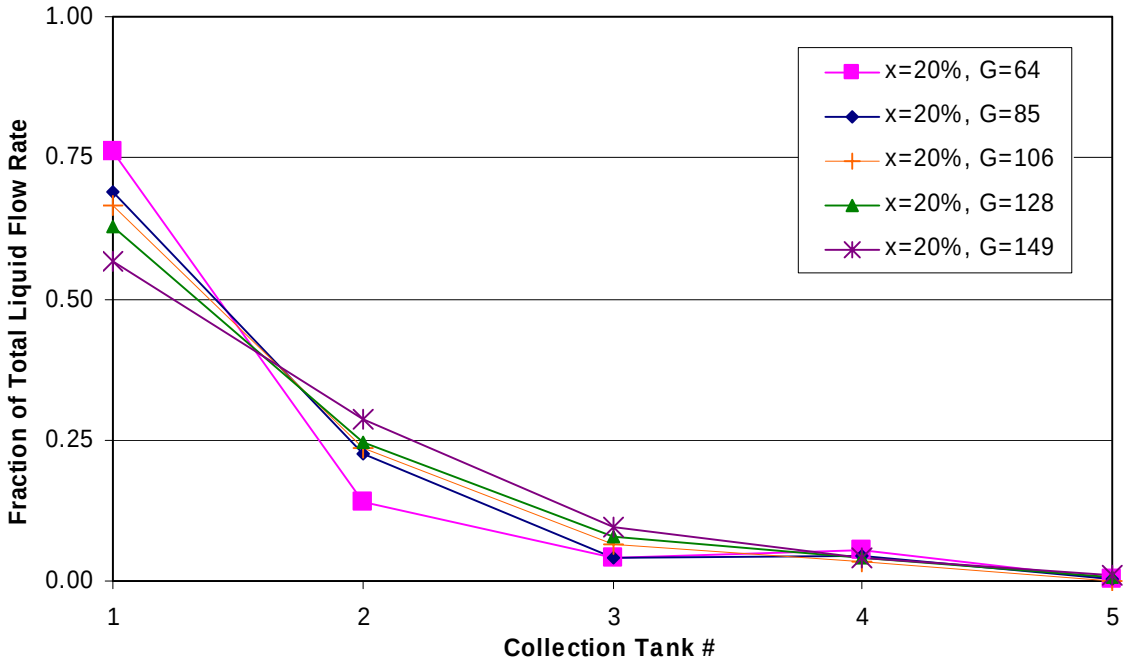

Figure B-57: 1/2 Depth Protrusion, Long Inlet, x=20%

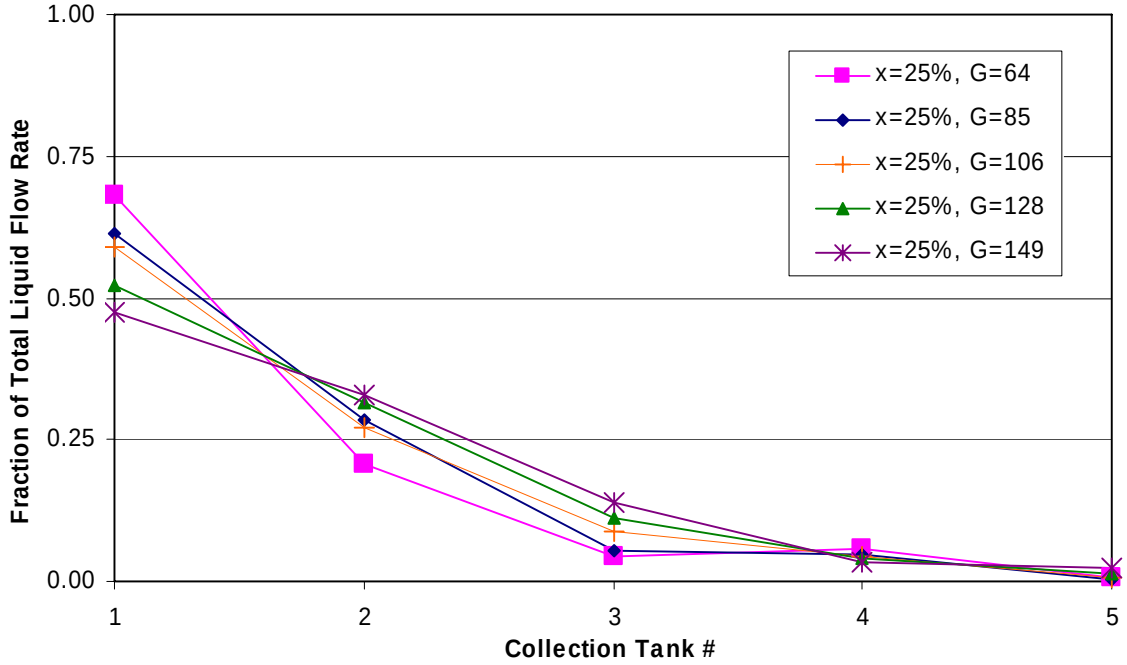

Figure B-58: 1/2 Depth Protrusion, Long Inlet, x=25%

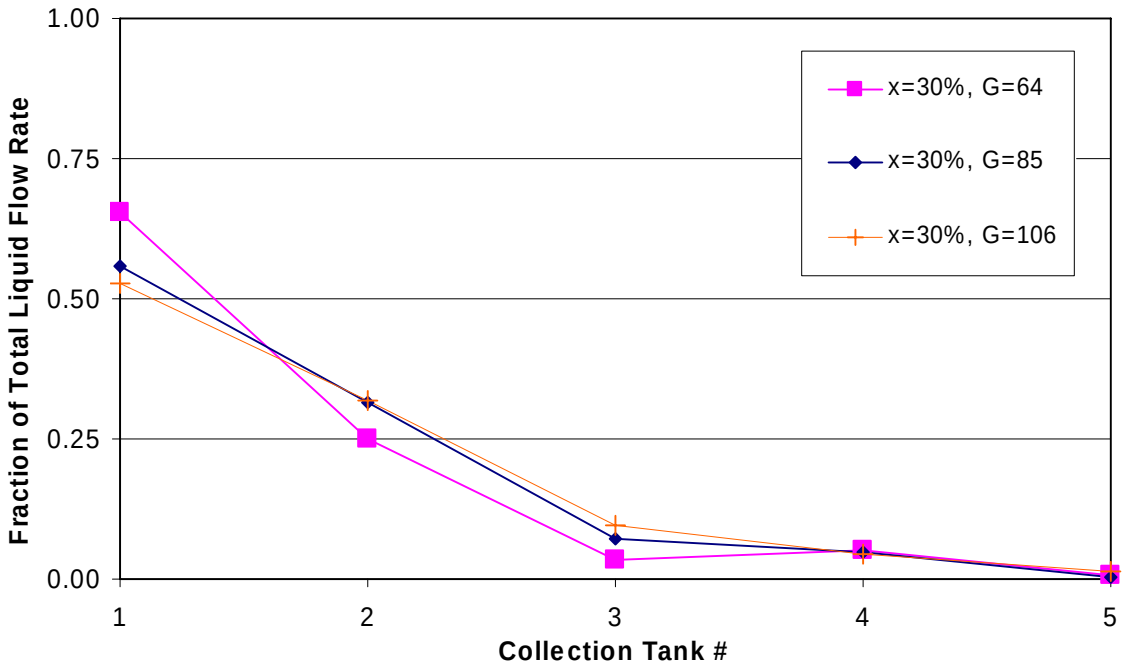

Figure B-59: 1/2 Depth Protrusion, Long Inlet, x=30%

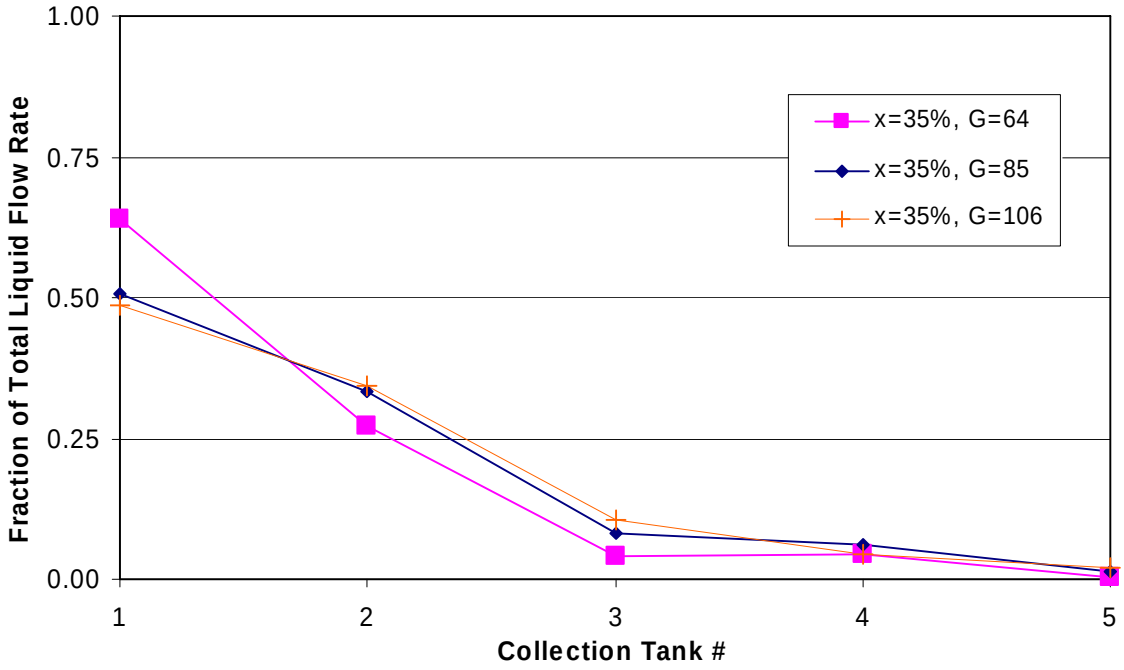

Figure B-60: 1/2 Depth Protrusion, Long Inlet, x=35%

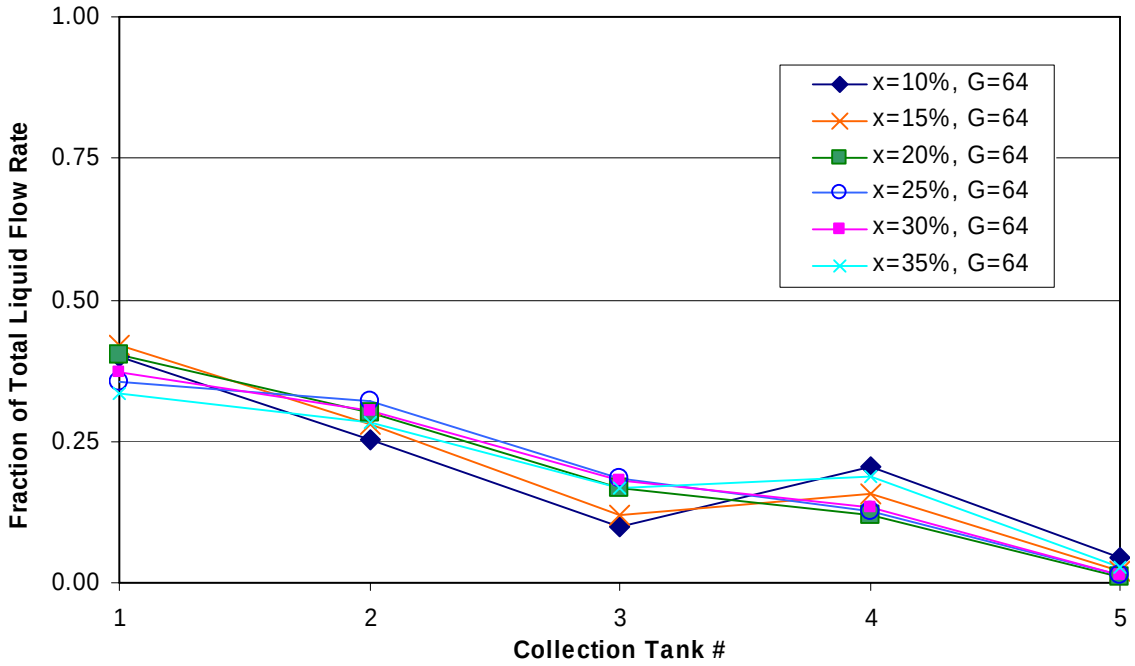

Figure B-61: 3/4 Depth Protrusion, Long Inlet, G=64 kg/m^{2}s

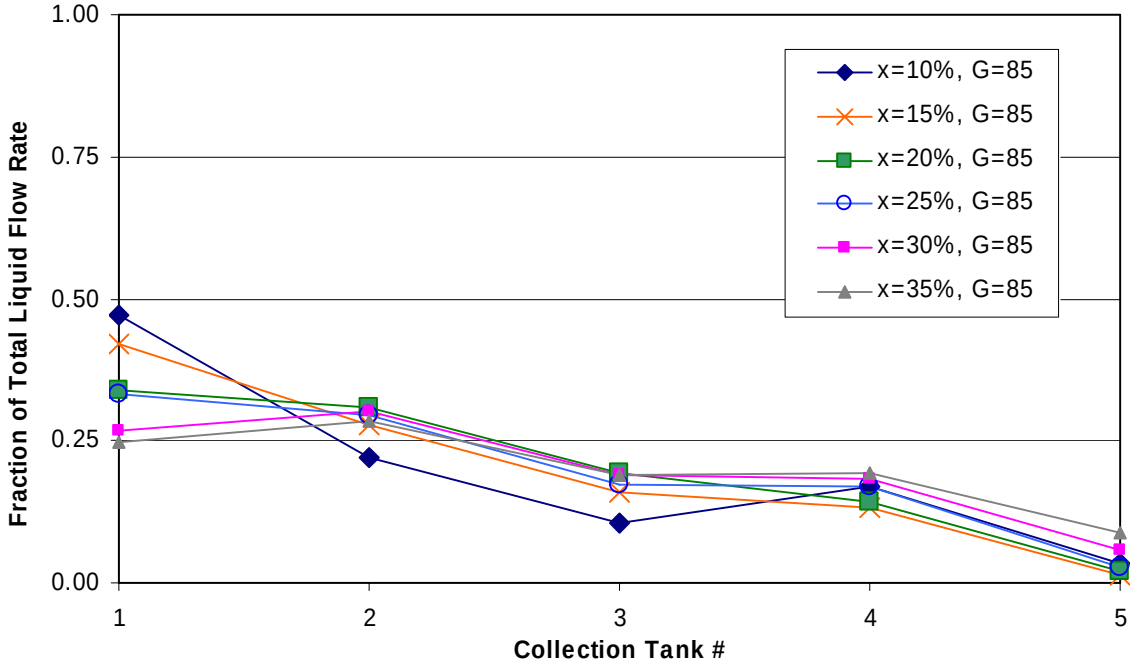

Figure B-62: 3/4 Depth Protrusion, Long Inlet, G=85 kg/m^{2}s

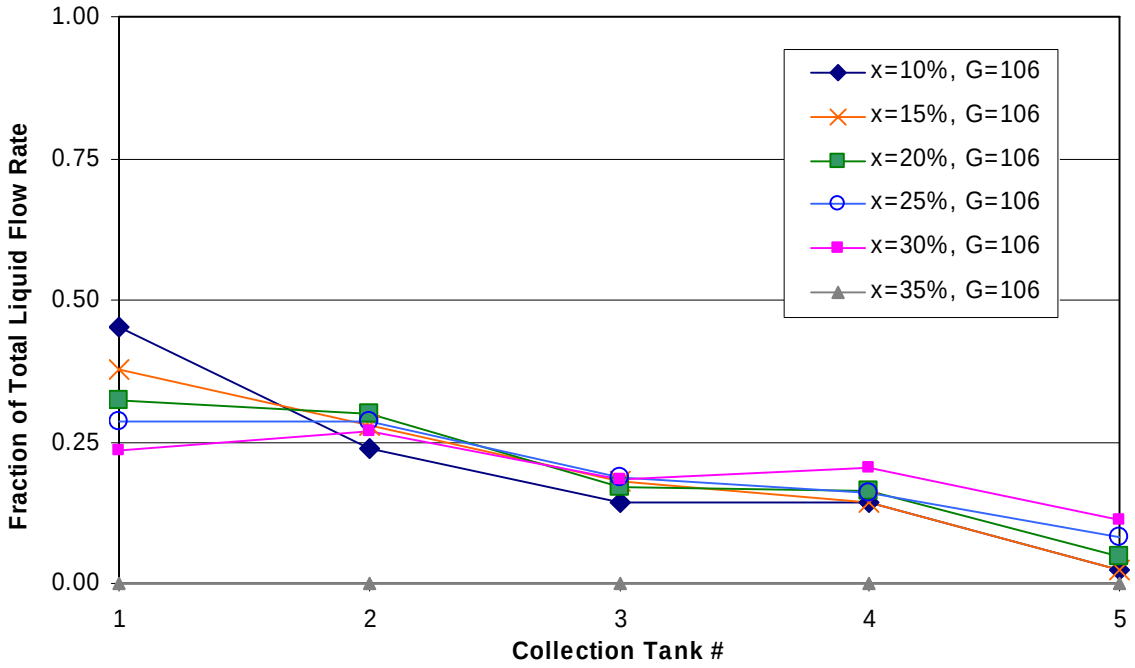

Figure B-63: 3/4 Depth Protrusion, Long Inlet, G=106 kg/m^{2}s

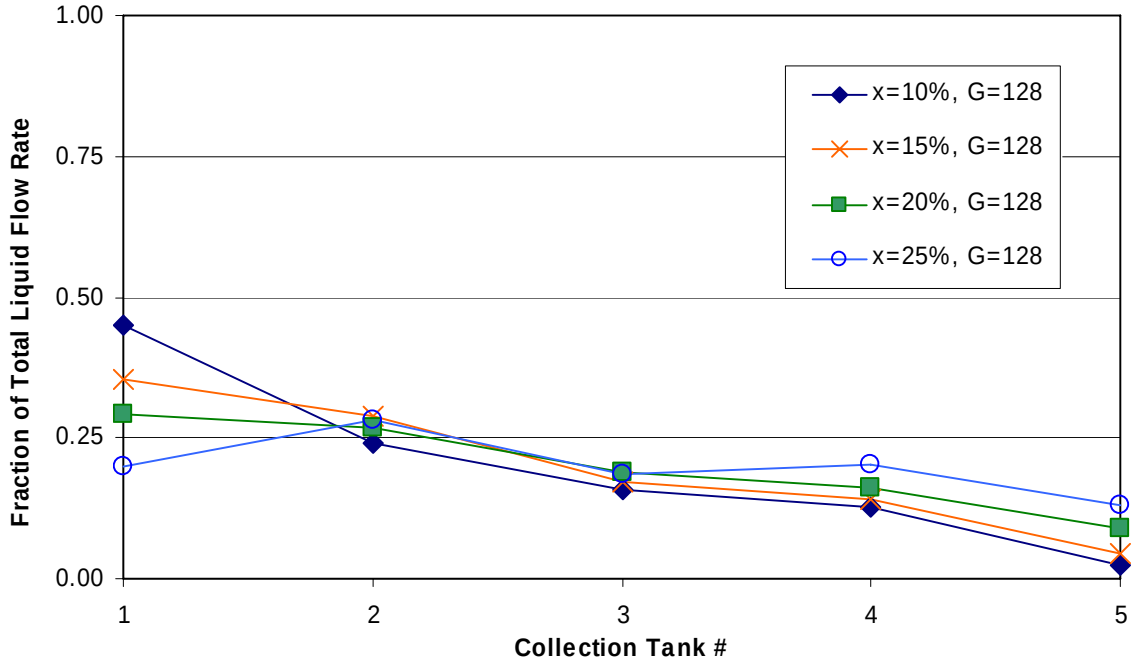

Figure B-64: 3/4 Depth Protrusion, Long Inlet, G=128 kg/m^{2}s

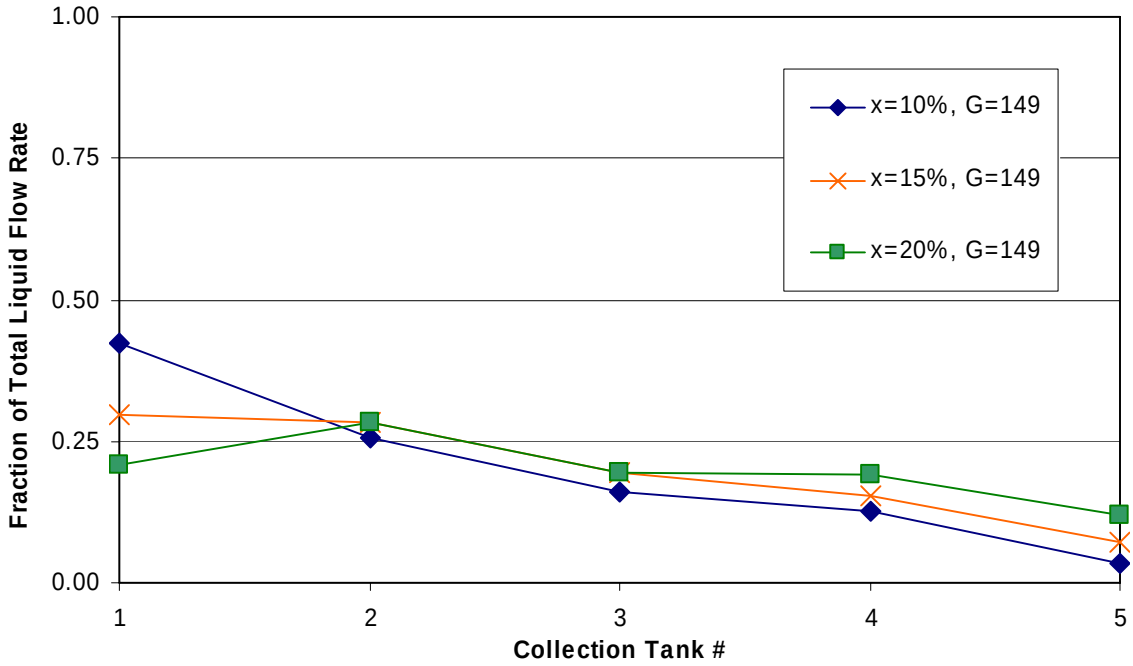

Figure B-65: 3/4 Depth Protrusion, Long Inlet, G=149 kg/m^{2}s

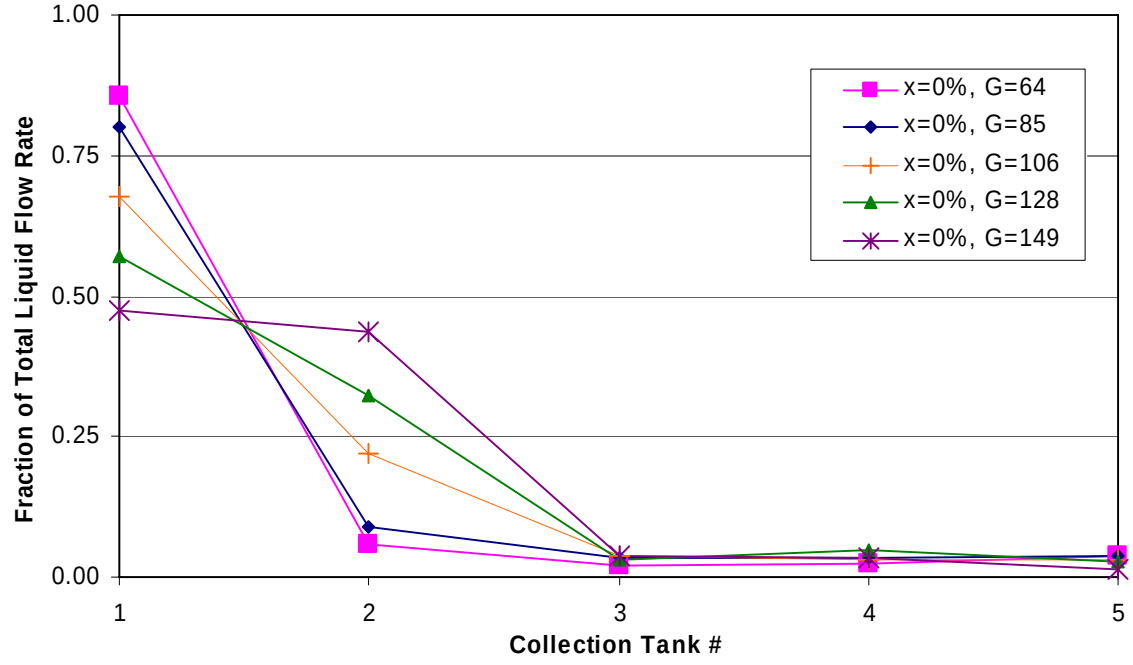

Figure B-66: 3/4 Depth Protrusion, Long Inlet, x=0%

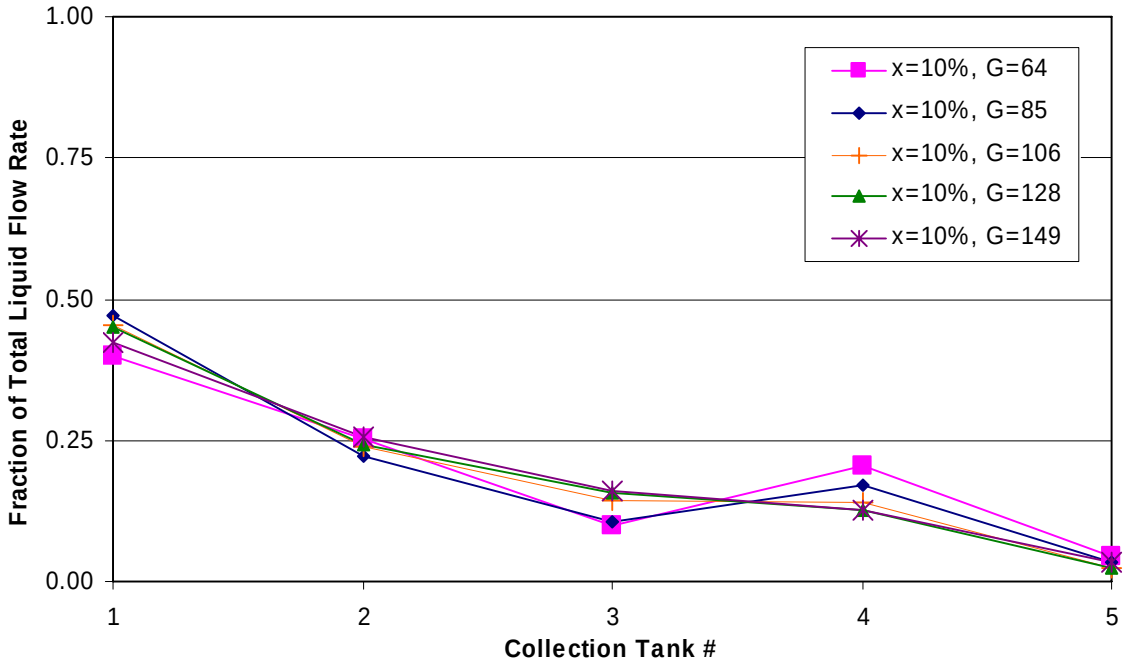

Figure B-67: 3/4 Depth Protrusion, Long Inlet, x=10%

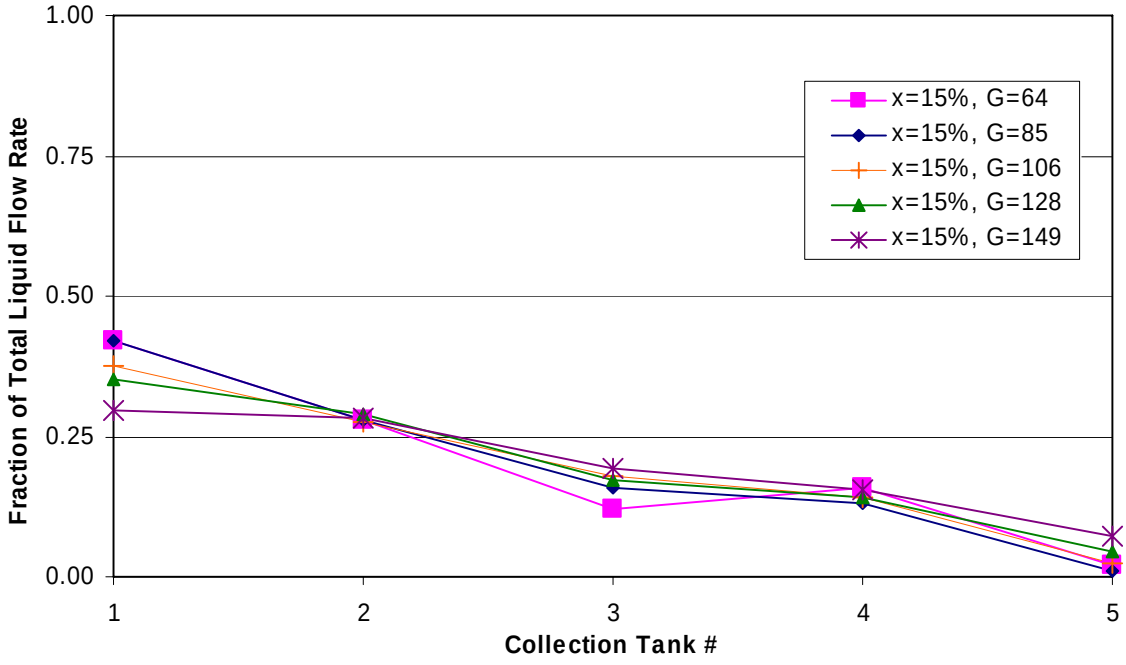

Figure B-68: 3/4 Depth Protrusion, Long Inlet, x=15%

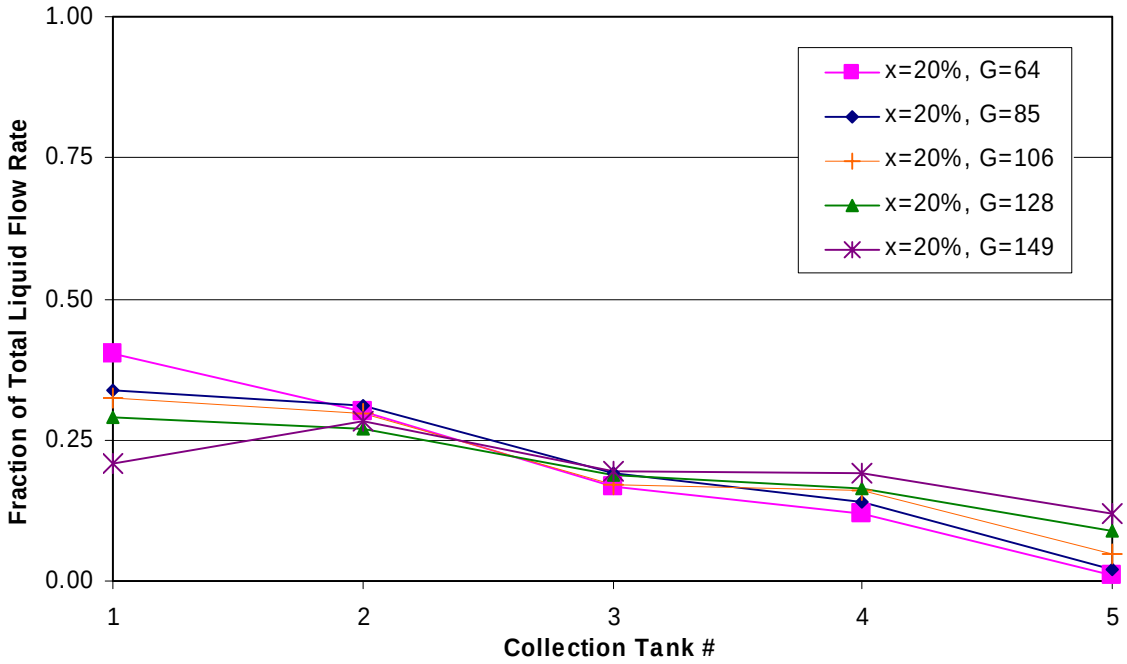

Figure B-69: 3/4 Depth Protrusion, Long Inlet, x=20%

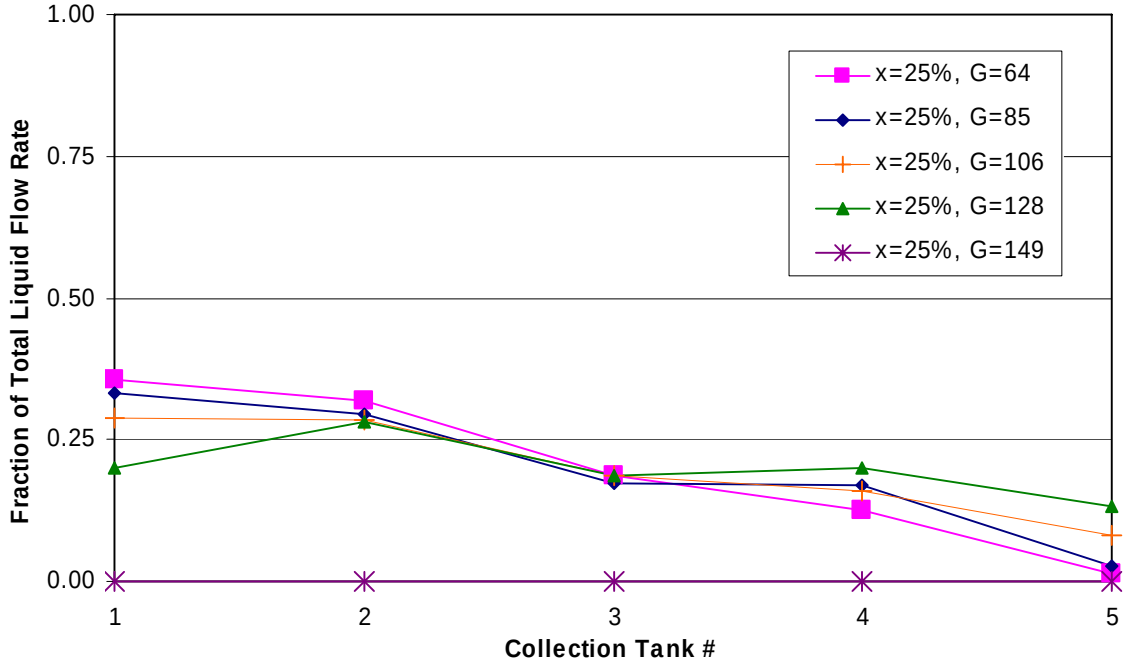

Figure B-70: 3/4 Depth Protrusion, Long Inlet, x=25%

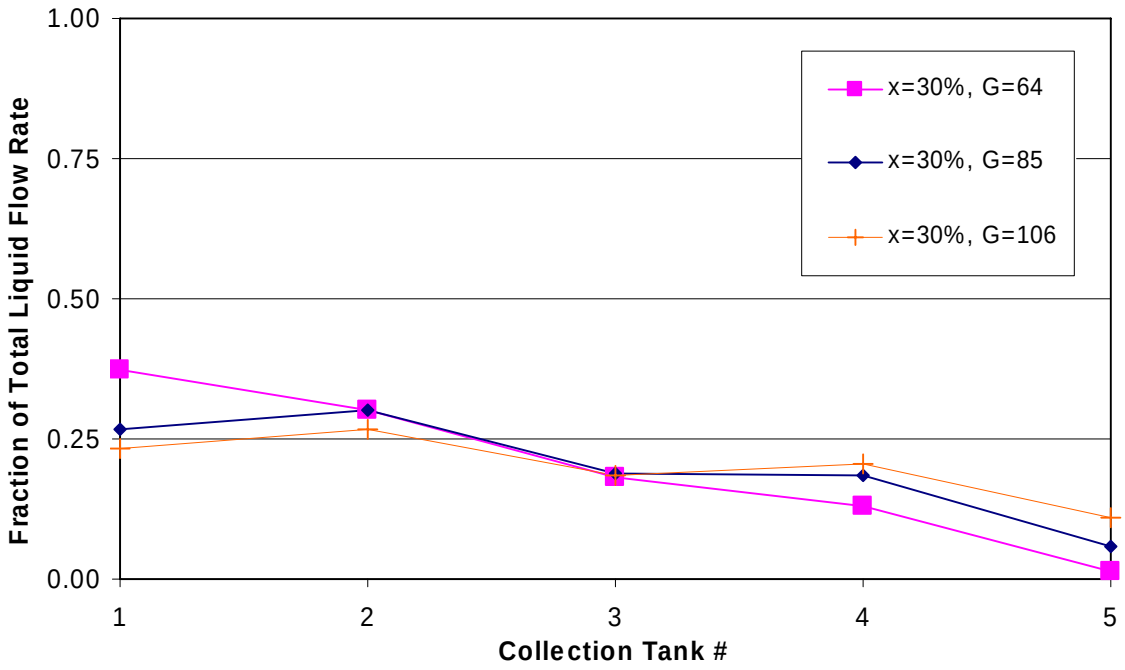

Figure B-71: 3/4 Depth Protrusion, Long Inlet, x=30%

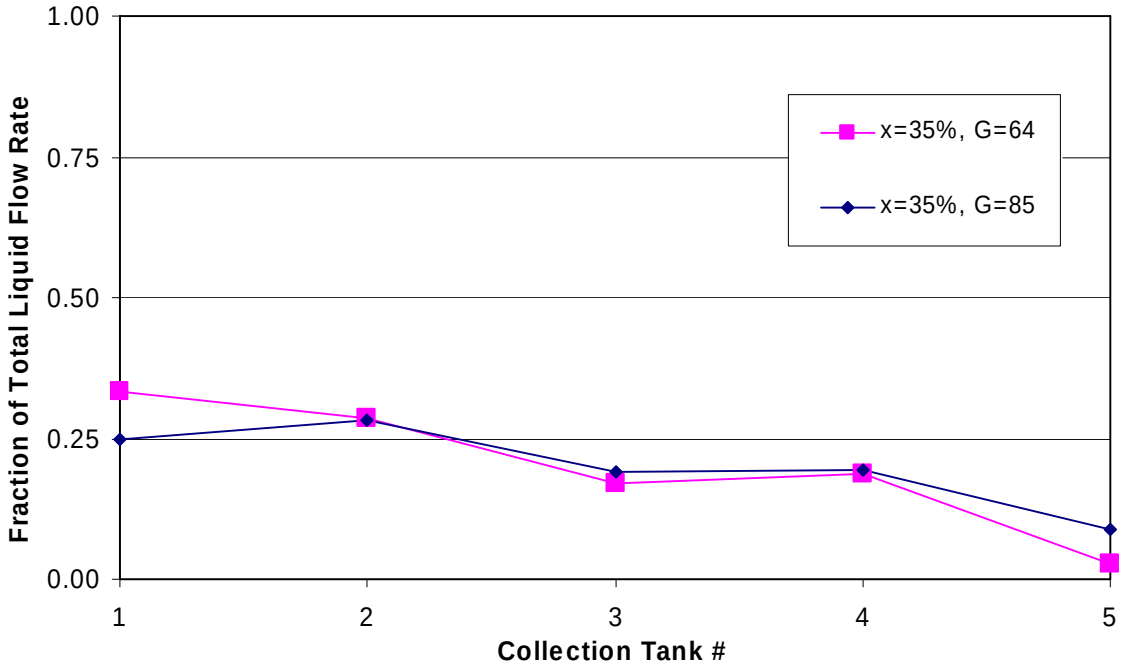

Figure B-72: 3/4 Depth Protrusion, Long Inlet, x=35%

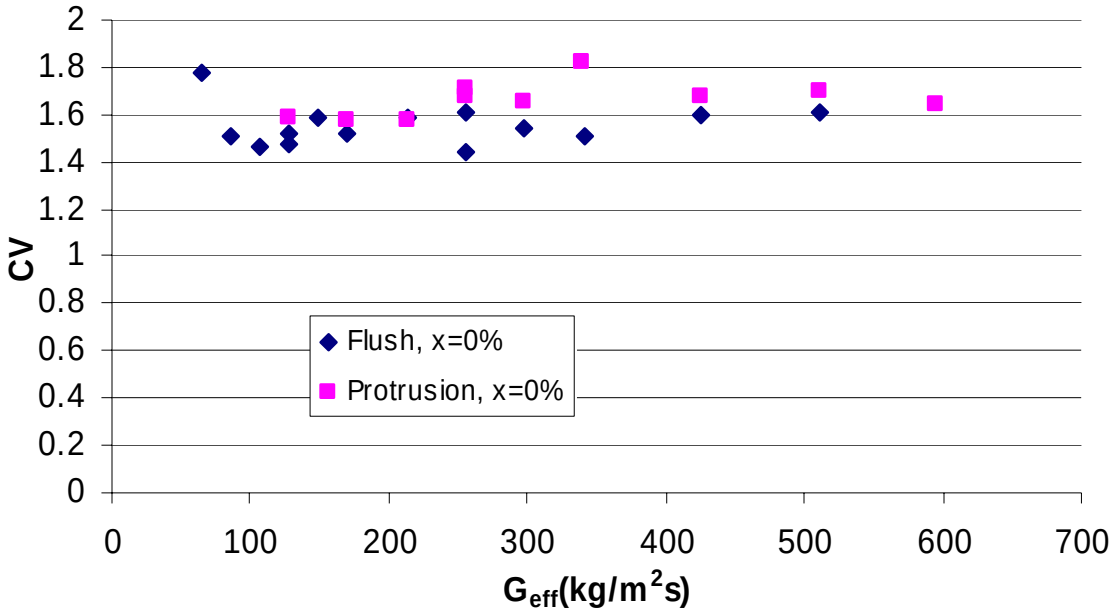

Figure B-73: Flush and Protrusion Comparison, Short Entrance, 0% Inlet Quality

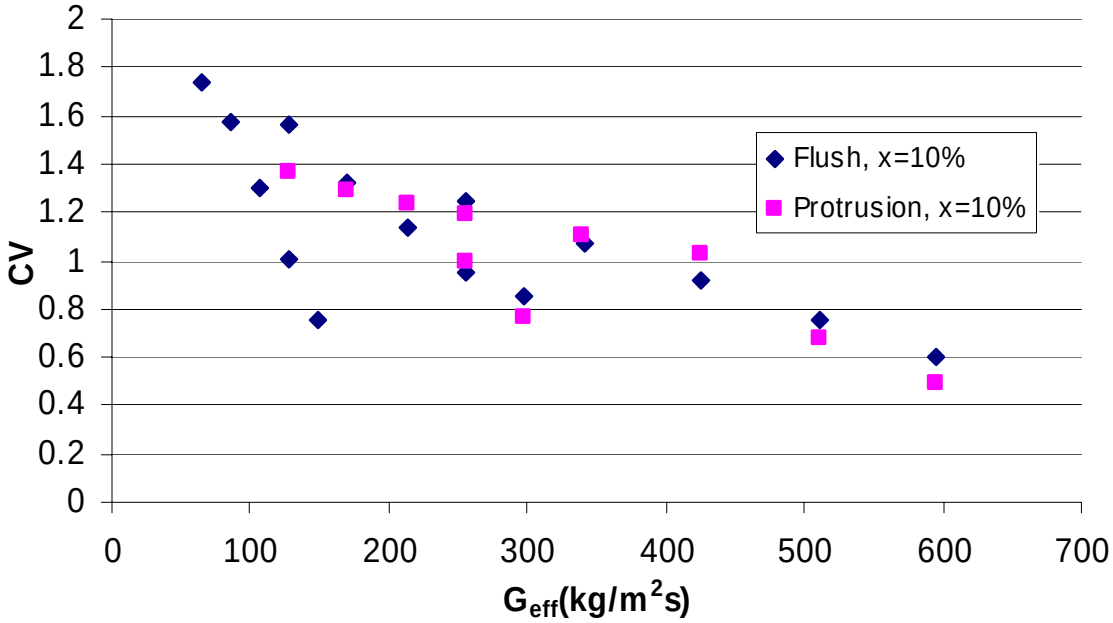

Figure B-74: Flush and Protrusion Comparison, Short Entrance, 10% Inlet Quality

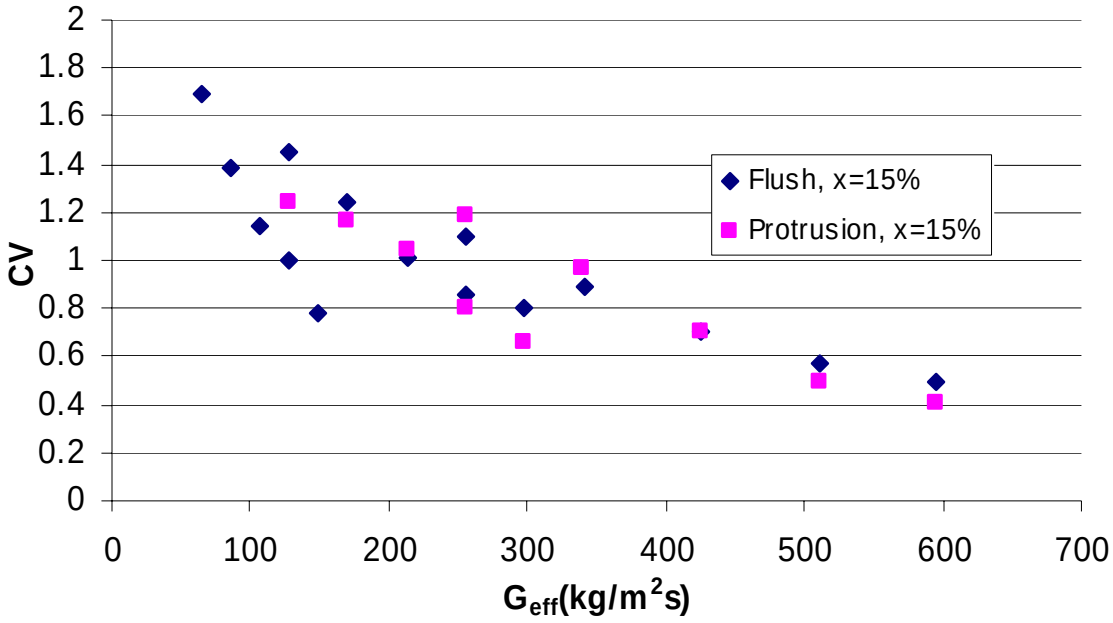

Figure B-75: Flush and Protrusion Comparison, Short Entrance, 15% Inlet Quality

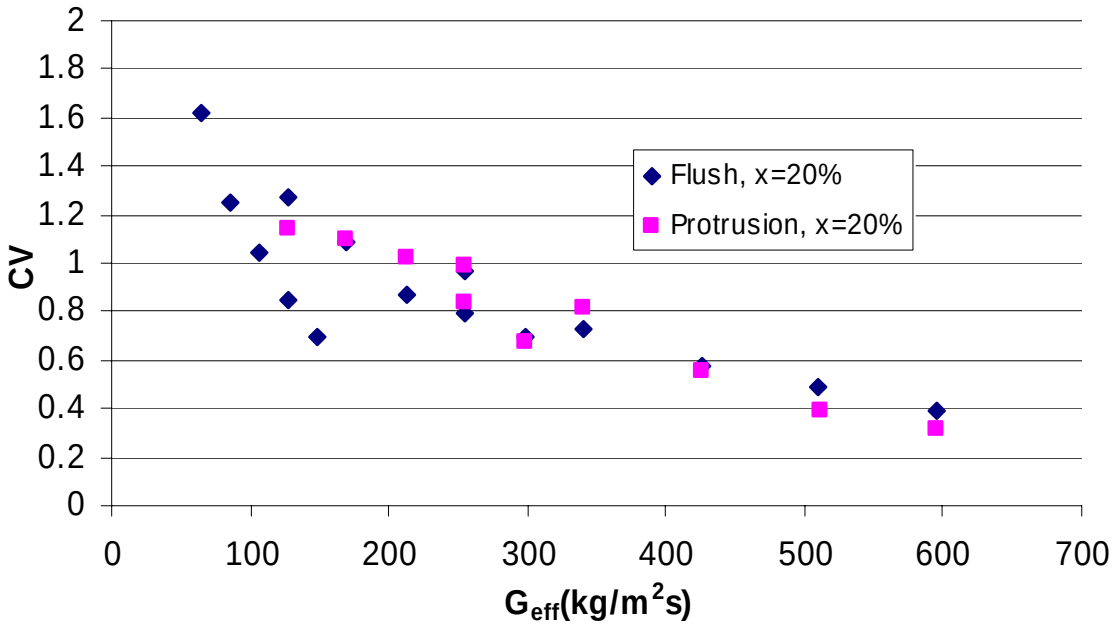

Figure B-76: Flush and Protrusion Comparison, Short Entrance, 20% Inlet Quality

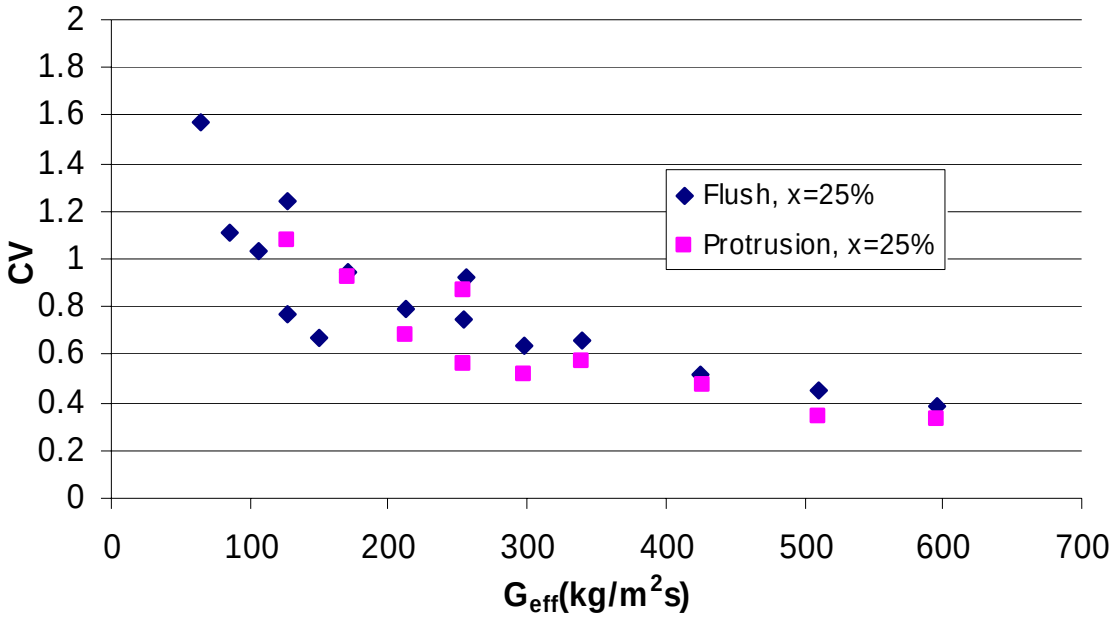

Figure B-77: Flush and Protrusion Comparison, Short Entrance, 25% Inlet Quality

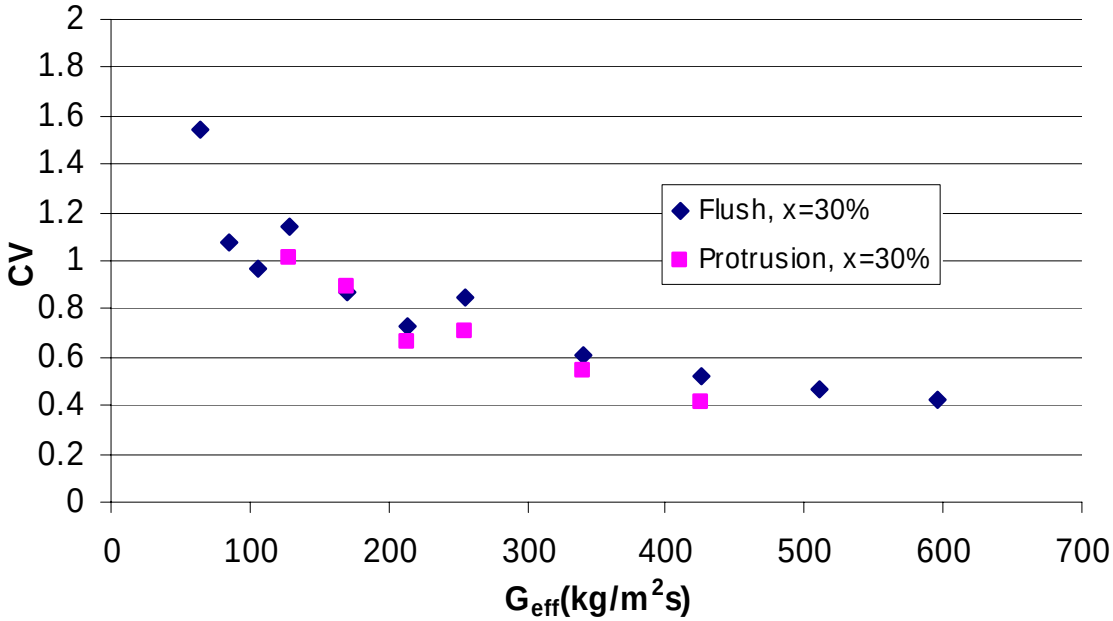

Figure B-78: Flush and Protrusion Comparison, Short Entrance, 30% Inlet Quality

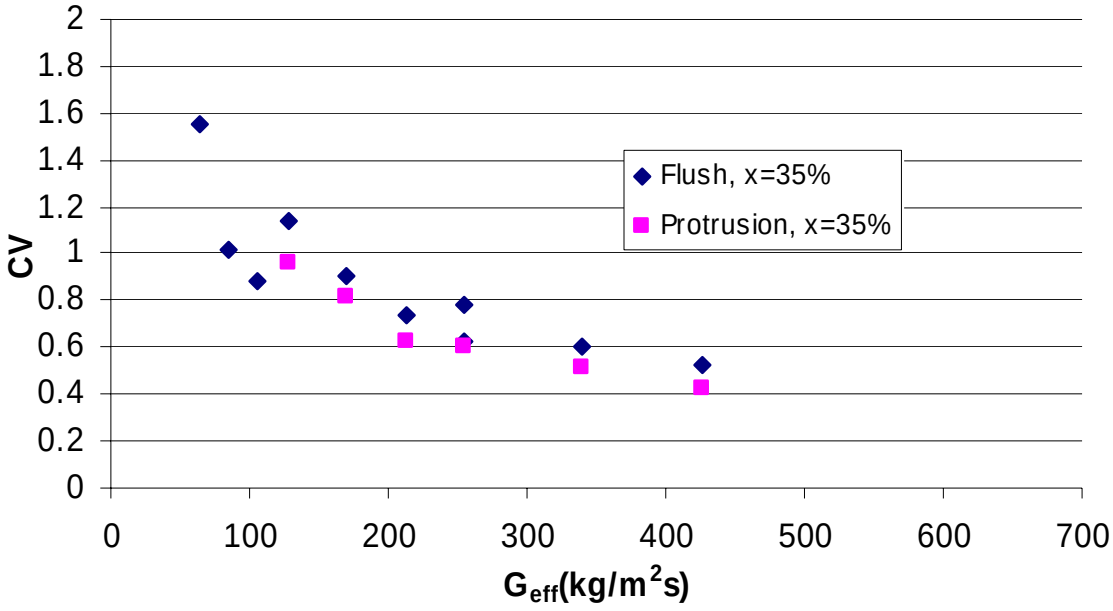

Figure B-79: Flush and Protrusion Comparison, Short Entrance, 35% Inlet Quality

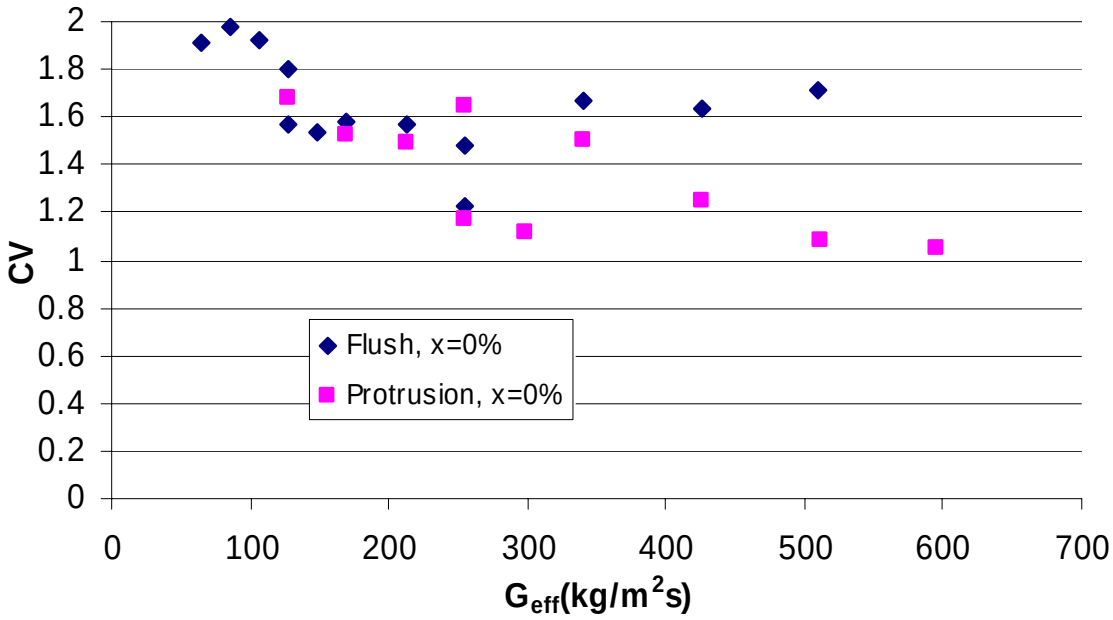

Figure B-80: Flush and Protrusion Comparison, Long Entrance, 0% Inlet Quality

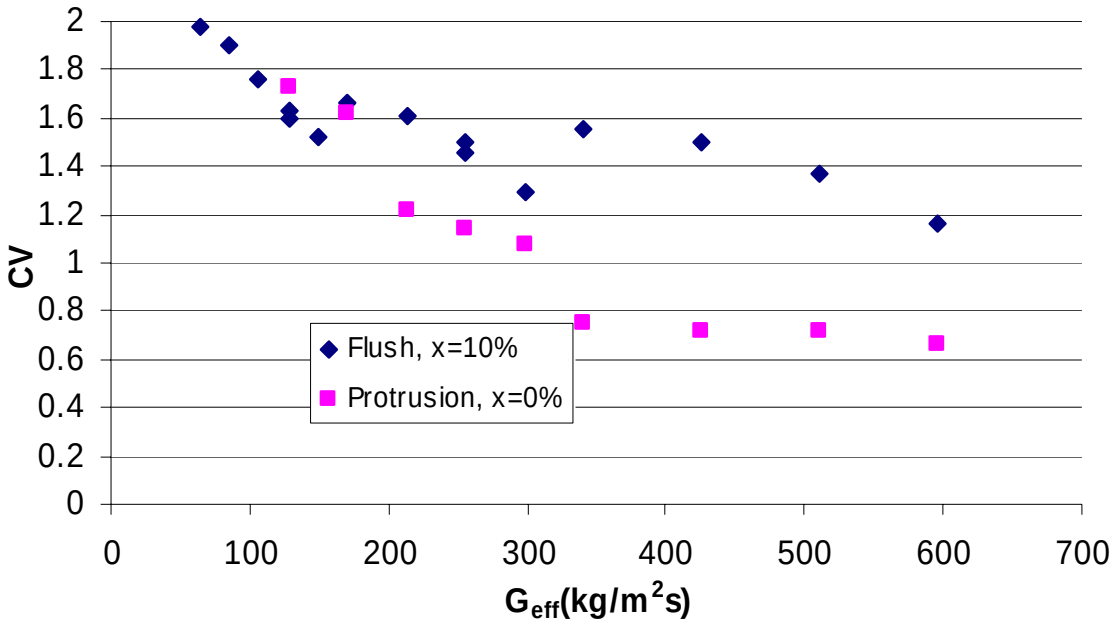

Figure B-81: Flush and Protrusion Comparison, Long Entrance, 10% Inlet Quality

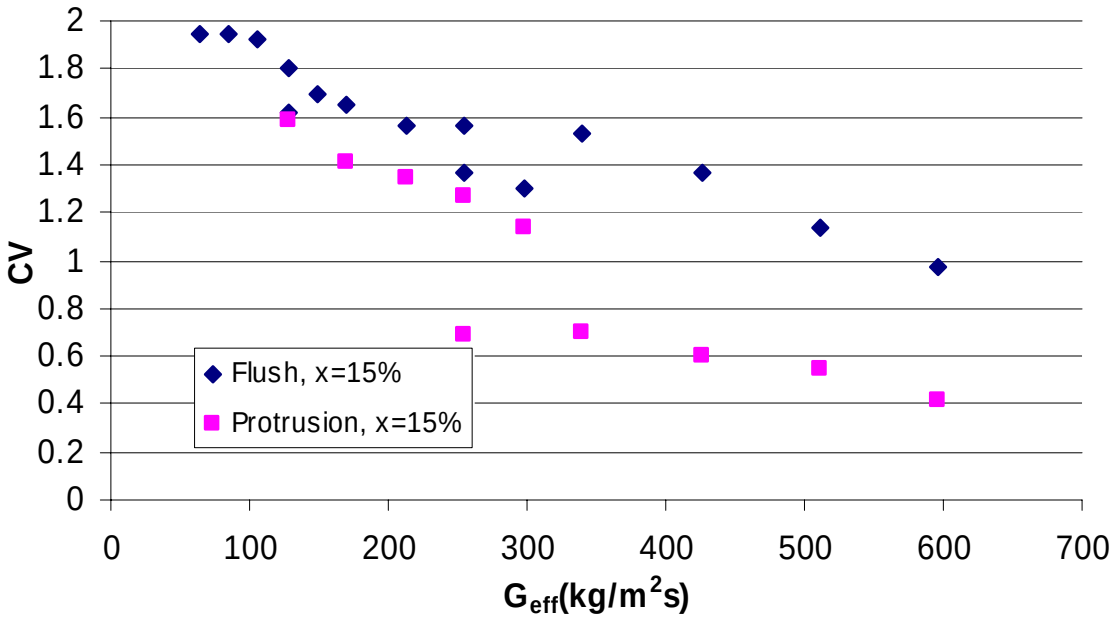

Figure B-82: Flush and Protrusion Comparison, Long Entrance, 15% Inlet Quality

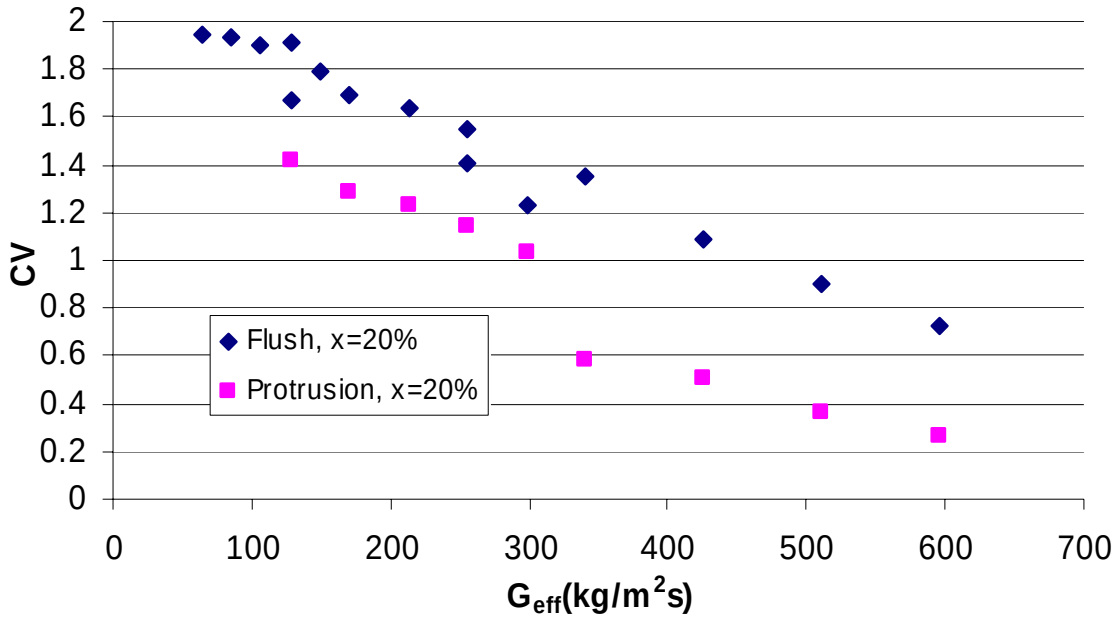

Figure B-83: Flush and Protrusion Comparison, Long Entrance, 20% Inlet Quality

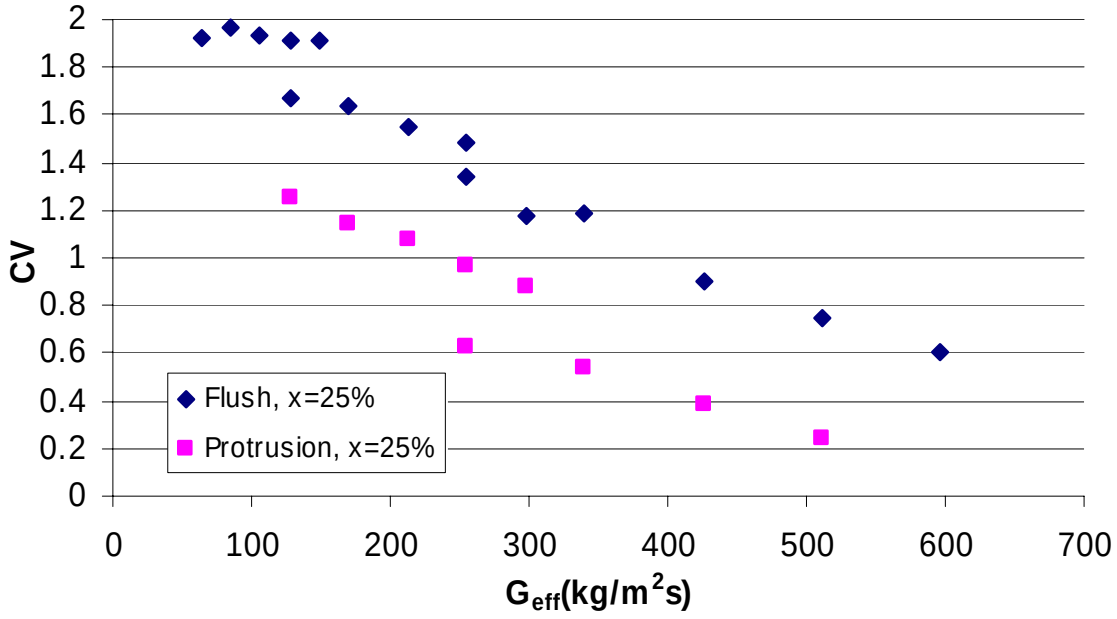

Figure B-84: Flush and Protrusion Comparison, Long Entrance, 25% Inlet Quality

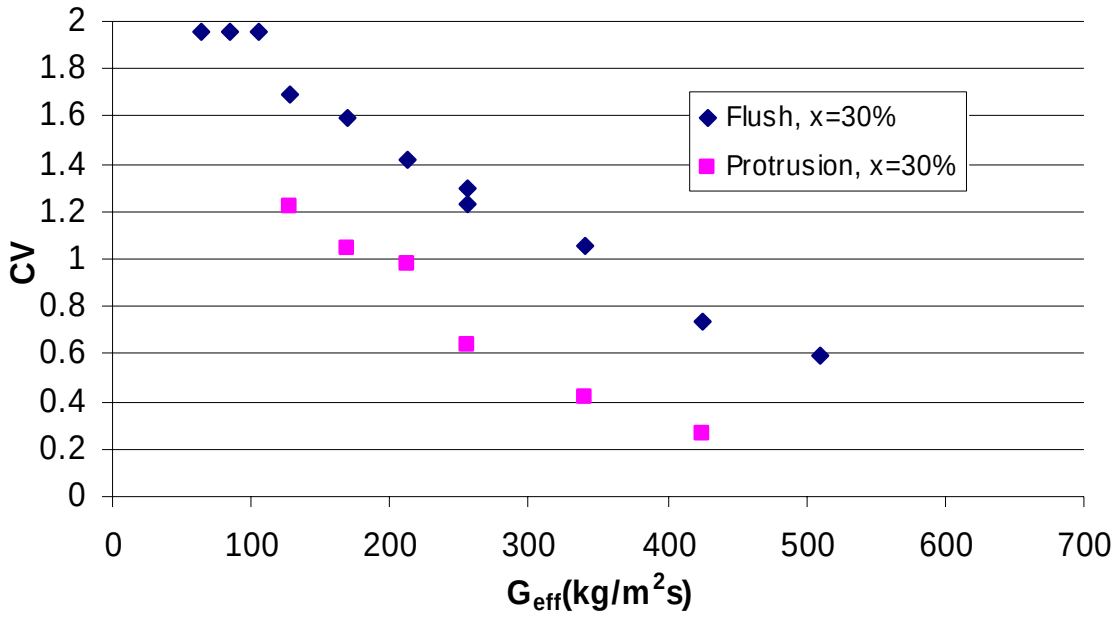

Figure B-85: Flush and Protrusion Comparison, Long Entrance, 30% Inlet Quality

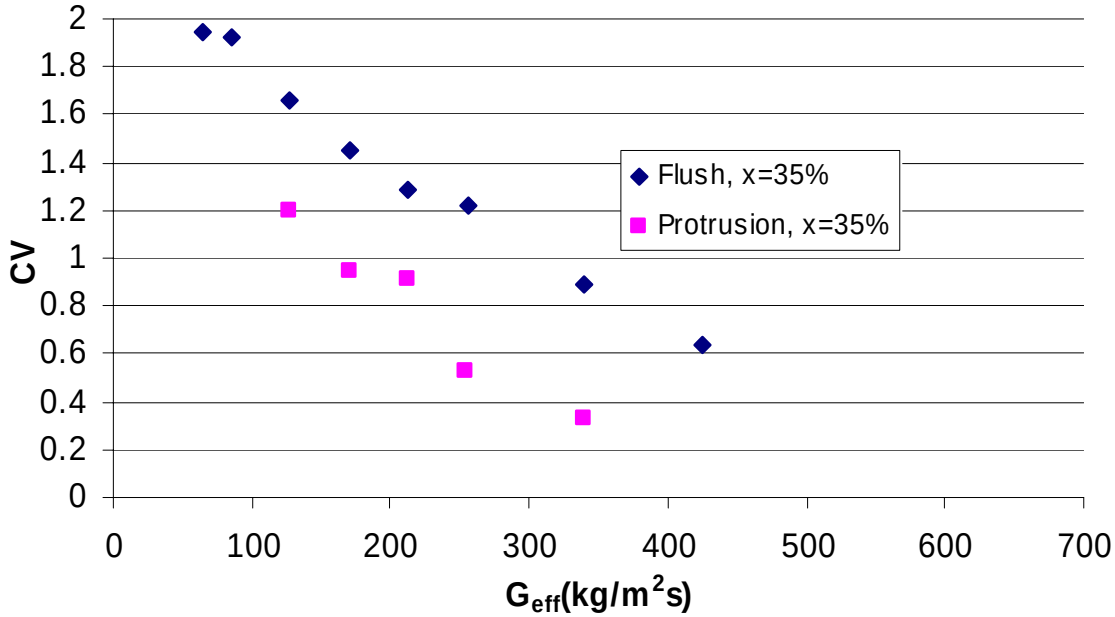

Figure B-86: Flush and Protrusion Comparison, Long Entrance, 35% Inlet Quality

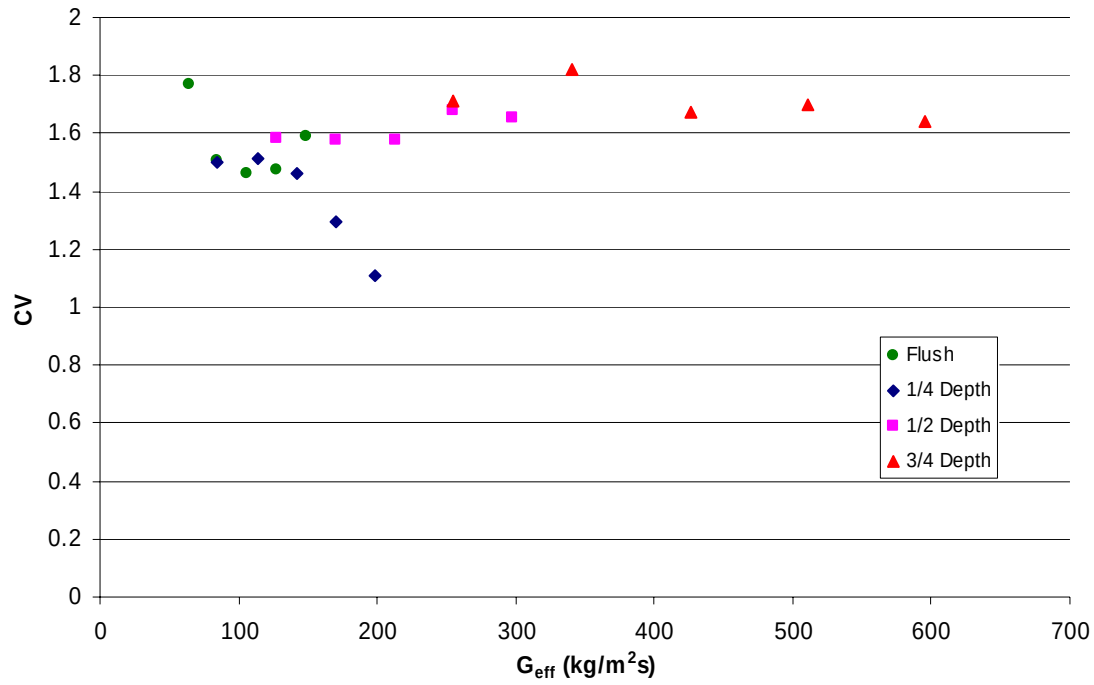

Figure B-87: Effective Mass Flux Effects, Short Entrance, 0% Inlet Quality

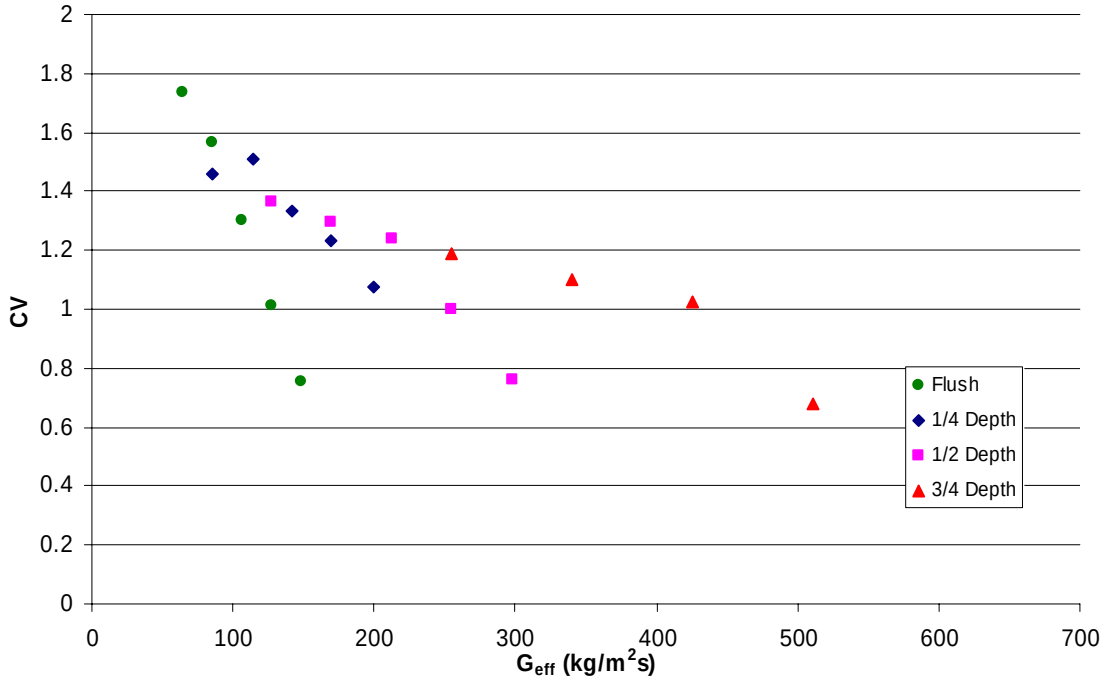

Figure B-88: Effective Mass Flux Effects, Short Entrance, 10% Inlet Quality

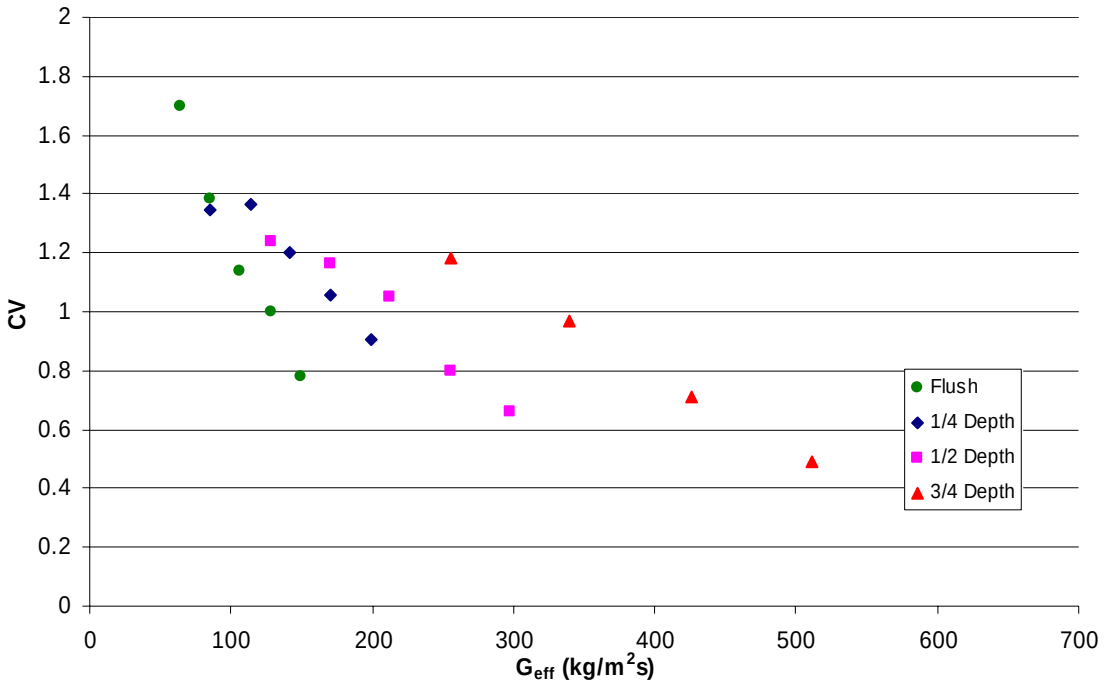

Figure B-89: Effective Mass Flux Effects, Short Entrance, 15% Inlet Quality

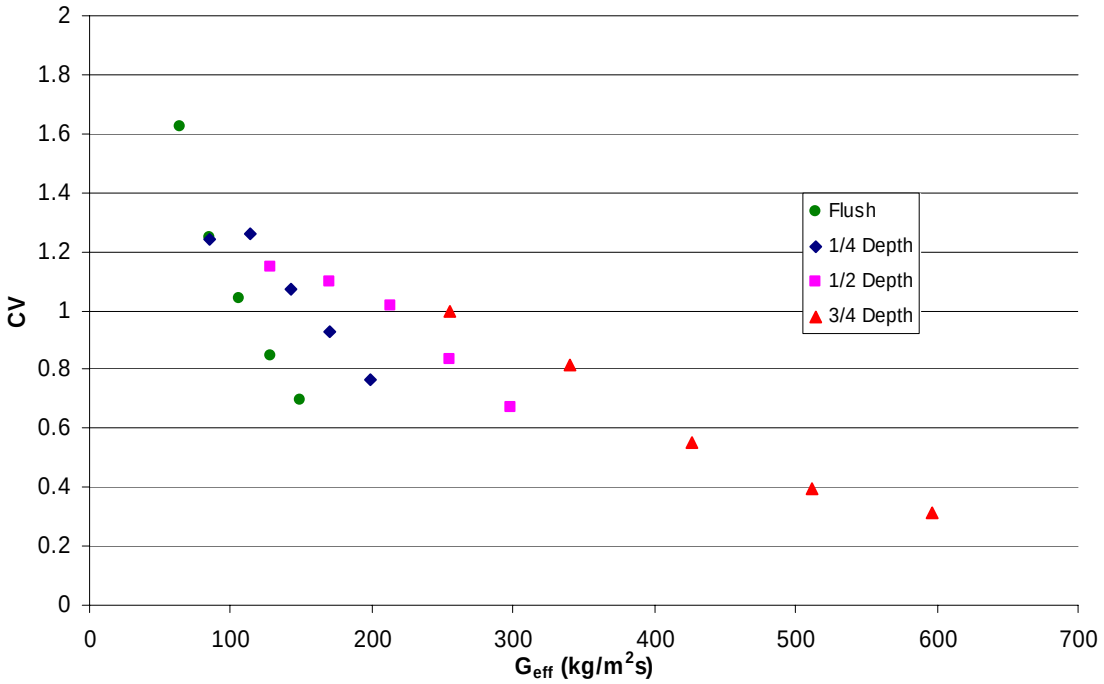

Figure B-90: Effective Mass Flux Effects, Short Entrance, 20% Inlet Quality

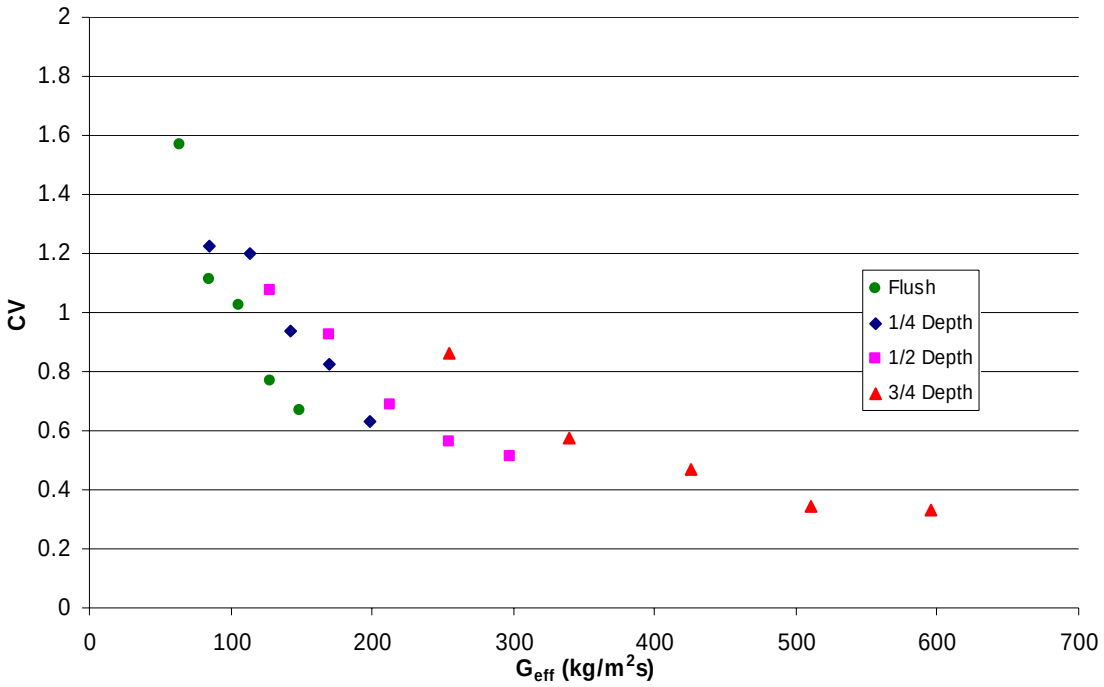

Figure B-91: Effective Mass Flux Effects, Short Entrance, 25% Inlet Quality

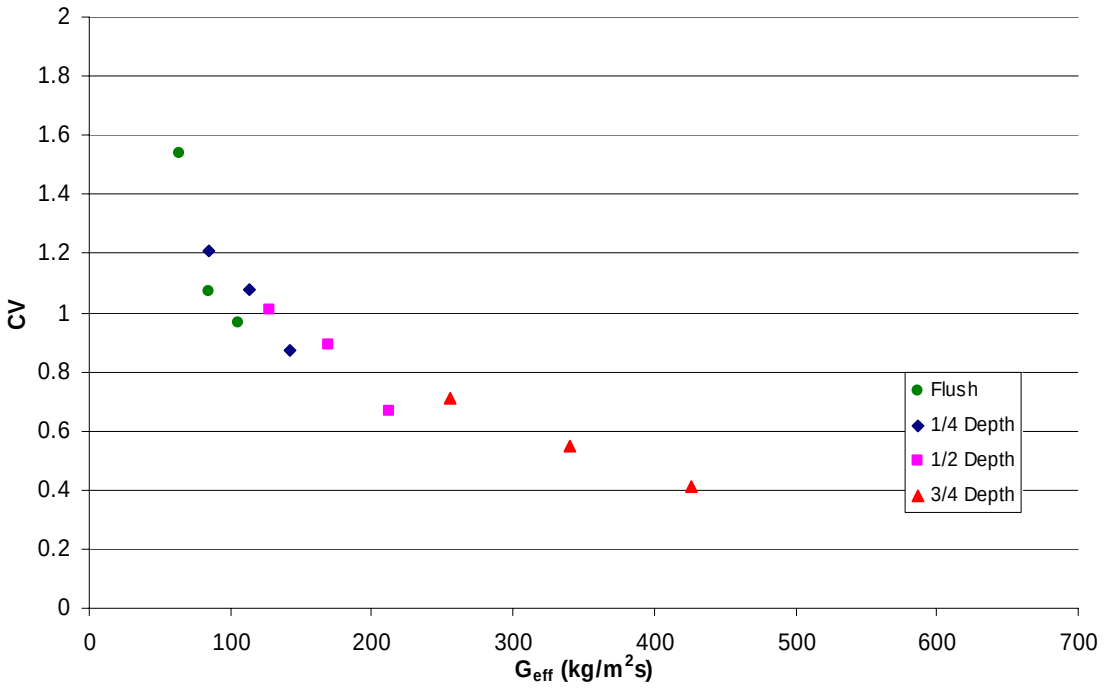

Figure B-92: Effective Mass Flux Effects, Short Entrance, 30% Inlet Quality

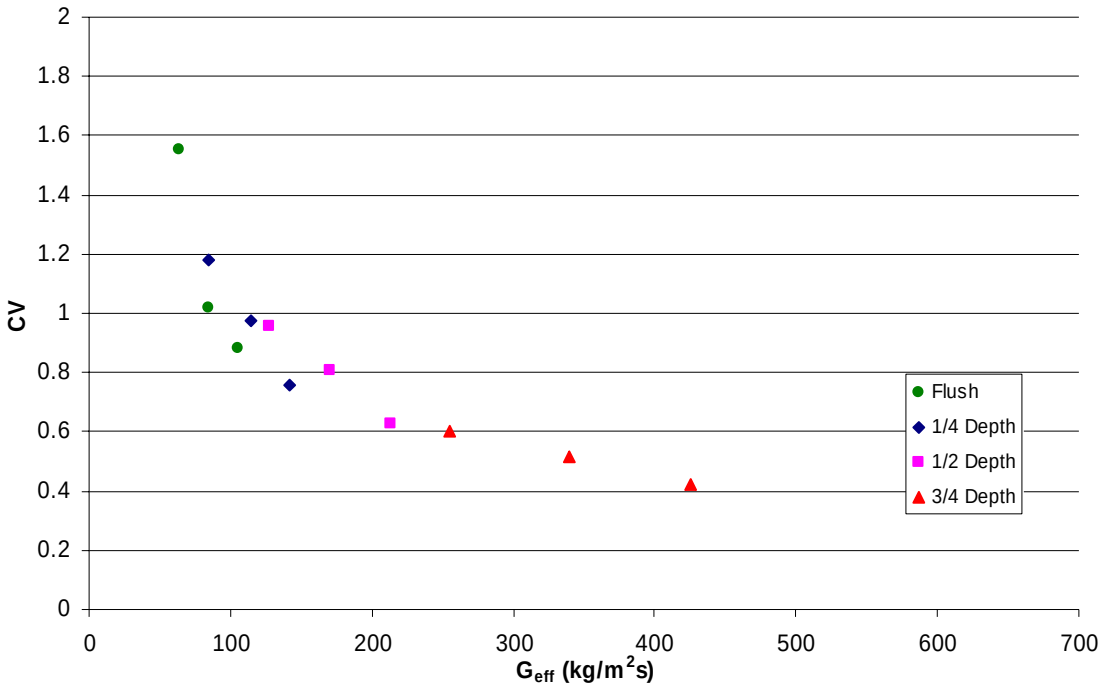

Figure B-93: Effective Mass Flux Effects, Short Entrance, 35% Inlet Quality

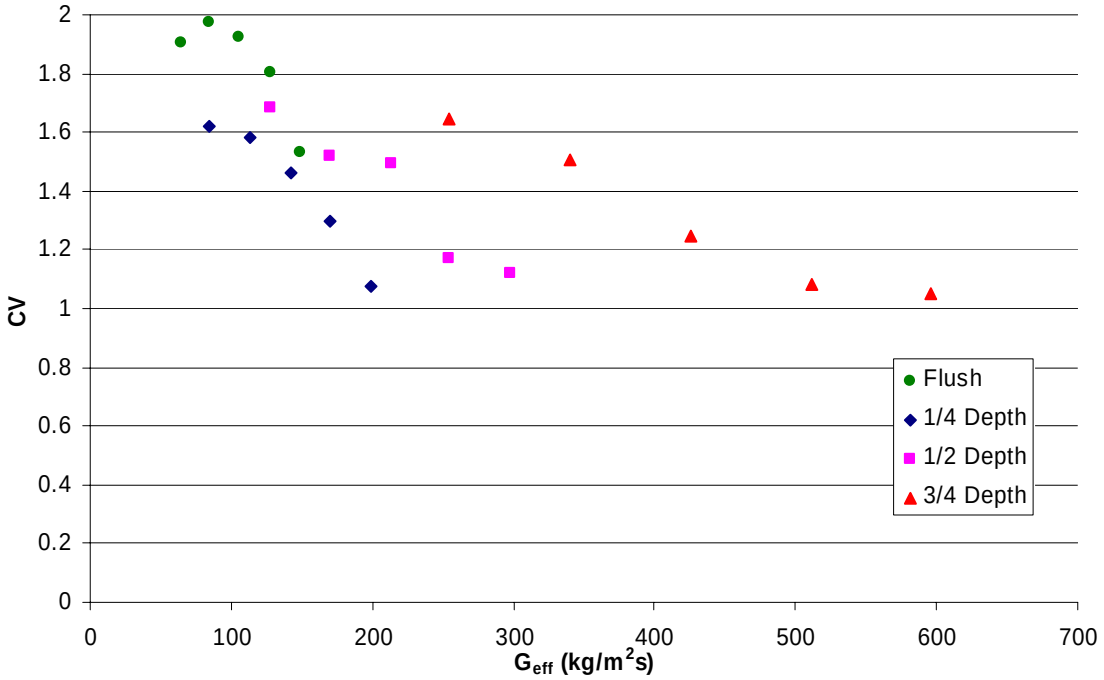

Figure B-94: Effective Mass Flux Effects, Long Entrance, 0% Inlet Quality

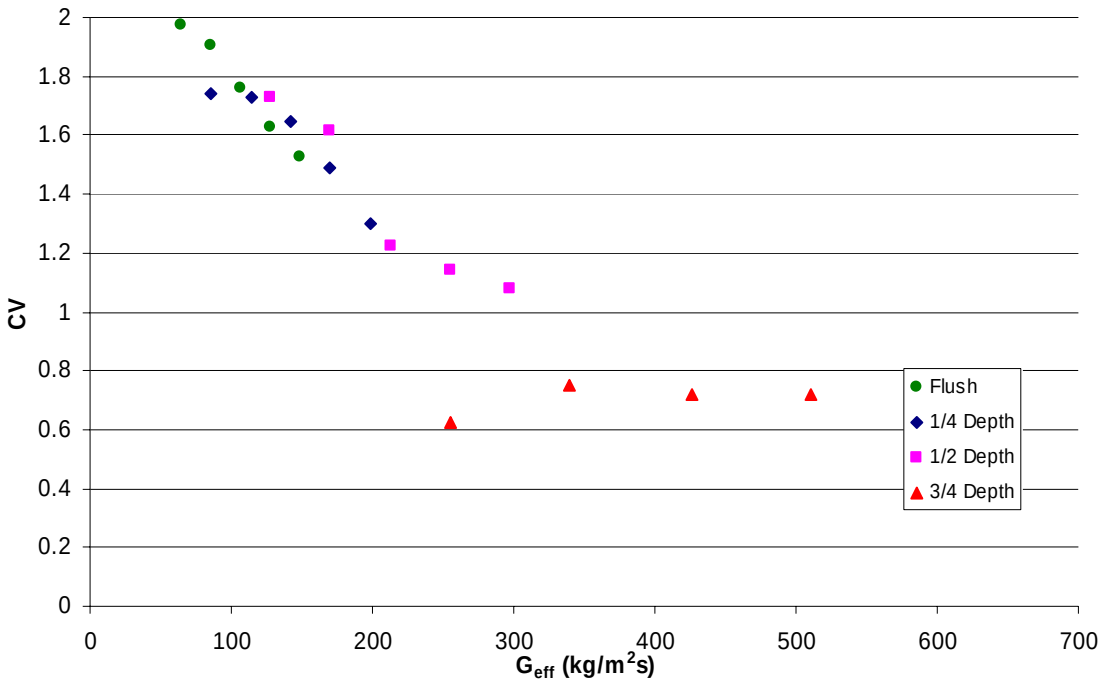

Figure B-95: Effective Mass Flux Effects, Long Entrance, 10% Inlet Quality

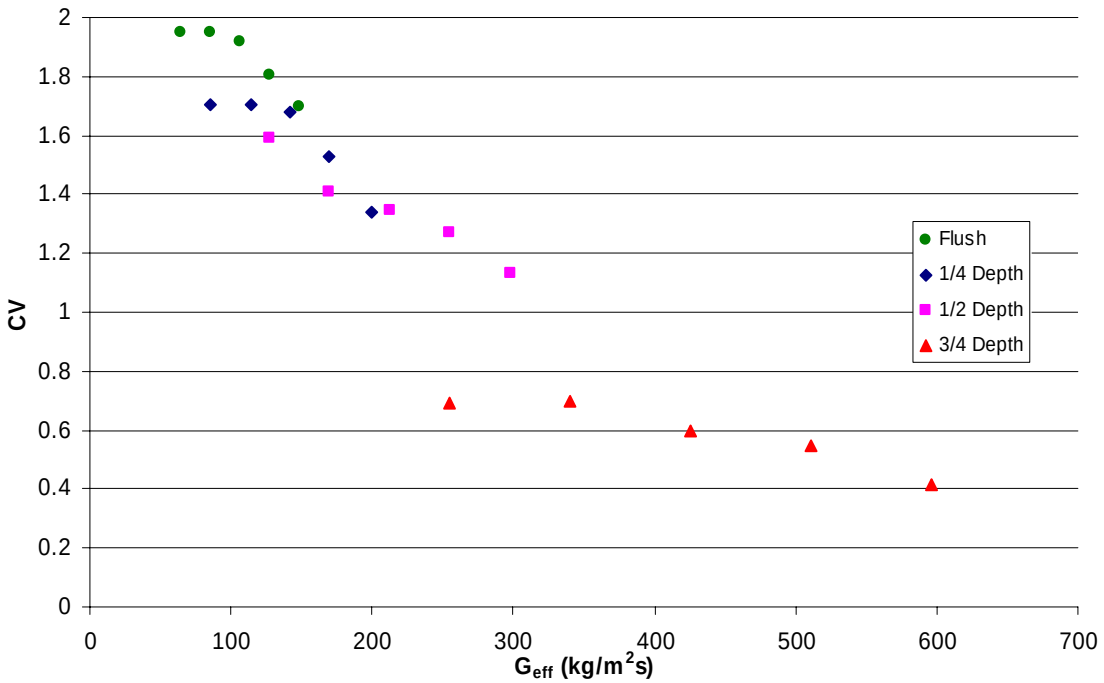

Figure B-96: Effective Mass Flux Effects, Long Entrance, 15% Inlet Quality

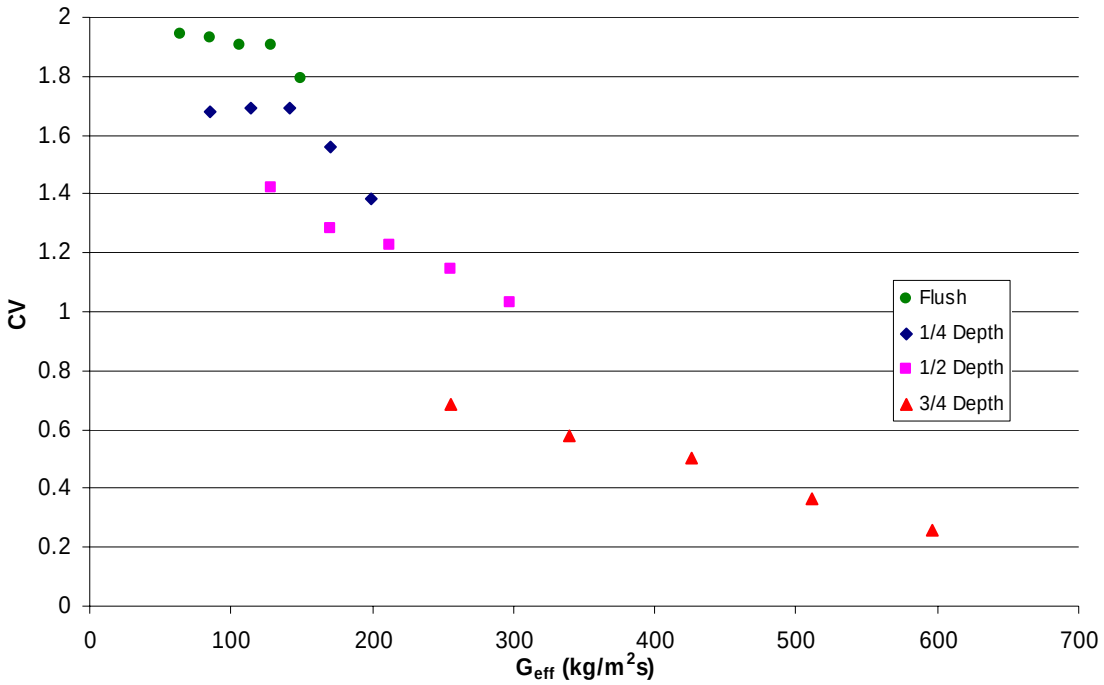

Figure B-97: Effective Mass Flux Effects, Long Entrance, 20% Inlet Quality

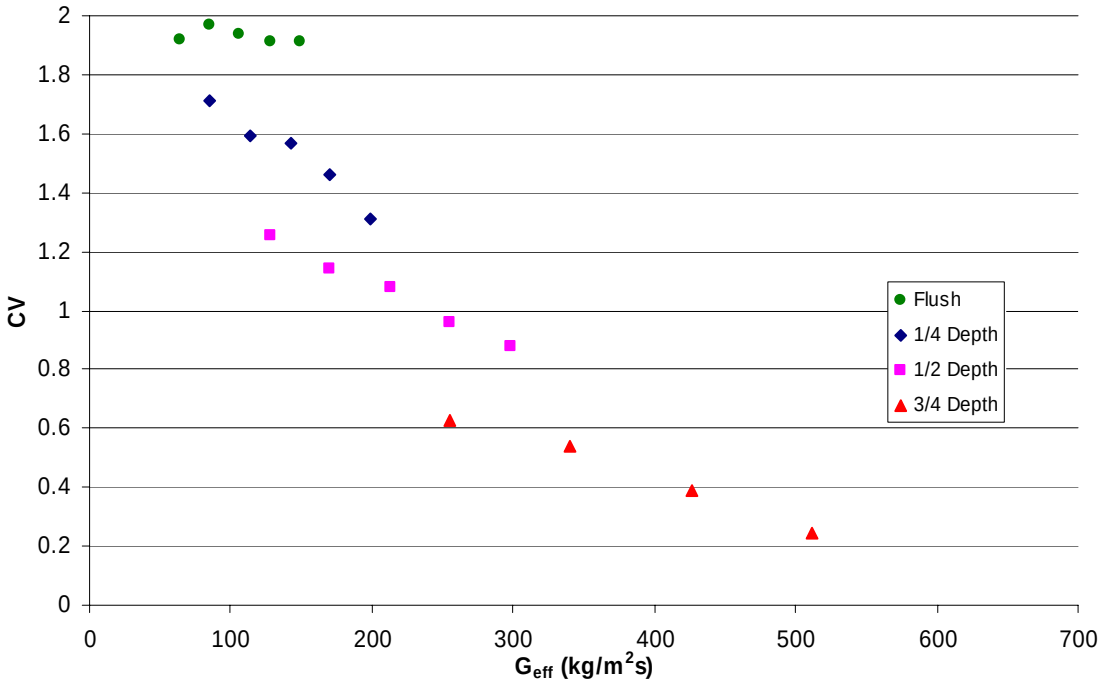

Figure B-98: Effective Mass Flux Effects, Long Entrance, 25% Inlet Quality

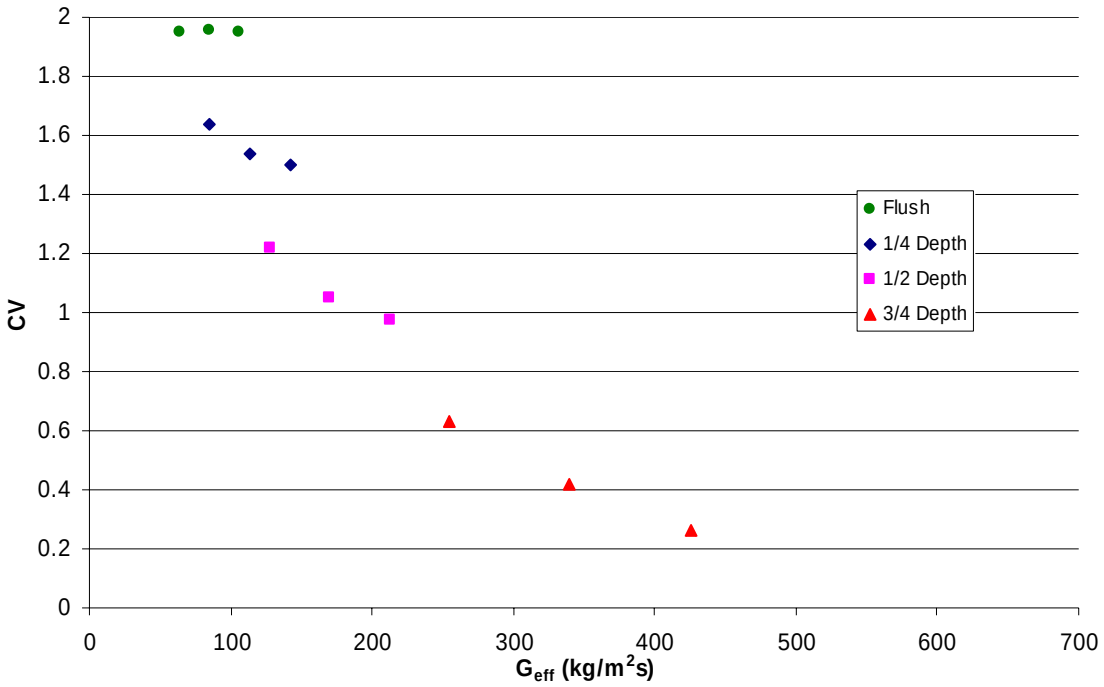

Figure B-99: Effective Mass Flux Effects, Long Entrance, 30% Inlet Quality

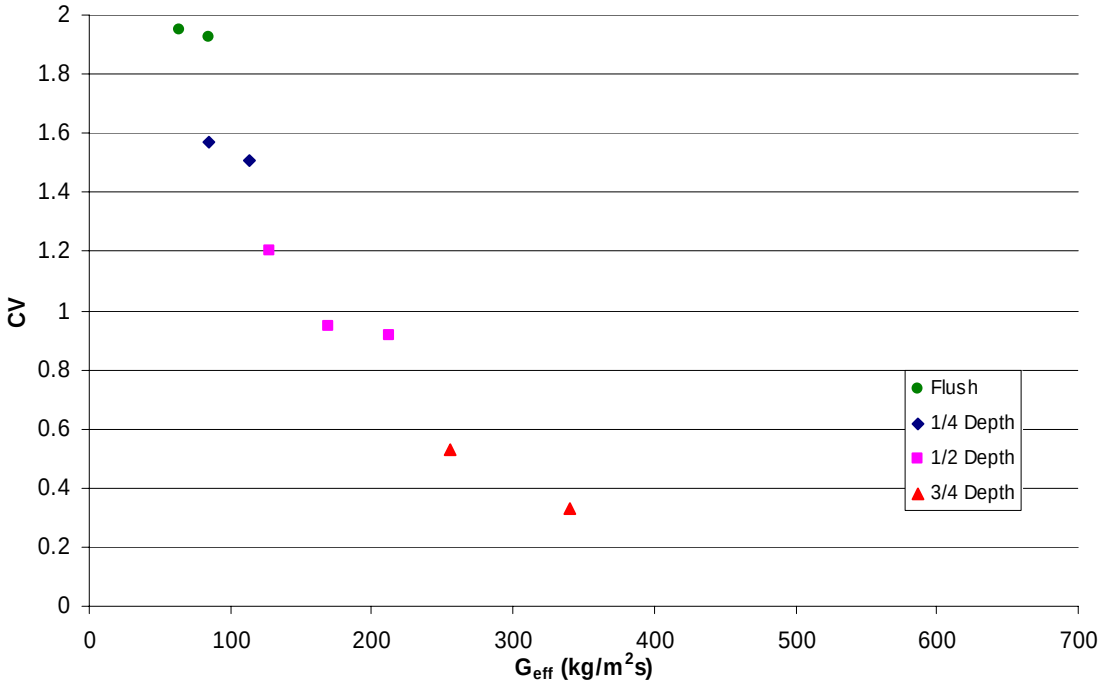

Figure B-100: Effective Mass Flux Effects, Long Entrance, 35% Inlet Quality

Appendix C. R134a Liquid Distribution Results for Cylindrical Manifold

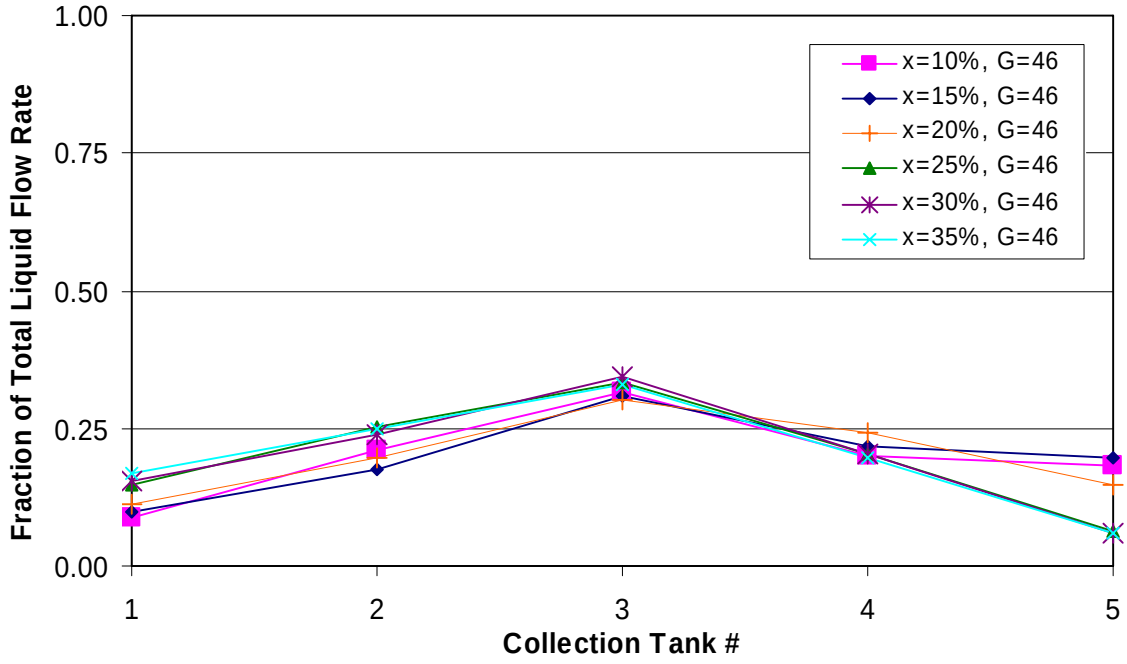

Figure C-1: 1/4 Depth Protrusion, Short Inlet, G=46 kg/m^{2}s

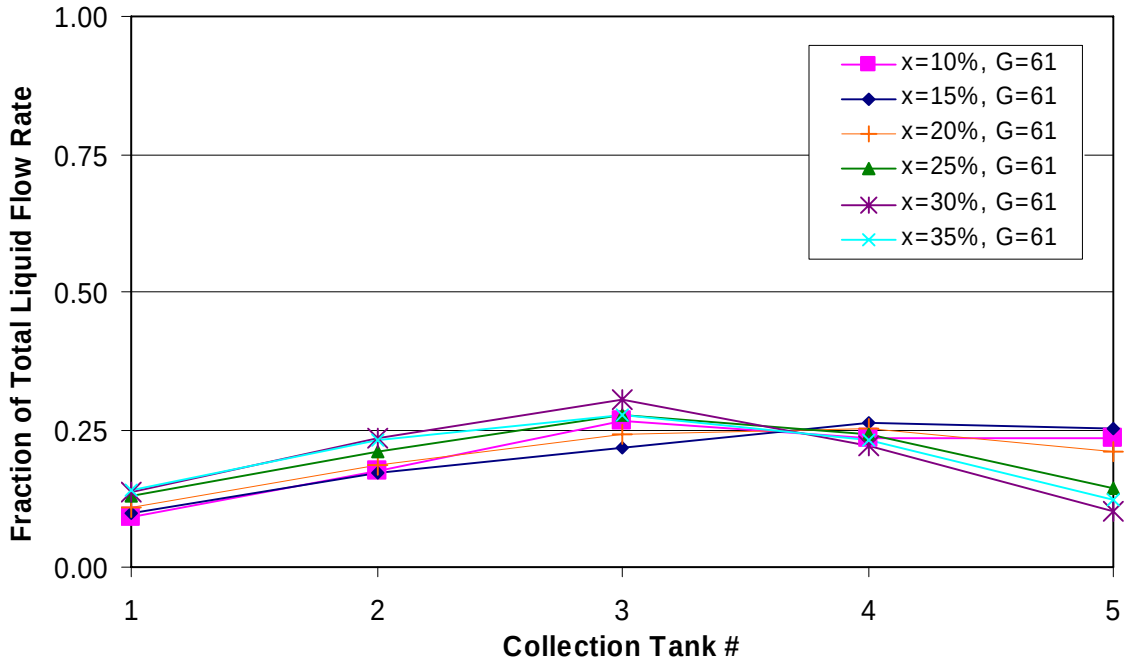

Figure C-2: 1/4 Depth Protrusion, Short Inlet, G=61 kg/m^{2}s

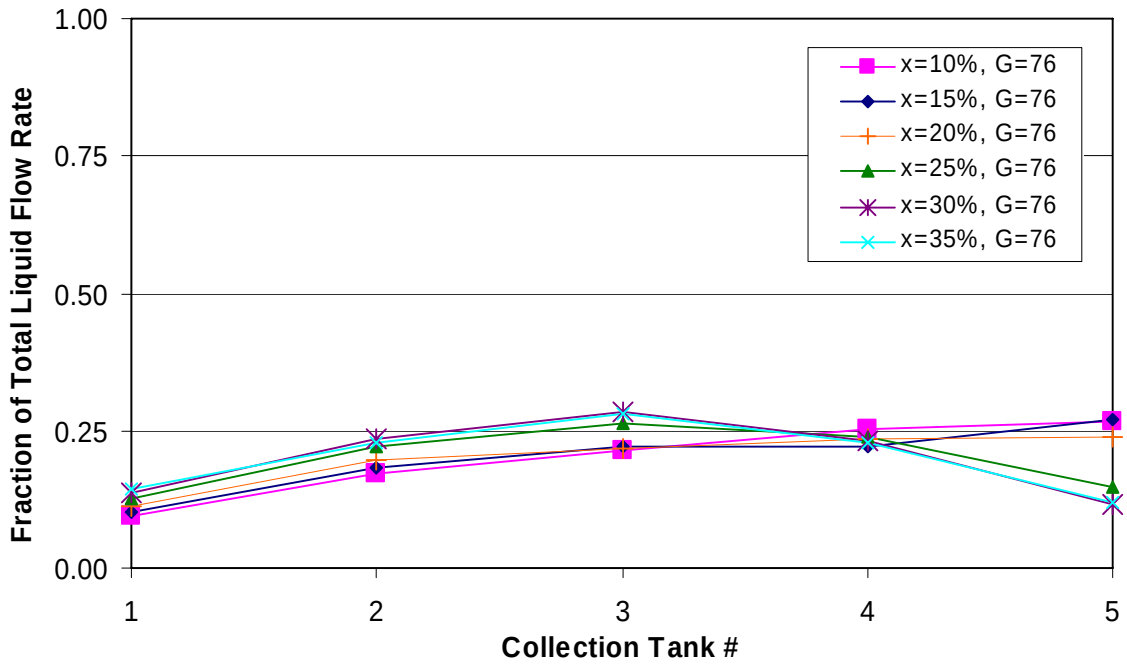

Figure C-3: 1/4 Depth Protrusion, Short Inlet, G=76 kg/m^{2}s

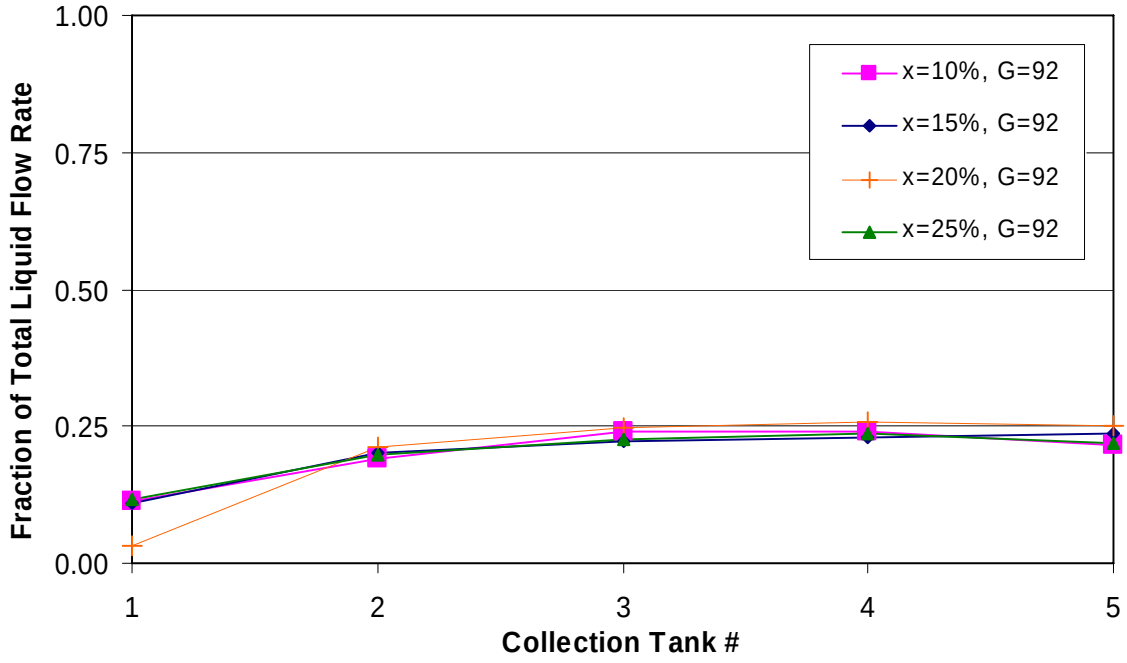

Figure C-4: 1/4 Depth Protrusion, Short Inlet, G=92 kg/m^{2}s

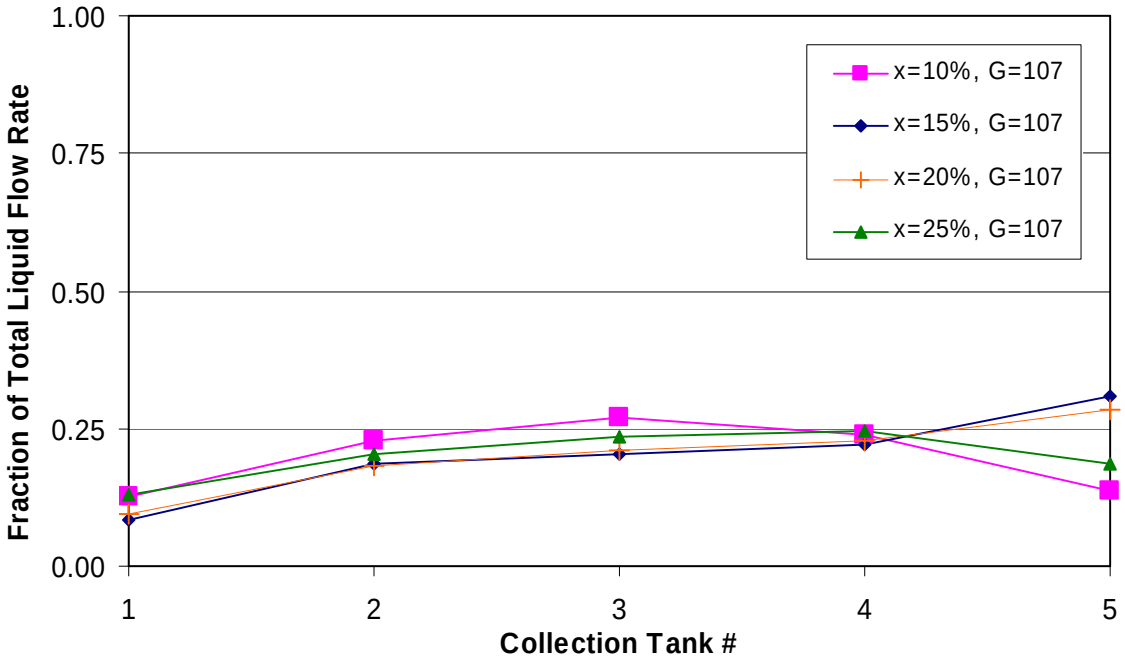

Figure C-5: 1/4 Depth Protrusion, Short Inlet, G=107 kg/m^{2}s

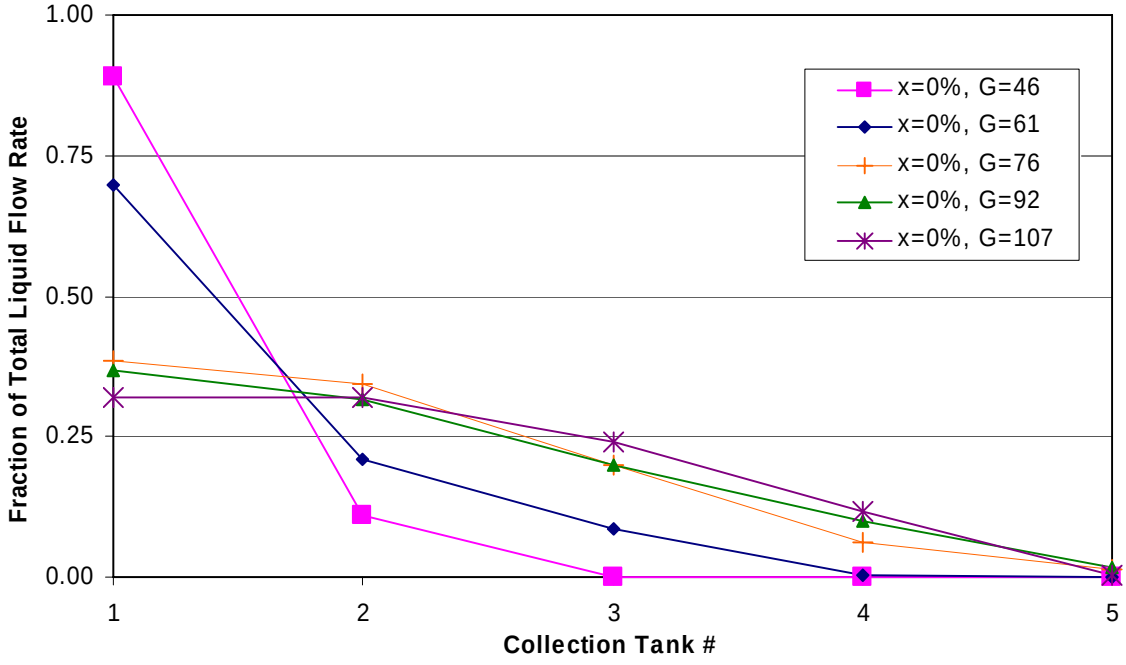

Figure C-6: 1/4 Depth Protrusion, Short Inlet, x=0%

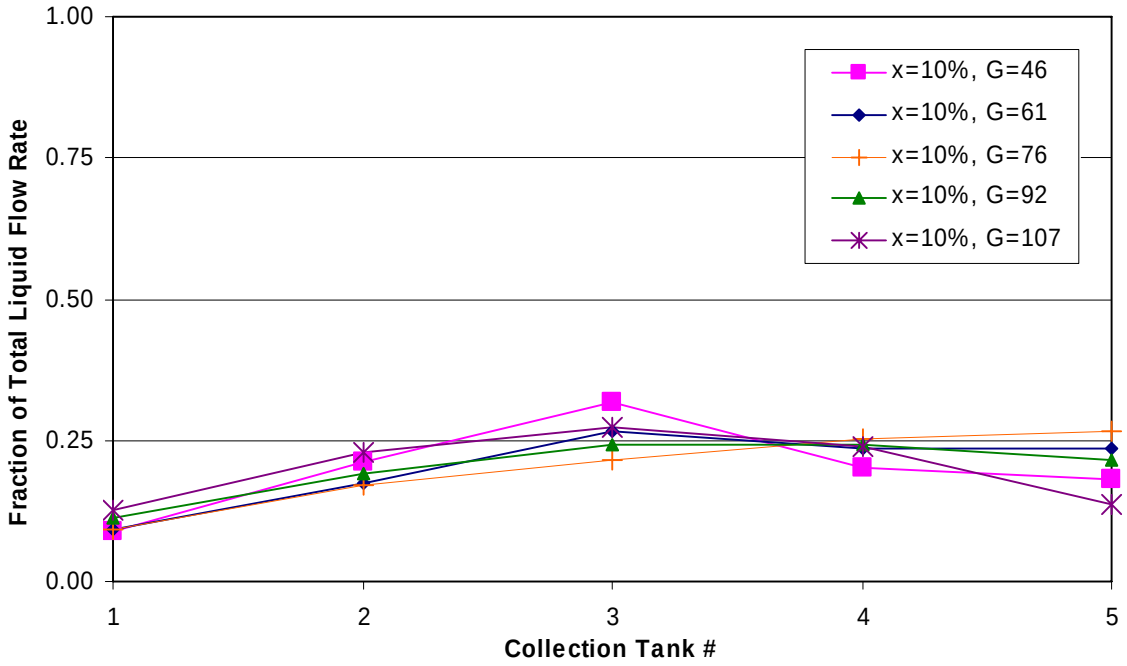

Figure C-7: 1/4 Depth Protrusion, Short Inlet, x=10%

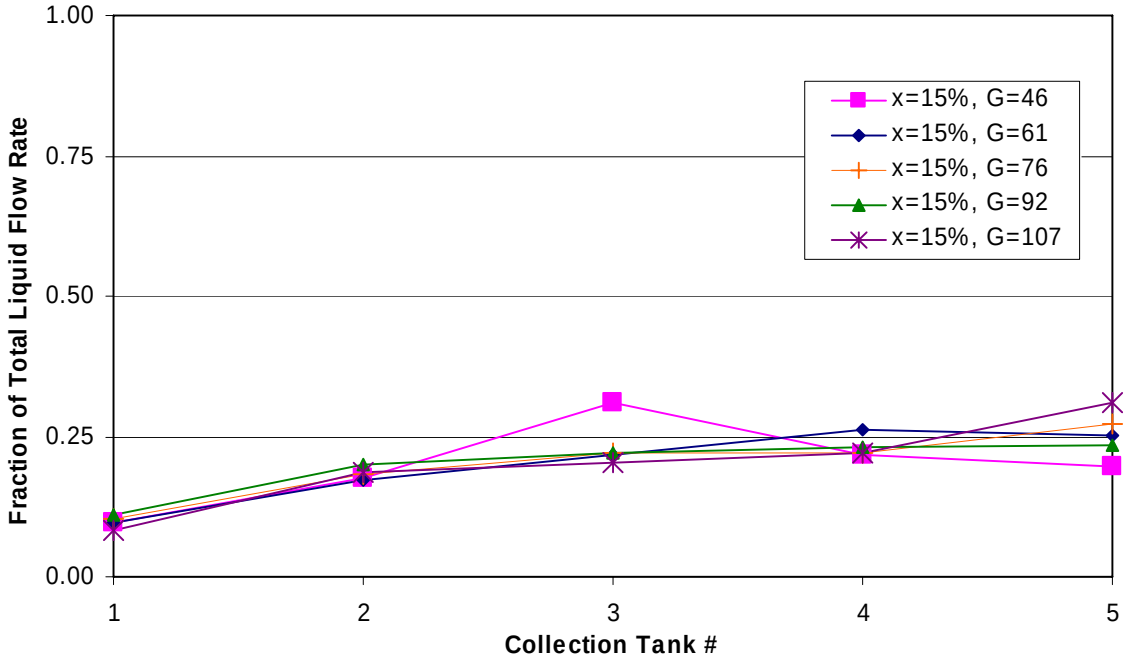

Figure C-8: 1/4 Depth Protrusion, Short Inlet, x=15%

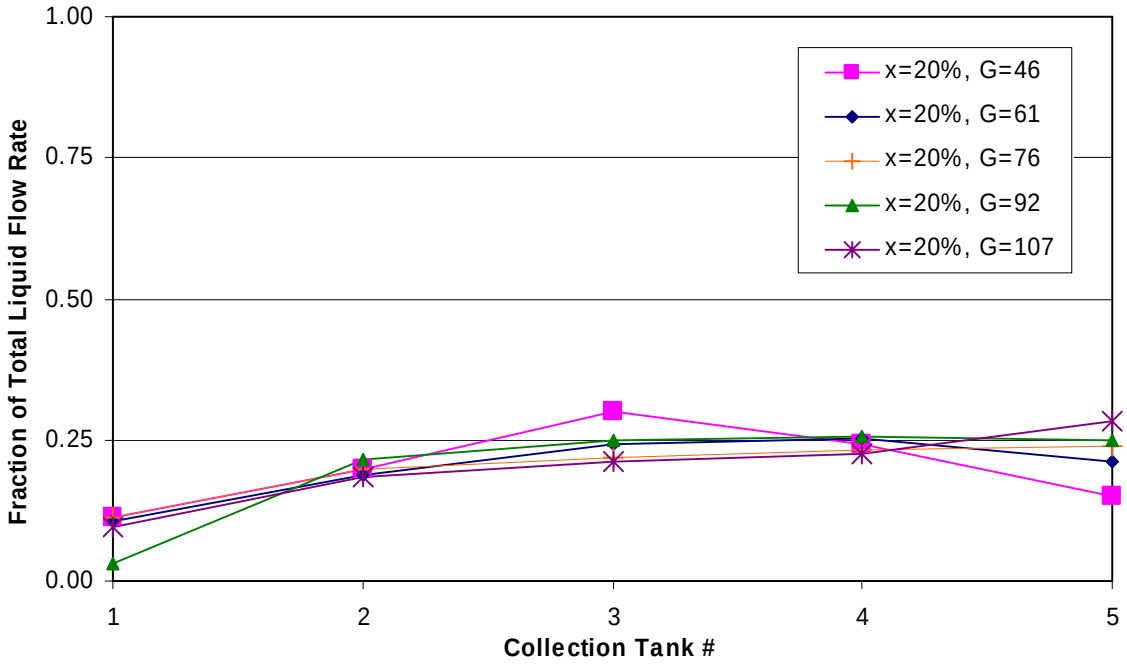

Figure C-9: 1/4 Depth Protrusion, Short Inlet, x=20%

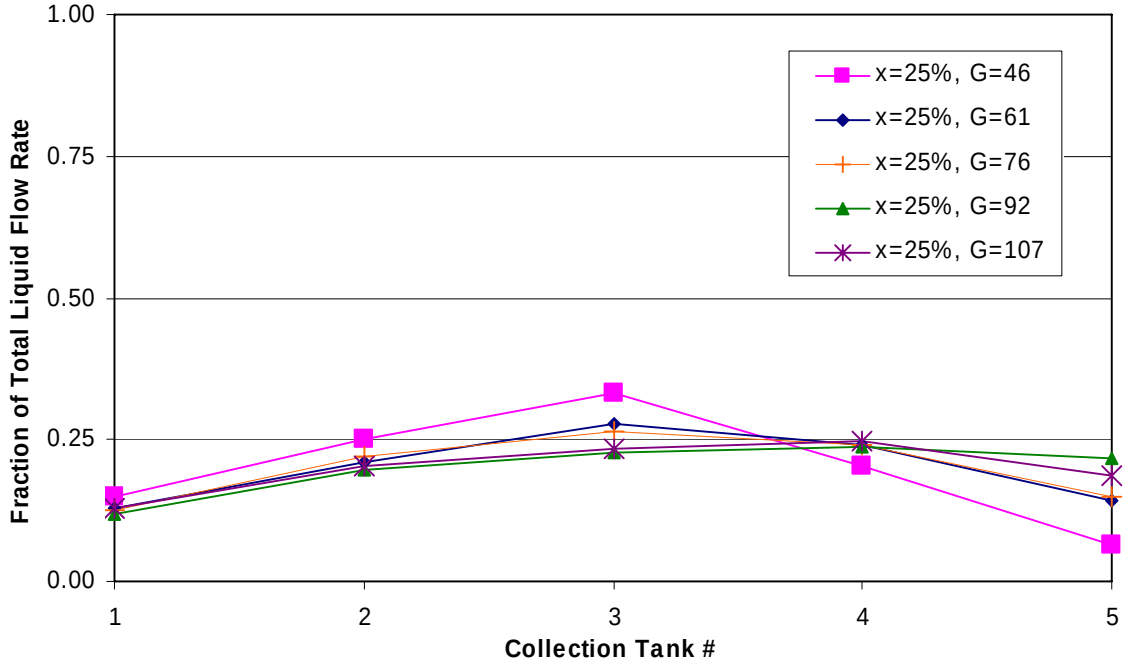

Figure C-10: 1/4 Depth Protrusion, Short Inlet, x=25%

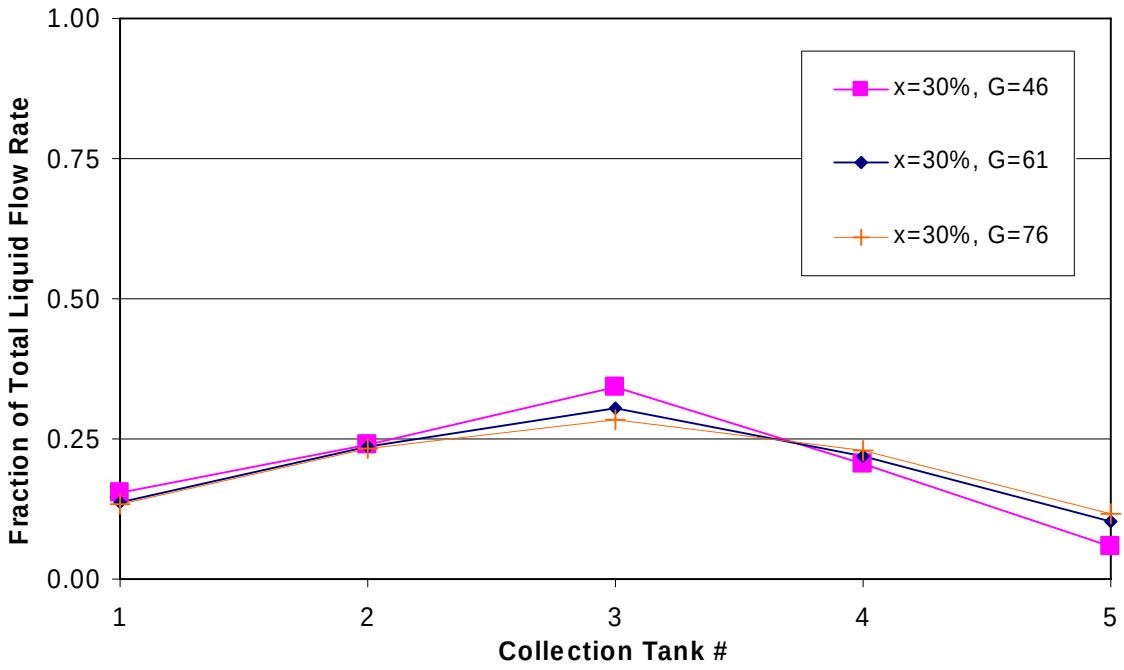

Figure C-11: 1/4 Depth Protrusion, Short Inlet, x=30%

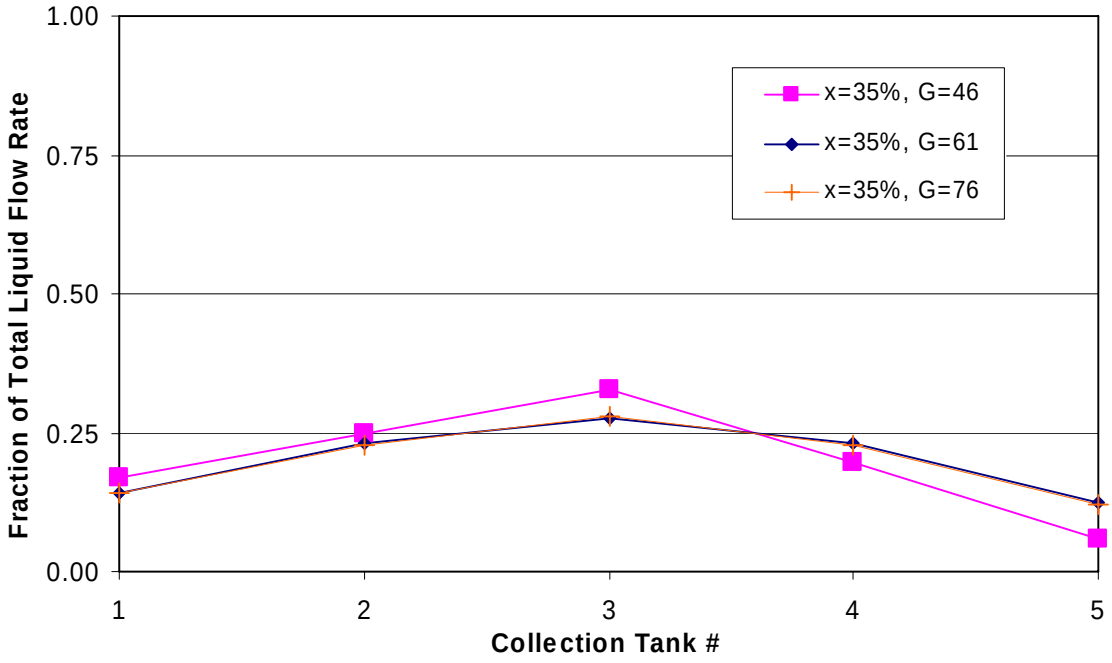

Figure C-12: 1/4 Depth Protrusion, Short Inlet, x=35%

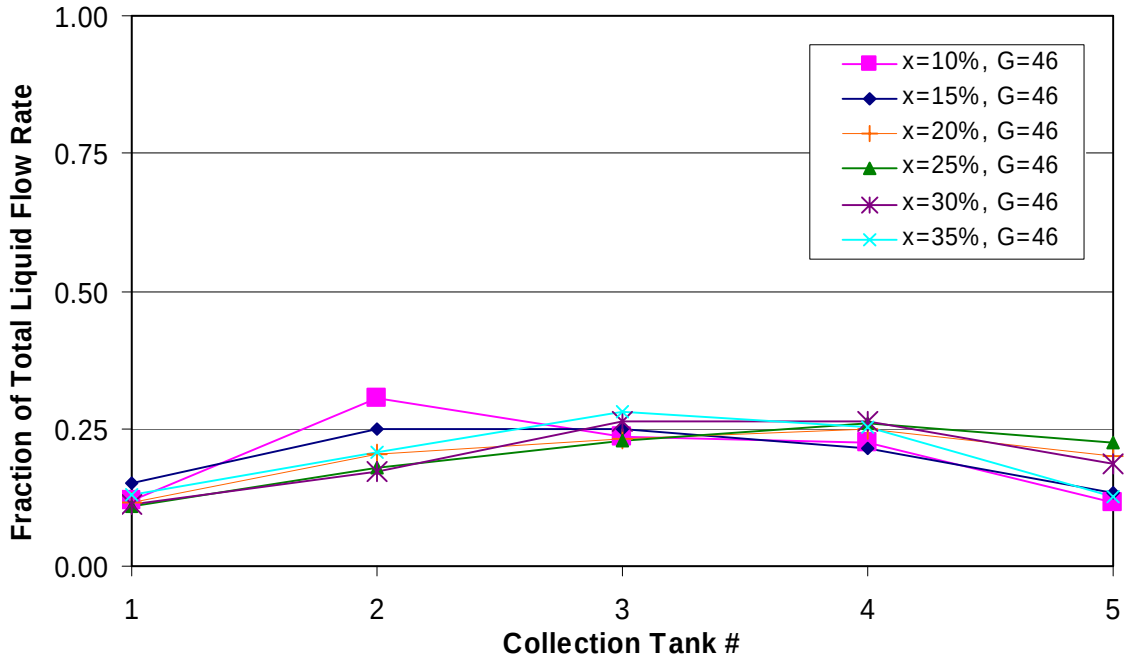

Figure C-13: 1/2 Depth Protrusion, Short Inlet, G=46 kg/m^{2}s

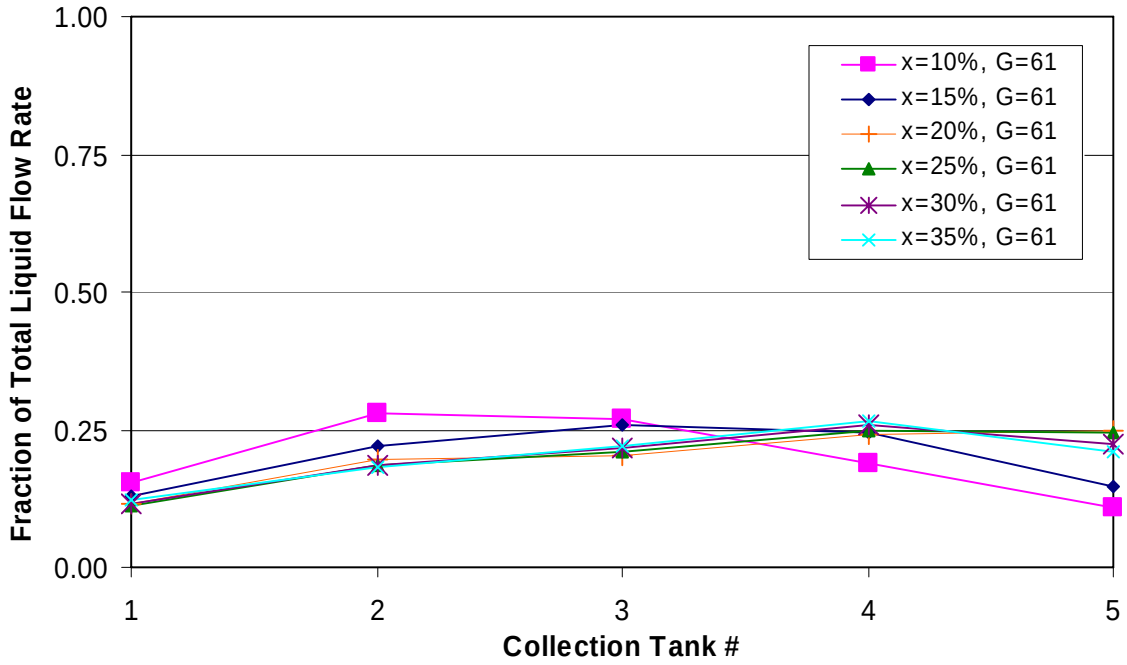

Figure C-14: 1/2 Depth Protrusion, Short Inlet, G=61 kg/m^{2}s

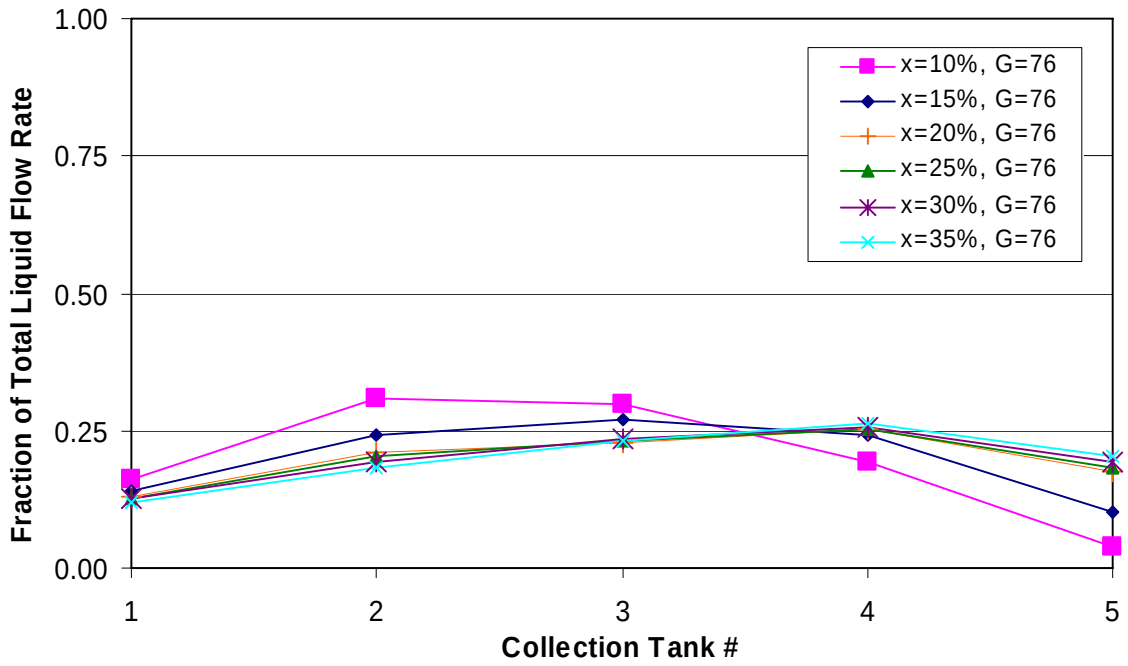

Figure C-15: 1/2 Depth Protrusion, Short Inlet, G=76 kg/m^{2}s

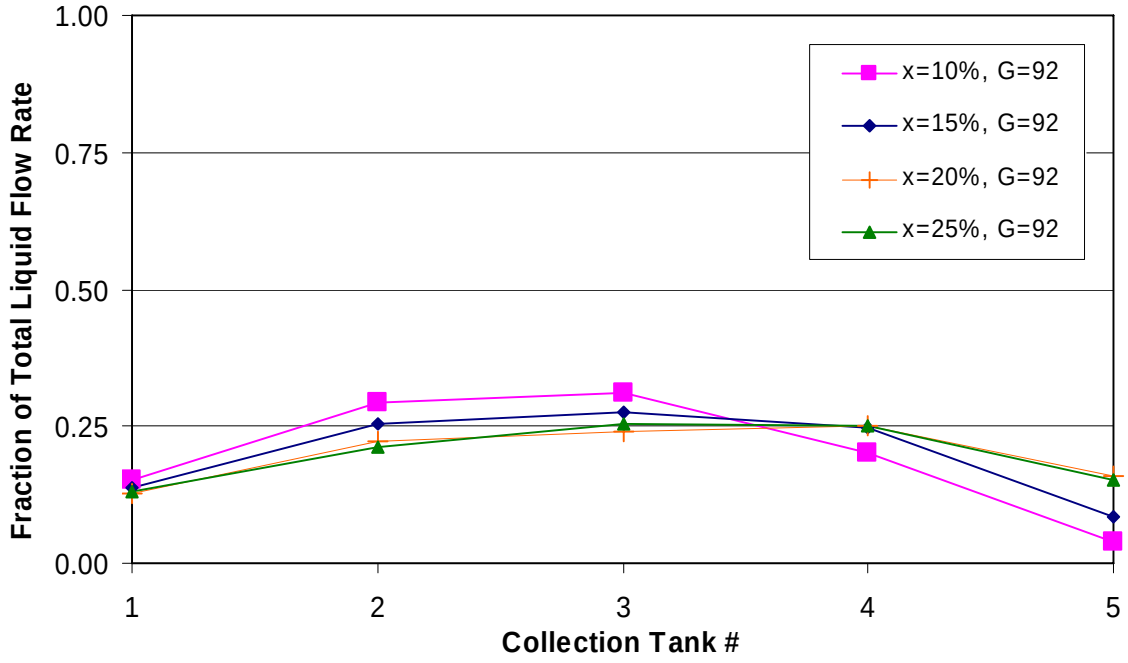

Figure C-16: 1/2 Depth Protrusion, Short Inlet, G=92 kg/m^{2}s

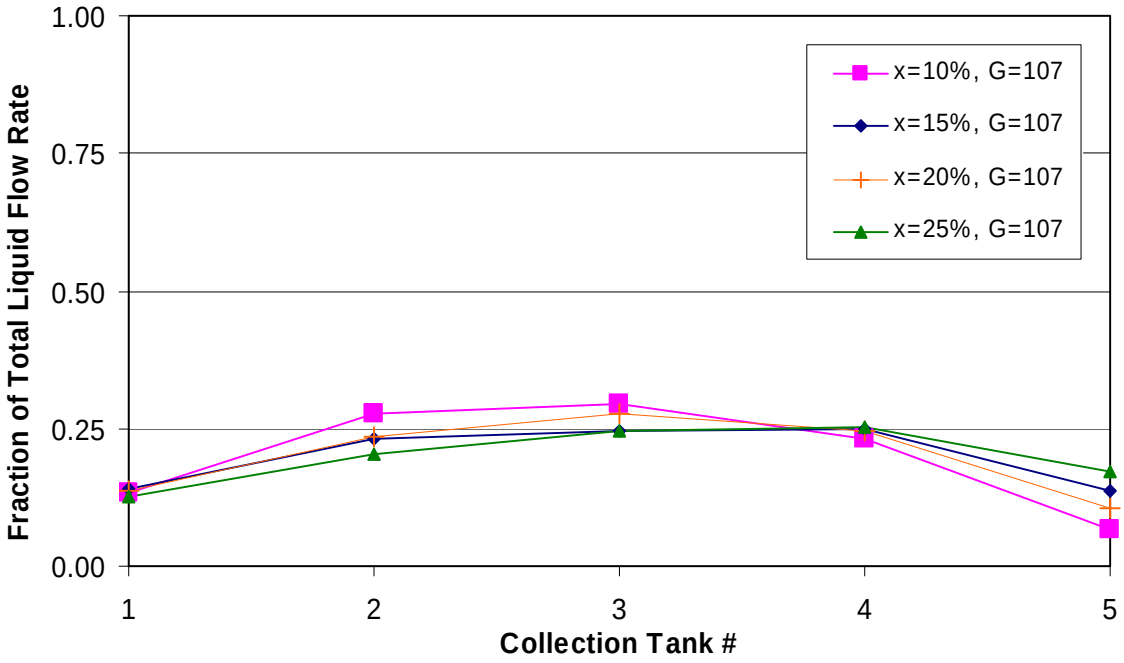

Figure C-17: 1/2 Depth Protrusion, Short Inlet, G=107 kg/m^{2}s

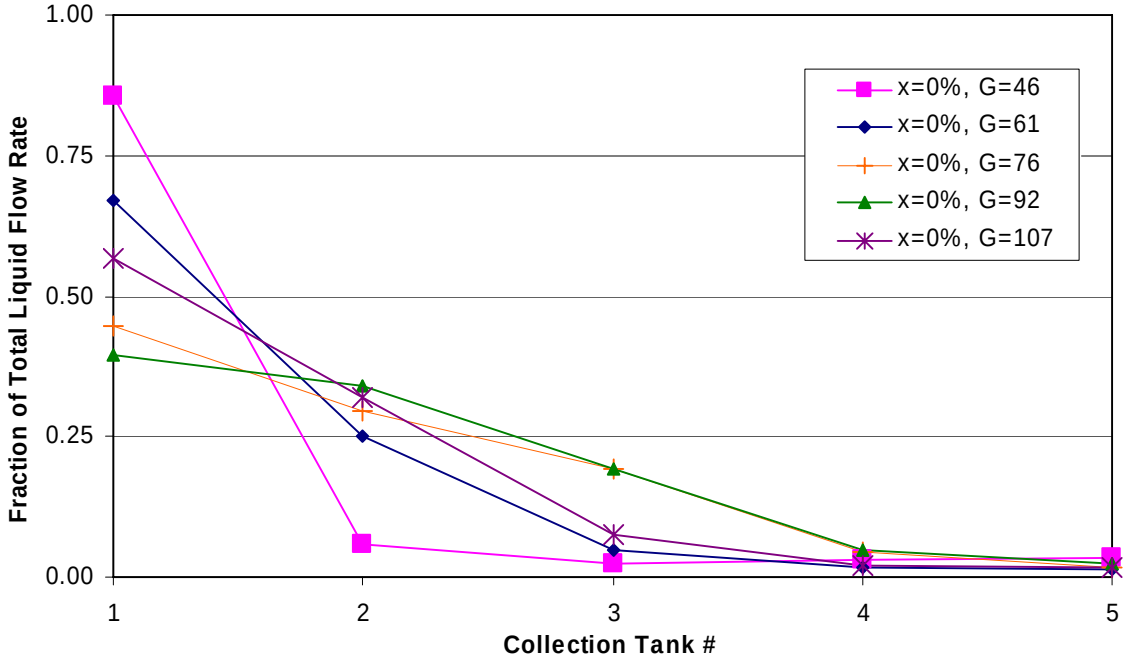

Figure C-18: 1/2 Depth Protrusion, Short Inlet, x=0%

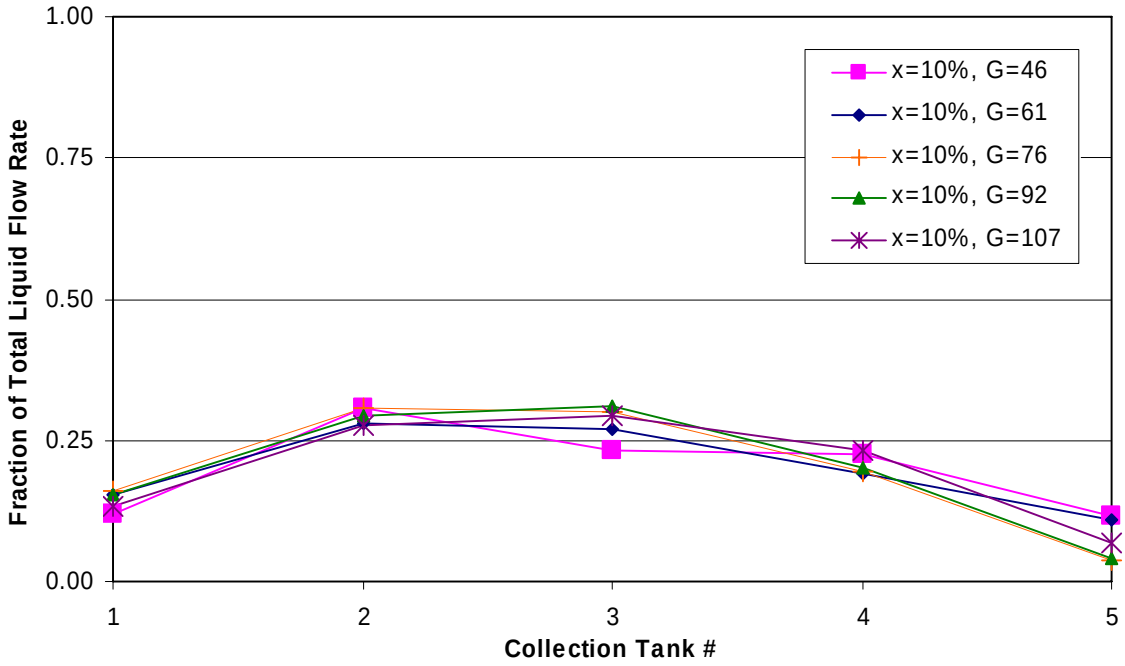

Figure C-19: 1/2 Depth Protrusion, Short Inlet, x=10%

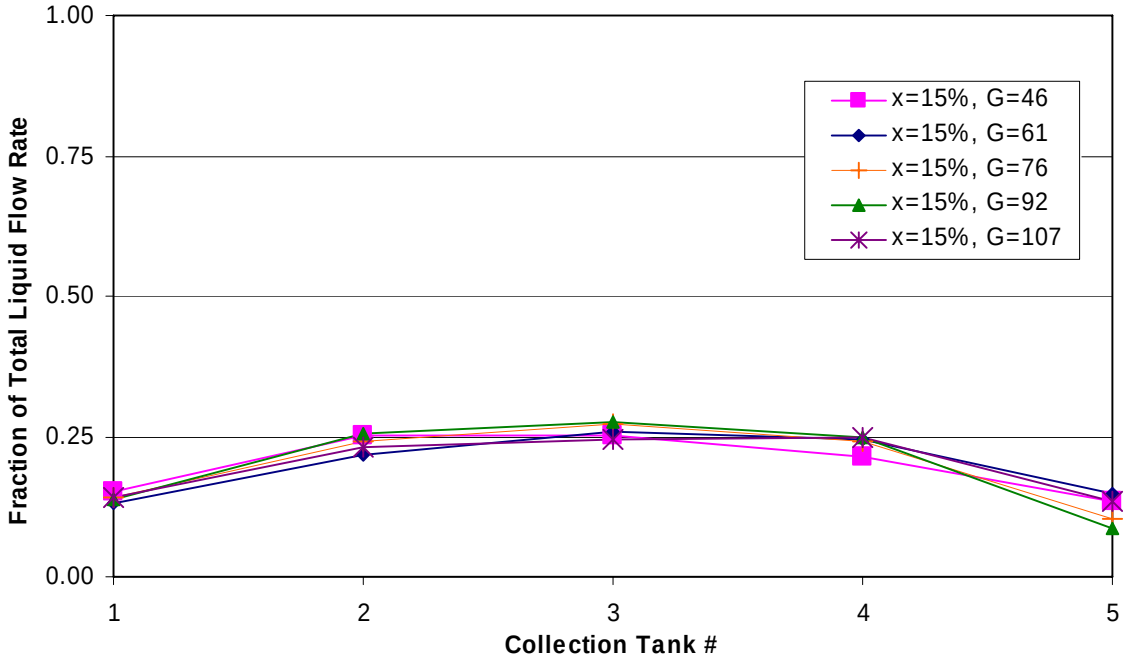

Figure C-20: 1/2 Depth Protrusion, Short Inlet, x=15%

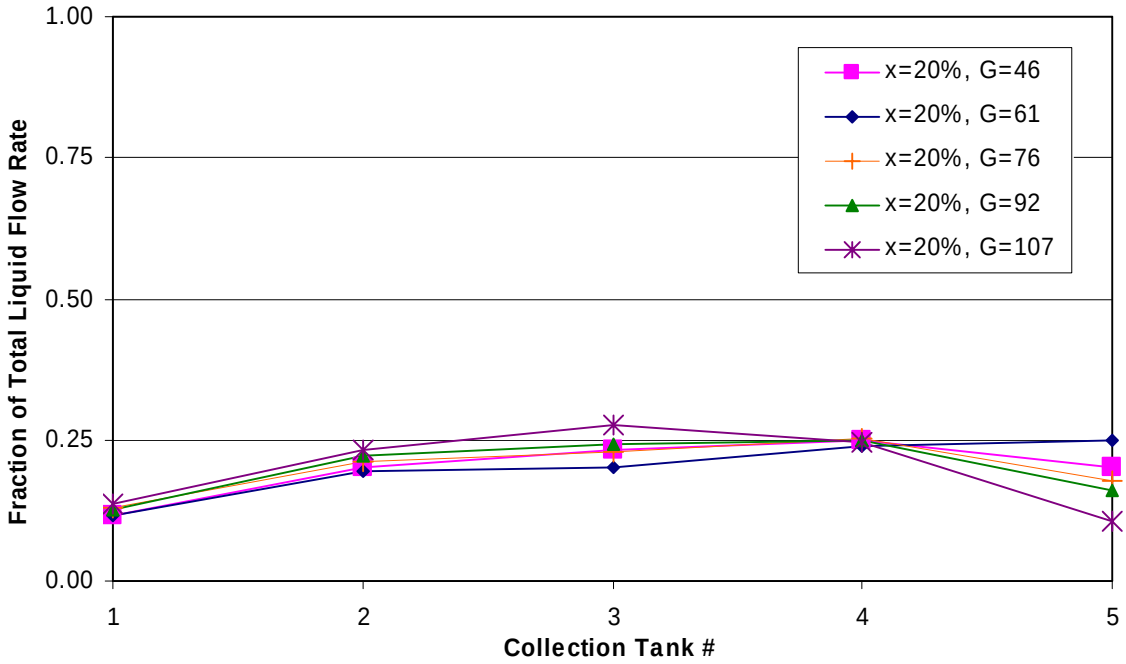

Figure C-21: 1/2 Depth Protrusion, Short Inlet, x=20%

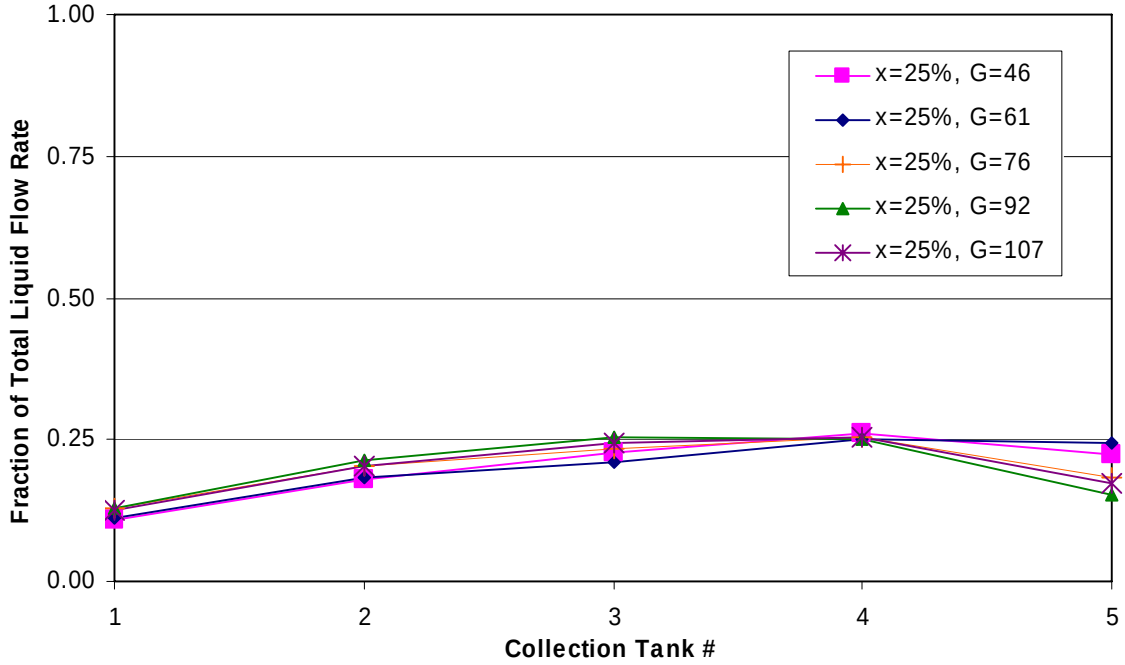

Figure C-22: 1/2 Depth Protrusion, Short Inlet, x=25%

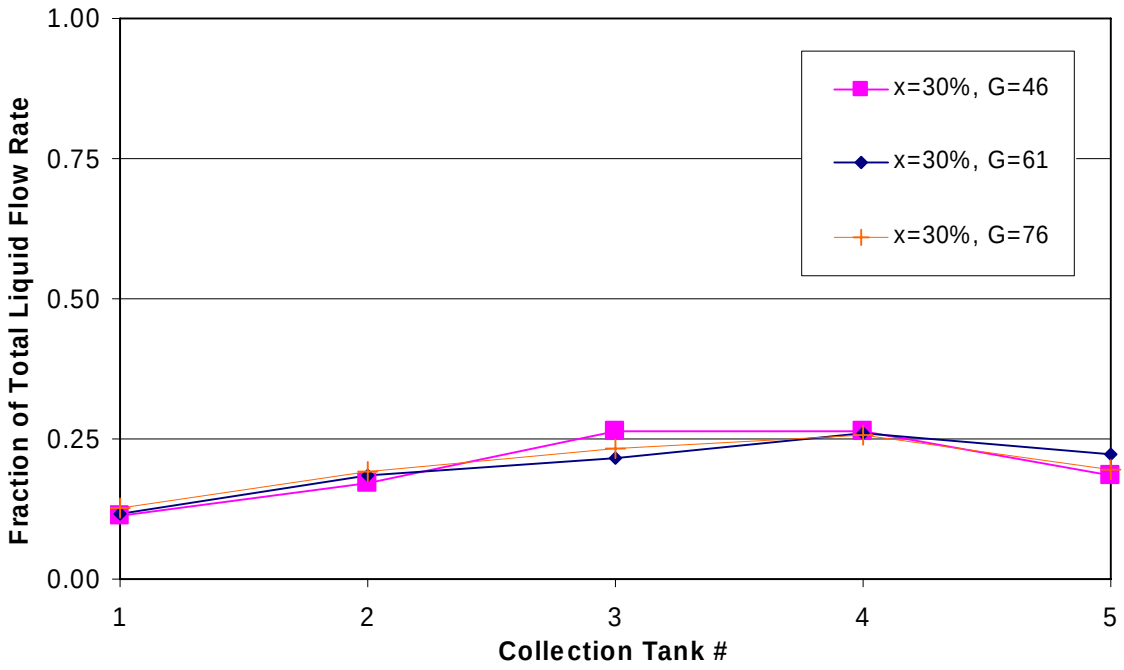

Figure C-23: 1/2 Depth Protrusion, Short Inlet, x=30%

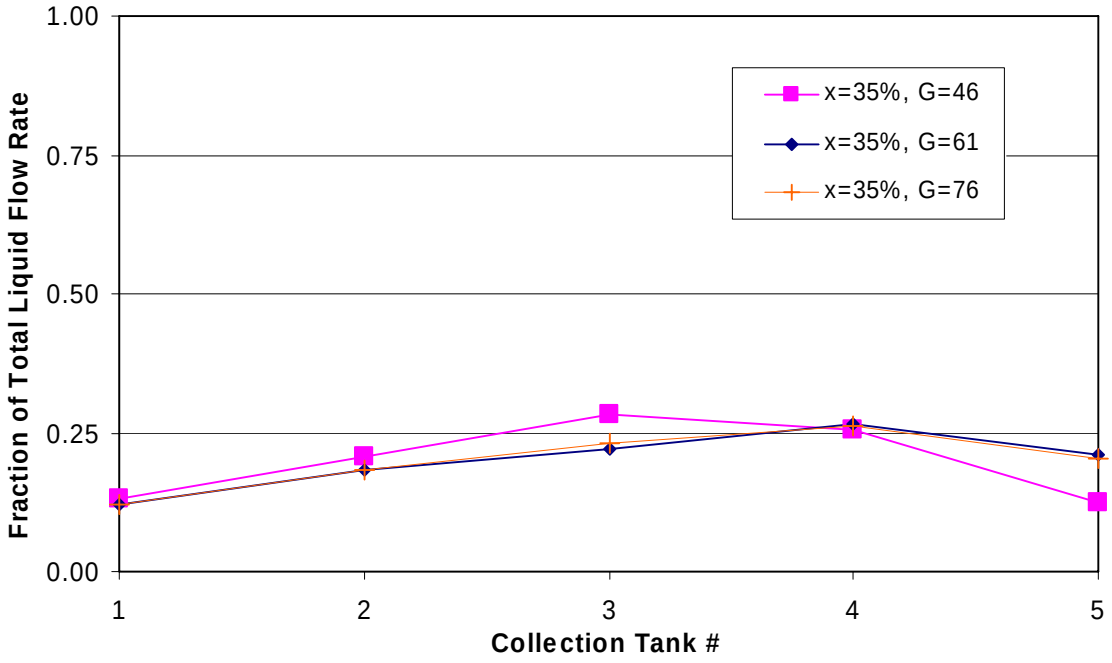

Figure C-24: 1/2 Depth Protrusion, Short Inlet, x=35%

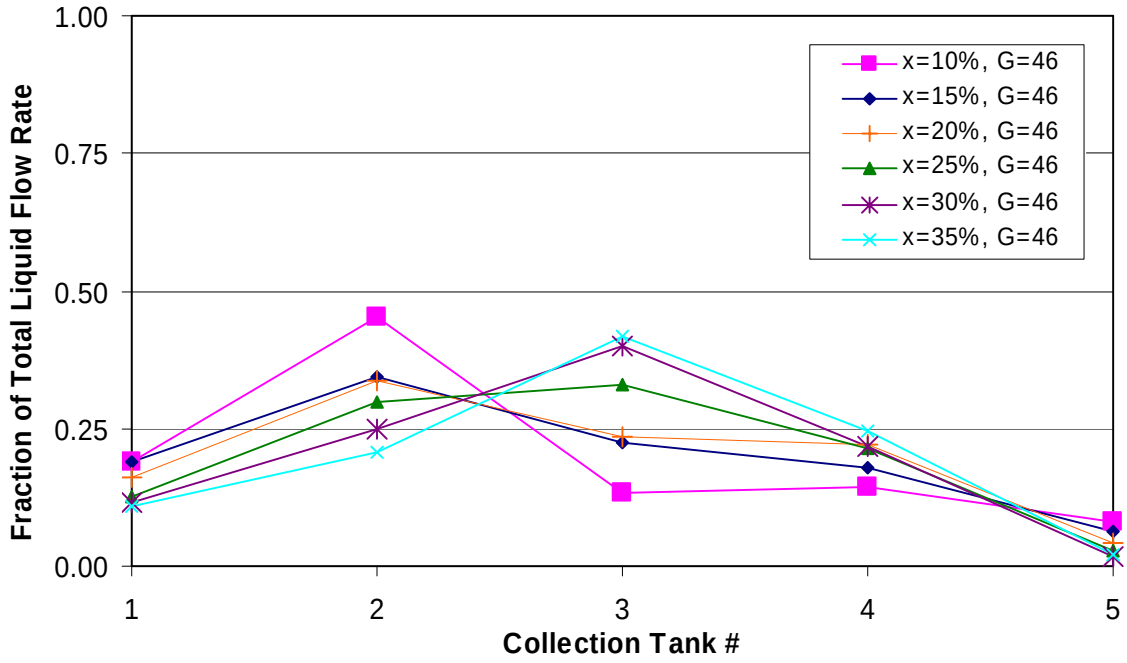

Figure C-25: 3/4 Depth Protrusion, Short Inlet, G=46 kg/m^{2}s

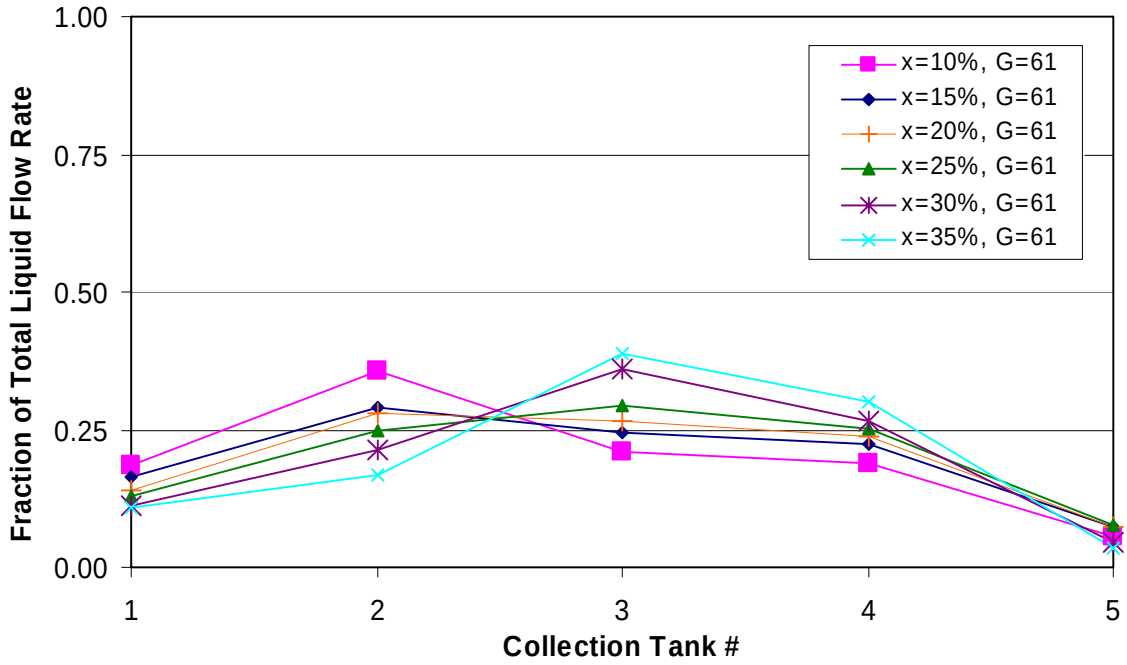

Figure C-26: 3/4 Depth Protrusion, Short Inlet, G=61kg/m^{2}s

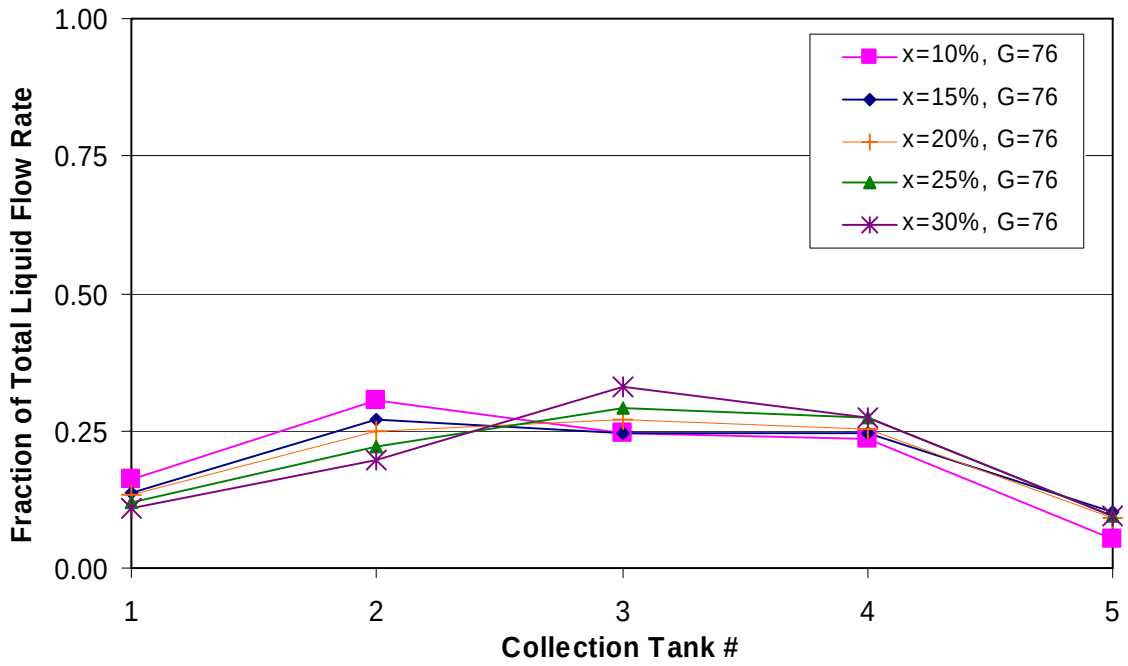

Figure C-27: 3/4 Depth Protrusion, Short Inlet, G=76 kg/m^{2}s

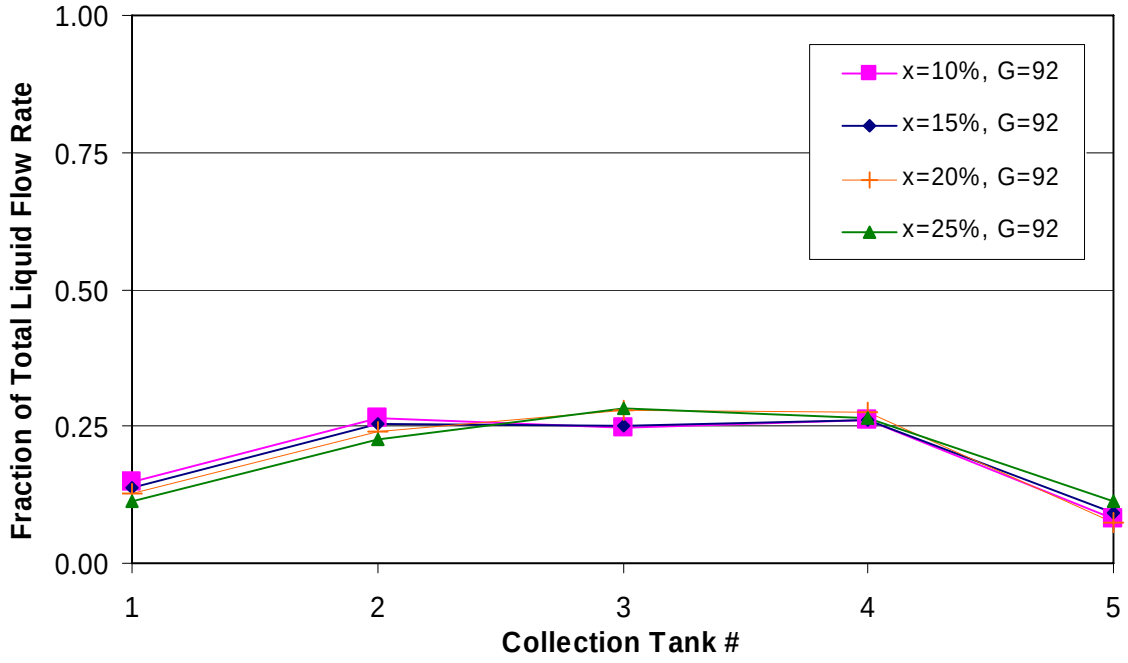

Figure C-28: 3/4 Depth Protrusion, Short Inlet, G=92 kg/m^{2}s

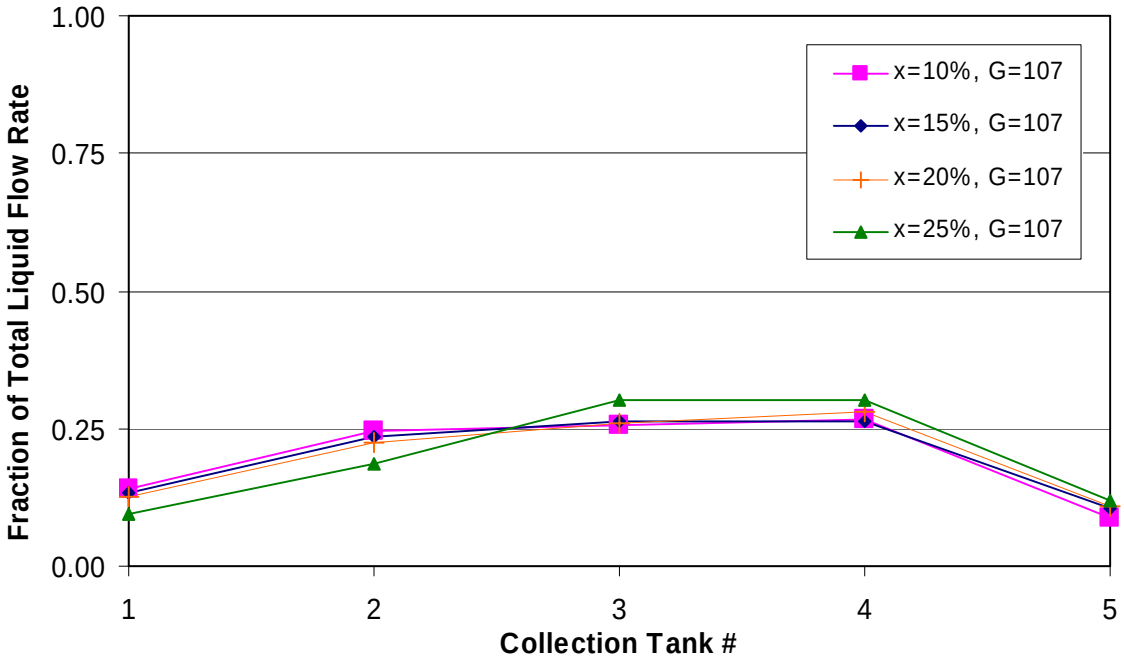

Figure C-29: 3/4 Depth Protrusion, Short Inlet, G=107 kg/m^{2}s

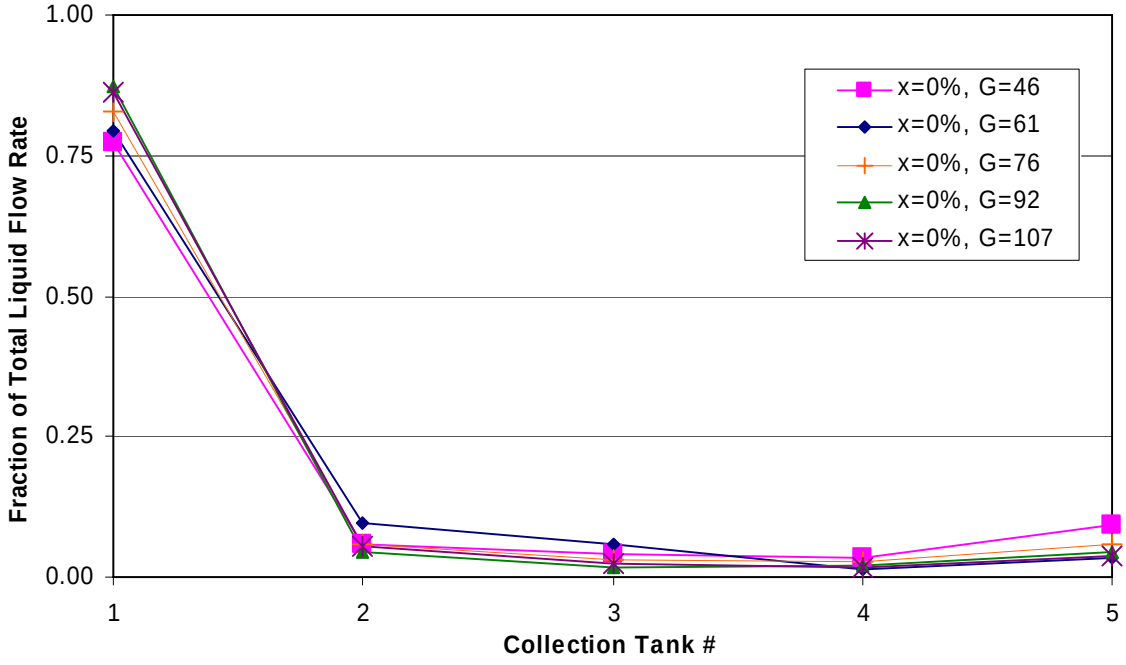

Figure C-30: 3/4 Depth Protrusion, Short Inlet, x=0%

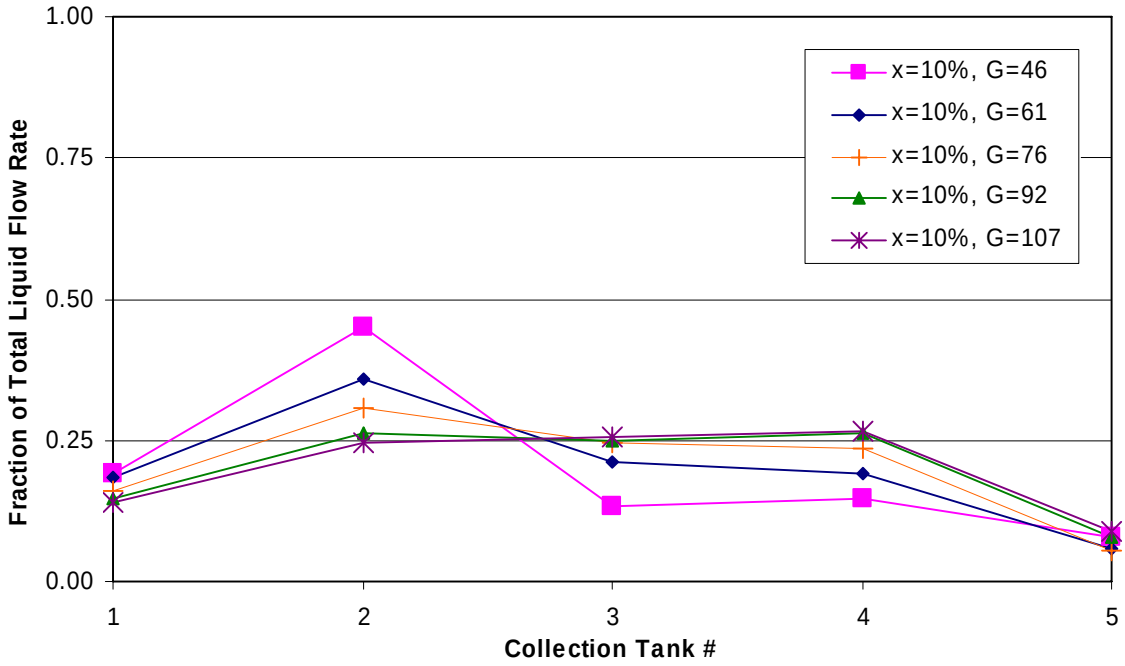

Figure C-31: 3/4 Depth Protrusion, Short Inlet, x=10%

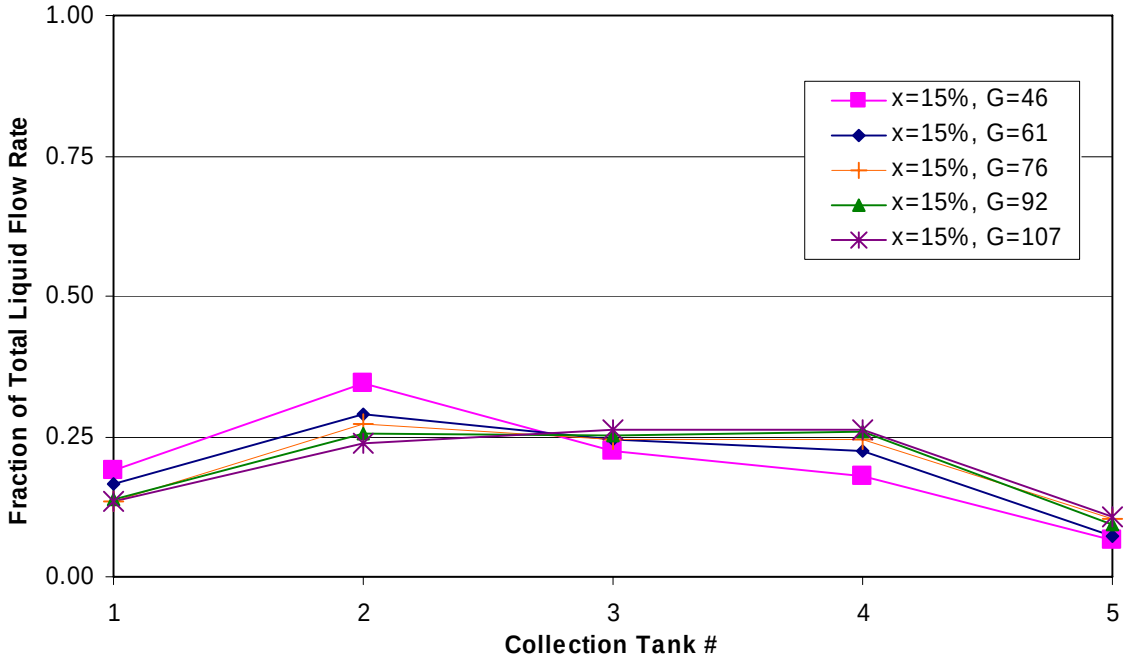

Figure C-32: 3/4 Depth Protrusion, Short Inlet, x=15%

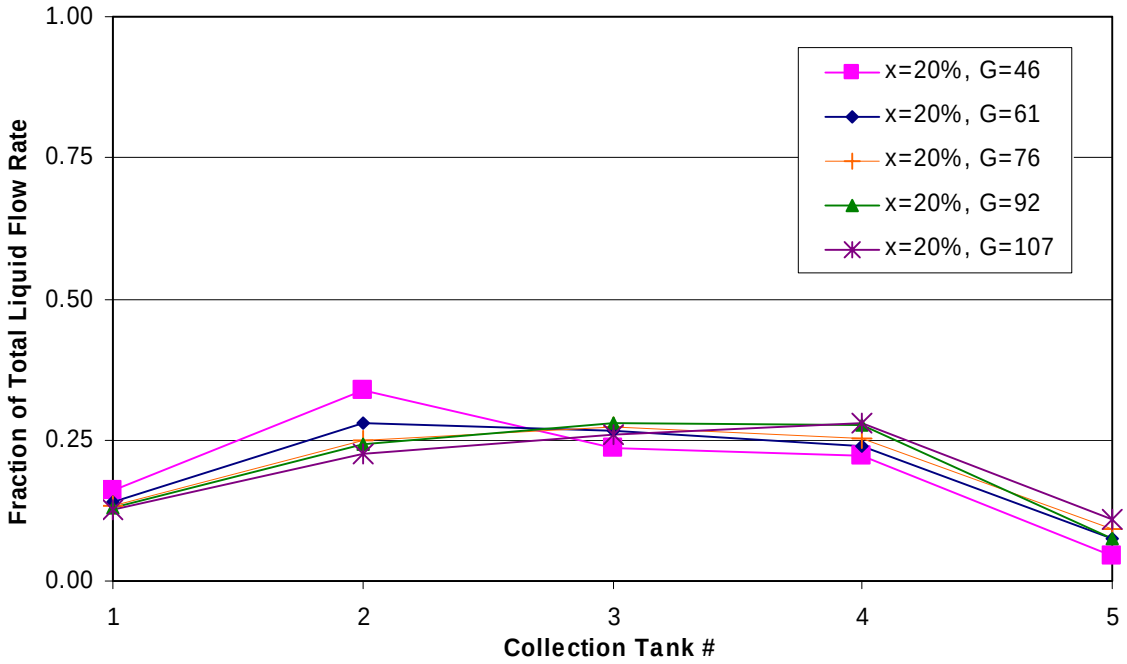

Figure C-33: 3/4 Depth Protrusion, Short Inlet, x=20%

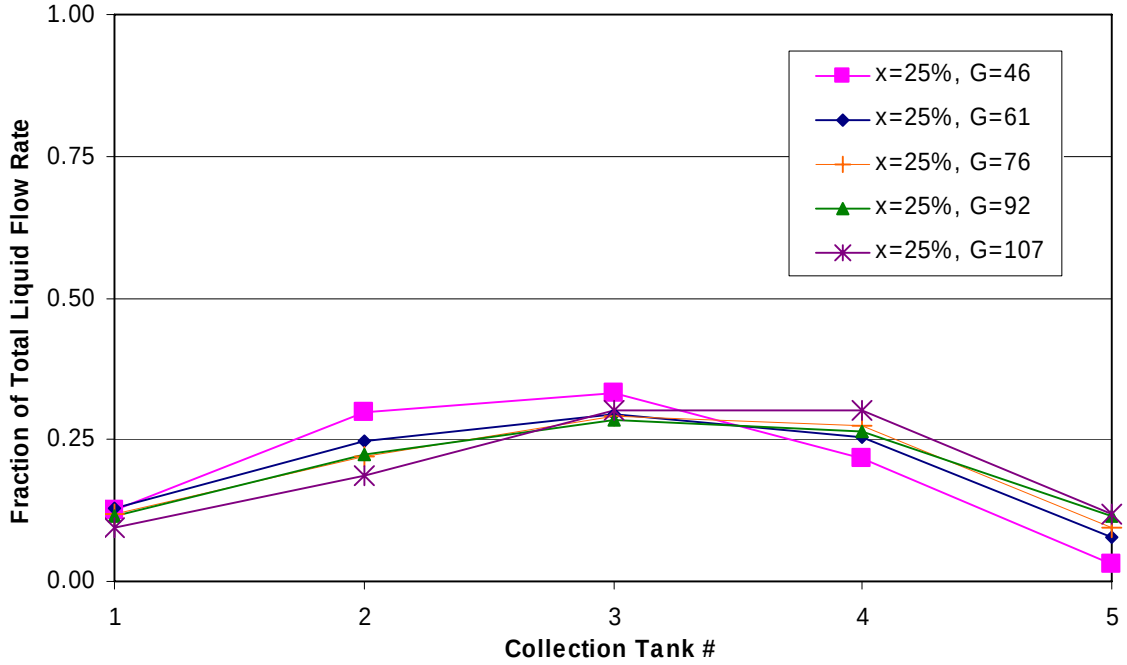

Figure C-34: 3/4 Depth Protrusion, Short Inlet, x=25%

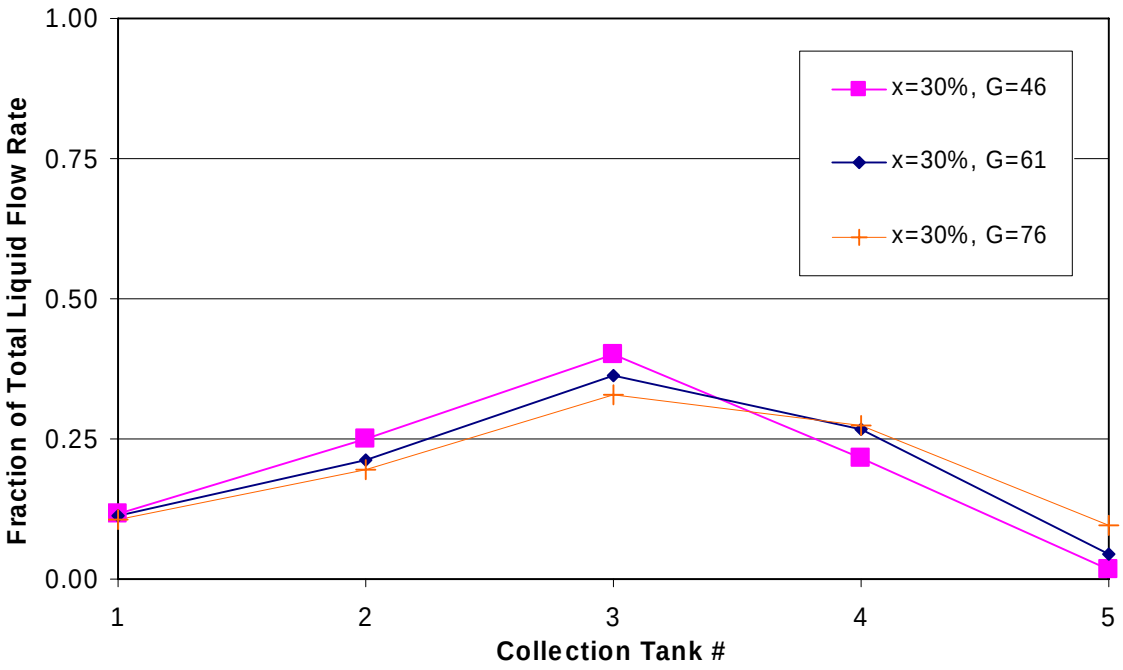

Figure C-35: 3/4 Depth Protrusion, Short Inlet, x=30%

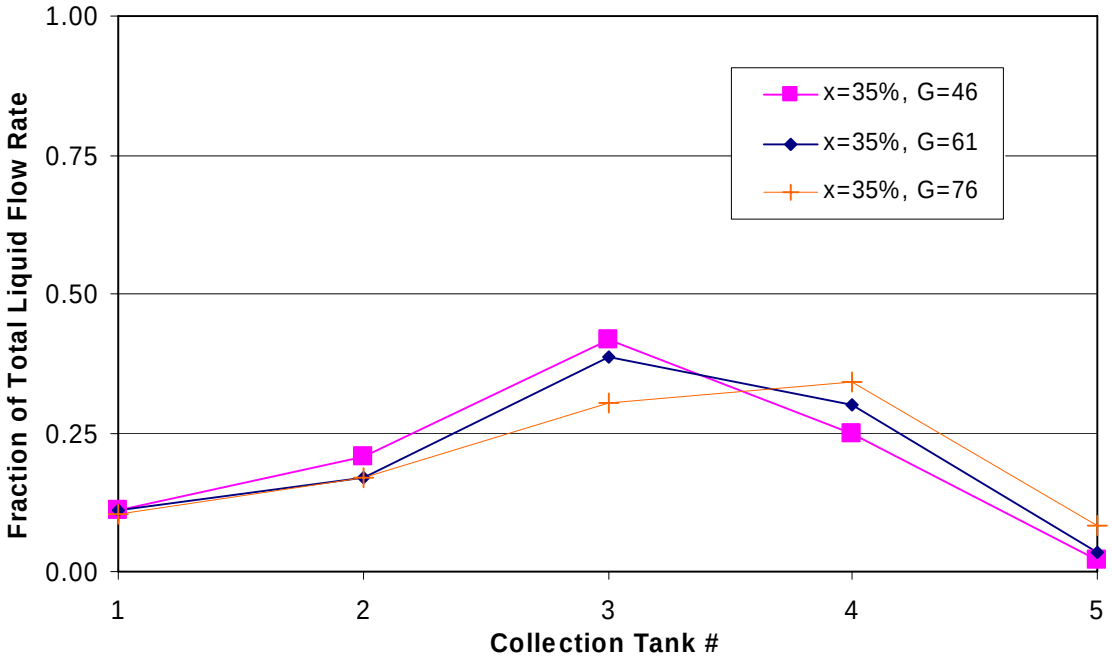

Figure C-36: 3/4 Depth Protrusion, Short Inlet, x=35%

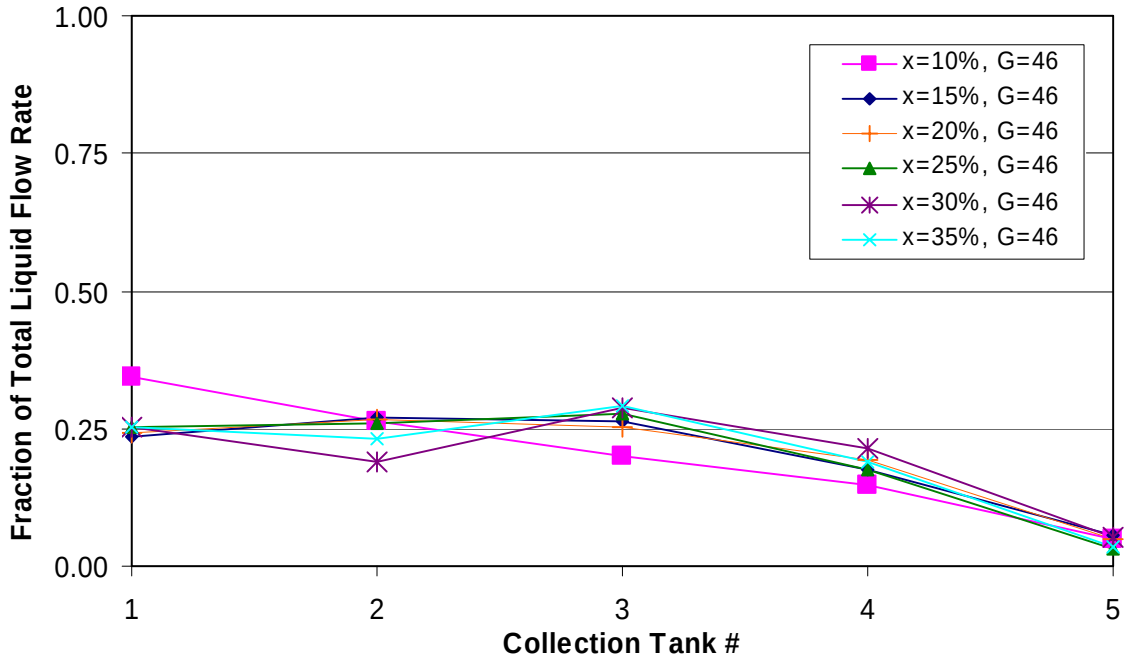

Figure C-37: Stagger Up Protrusion, Short Inlet, G=46 kg/m^{2}s

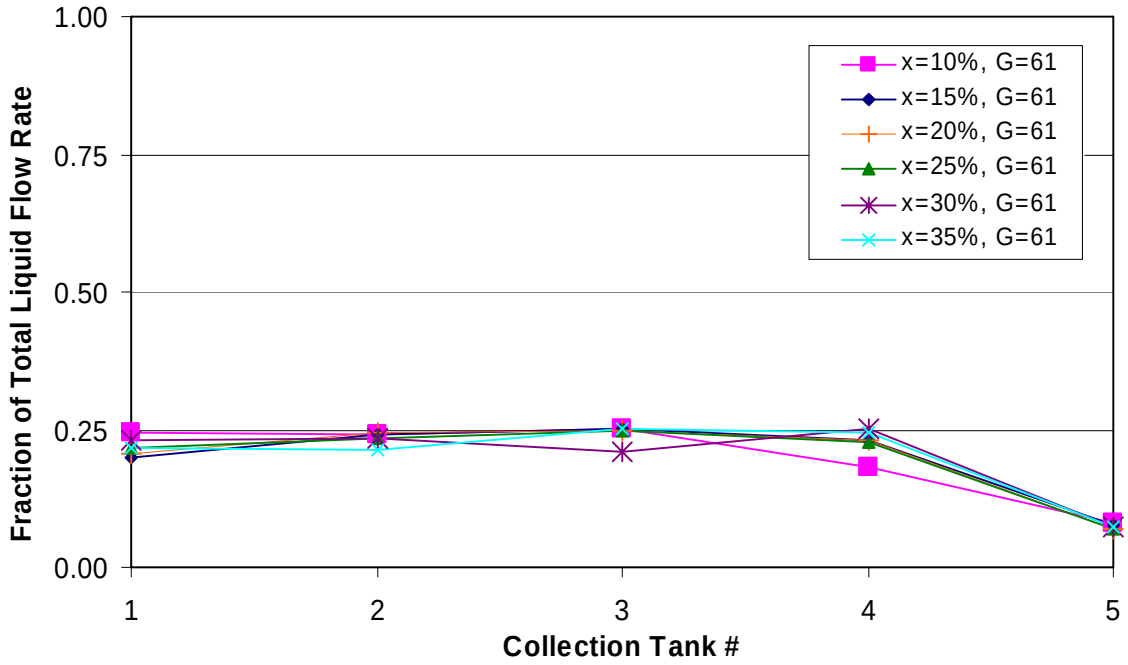

Figure C-38: Stagger Up Protrusion, Short Inlet, G=61 kg/m^{2}s

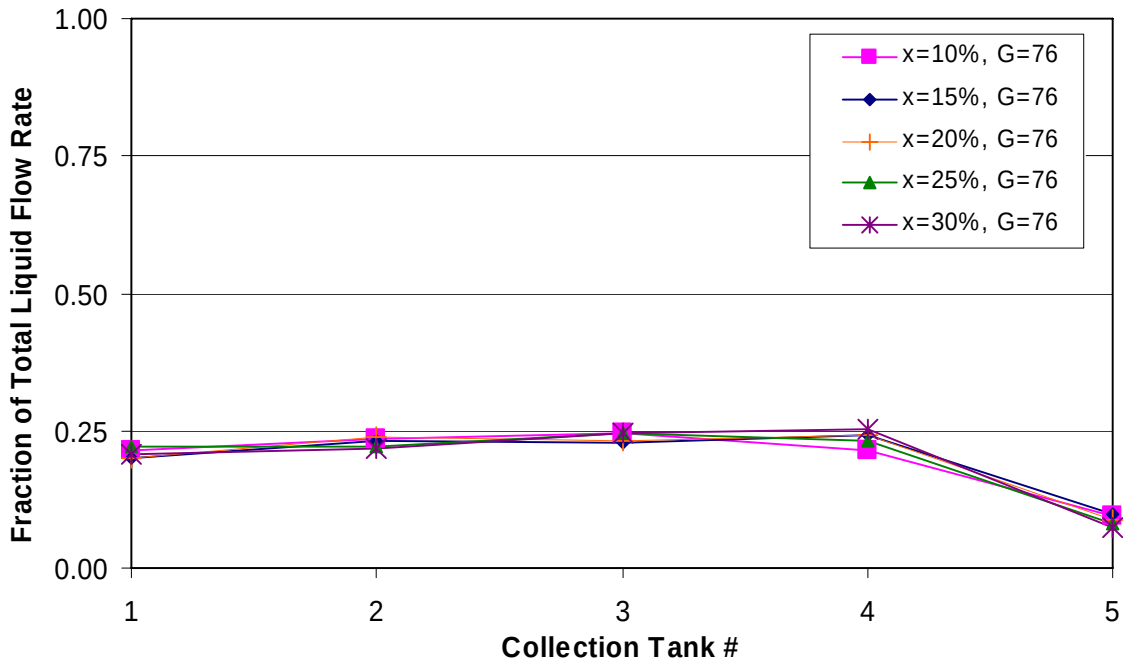

Figure C-39: Stagger Up Protrusion, Short Inlet, G=76 kg/m^{2}s

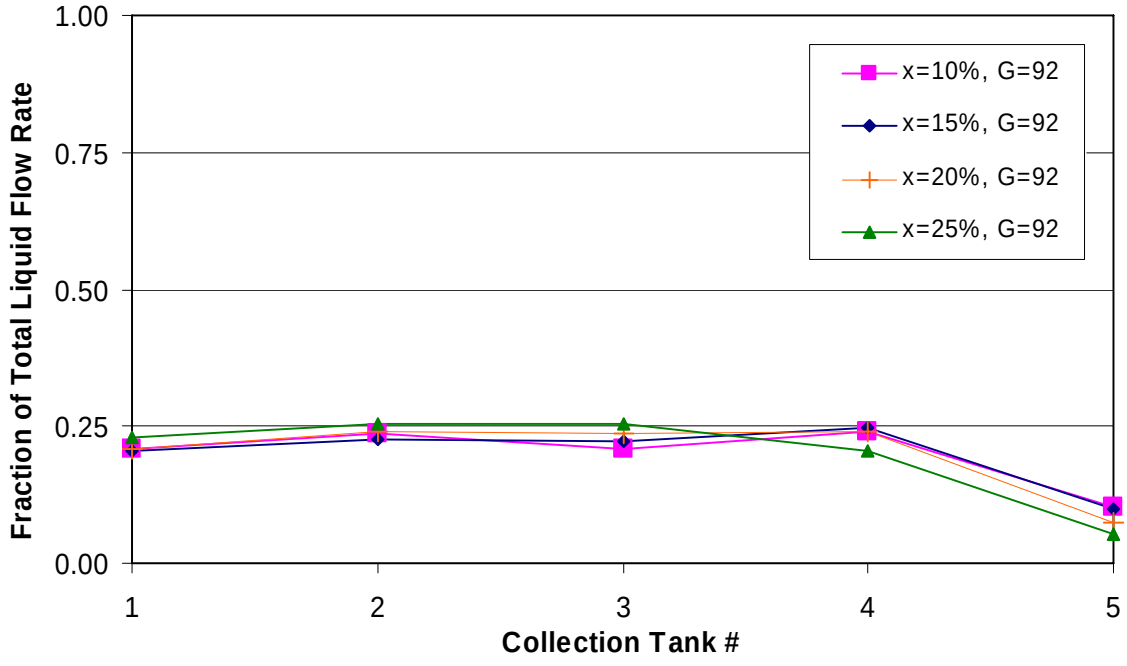

Figure C-40: Stagger Up Protrusion, Short Inlet, G=92 kg/m^{2}s

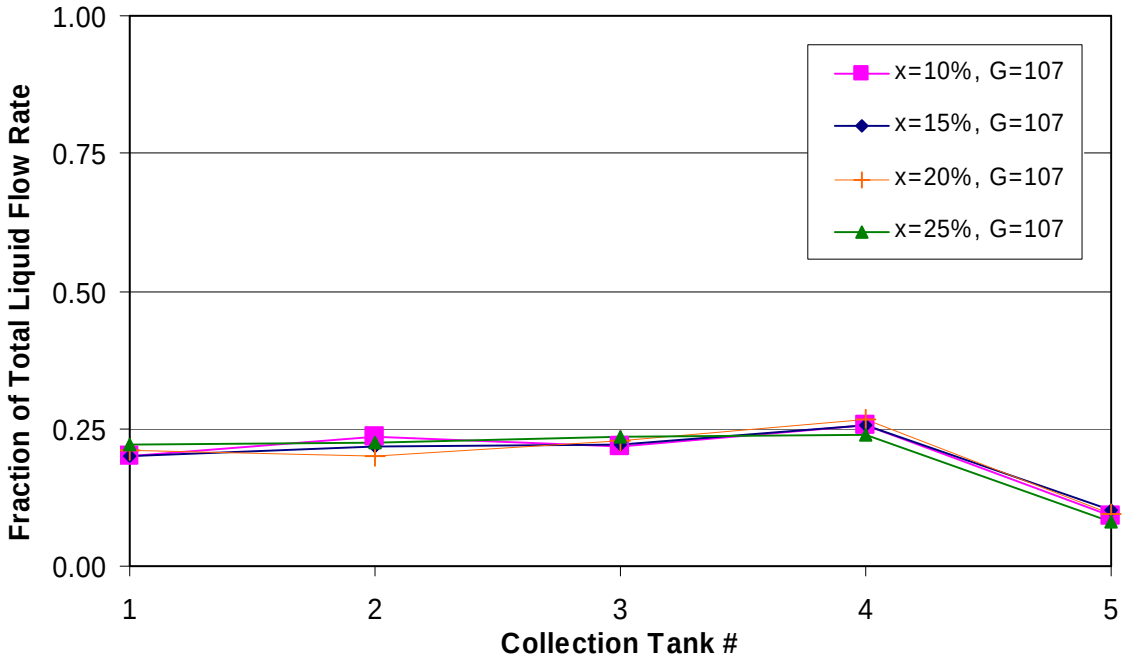

Figure C-41: Stagger Up Protrusion, Short Inlet, G=107 kg/m^{2}s

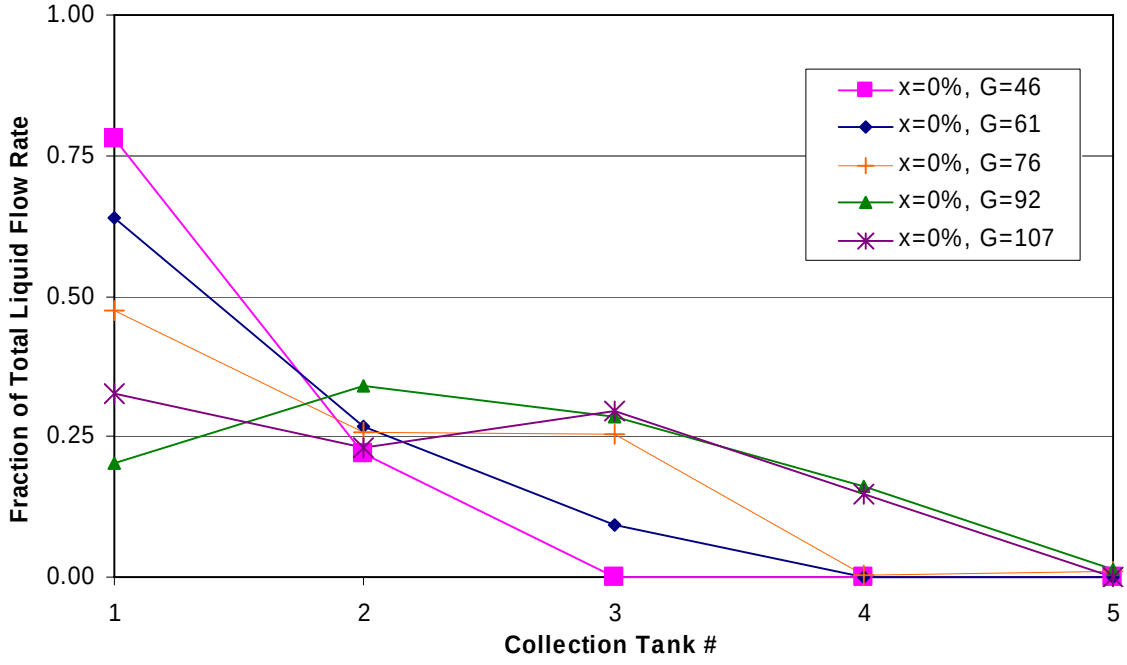

Figure C-42: Stagger Up Protrusion, Short Inlet, x=0%

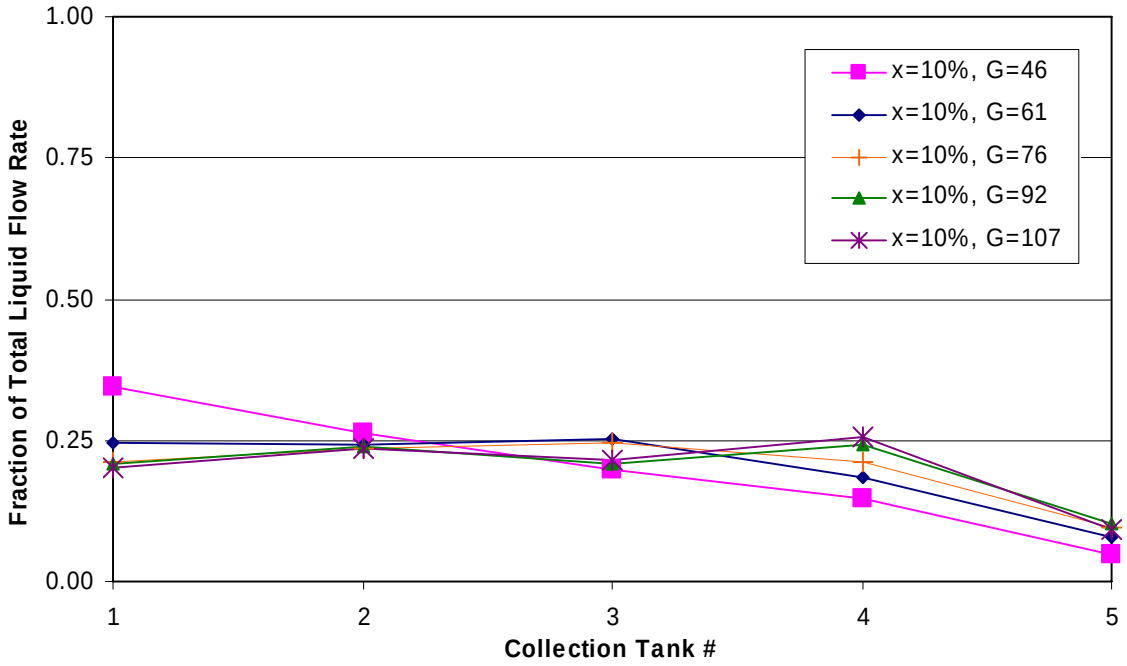

Figure C-43: Stagger Up Protrusion, Short Inlet, x=10%

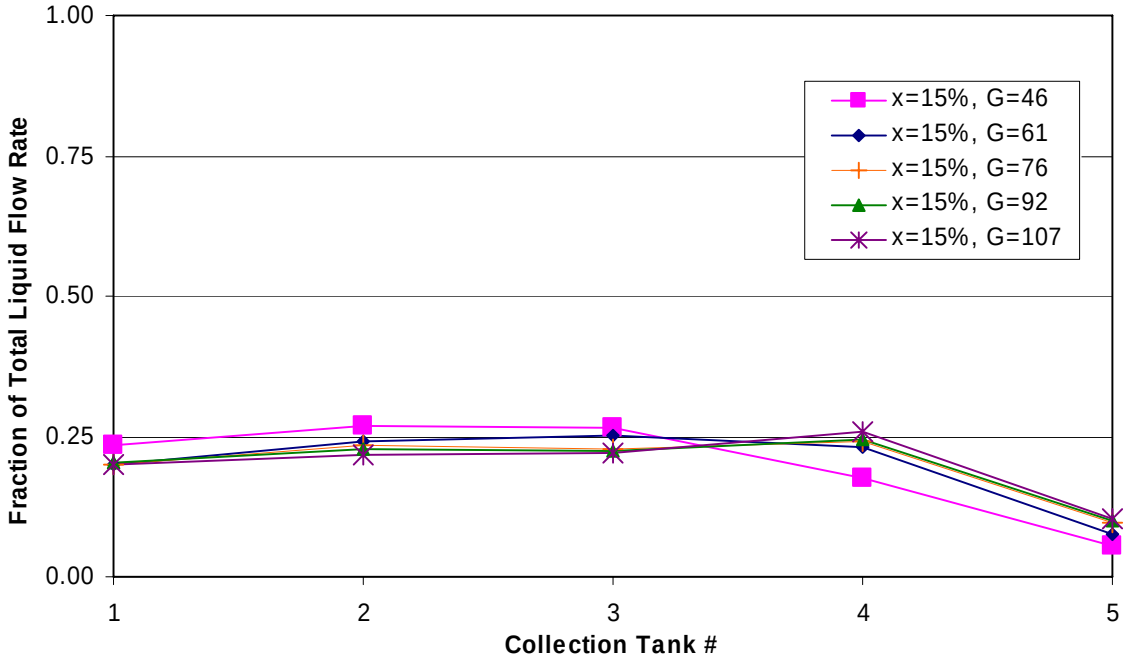

Figure C-44: Stagger Up Protrusion, Short Inlet, x=15%

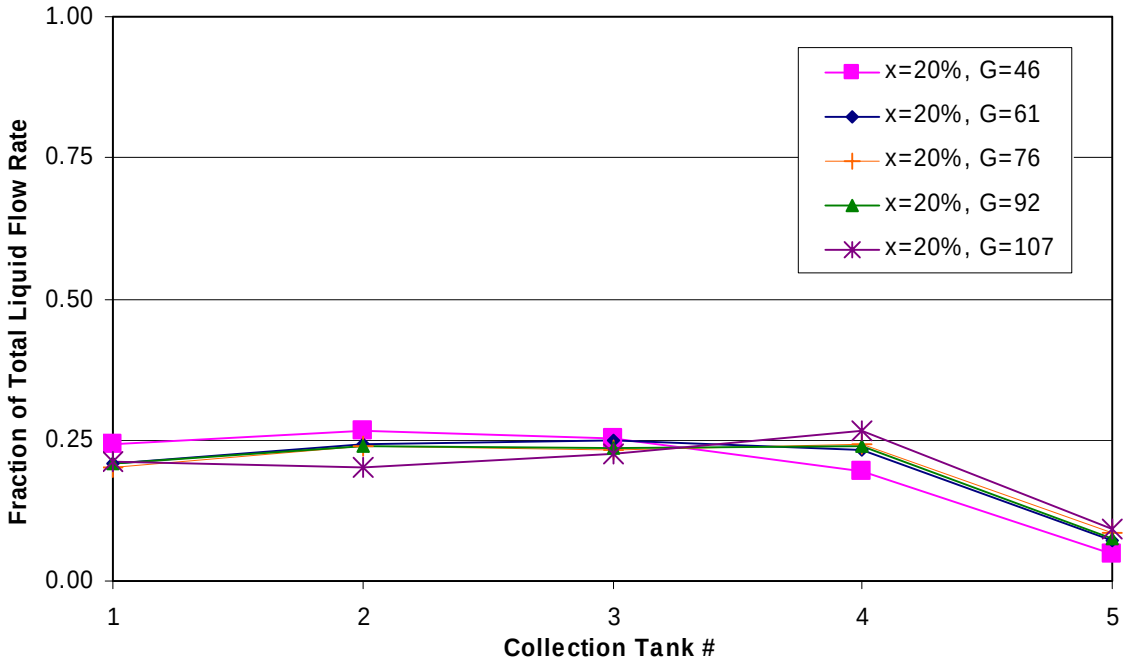

Figure C-45: Stagger Up Protrusion, Short Inlet, x=20%

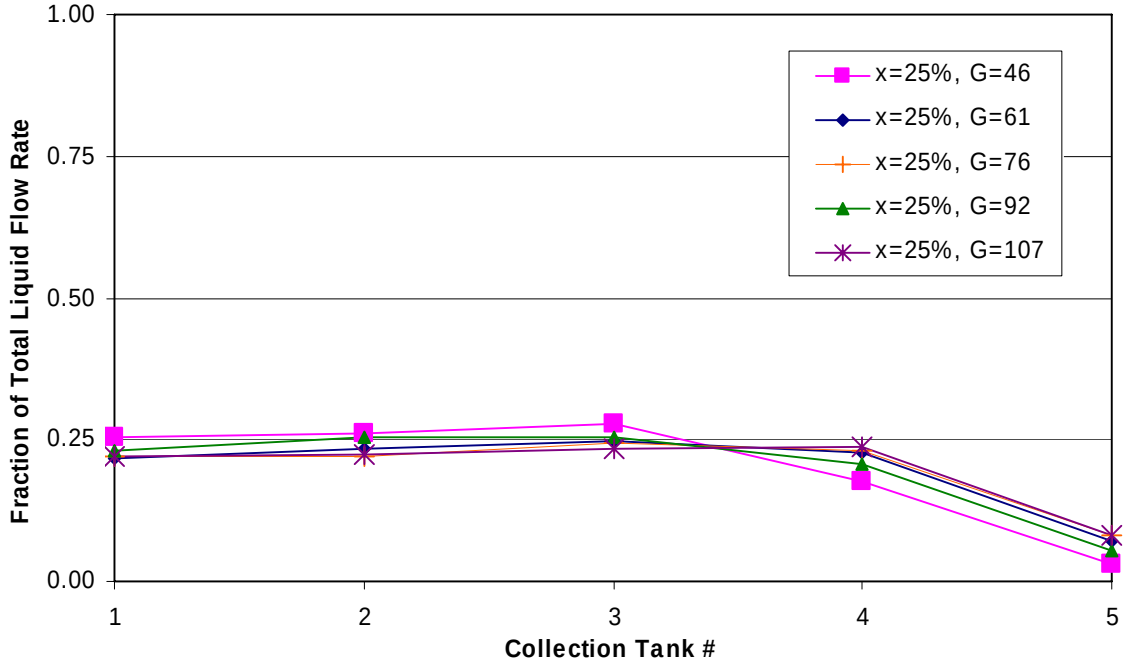

Figure C-46: Stagger Up Protrusion, Short Inlet, x=25%

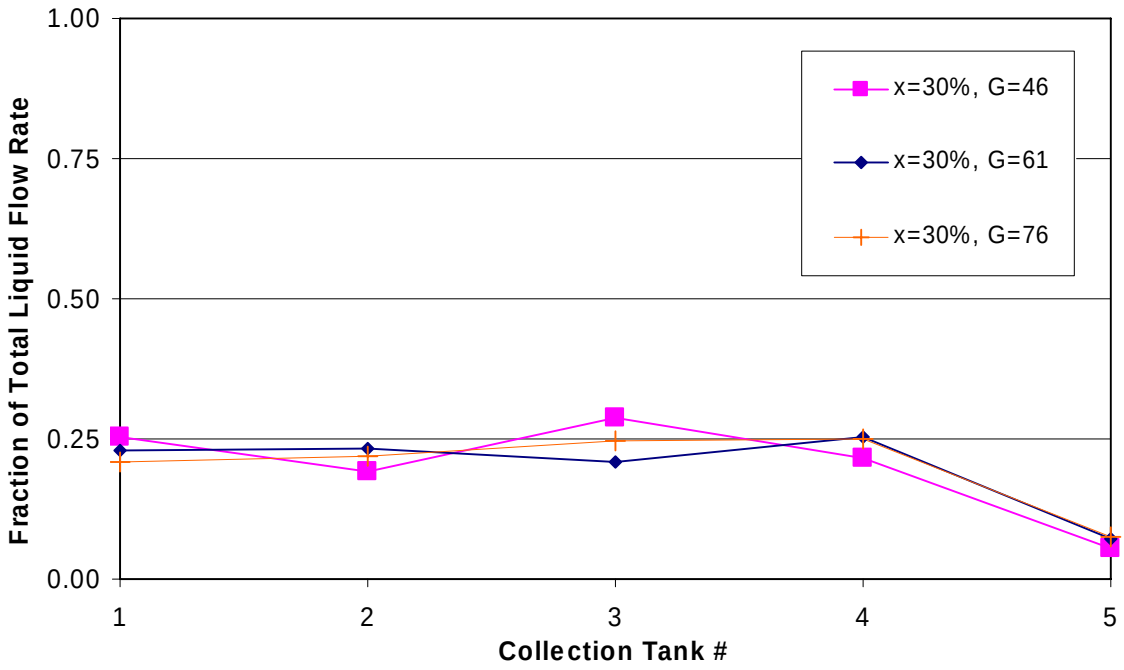

Figure C-47: Stagger Up Protrusion, Short Inlet, x=30%

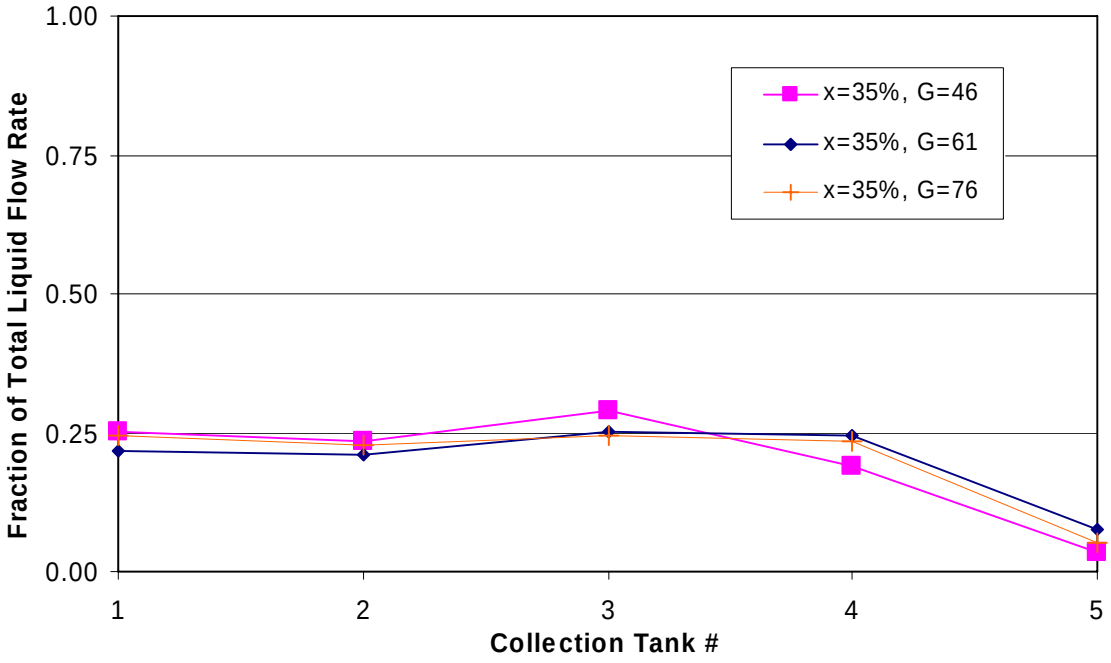

Figure C-48: Stagger Up Protrusion, Short Inlet, x=35%

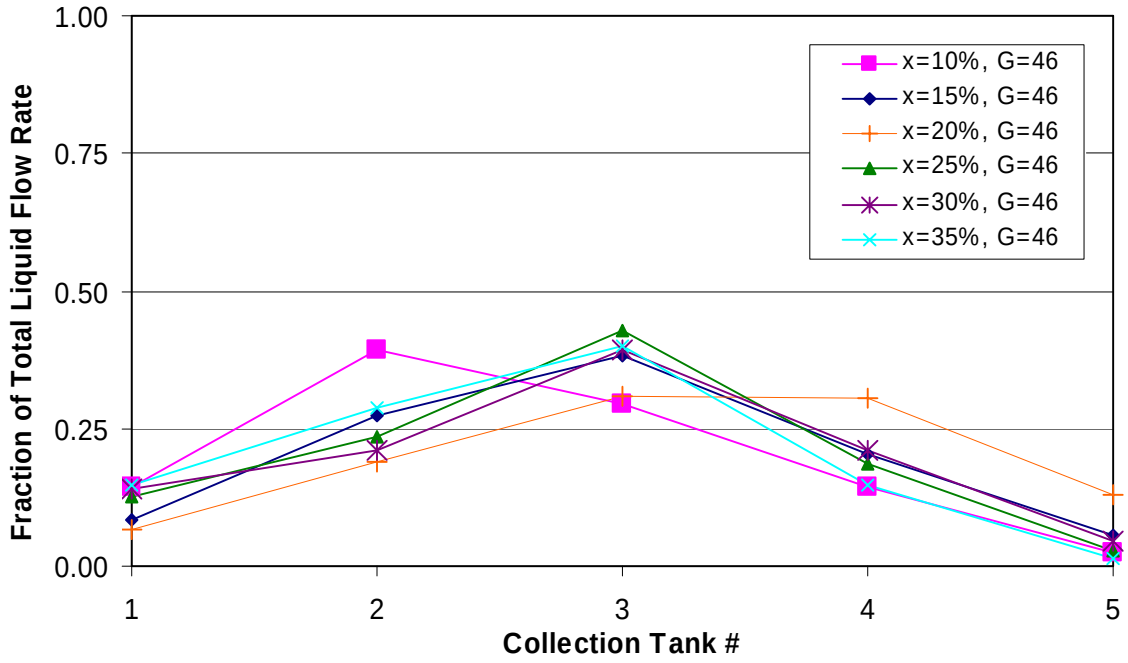

Figure C-49: Stagger Down Protrusion, Short Inlet, G=46 kg/m^{2}s

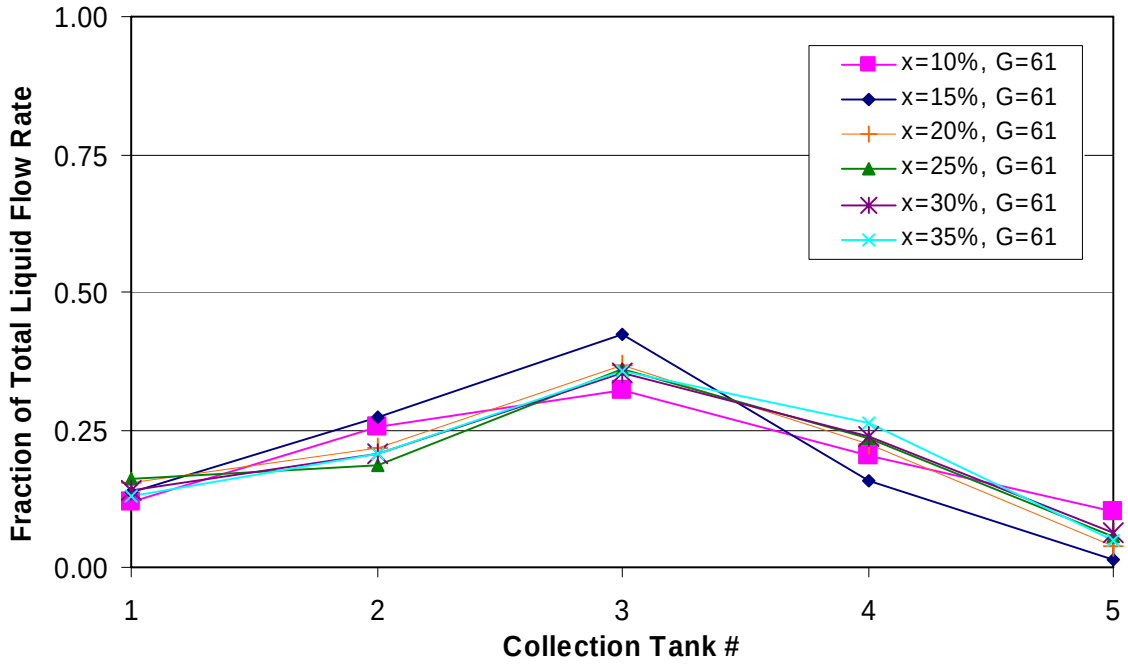

Figure C-50: Stagger Down Protrusion, Short Inlet, G=61 kg/m^{2}s

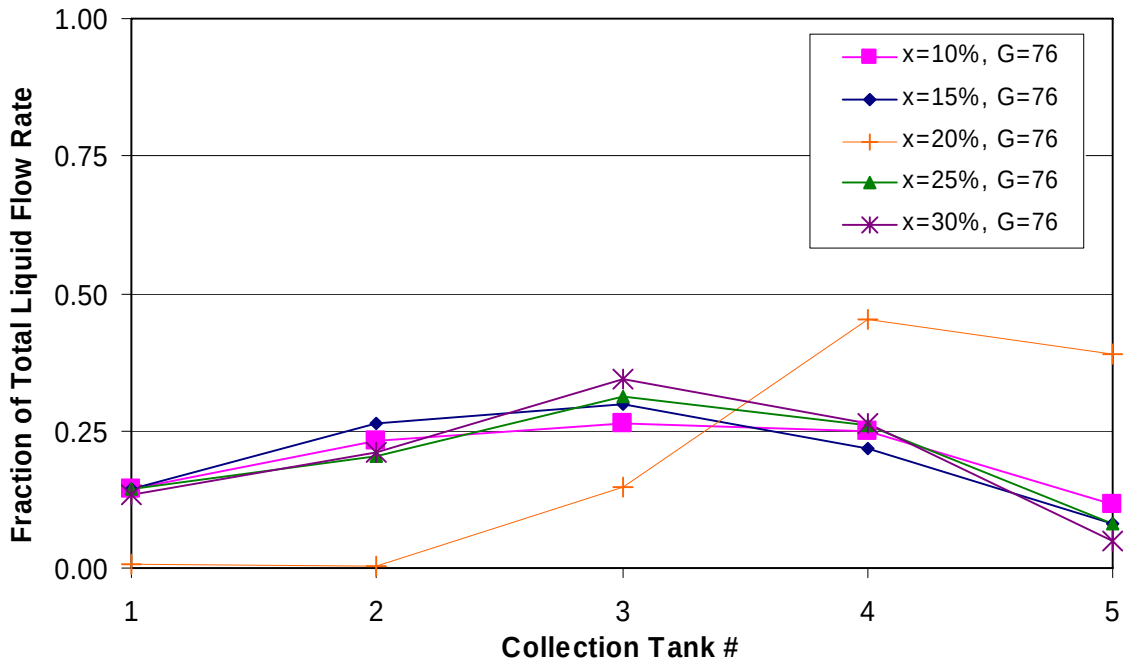

Figure C-51: Stagger Down Protrusion, Short Inlet, G=76 kg/m^{2}s

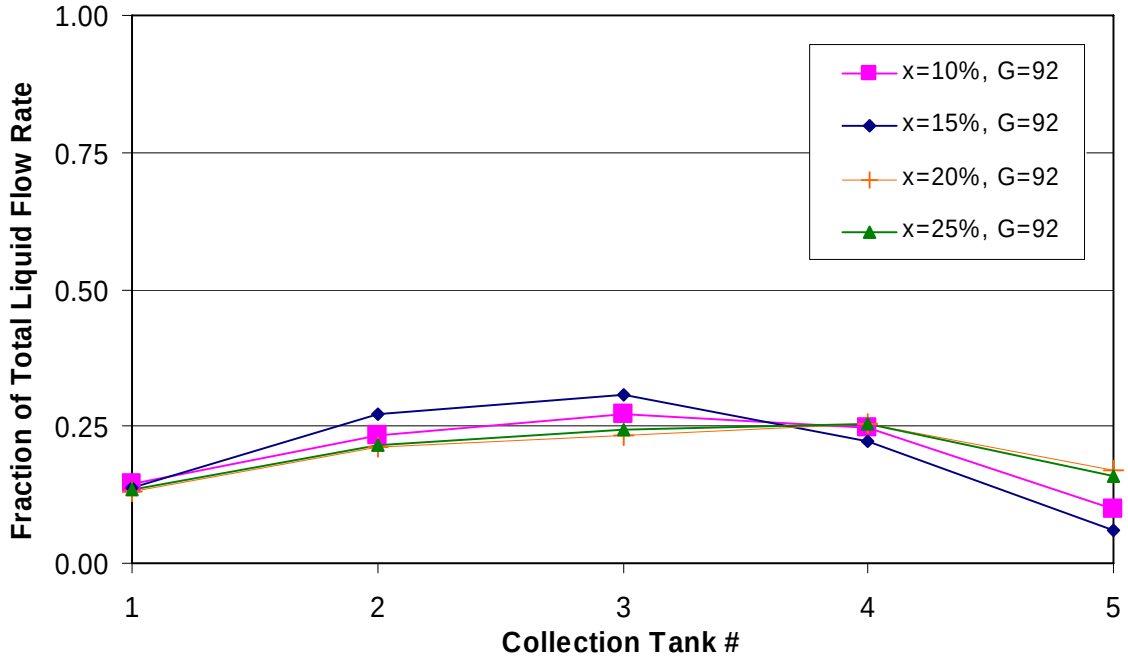

Figure C-52: Stagger Down Protrusion, Short Inlet, G=92 kg/m^{2}s

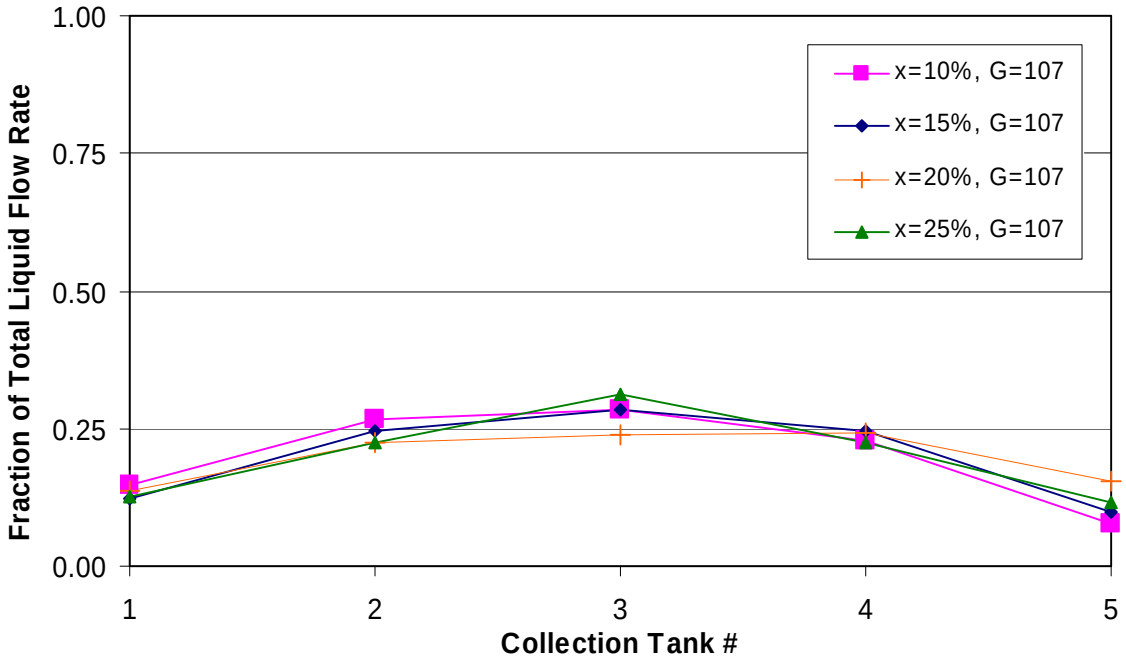

Figure C-53: Stagger Down Protrusion, Short Inlet, G=107 kg/m^{2}s

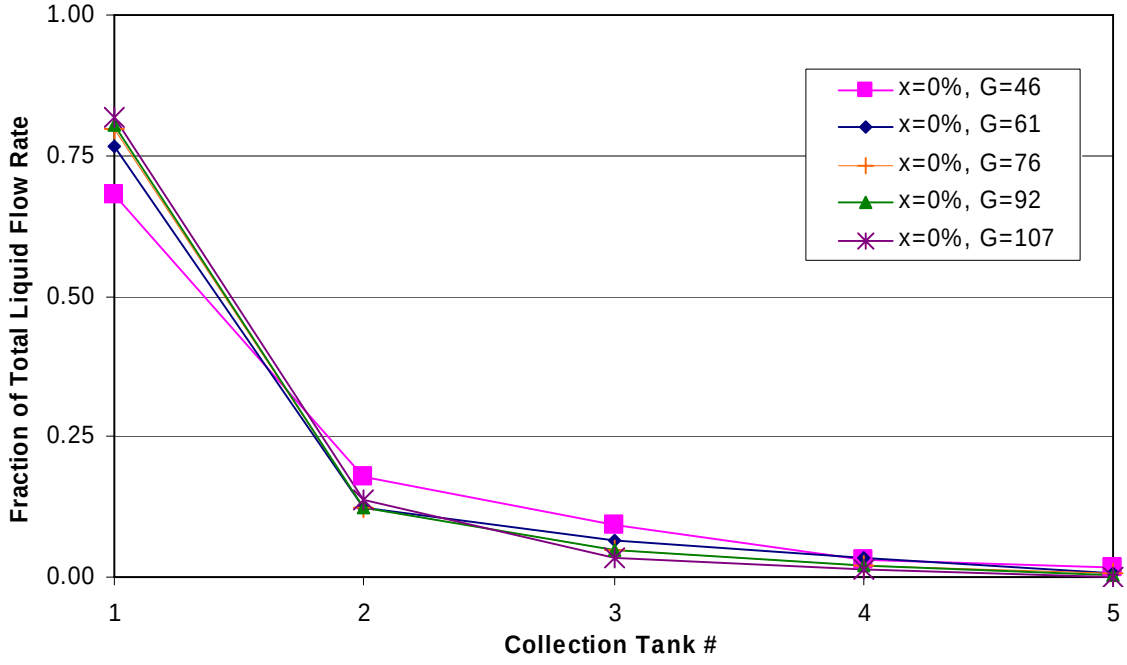

Figure C-54: Stagger Down Protrusion, Short Inlet, x=0%

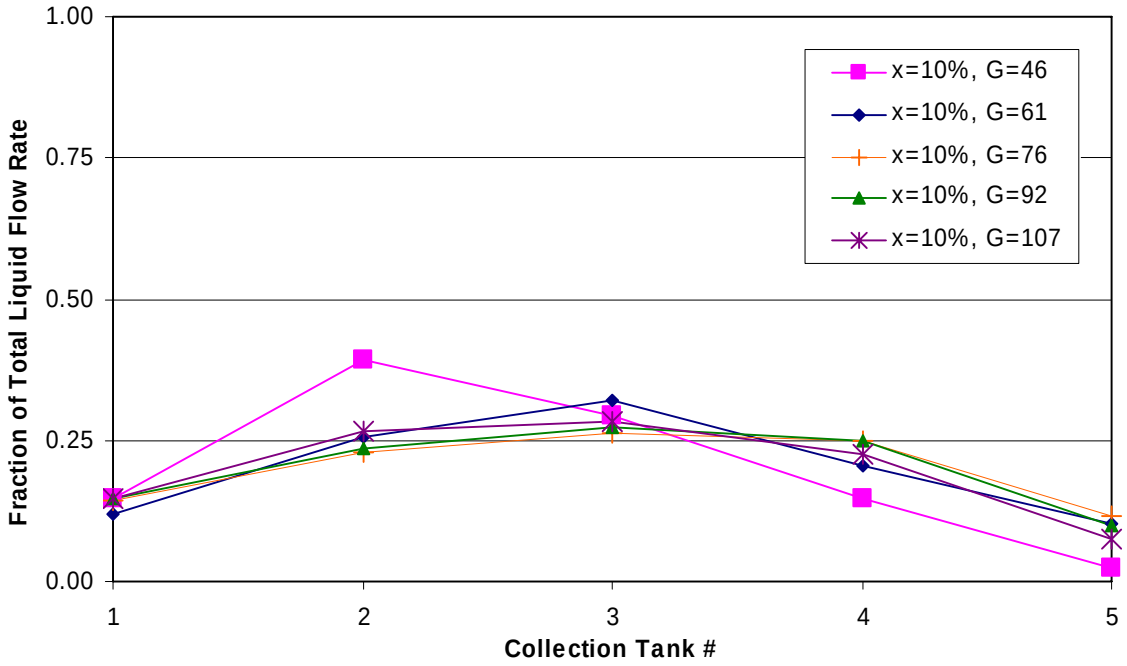

Figure C-55: Stagger Down Protrusion, Short Inlet, x=10%

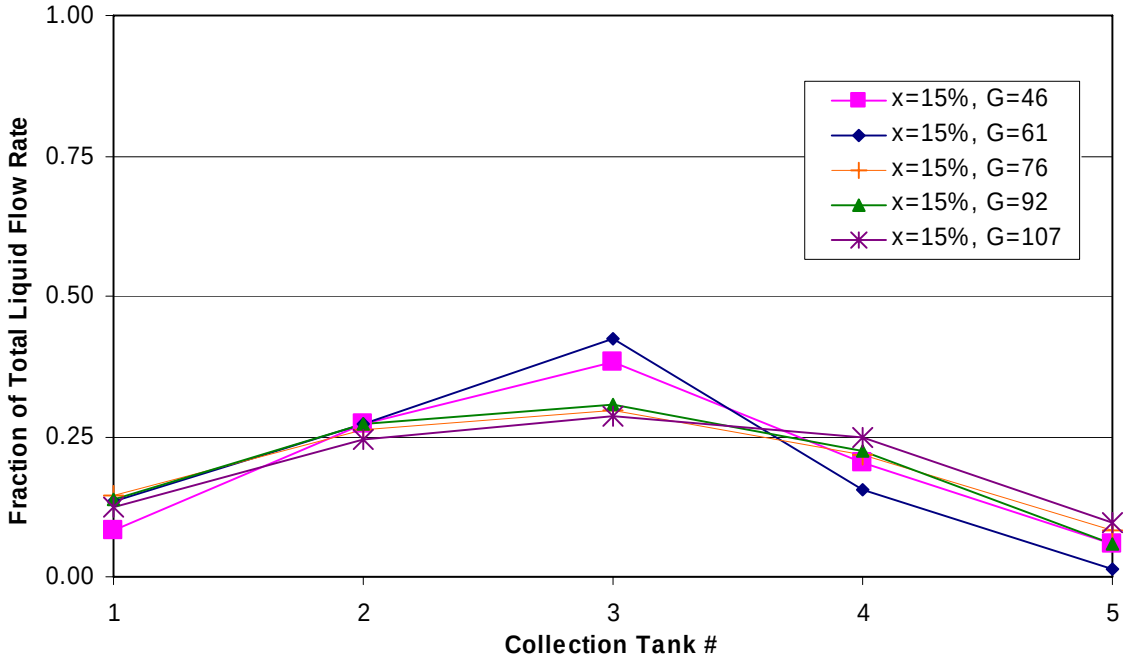

Figure C-56: Stagger Down Protrusion, Short Inlet, x=15%

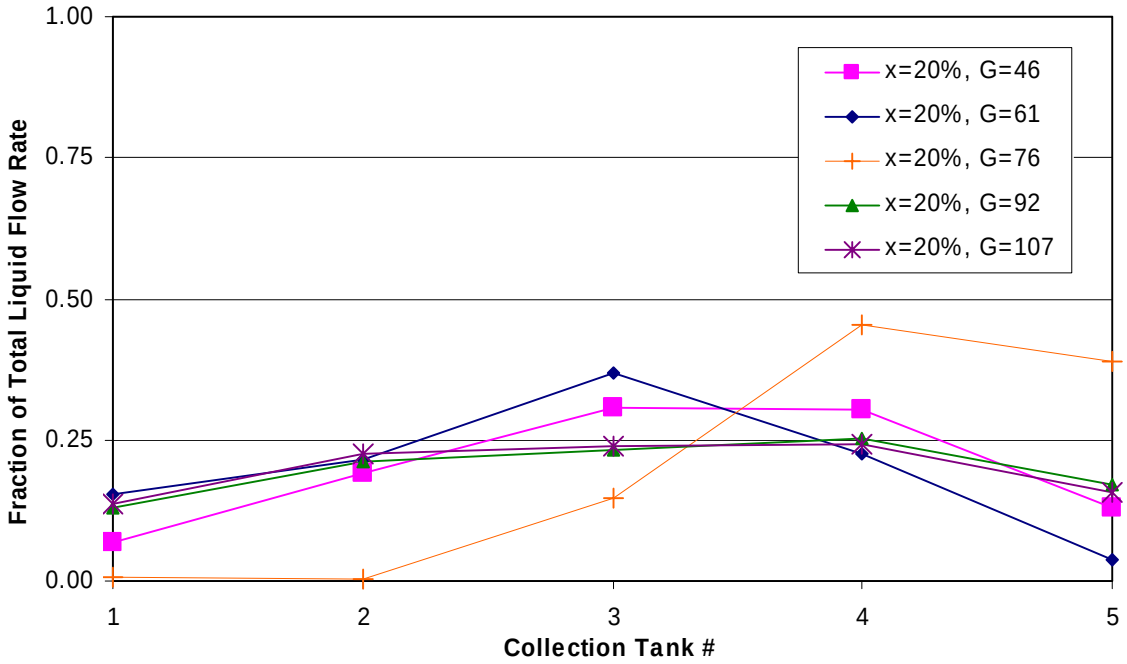

Figure C-57: Stagger Down Protrusion, Short Inlet, x=20%

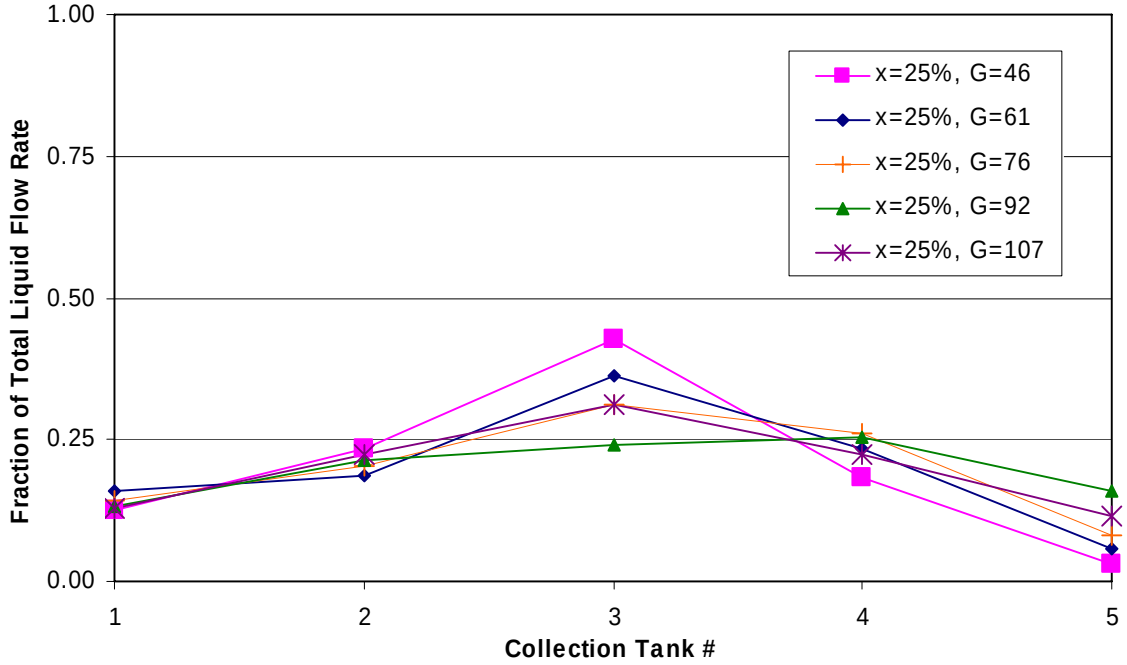

Figure C-58: Stagger Down Protrusion, Short Inlet, x=25%

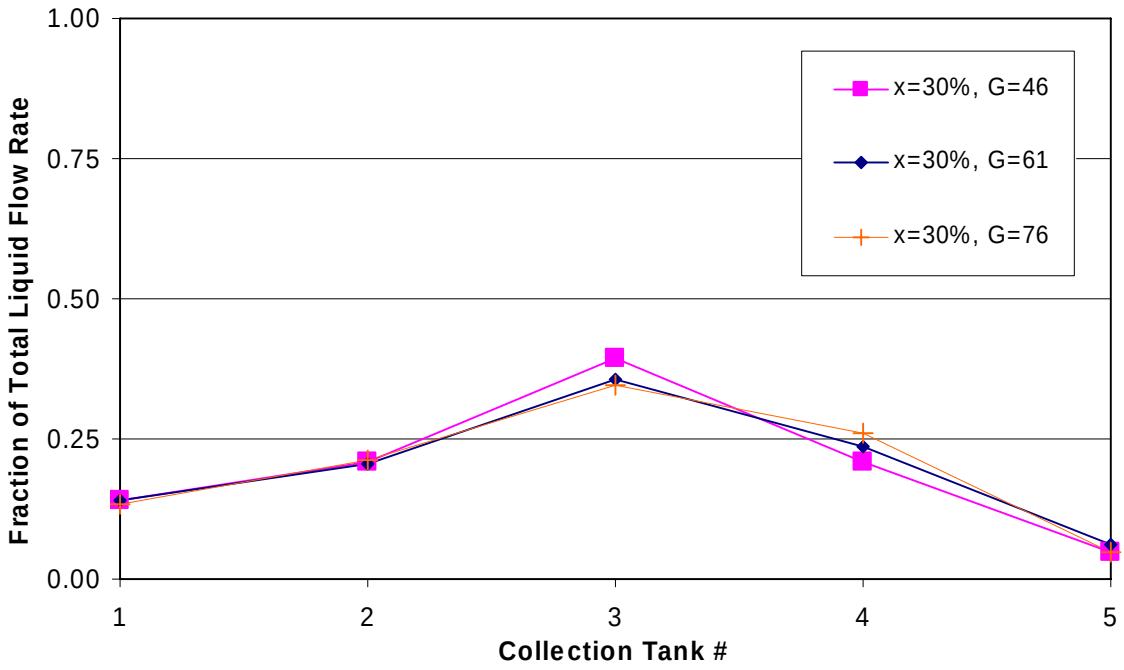

Figure C-59: Stagger Down Protrusion, Short Inlet, x=30%

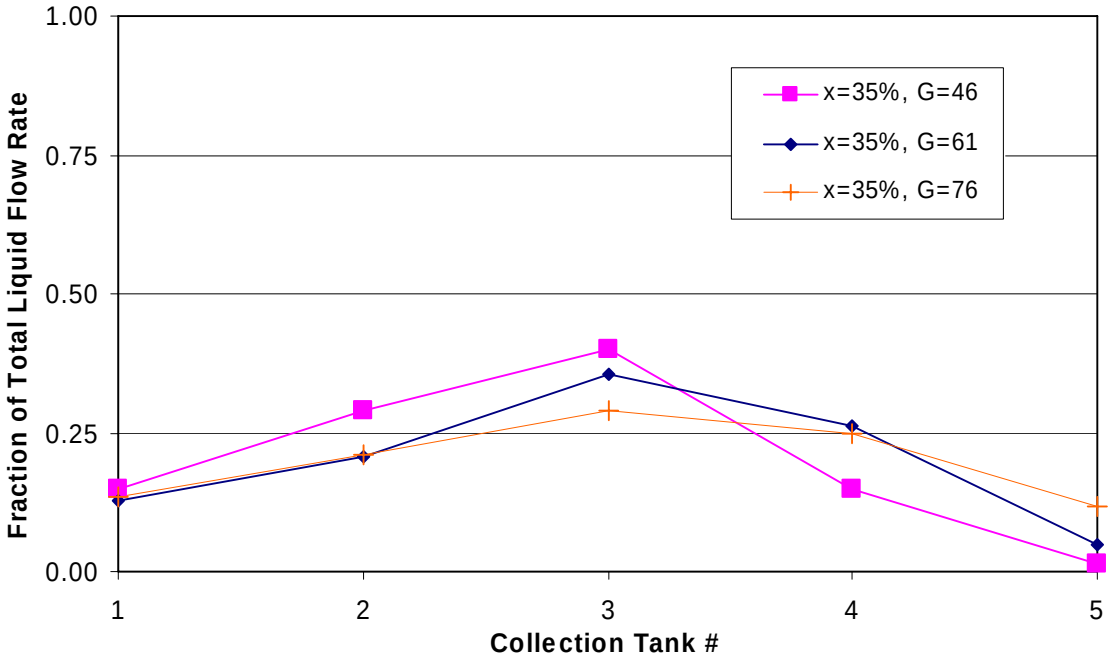

Figure C-60: Stagger Down Protrusion, Short Inlet, x=35%

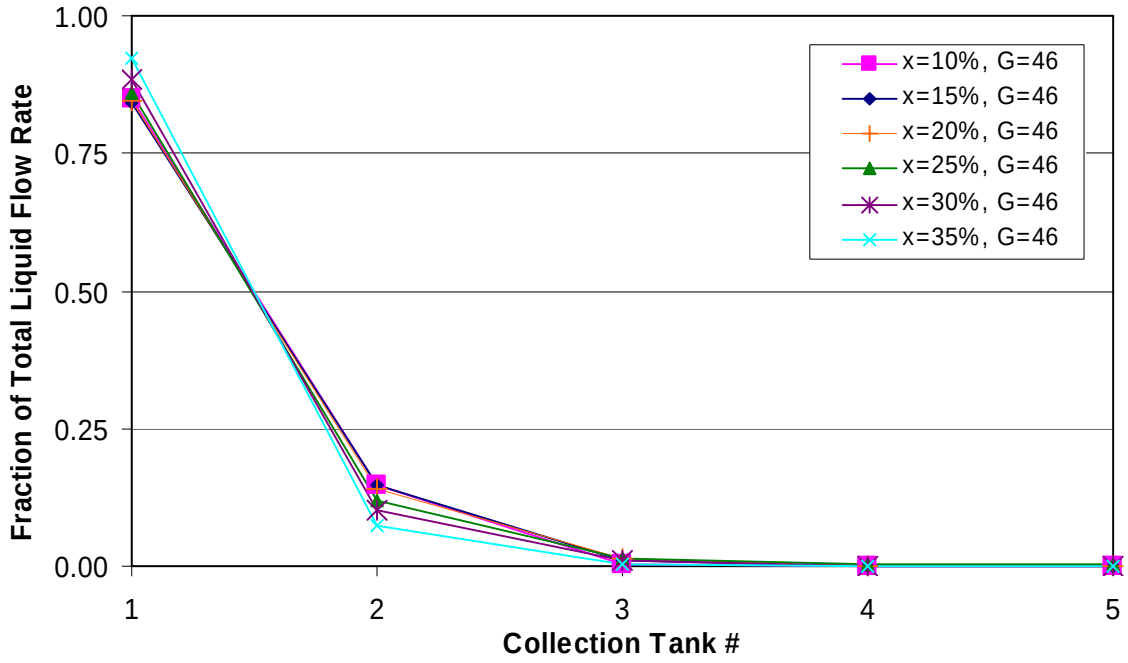

Figure C-61: 1/4 Depth Protrusion, Long Inlet, G=46 kg/m^{2}s

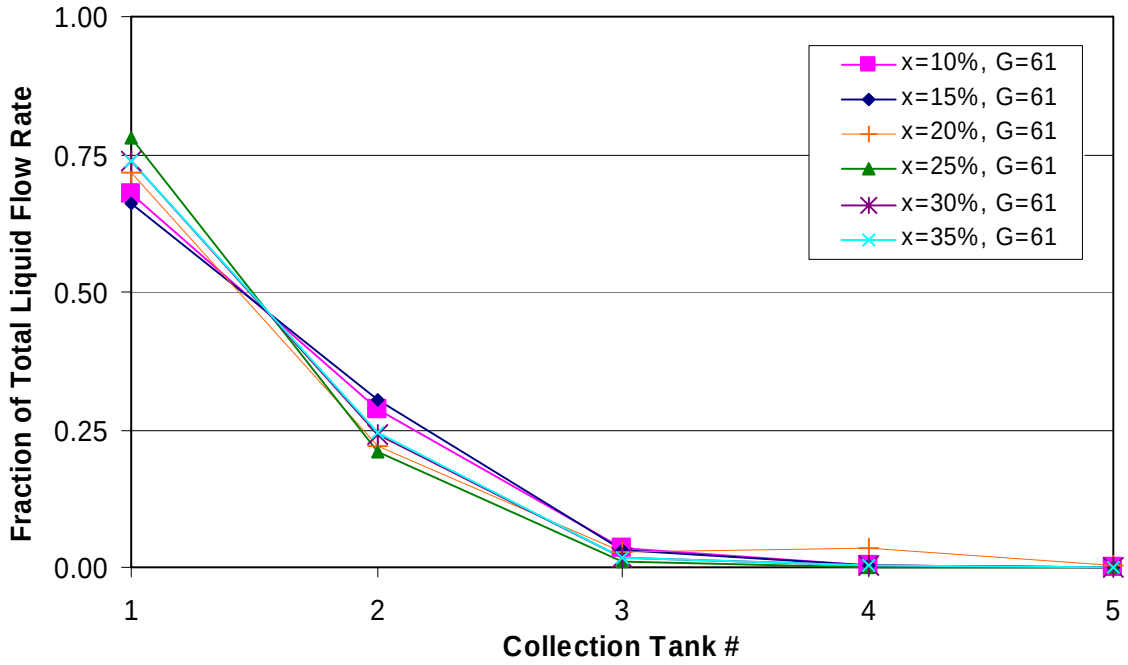

Figure C-62: 1/4 Depth Protrusion, Long Inlet, G=61 kg/m^{2}s

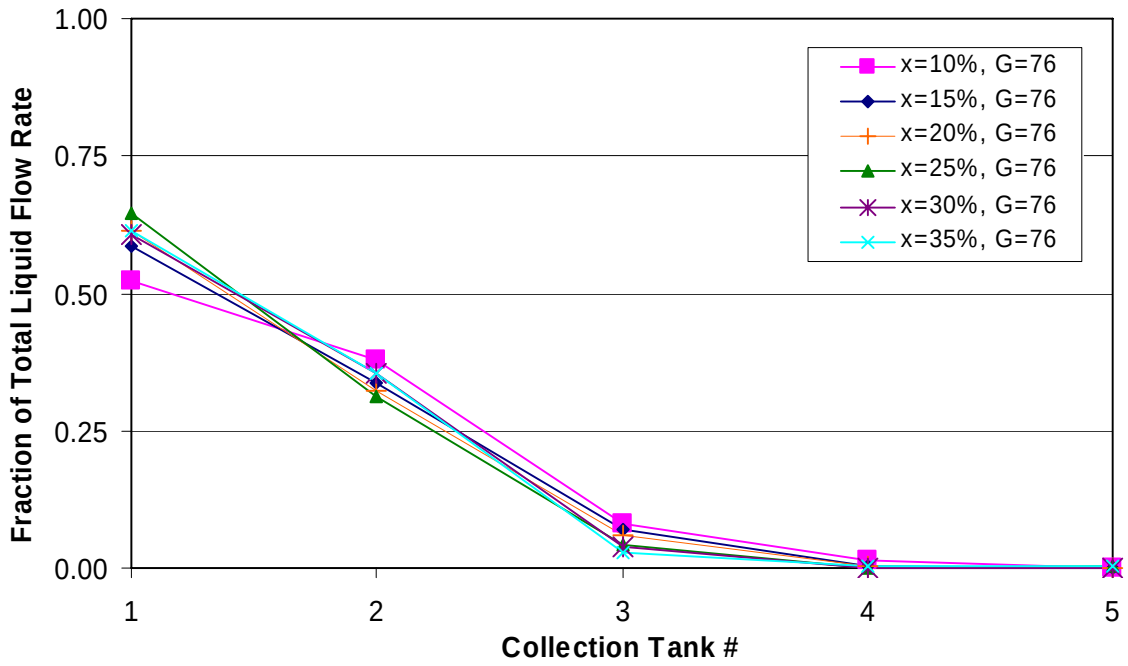

Figure C-63: 1/4 Depth Protrusion, Long Inlet, G=76 kg/m^{2}s

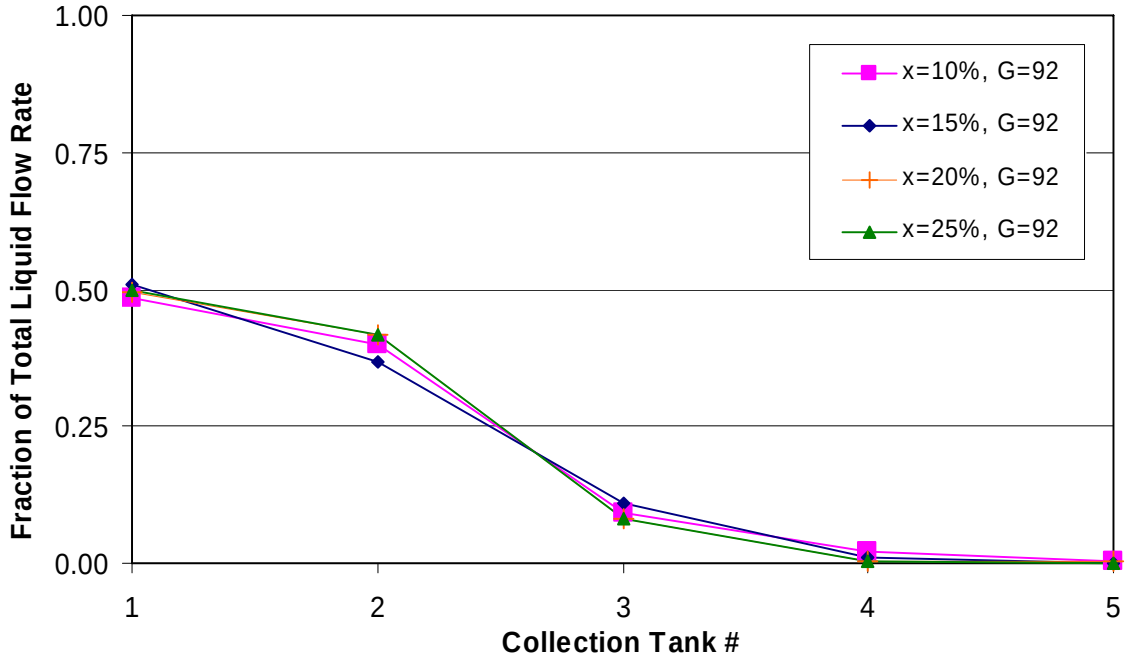

Figure C-64: 1/4 Depth Protrusion, Long Inlet, G=92 kg/m^{2}s

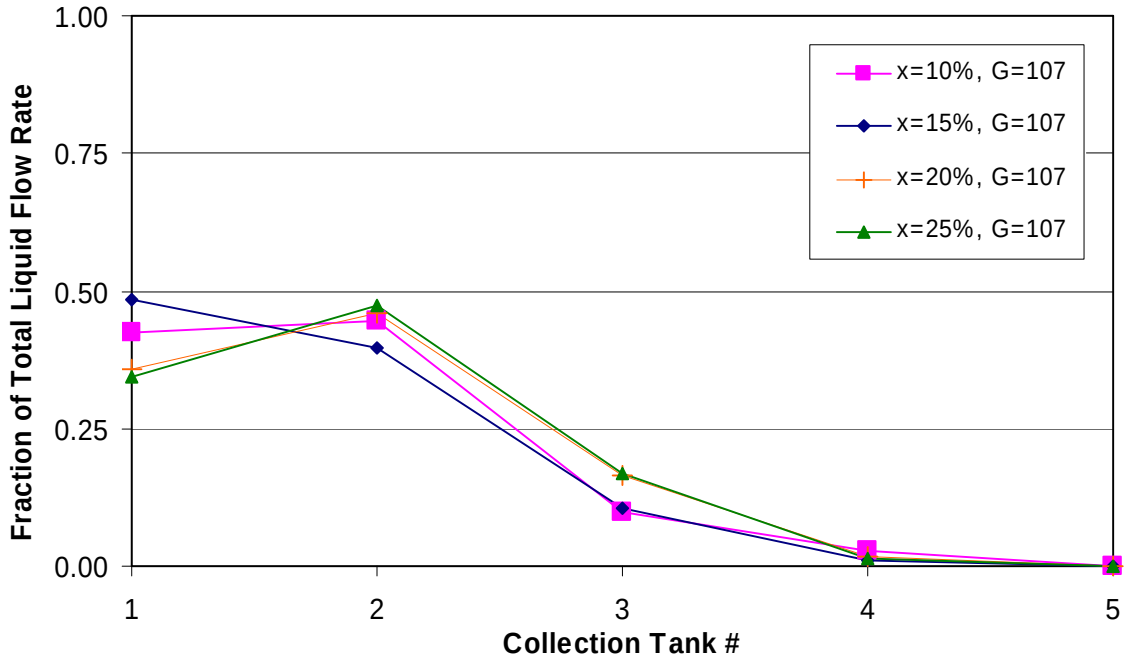

Figure C-65: 1/4 Depth Protrusion, Long Inlet, G=107 kg/m^{2}s

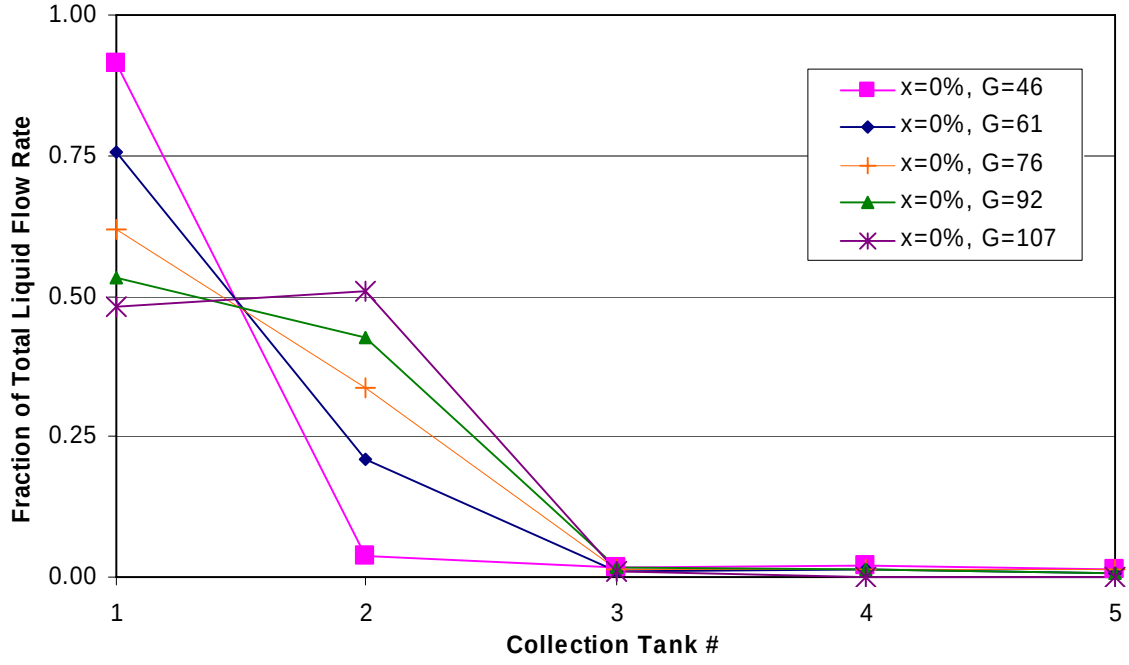

Figure C-66: 1/4 Depth Protrusion, Long Inlet, x=0%

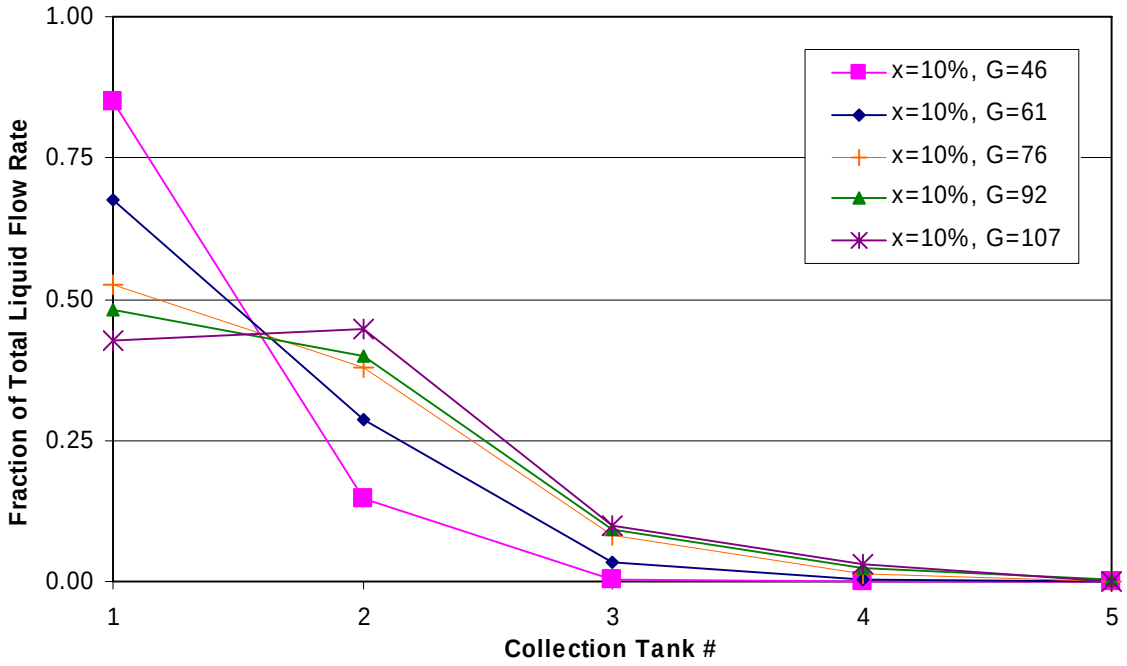

Figure C-67: 1/4 Depth Protrusion, Long Inlet, x=10%

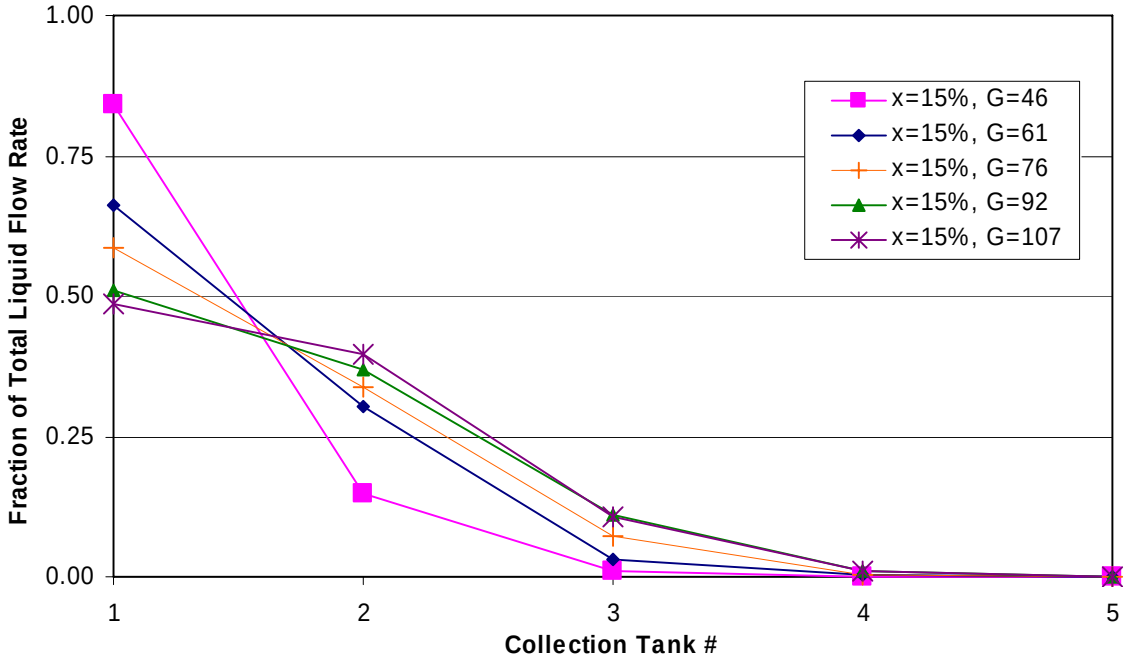

Figure C-68: 1/4 Depth Protrusion, Long Inlet, x=15%

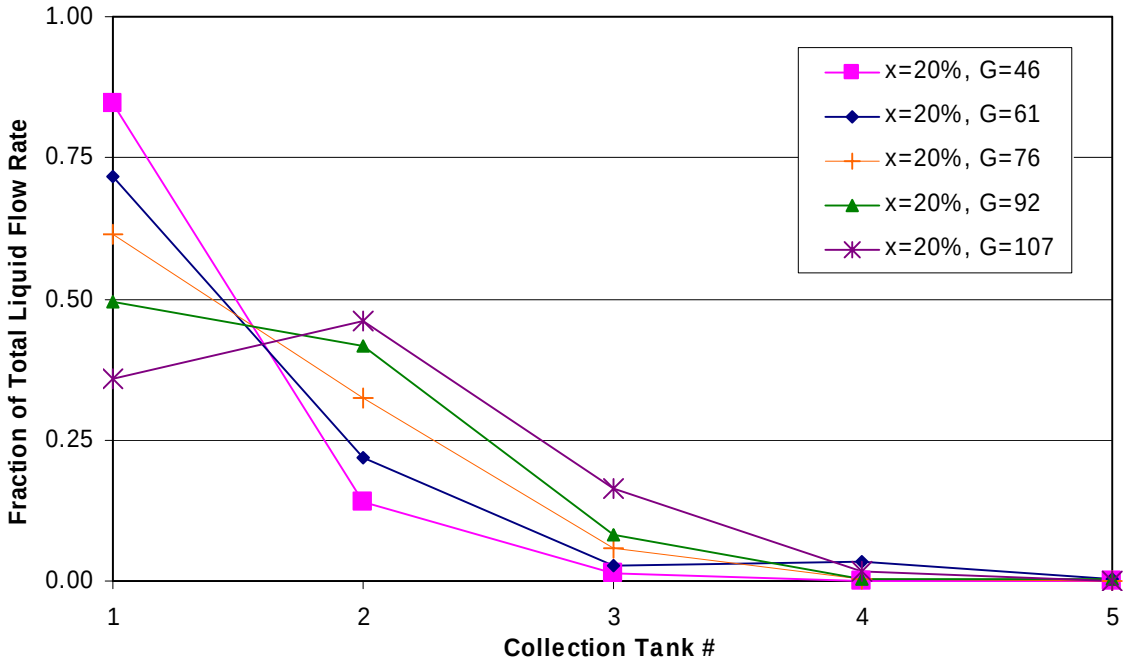

Figure C-69: 1/4 Depth Protrusion, Long Inlet, x=20%

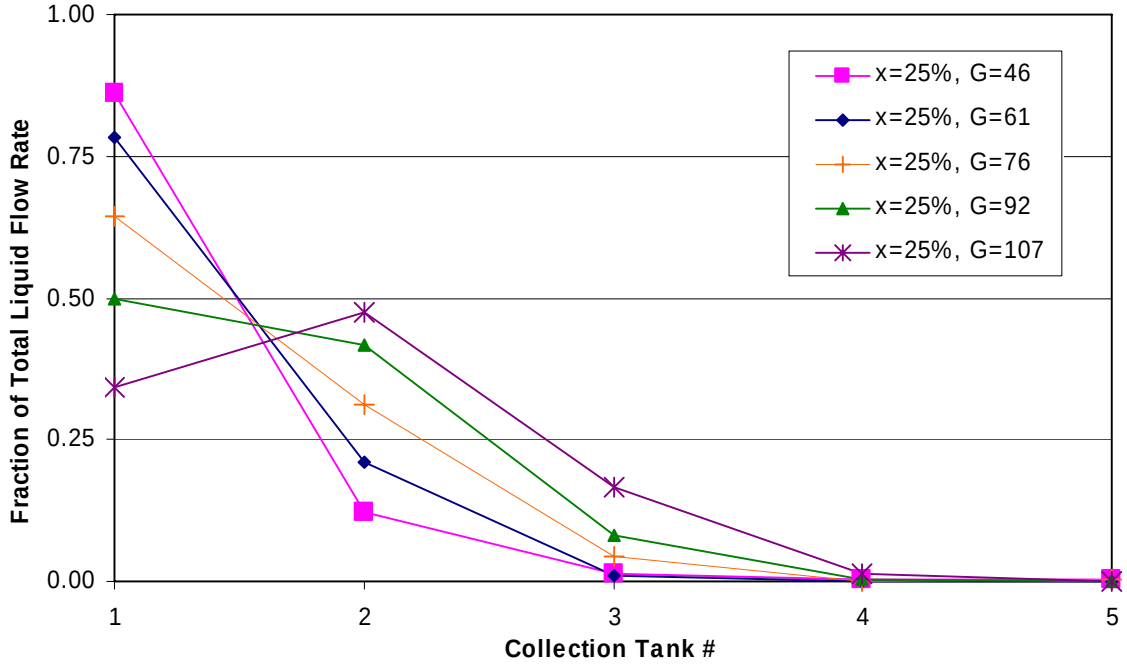

Figure C-70: 1/4 Depth Protrusion, Long Inlet, x=25%

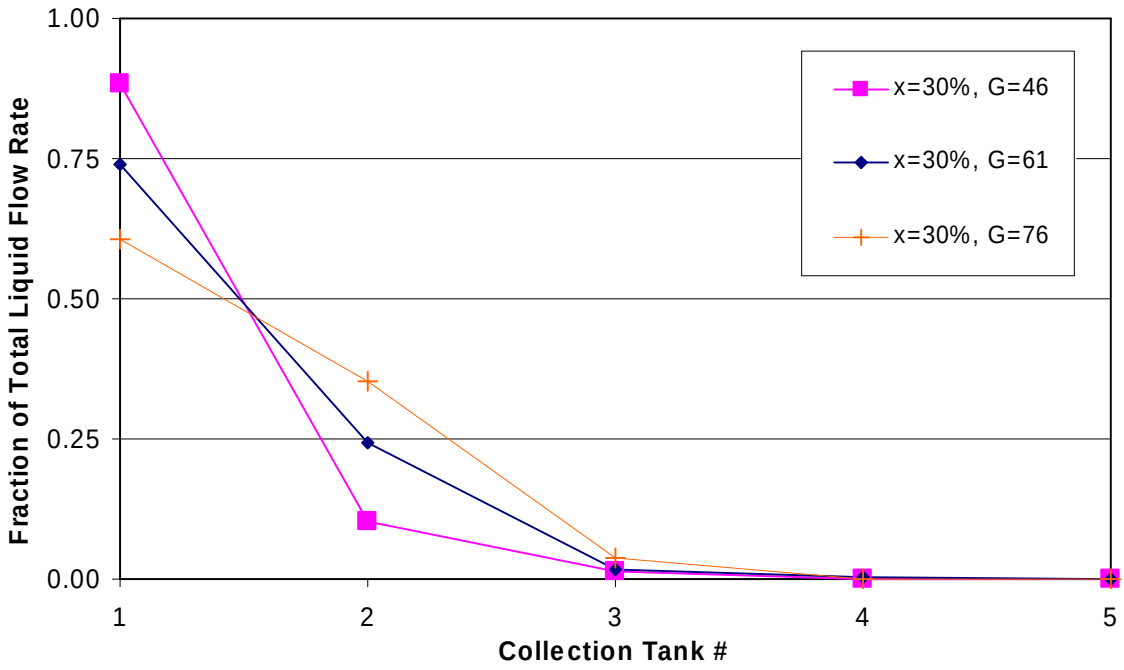

Figure C-71: 1/4 Depth Protrusion, Long Inlet, x=30%

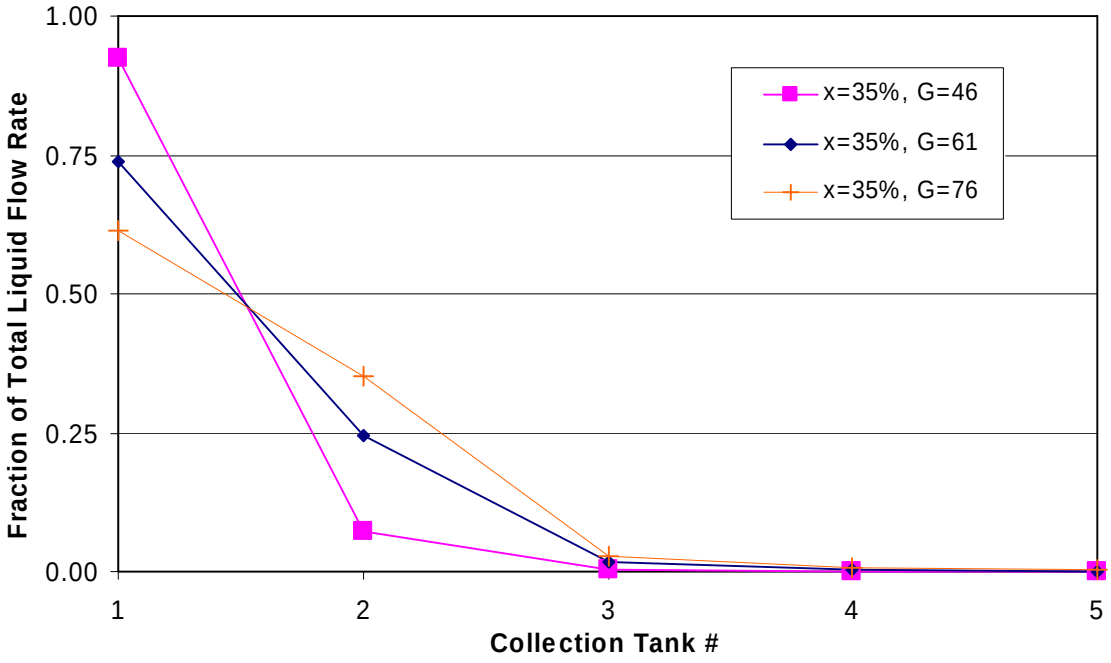

Figure C-72: 1/4 Depth Protrusion, Long Inlet, x=35%

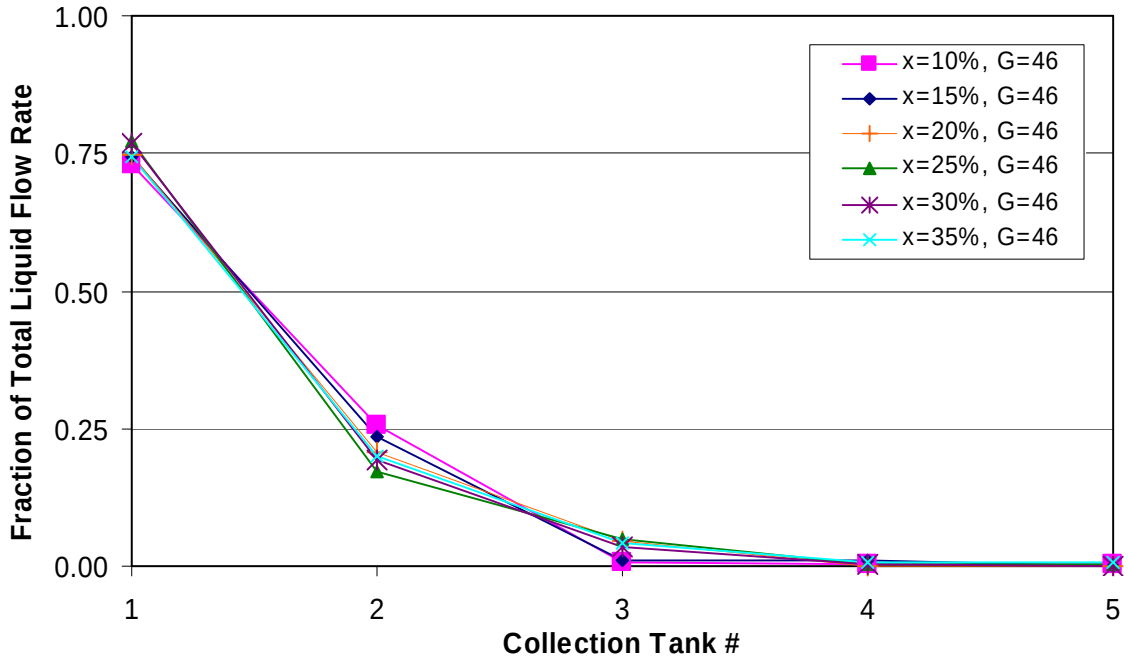

Figure C-73: 1/2 Depth Protrusion, Long Inlet, G=46 kg/m^{2}s

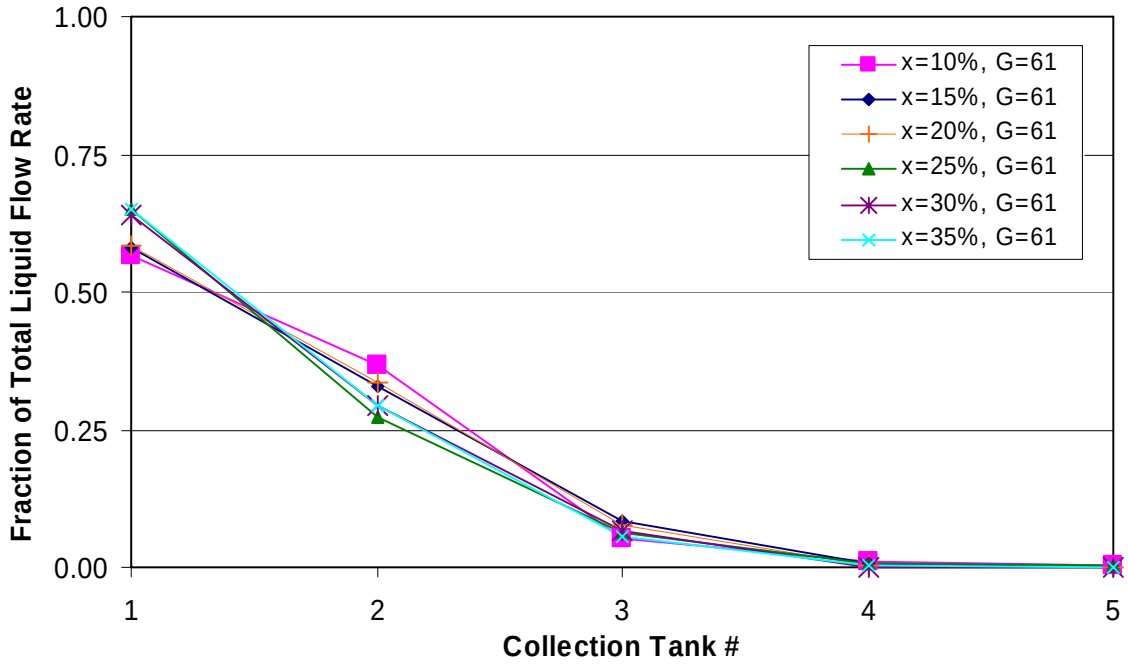

Figure C-74: 1/2 Depth Protrusion, Long Inlet, G=61 kg/m^{2}s

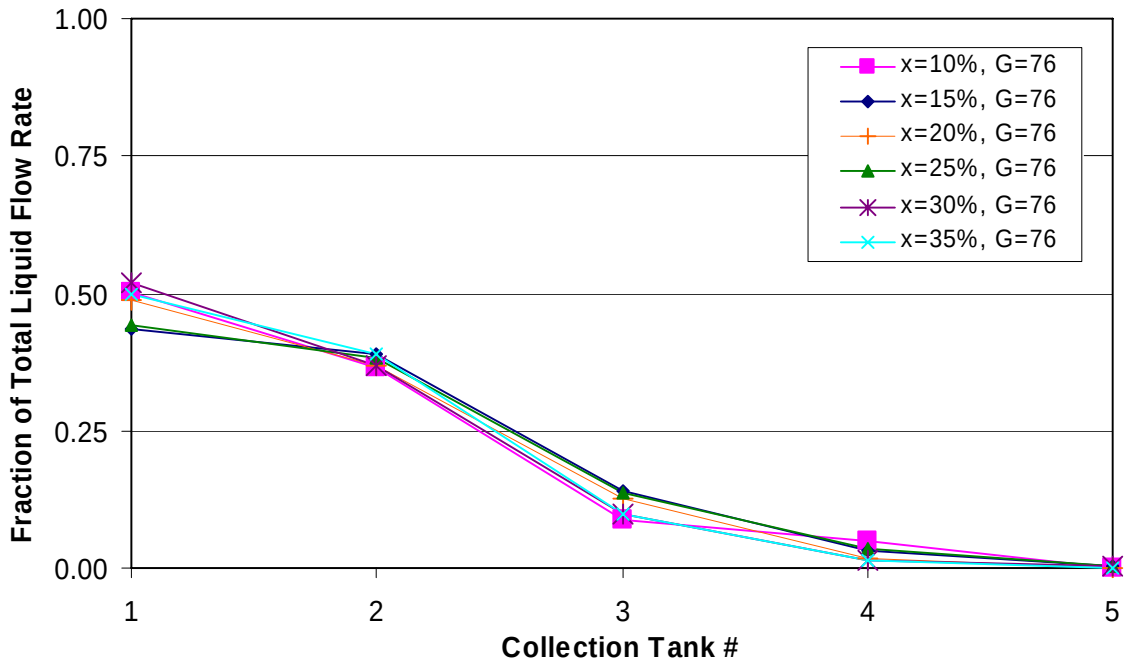

Figure C-75: 1/2 Depth Protrusion, Long Inlet, G=76 kg/m^{2}s

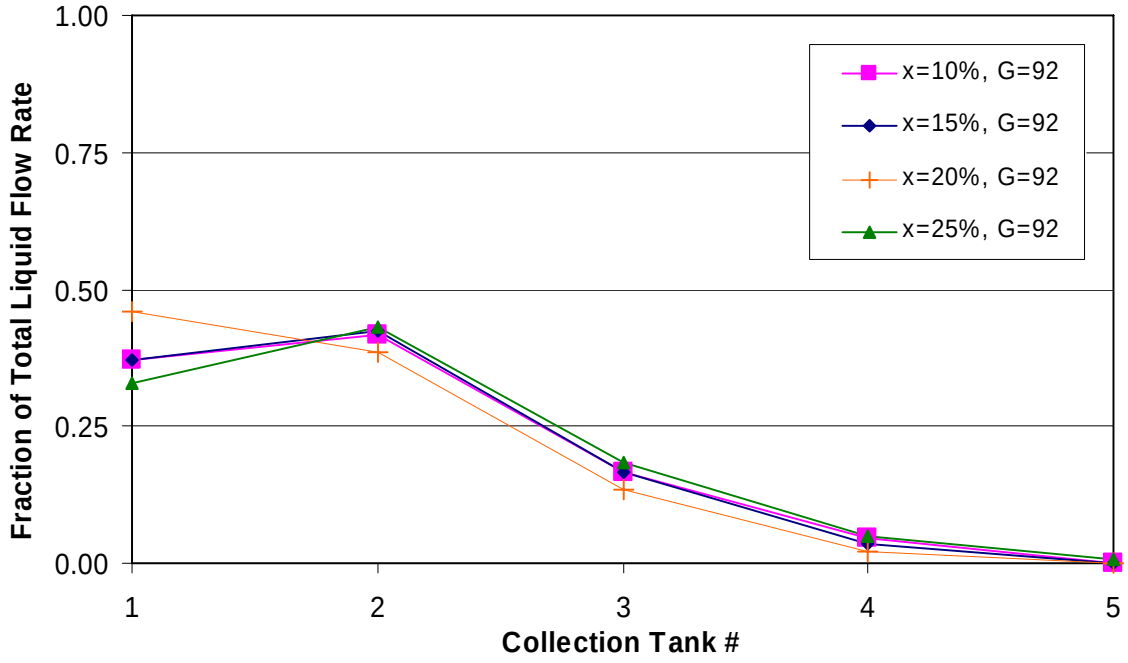

Figure C-76: 1/2 Depth Protrusion, Long Inlet, G=92 kg/m^{2}s

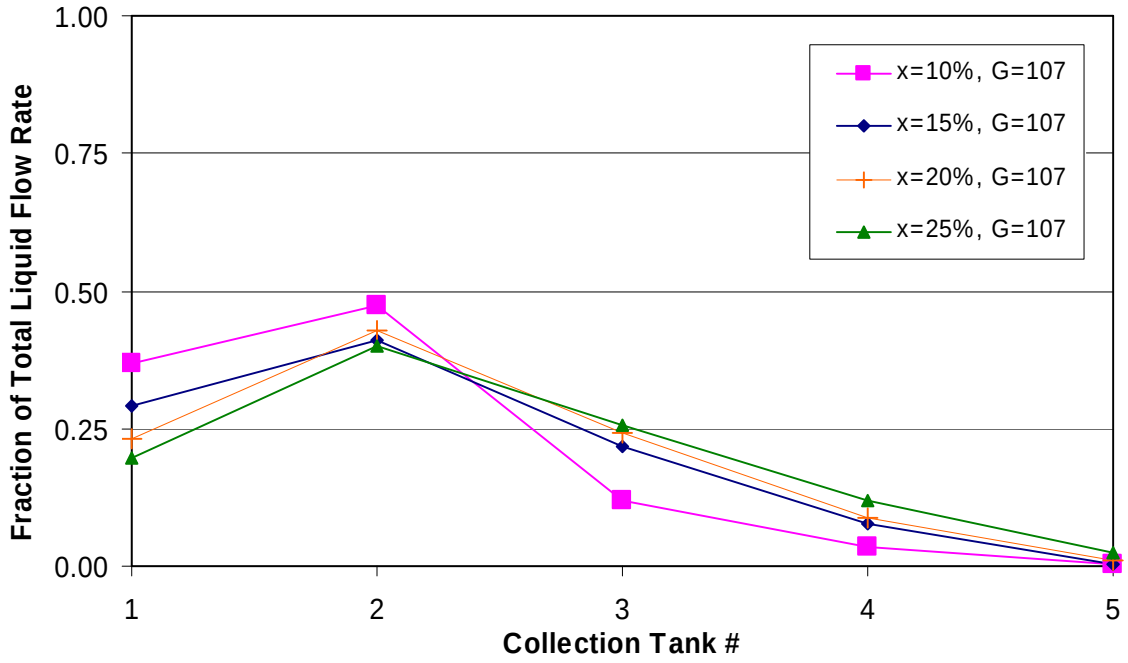

Figure C-77: 1/2 Depth Protrusion, Long Inlet, G=107 kg/m^{2}s

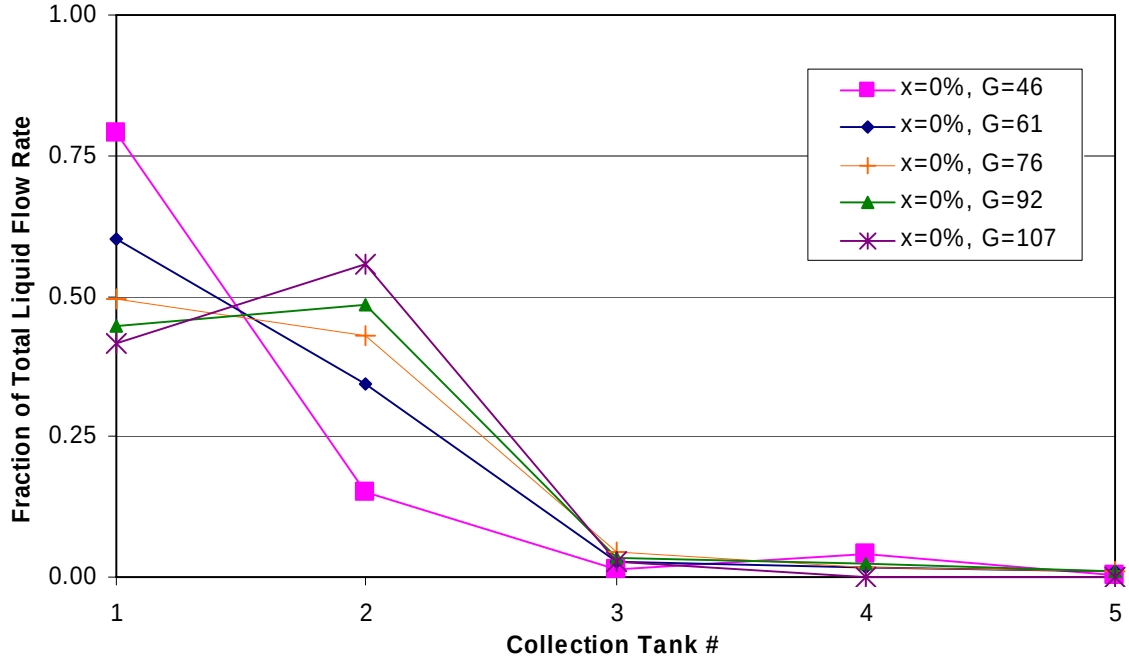

Figure C-78: 1/2 Depth Protrusion, Long Inlet, x=0%

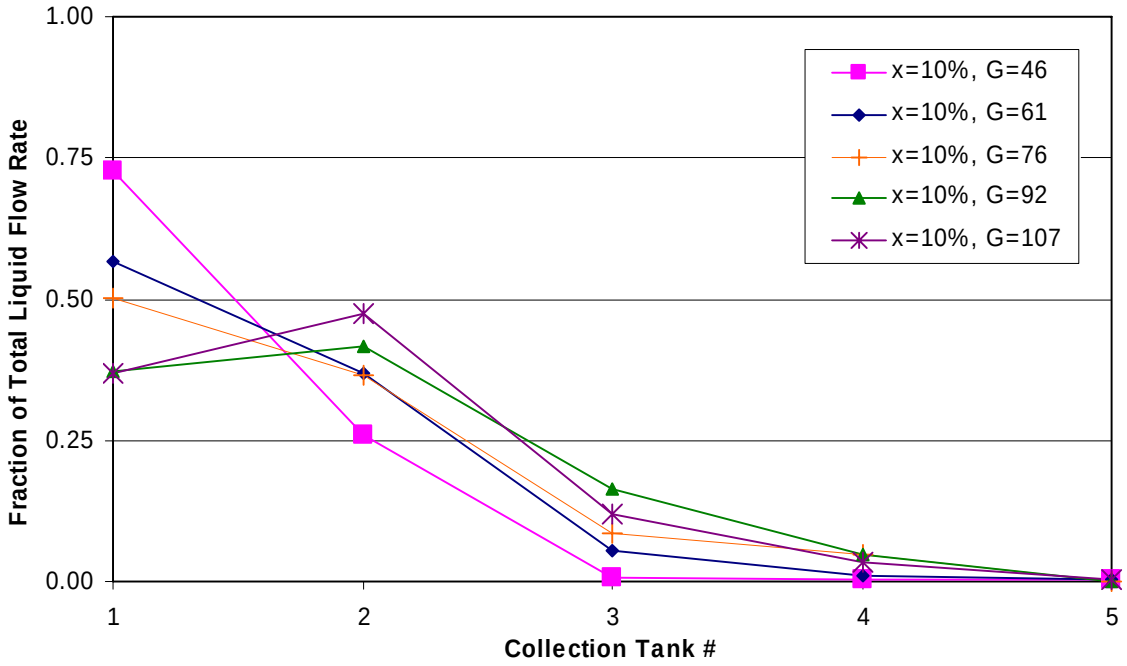

Figure C-79: 1/2 Depth Protrusion, Long Inlet, x=10%

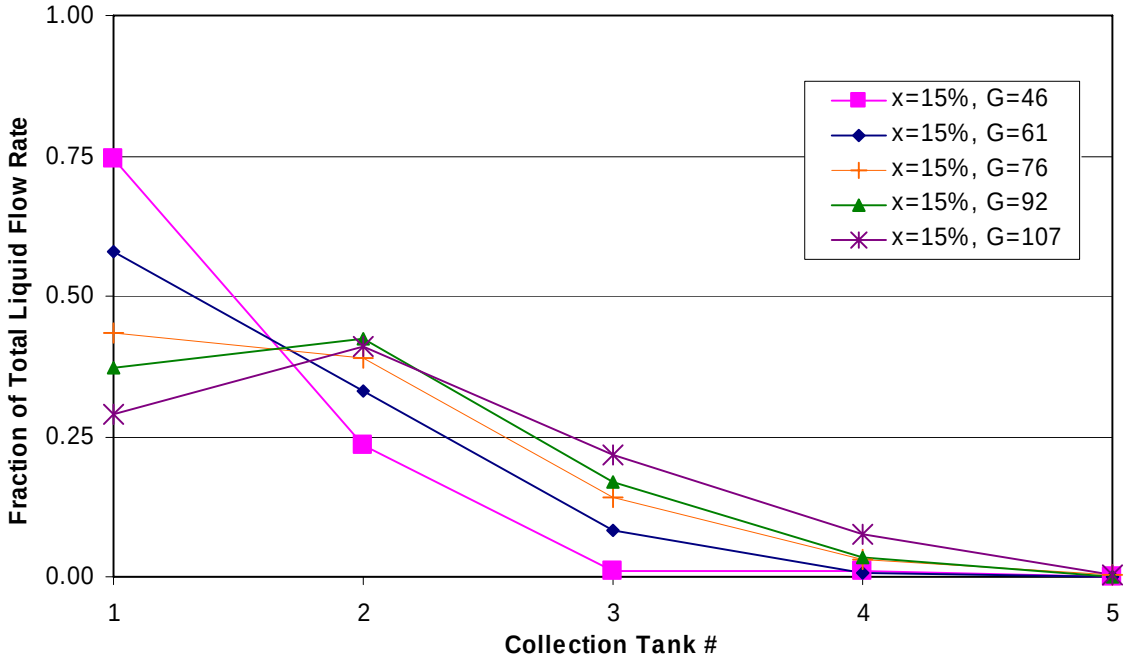

Figure C-80: 1/2 Depth Protrusion, Long Inlet, x=15%

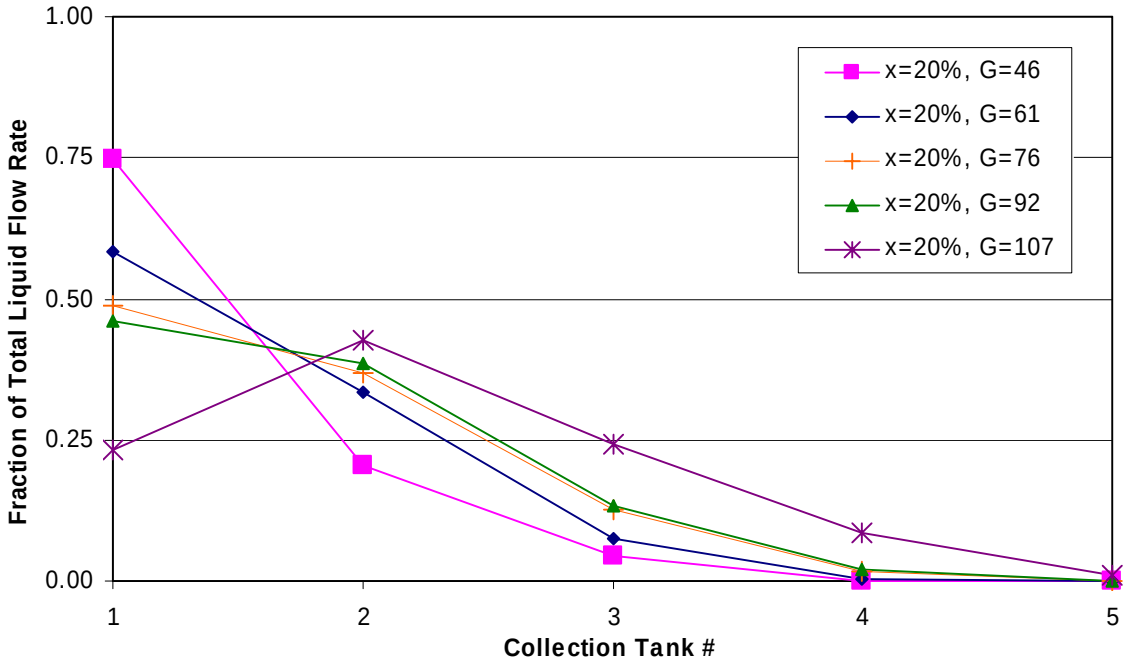

Figure C-81: 1/2 Depth Protrusion, Long Inlet, x=20%

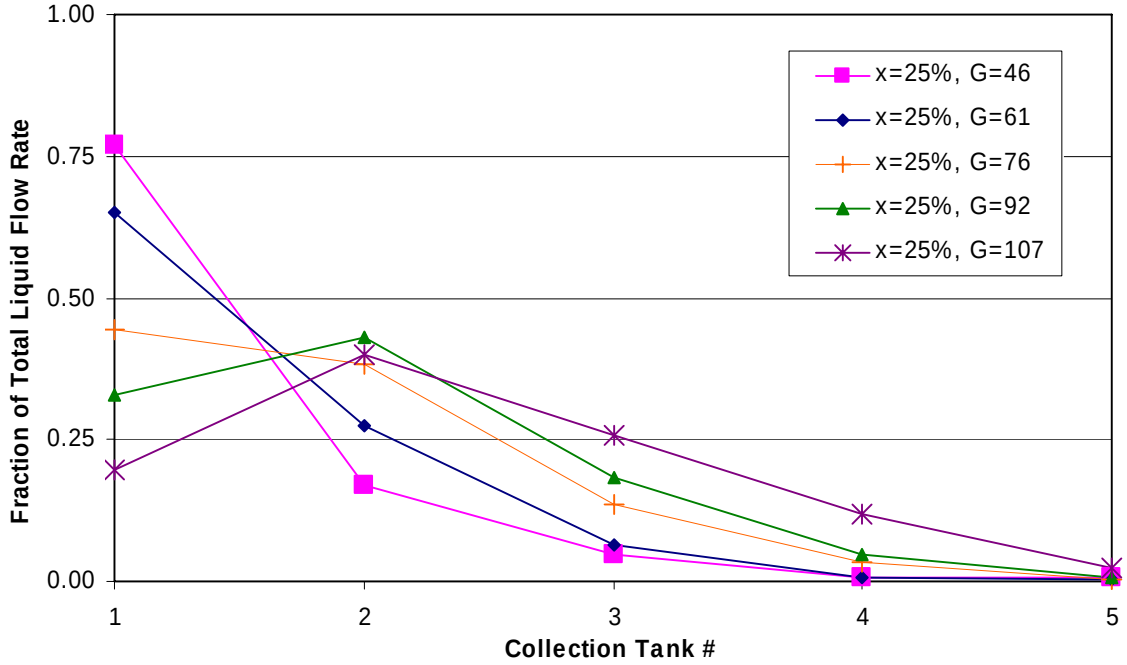

Figure C-82: 1/2 Depth Protrusion, Long Inlet, x=25%

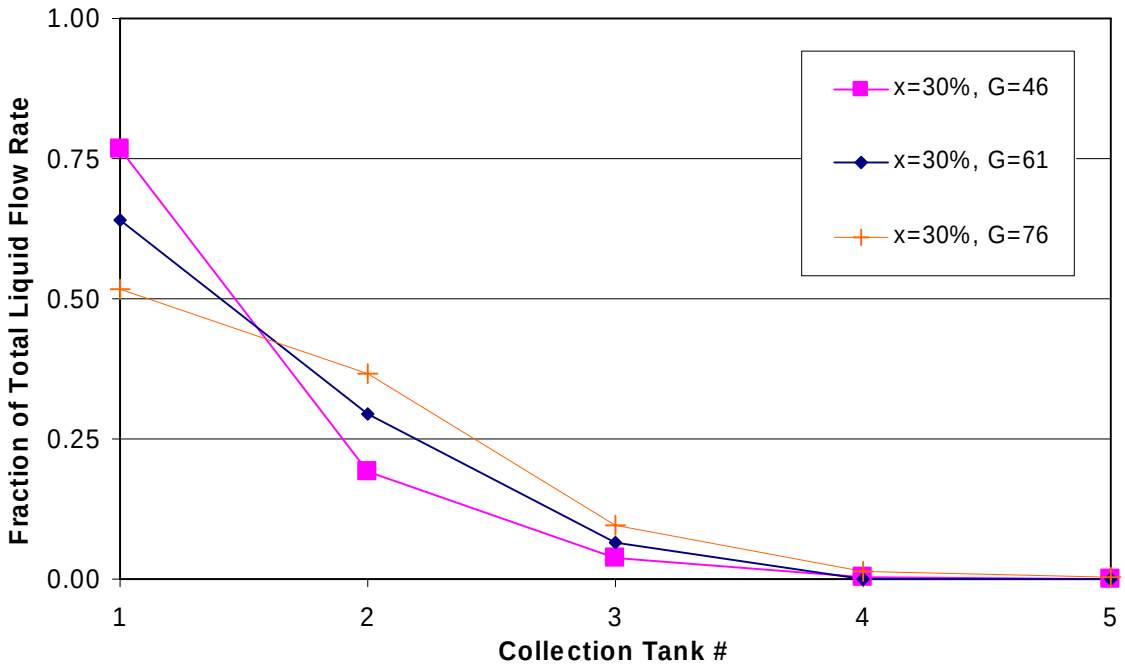

Figure C-83: 1/2 Depth Protrusion, Long Inlet, x=30%

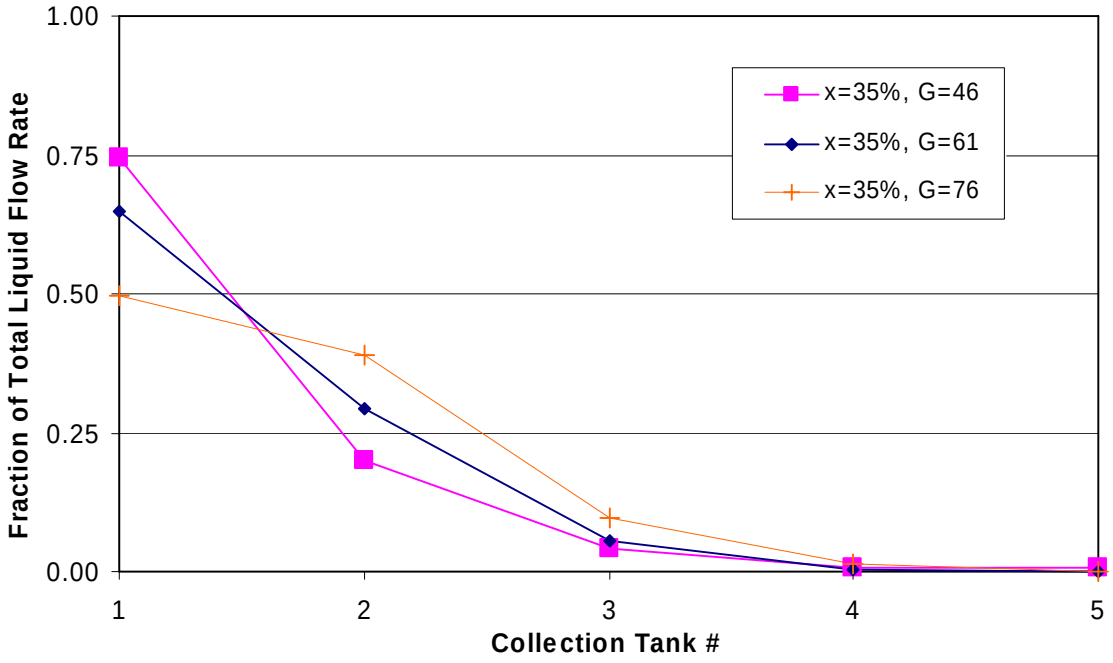

Figure C-84: 1/2 Depth Protrusion, Long Inlet, x=35%

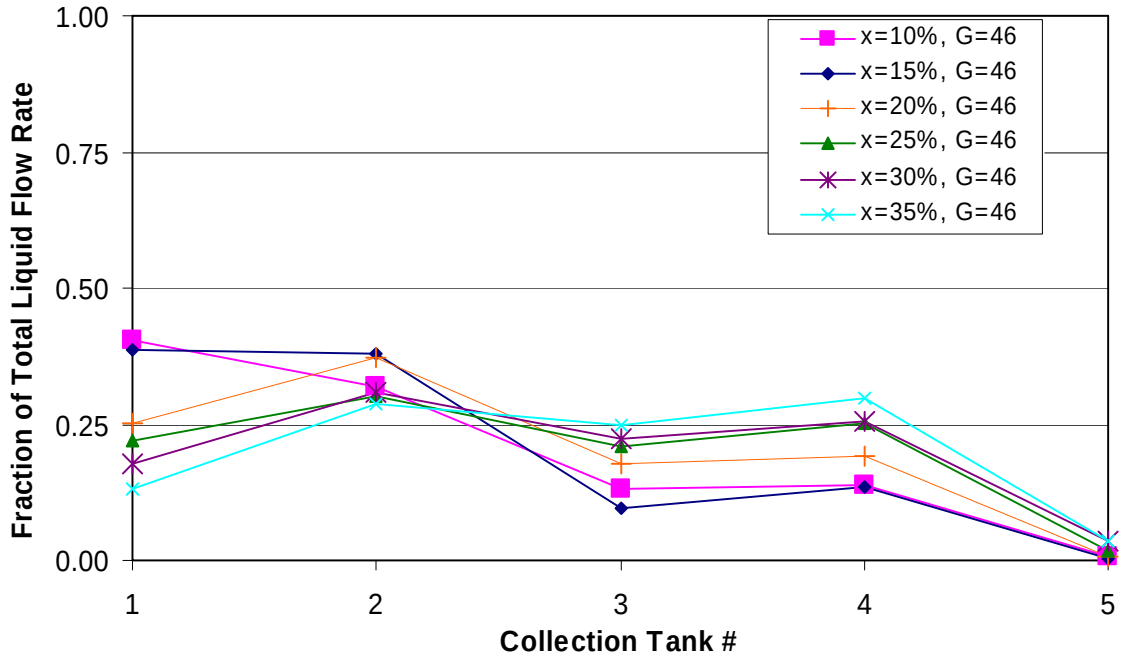

Figure C-85: 3/4 Depth Protrusion, Long Inlet, G=46kg/m^{2}s

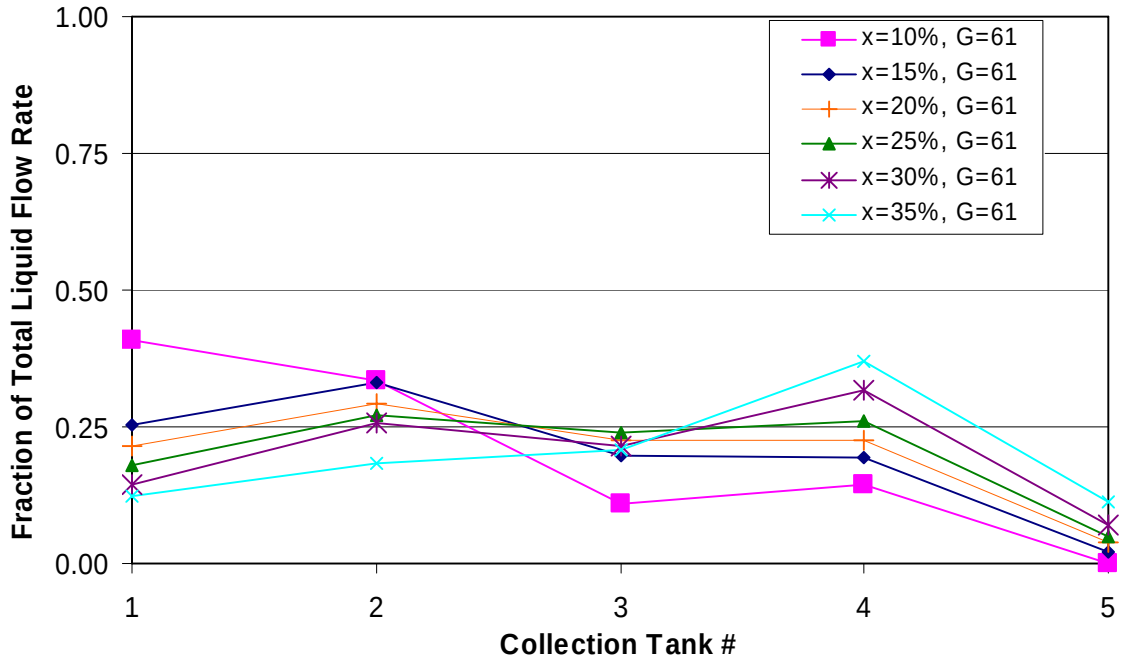

Figure C-86: 3/4 Depth Protrusion, Long Inlet, G=61 kg/m^{2}s

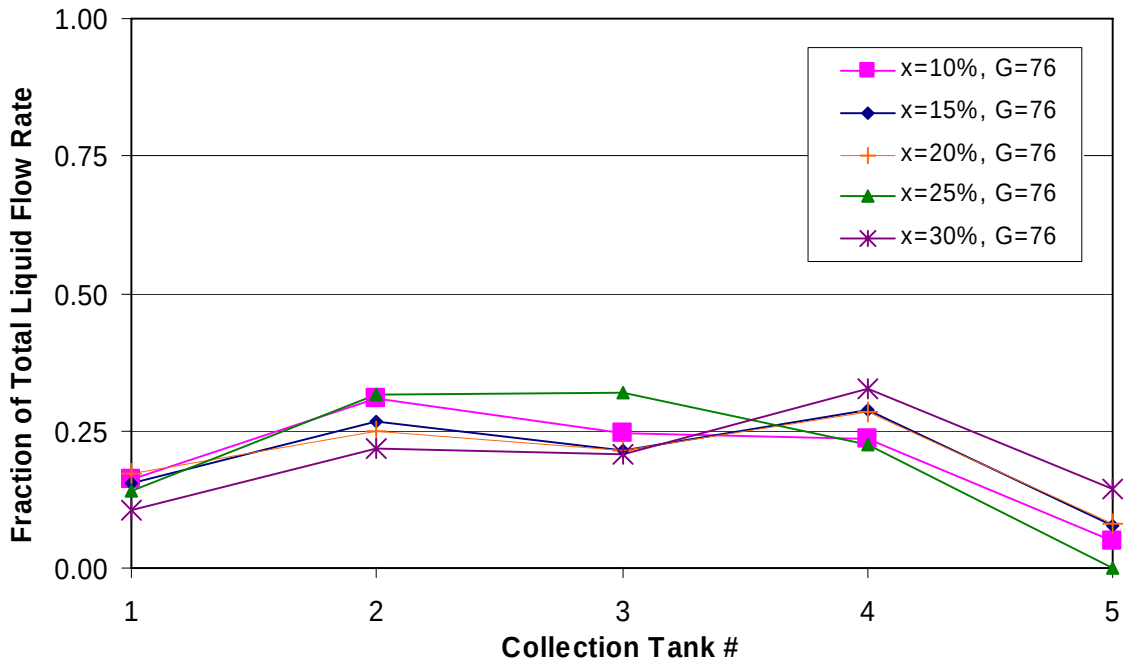

Figure C-87: 3/4 Depth Protrusion, Long Inlet, G=76 kg/m^{2}s

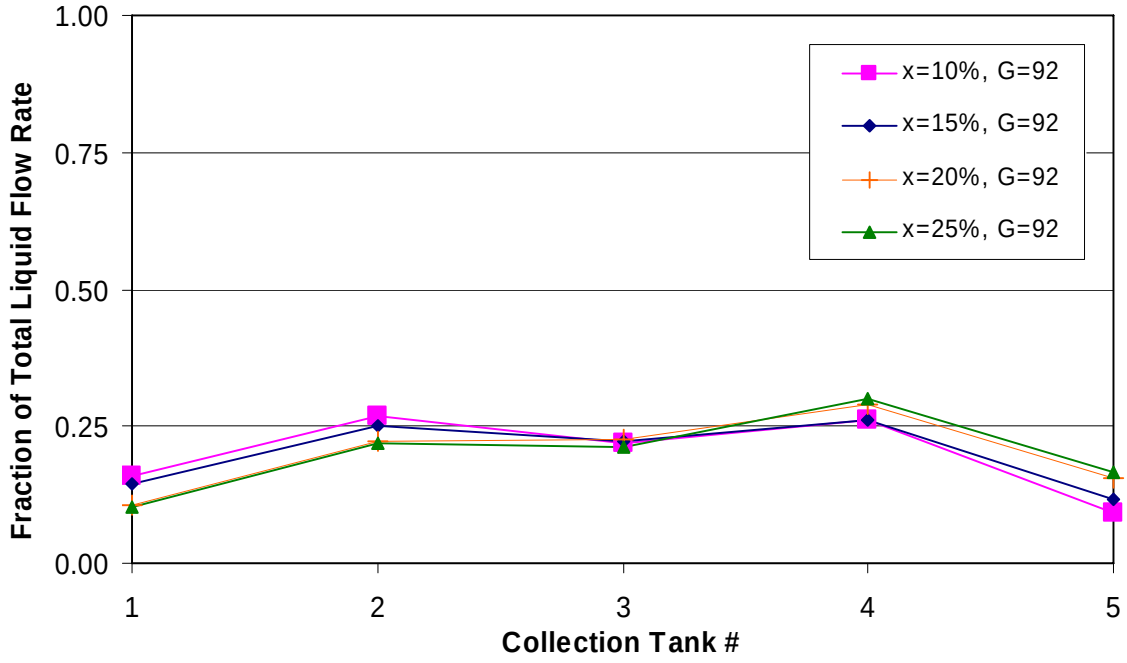

Figure C-88: 3/4 Depth Protrusion, Long Inlet, G=92 kg/m^{2}s

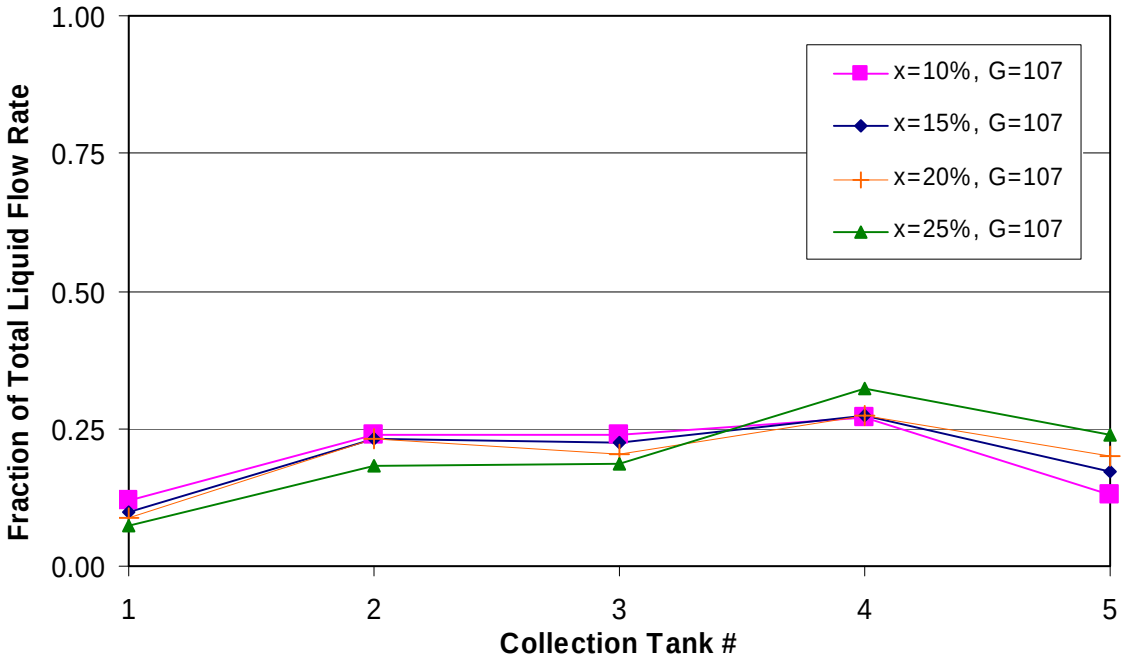

Figure C-89: 3/4 Depth Protrusion, Long Inlet, G=107kg/m^{2}s

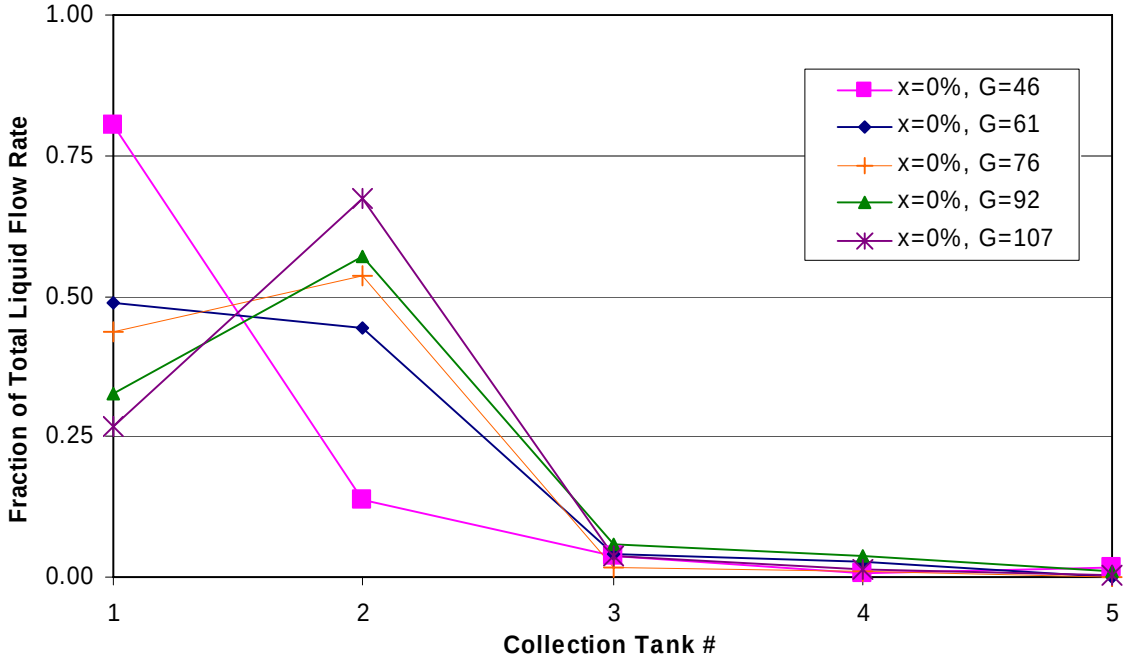

Figure C-90: 3/4 Depth Protrusion, Long Inlet, x=0%

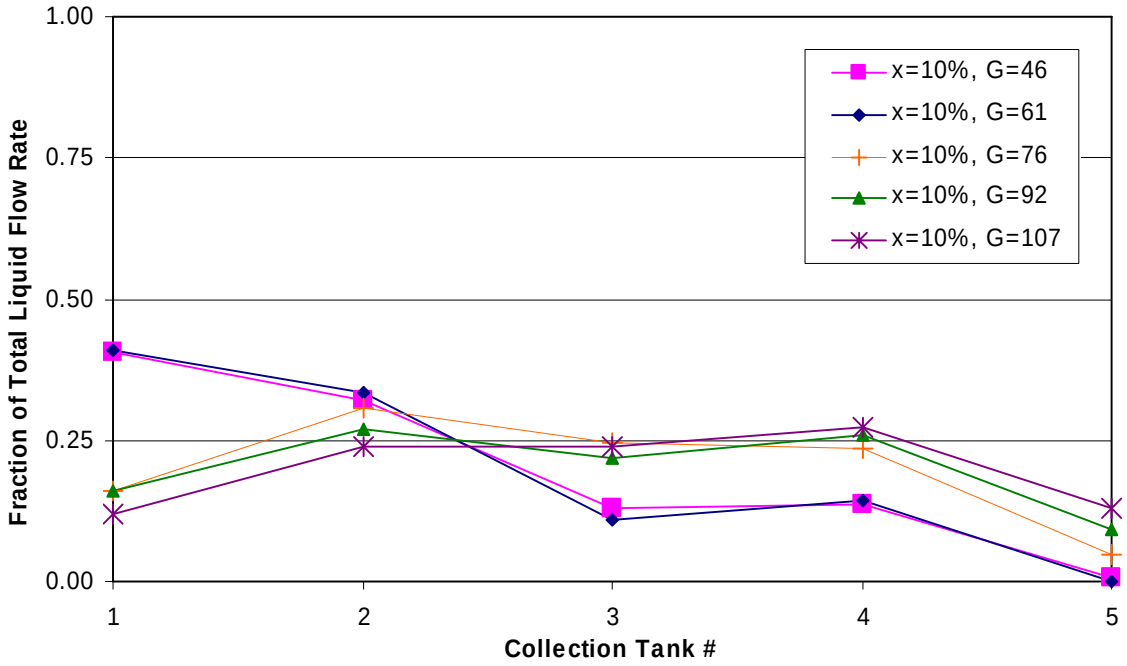

Figure C-91: 3/4 Depth Protrusion, Long Inlet, x=10%

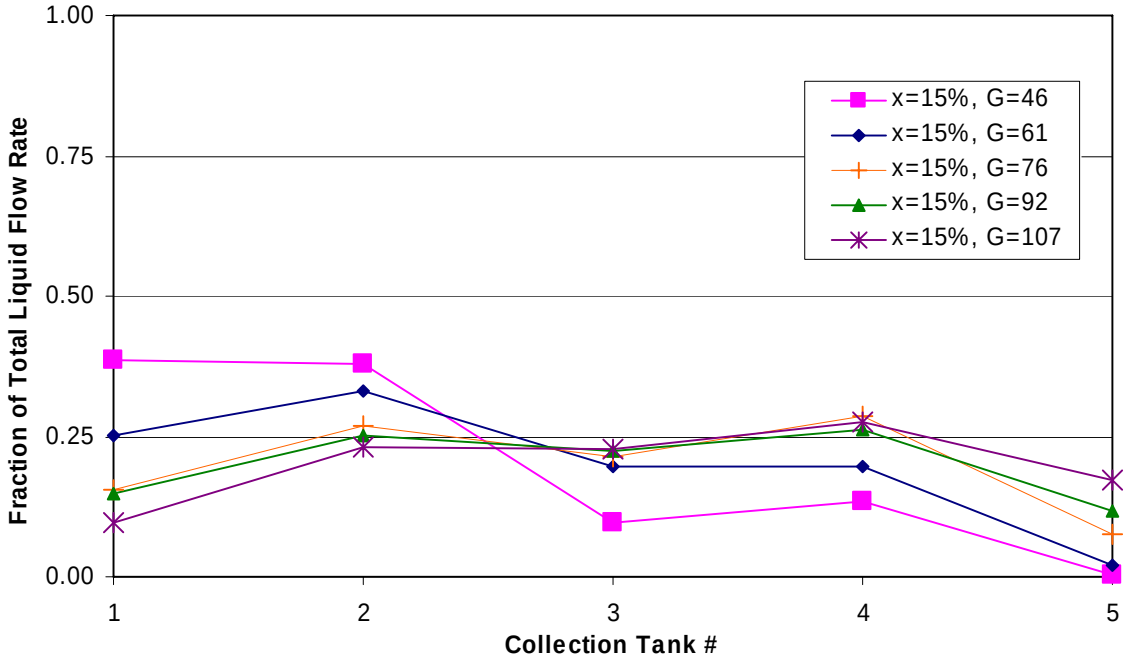

Figure C-92: 3/4 Depth Protrusion, Long Inlet, x=15%

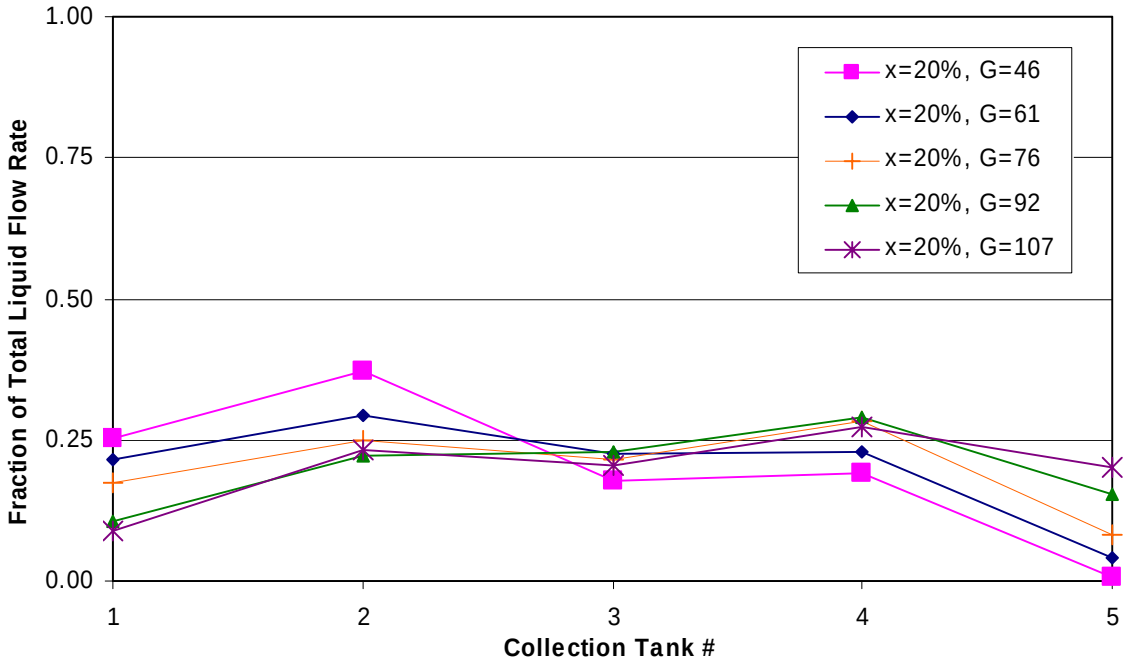

Figure C-93: 3/4 Depth Protrusion, Long Inlet, x=20%

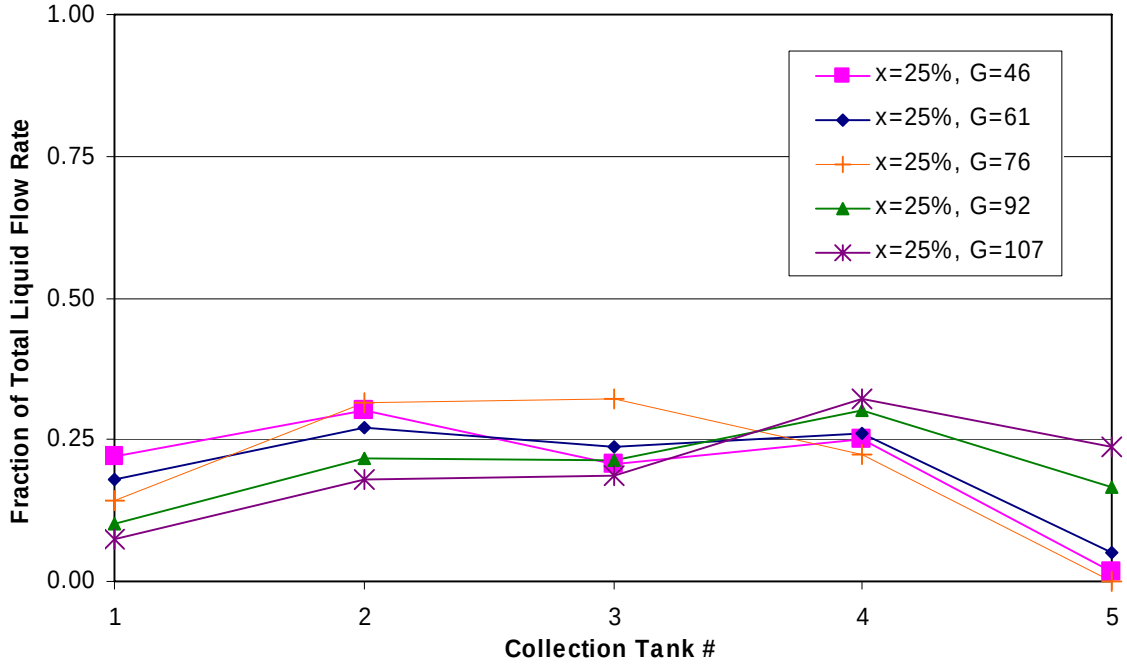

Figure C-94: 3/4 Depth Protrusion, Long Inlet, x=25%

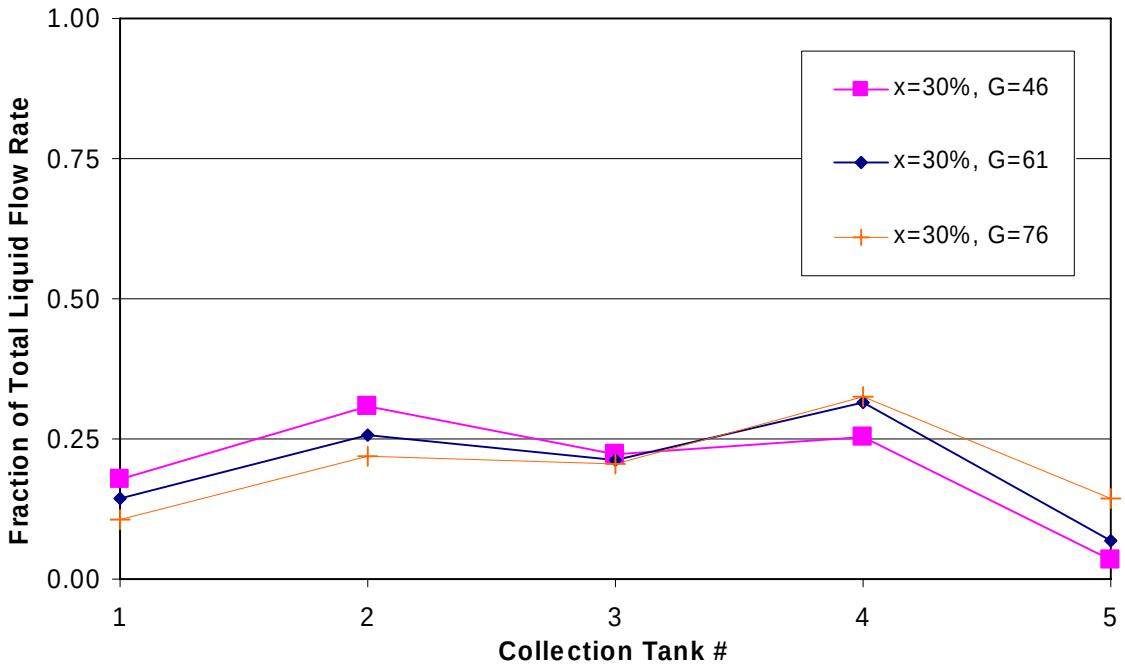

Figure C-95: 3/4 Depth Protrusion, Long Inlet, x=30%

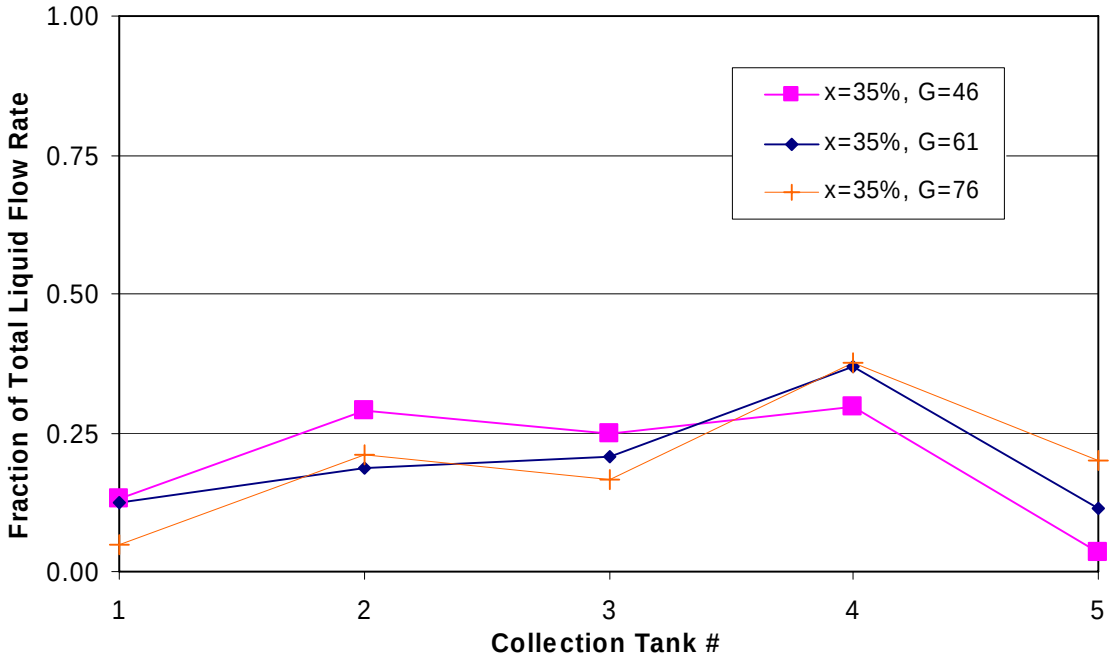

Figure C-96: 3/4 Depth Protrusion, Long Inlet, x=35%

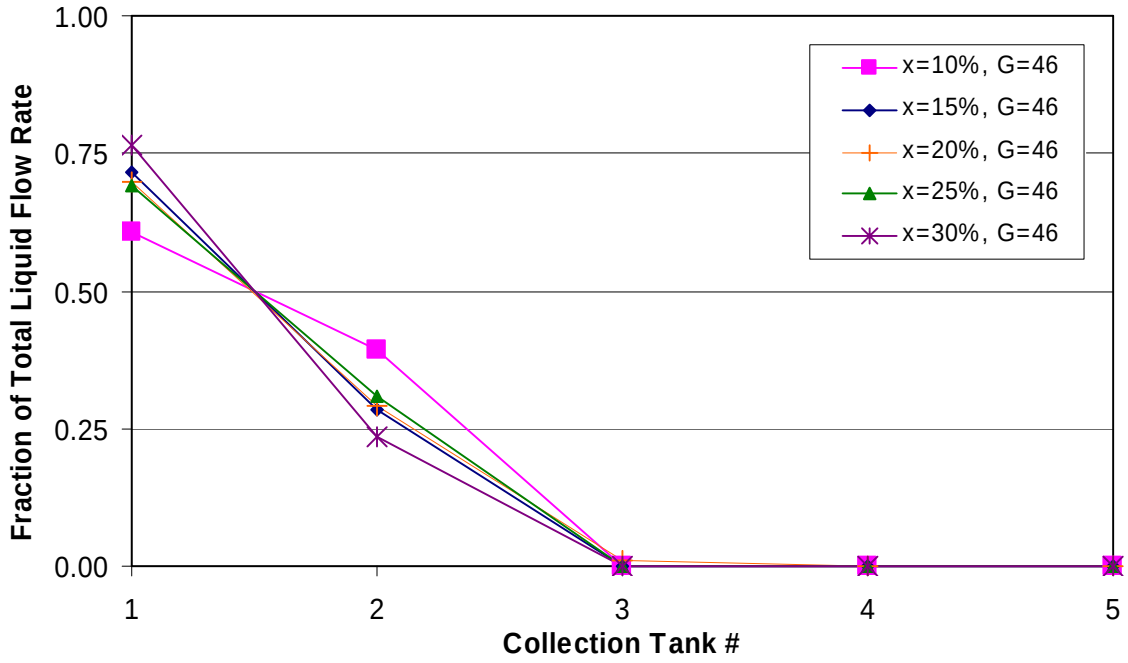

Figure C-97: Stagger Up Protrusion, Long Inlet, G=46 kg/m^{2}s

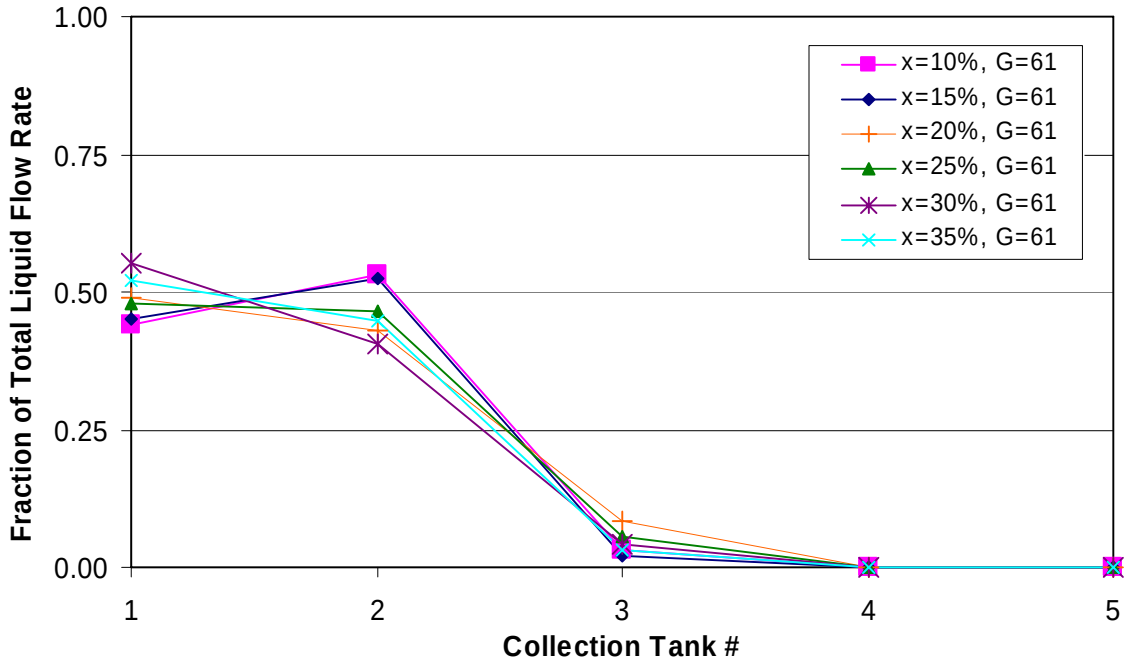

Figure C-98: Stagger Up Protrusion, Long Inlet, G=61 kg/m^{2}s

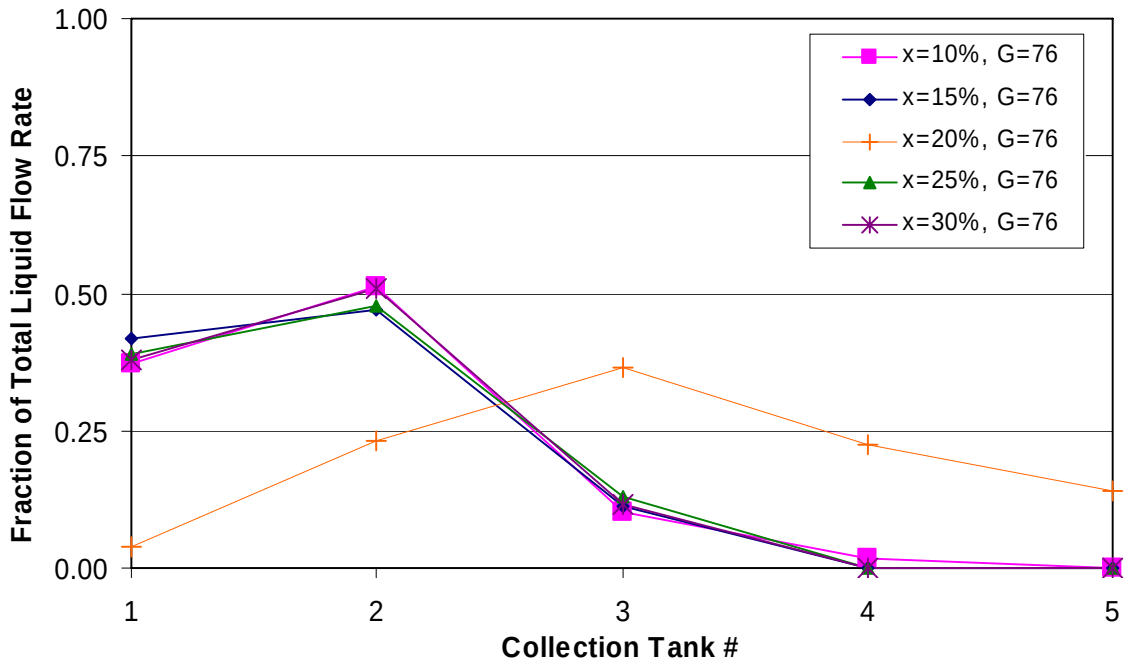

Figure C-99: Stagger Up Protrusion, Long Inlet, G=76 kg/m^{2}s

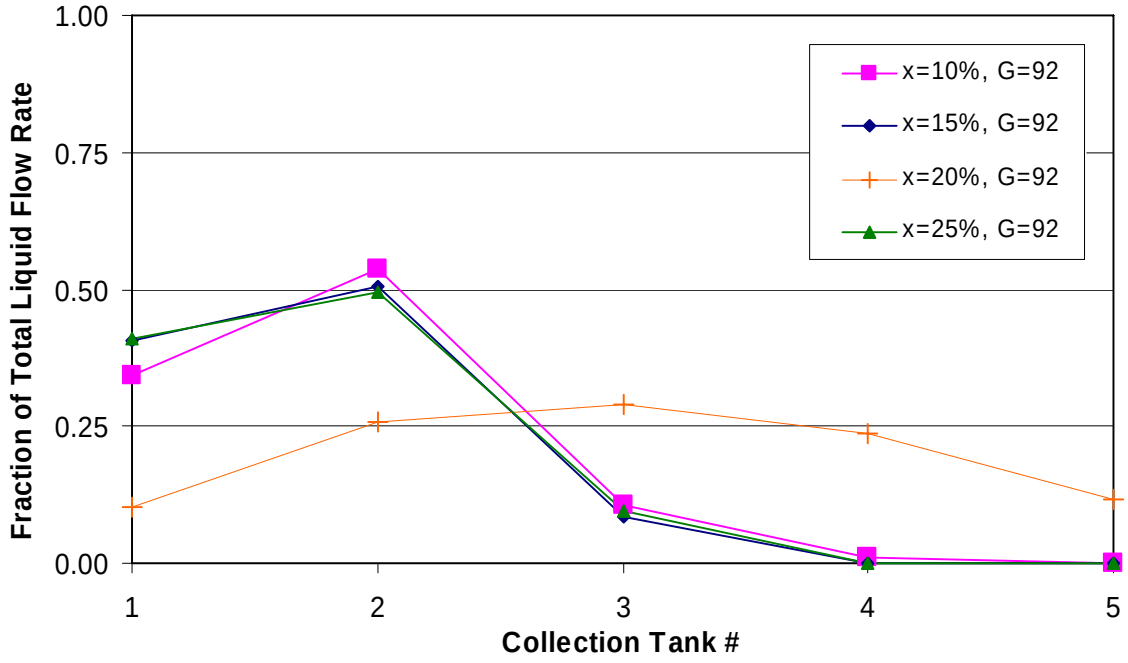

Figure C-100: Stagger Up Protrusion, Long Inlet, G=92 kg/m^{2}s

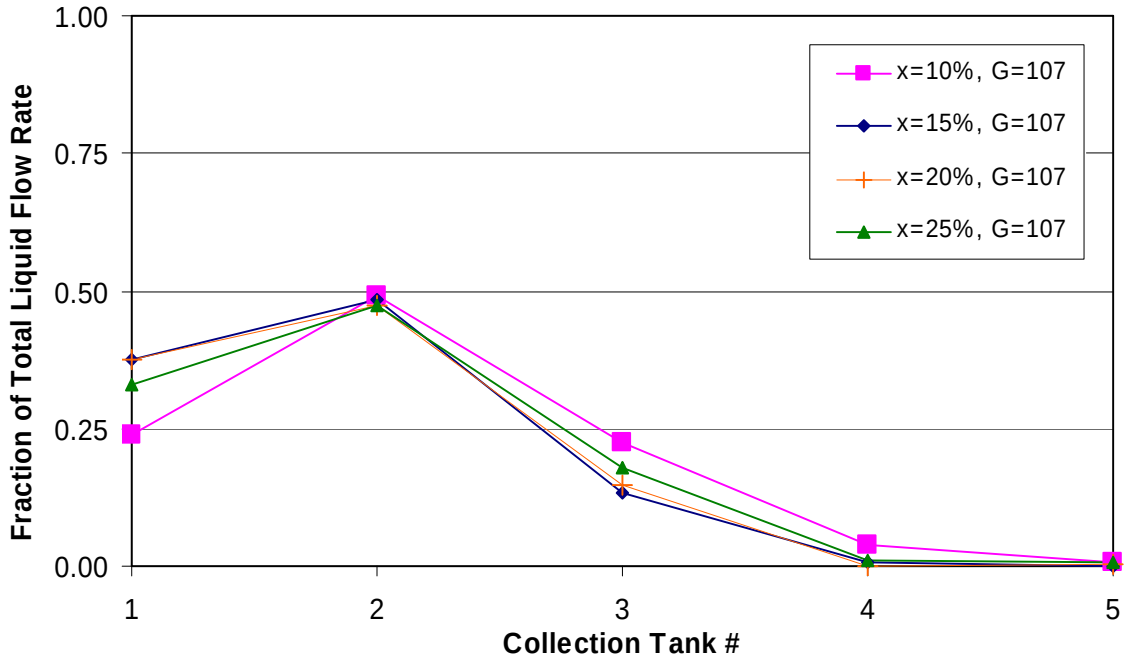

Figure C-101: Stagger Up Protrusion, Long Inlet, G=107 kg/m^{2}s

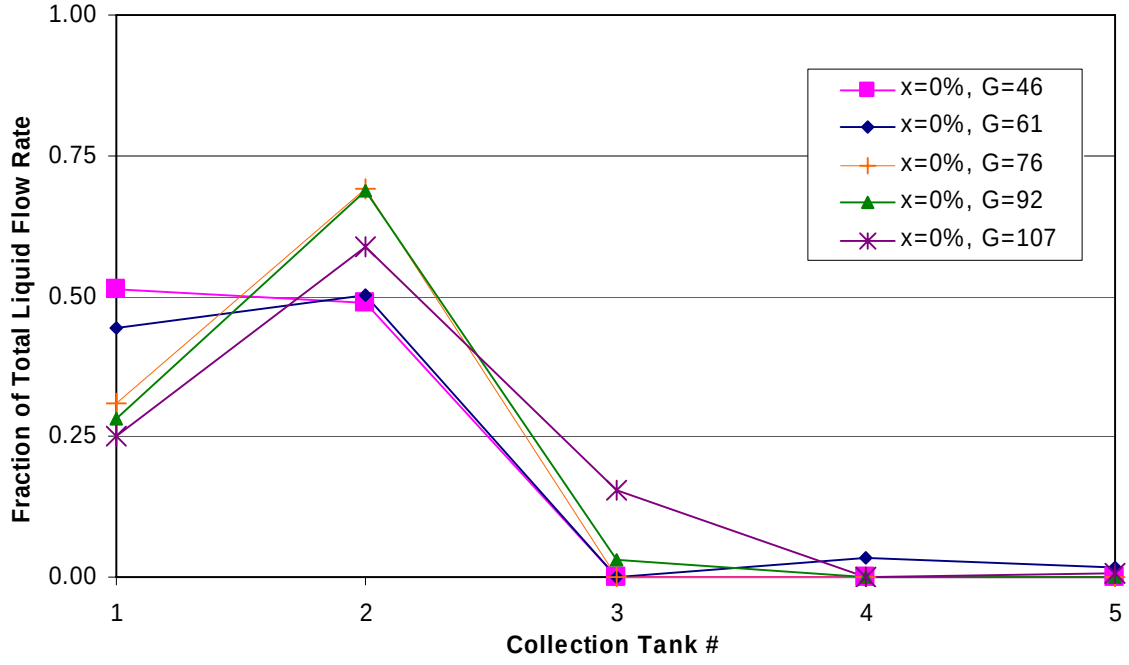

Figure C-102: Stagger Up Protrusion, Long Inlet, x=0%

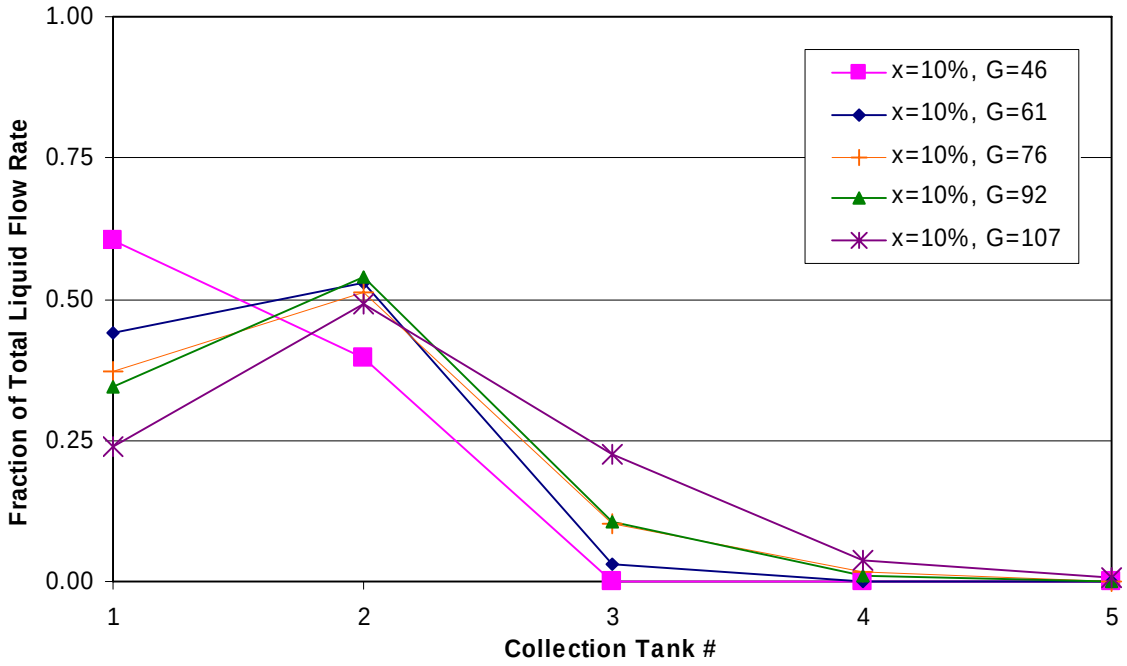

Figure C-103: Stagger Up Protrusion, Long Inlet, x=10%

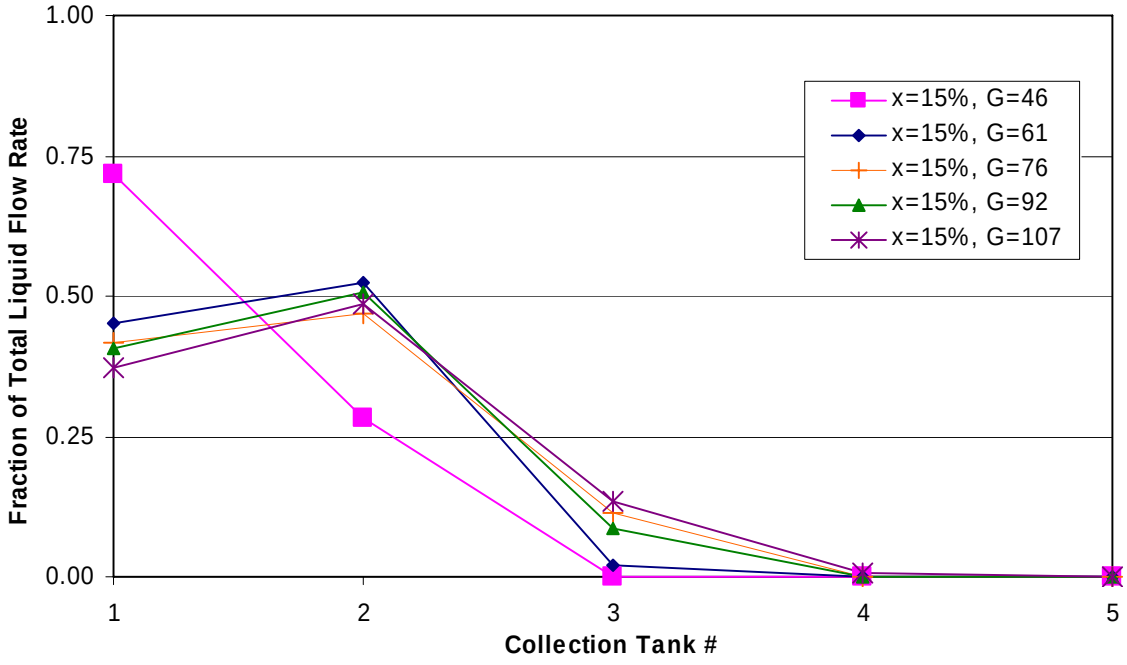

Figure C-104: Stagger Up Protrusion, Long Inlet, x=15%

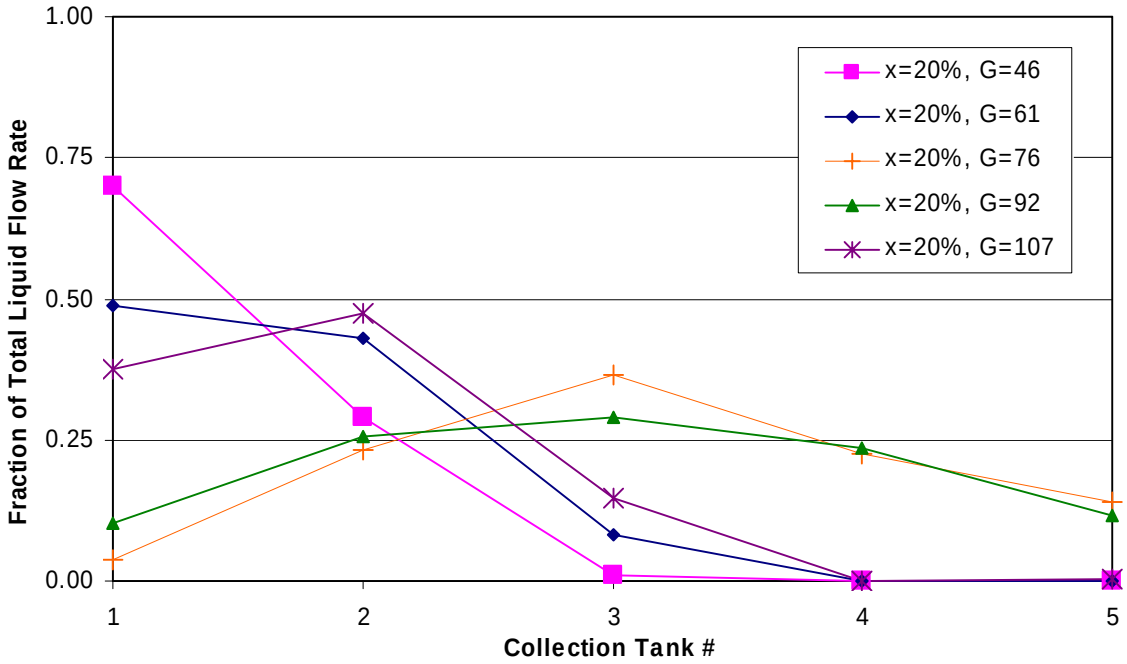

Figure C-105: Stagger Up Protrusion, Long Inlet, x=20%

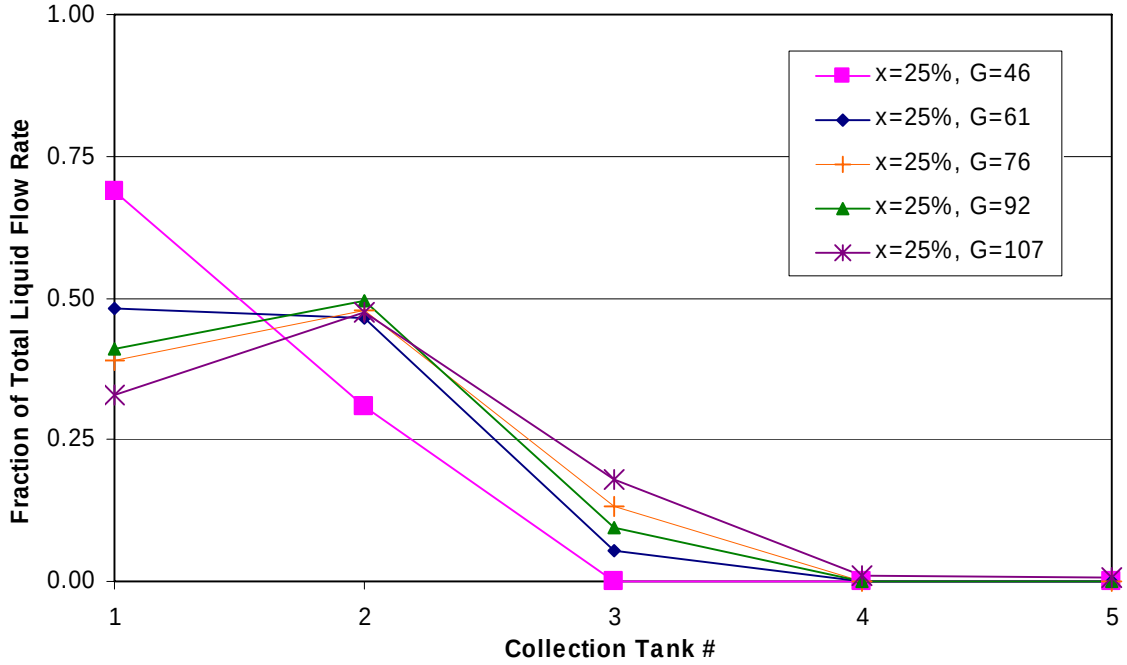

Figure C-106: Stagger Up Protrusion, Long Inlet, x=25%

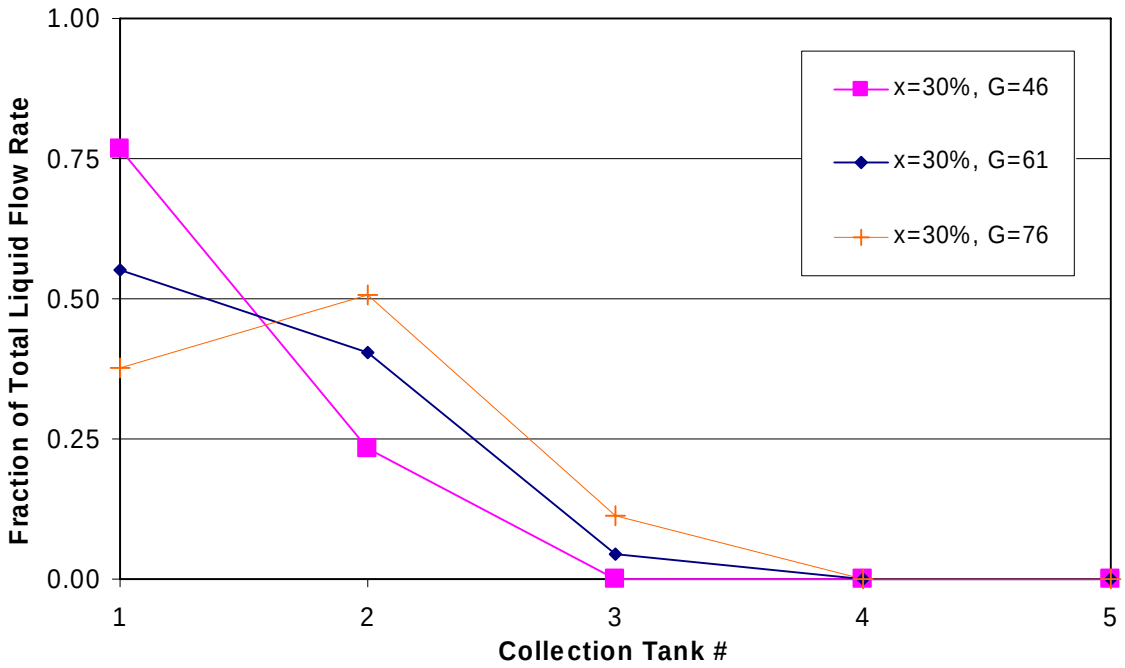

Figure C-107: Stagger Up Protrusion, Long Inlet, x=30%

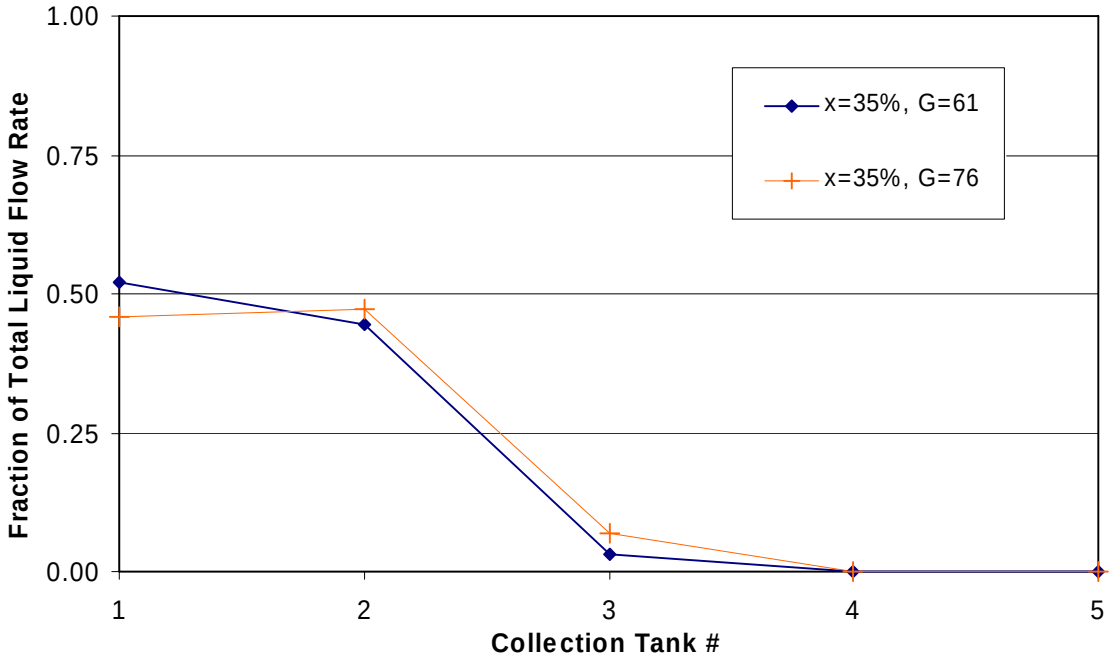

Figure C-108: Stagger Up Protrusion, Long Inlet, x=35%

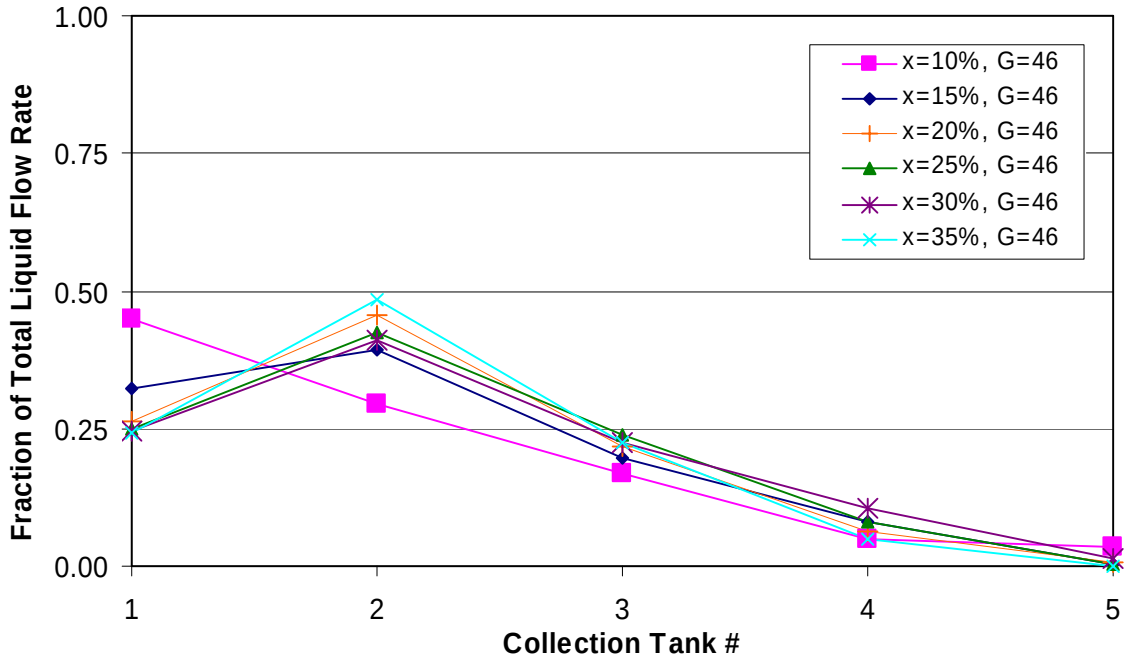

Figure C-109: Stagger Down Protrusion, Long Inlet, G=46 kg/m^{2}s

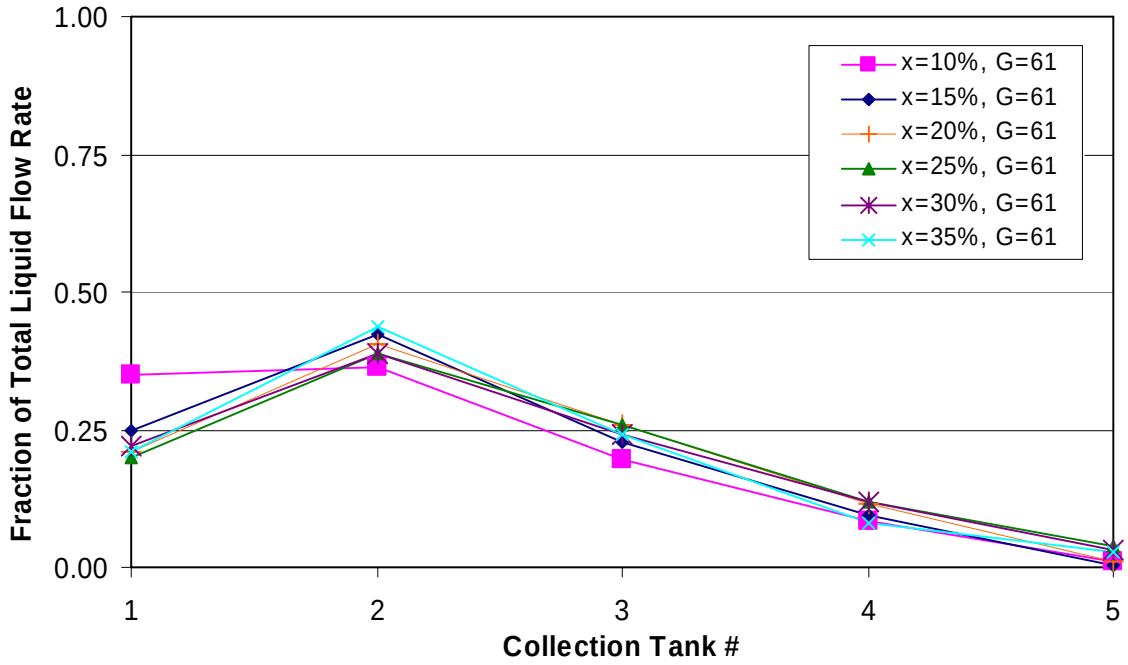

Figure C-110: Stagger Down Protrusion, Long Inlet, G=61 kg/m^{2}s

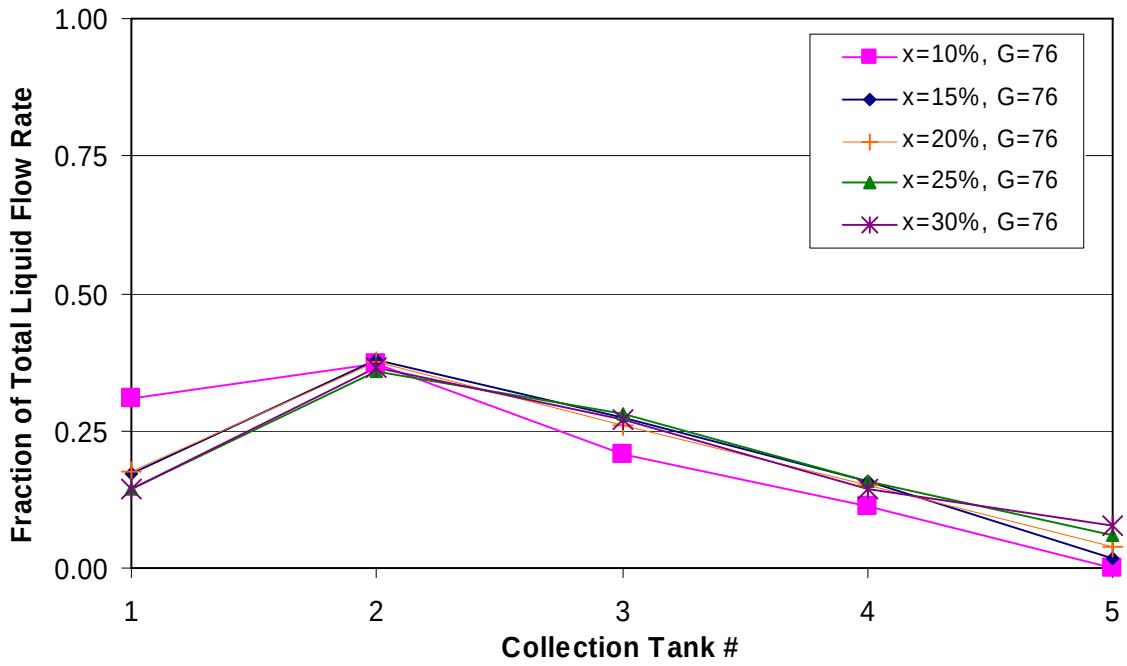

Figure C-111: Stagger Down Protrusion, Long Inlet, G=76 kg/m^{2}s

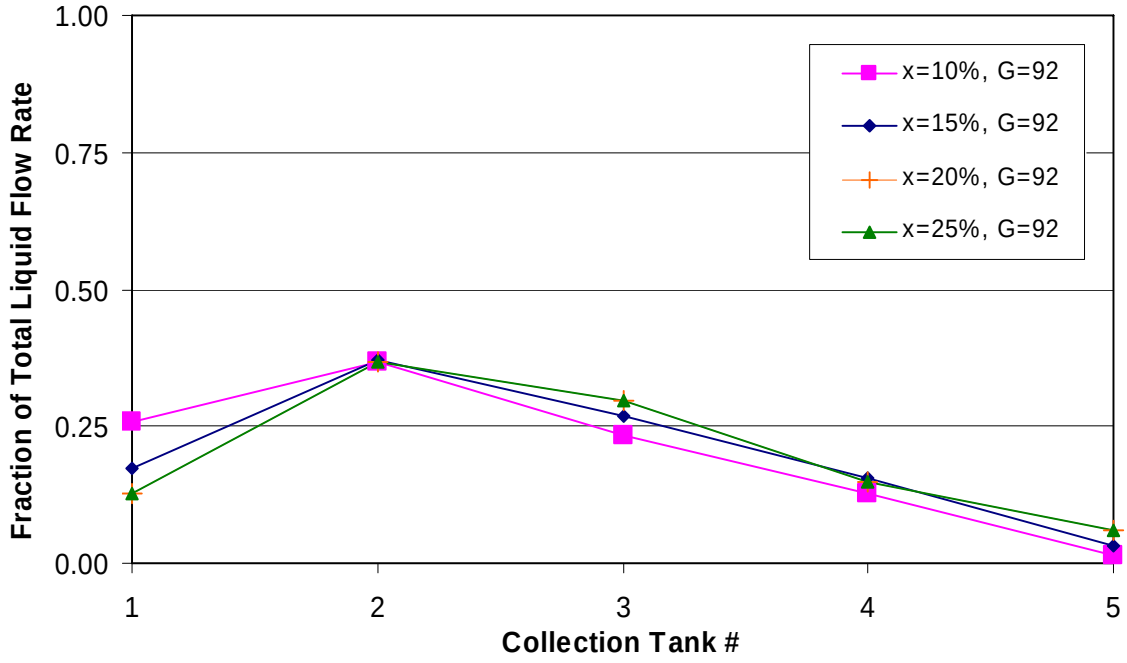

Figure C-112: Stagger Down Protrusion, Long Inlet, G=92 kg/m^{2}s

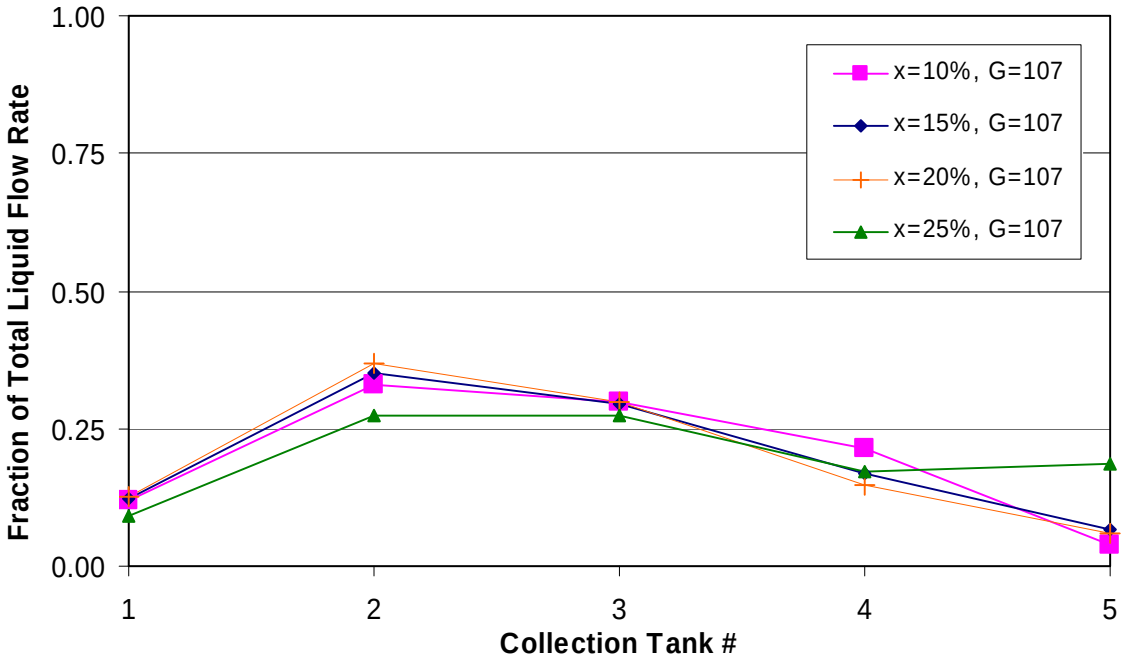

Figure C-113: Stagger Down Protrusion, Long Inlet, G=107 kg/m^{2}s

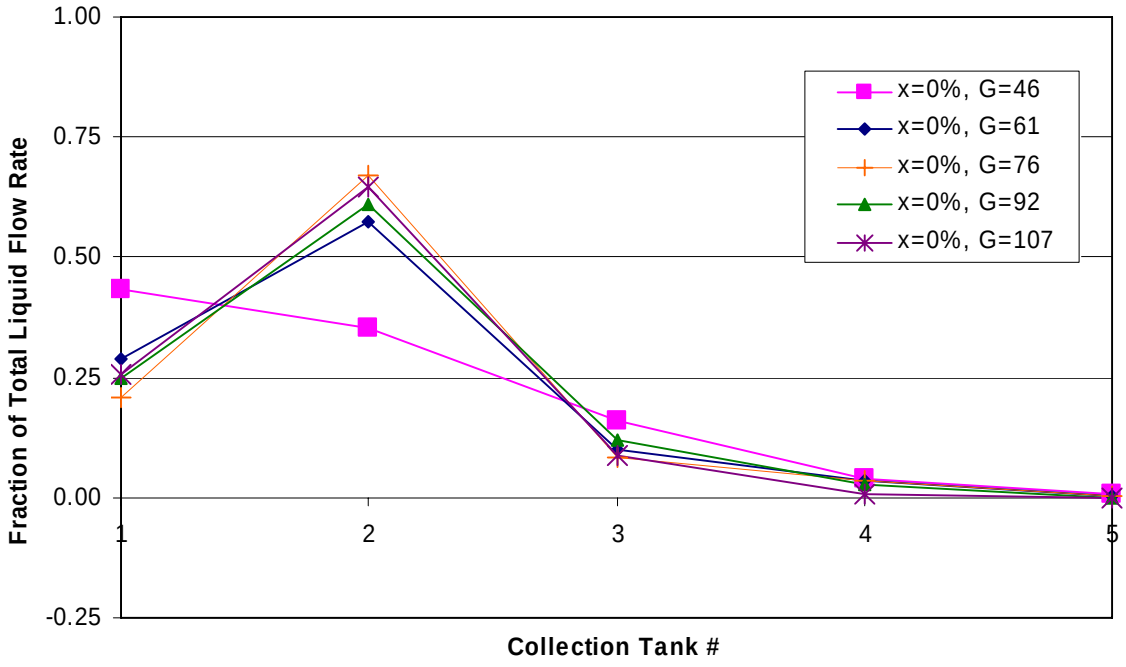

Figure C-114: Stagger Down Protrusion, Long Inlet, x=0%

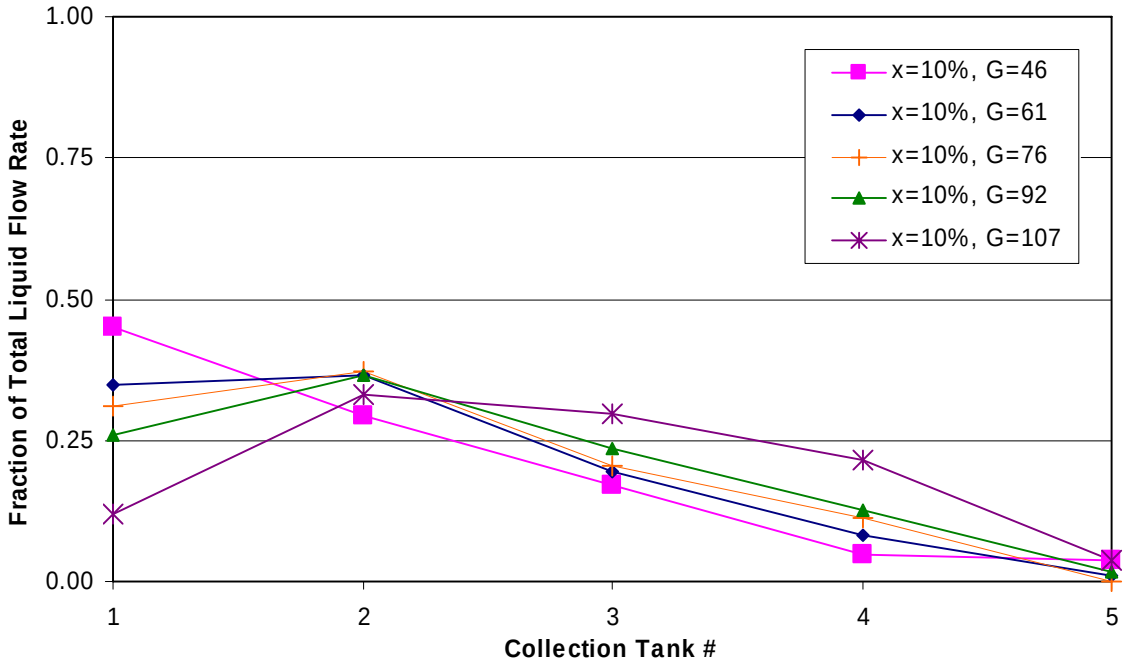

Figure C-115: Stagger Down Protrusion, Long Inlet, x=10%

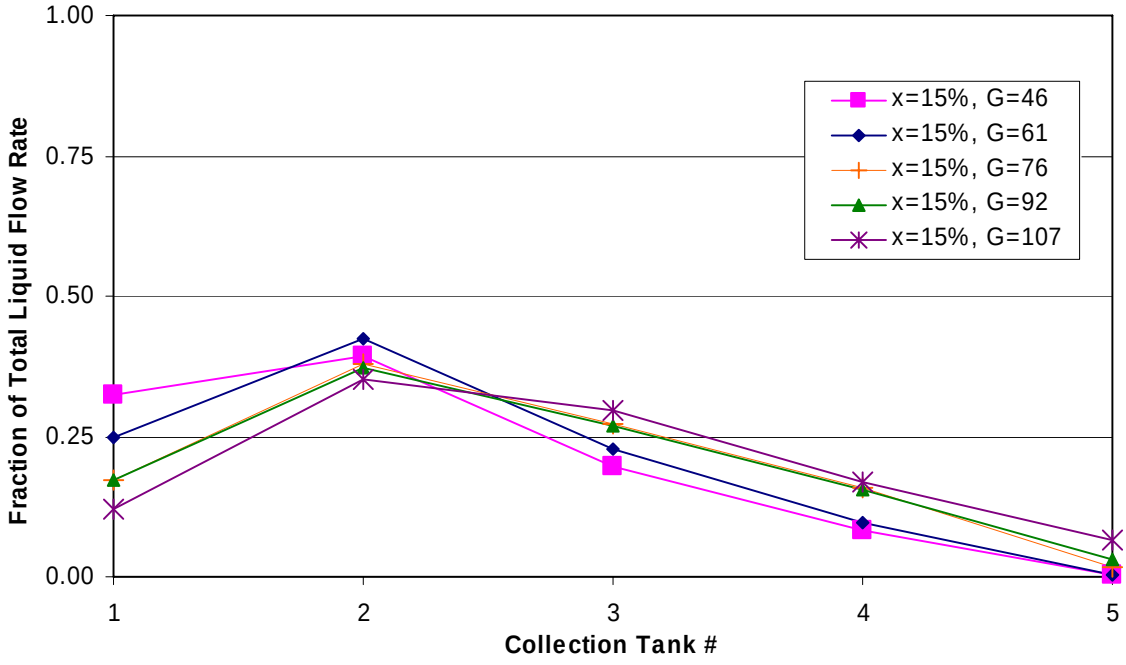

Figure C-116: Stagger Down Protrusion, Long Inlet, x=15%

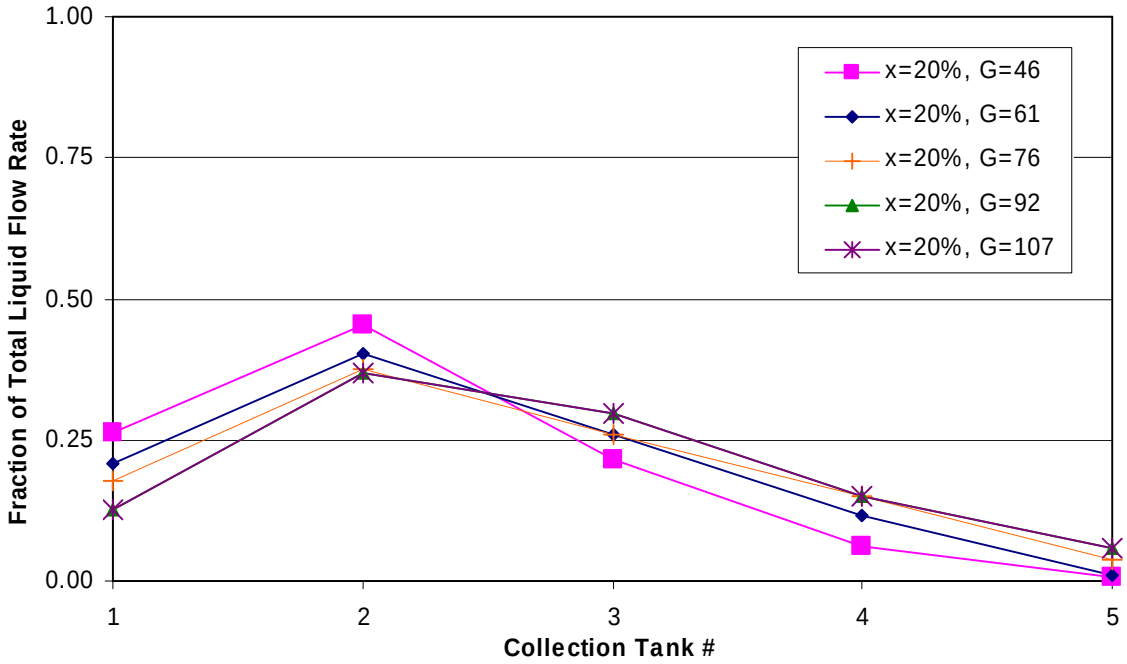

Figure C-117: Stagger Down Protrusion, Long Inlet, x=20%

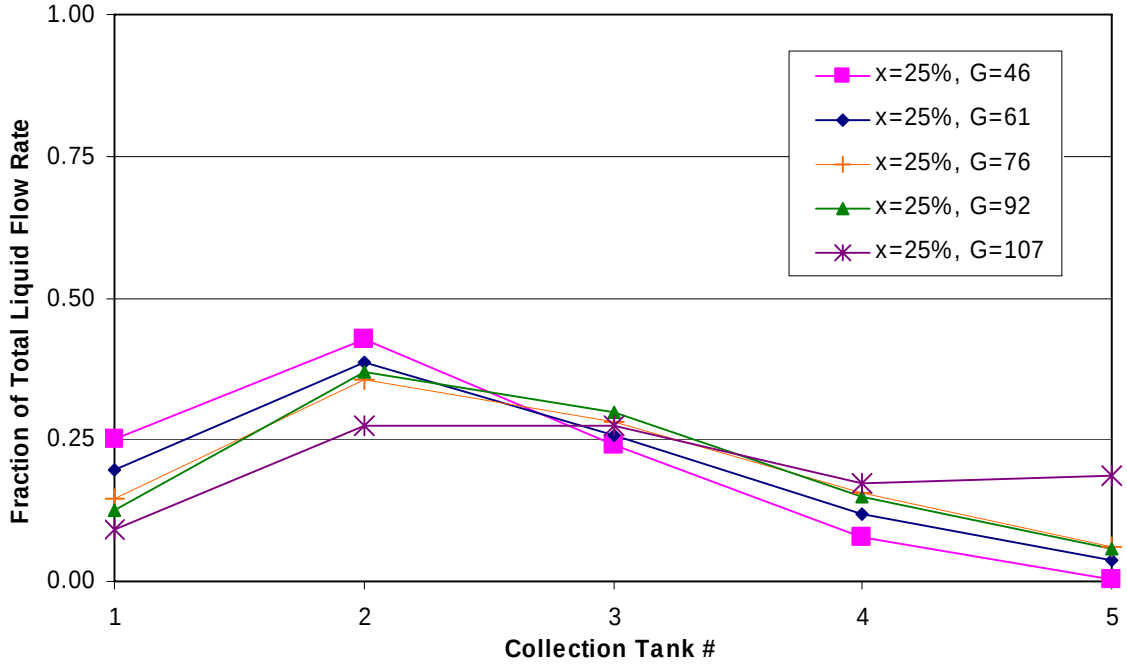

Figure C-118: Stagger Down Protrusion, Long Inlet, x=25%

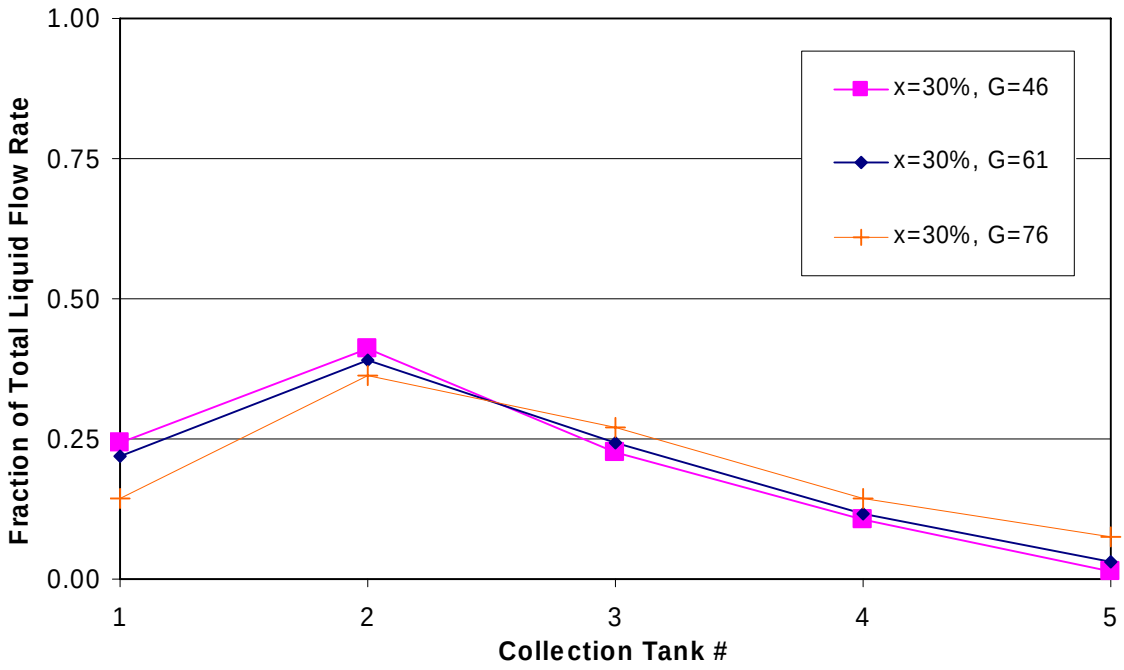

Figure C-119: Stagger Down Protrusion, Long Inlet, x=30%

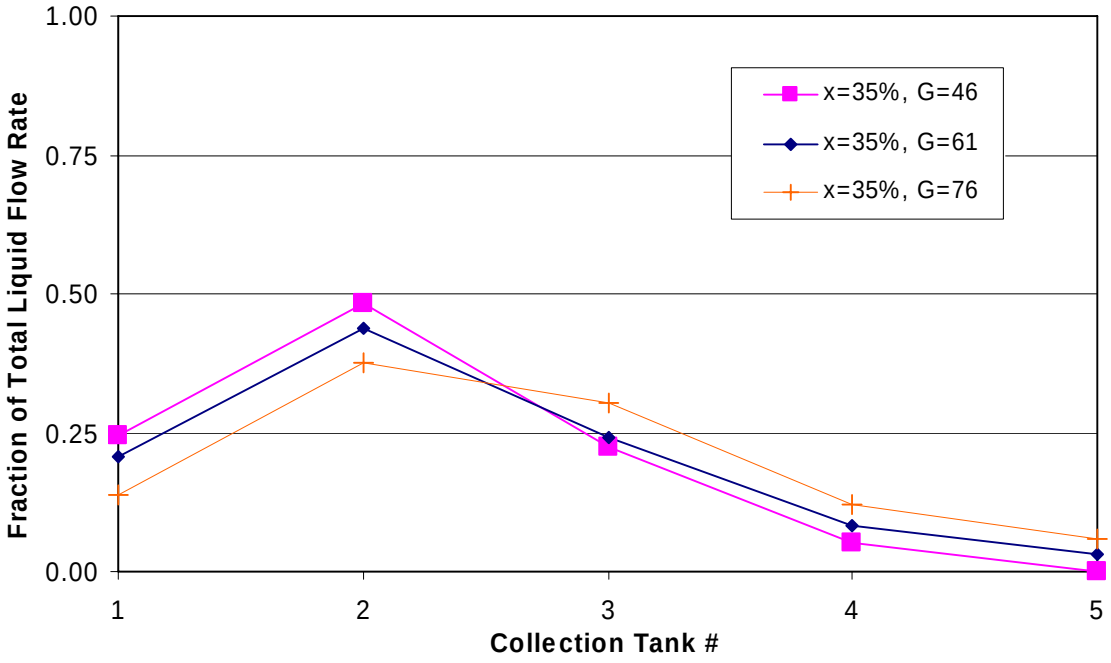

Figure C-120: Stagger Down Protrusion, Long Inlet, x=35%

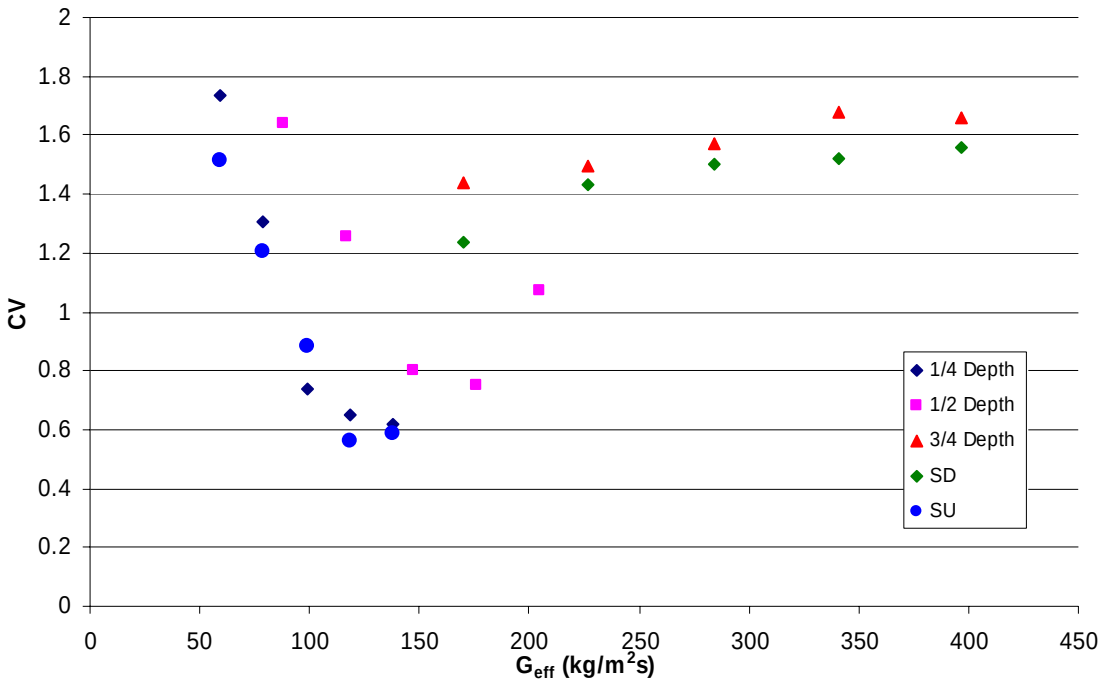

Figure C-121: Effective Mass Flux Effects, Short Entrance, 0% Inlet Quality

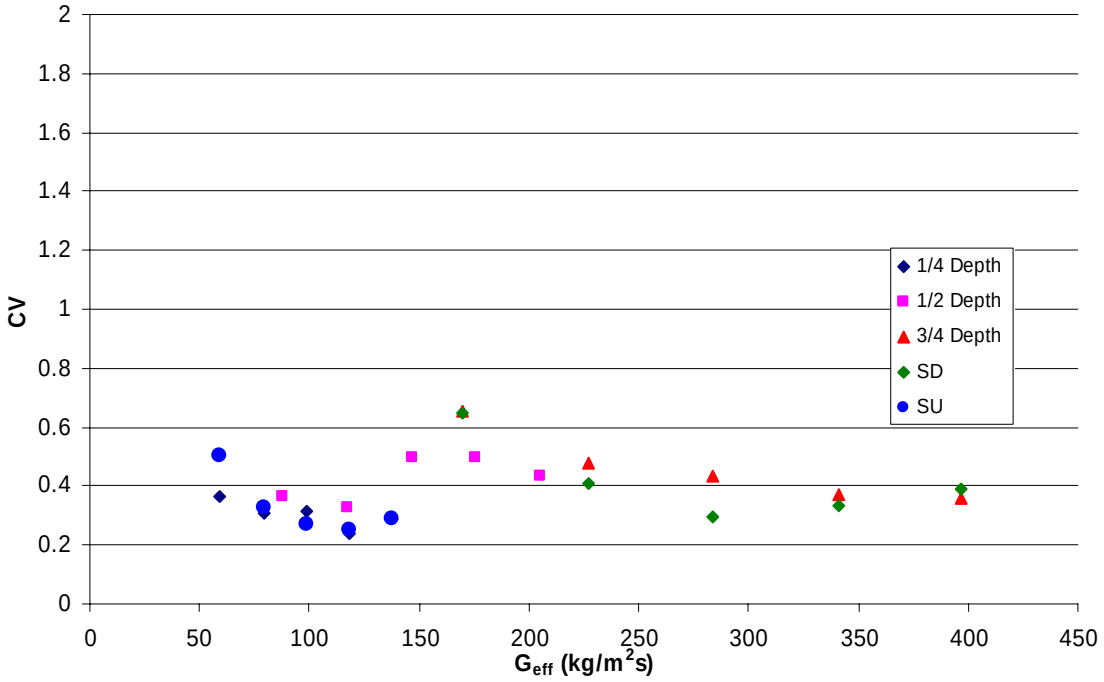

Figure C-122: Effective Mass Flux Effects, Short Entrance, 10% Inlet Quality

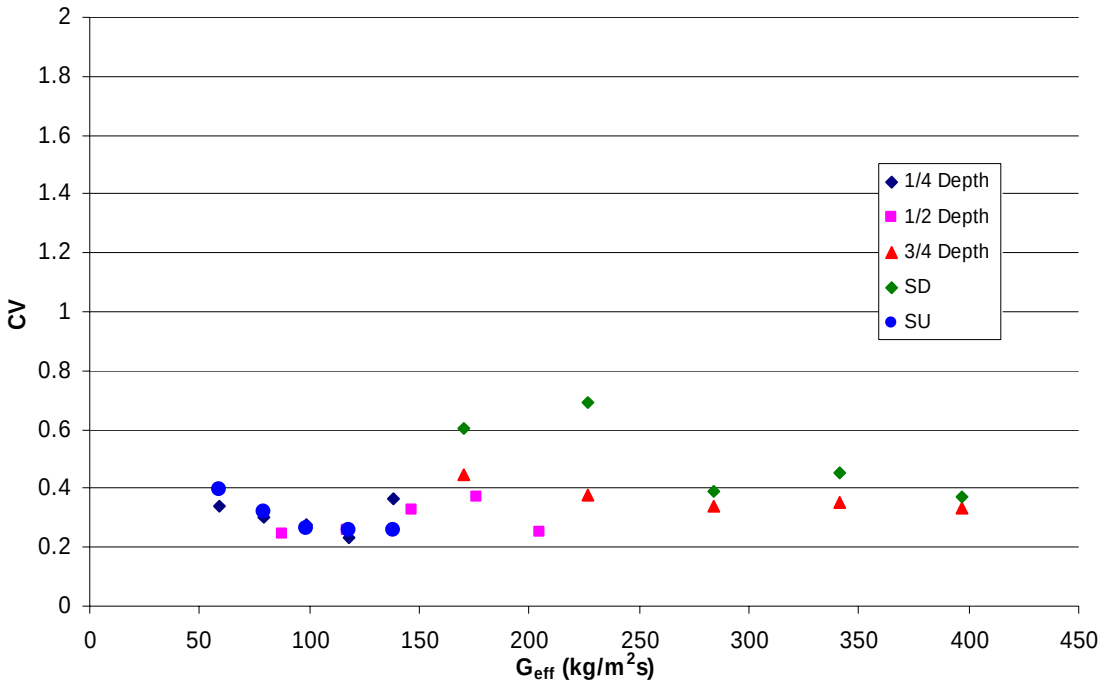

Figure C-123: Effective Mass Flux Effects, Short Entrance, 15% Inlet Quality

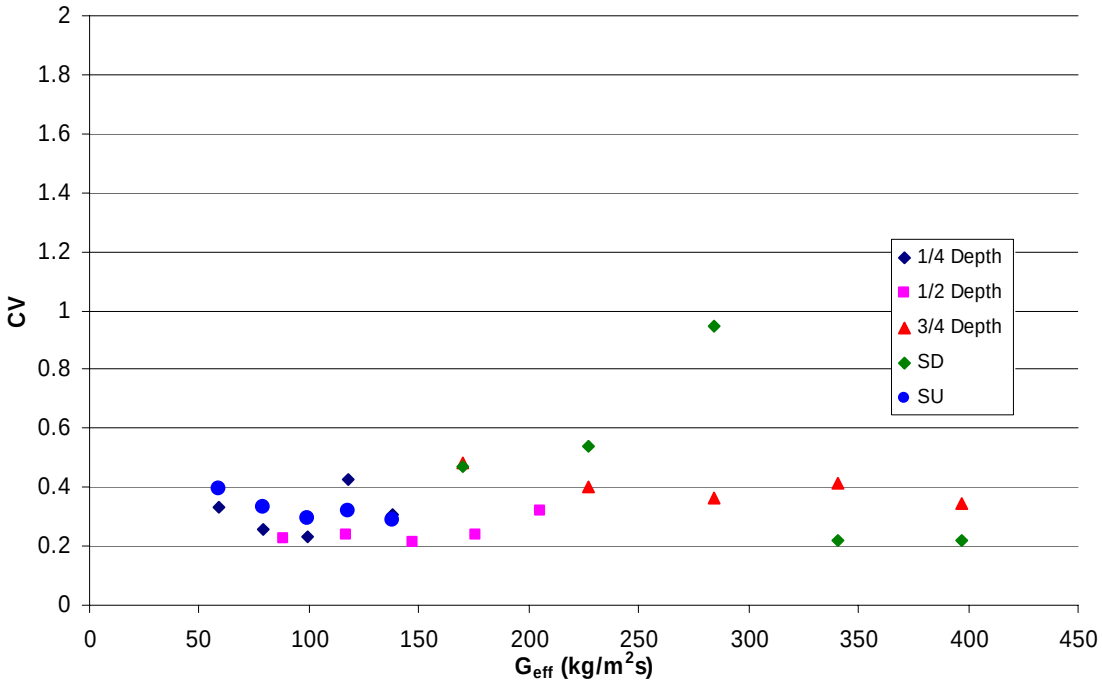

Figure C-124: Effective Mass Flux Effects, Short Entrance, 20% Inlet Quality

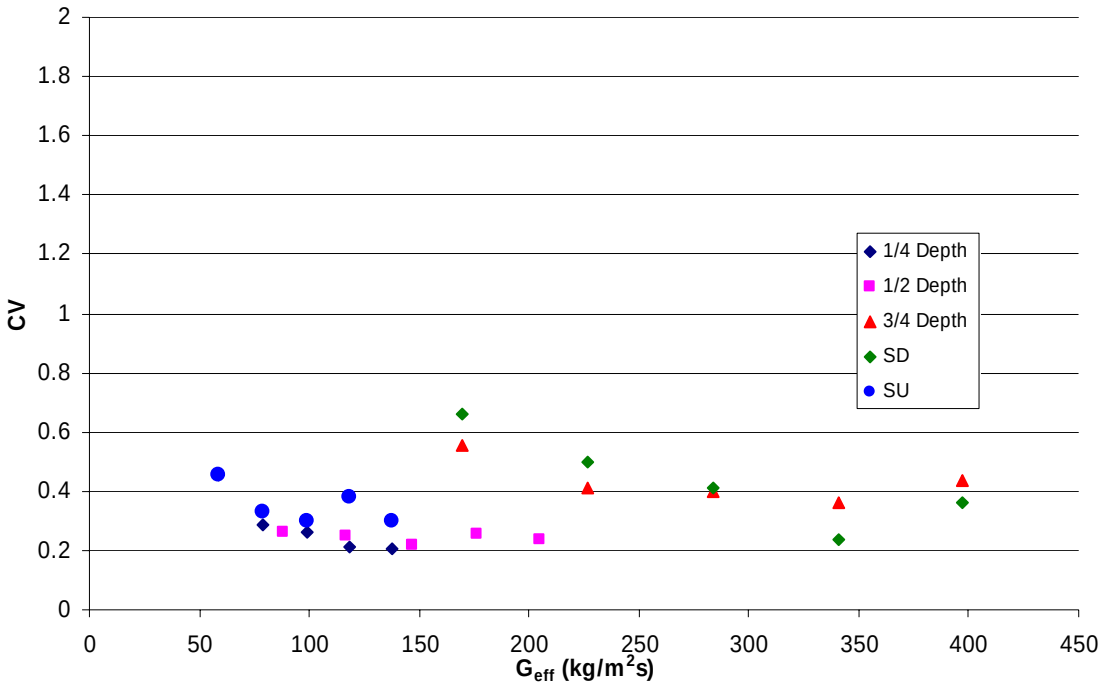

Figure C-125: Effective Mass Flux Effects, Short Entrance, 25% Inlet Quality

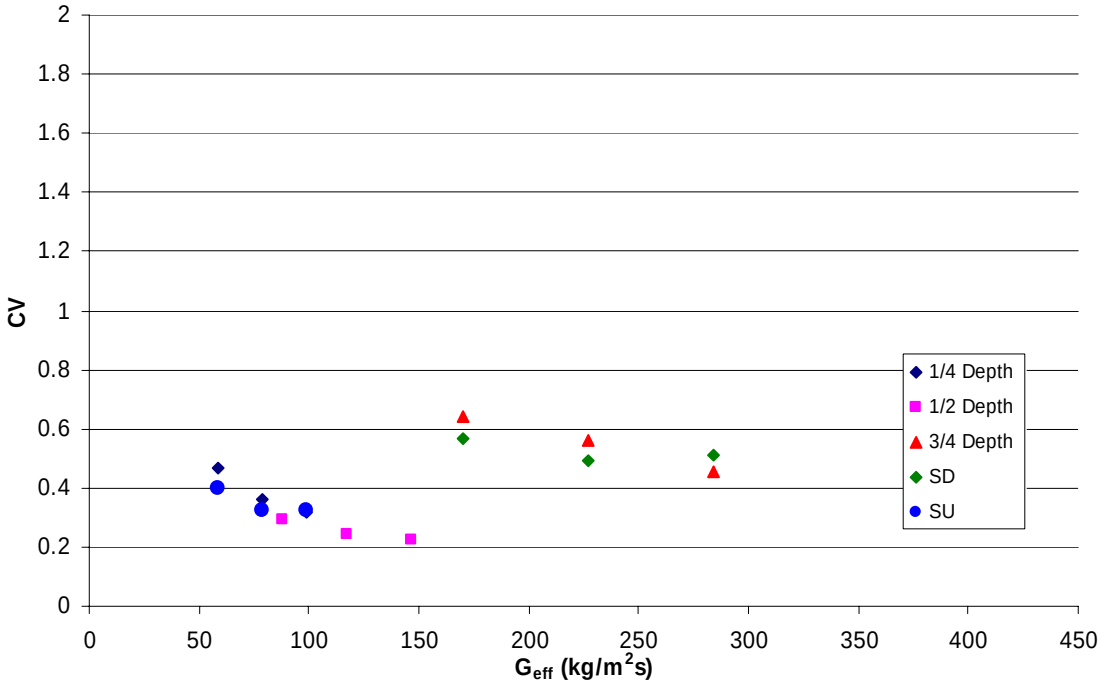

Figure C-126: Effective Mass Flux Effects, Short Entrance, 30% Inlet Quality

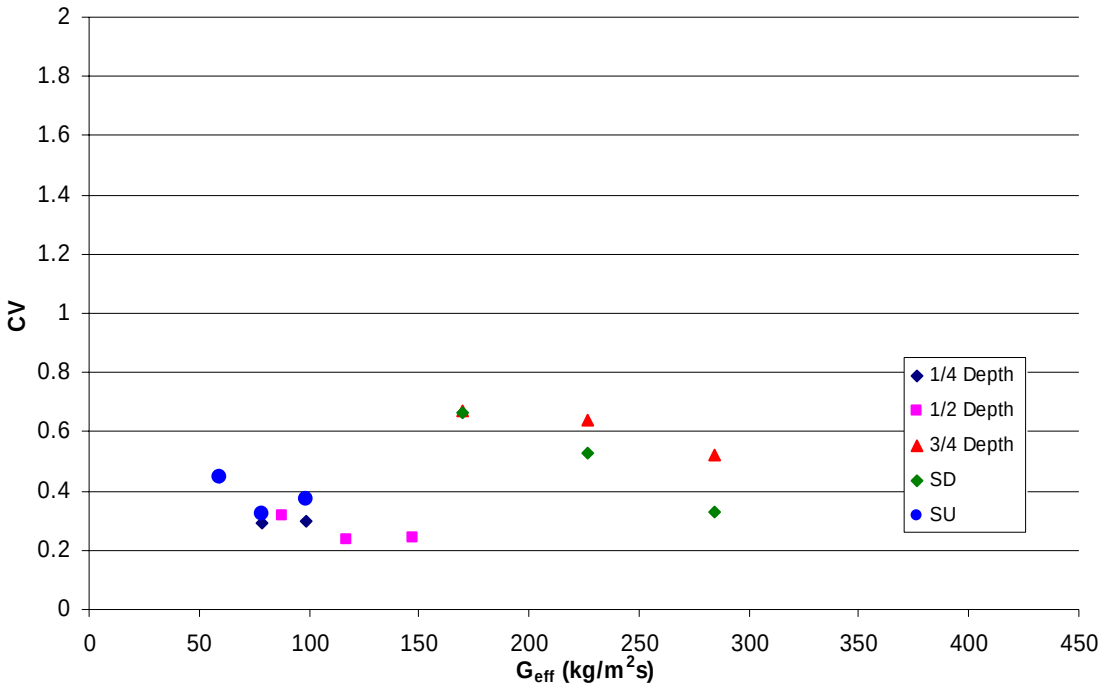

Figure C-127: Effective Mass Flux Effects, Short Entrance, 35% Inlet Quality

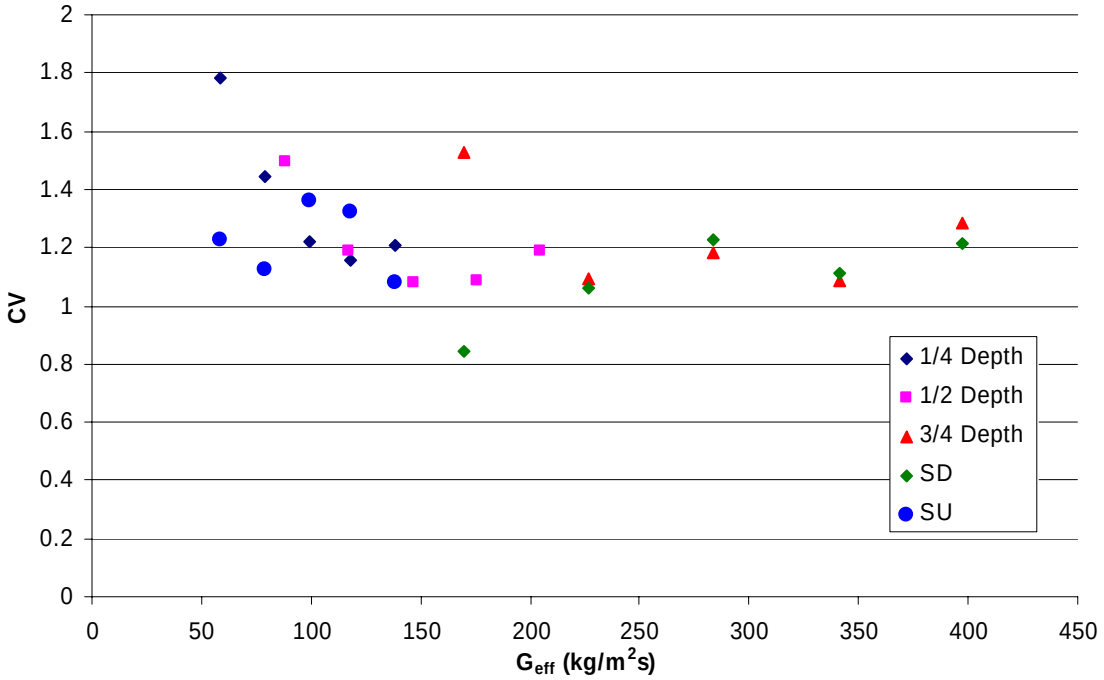

Figure C-128: Effective Mass Flux Effects, Long Entrance, 0% Inlet Quality

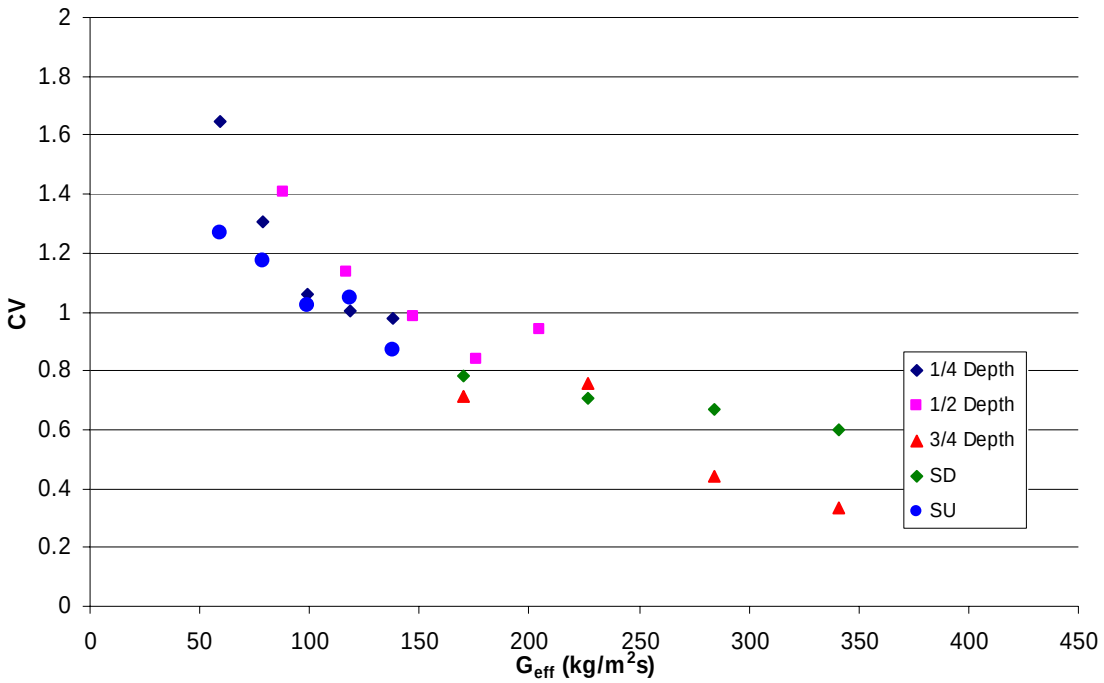

Figure C-129: Effective Mass Flux Effects, Long Entrance, 10% Inlet Quality

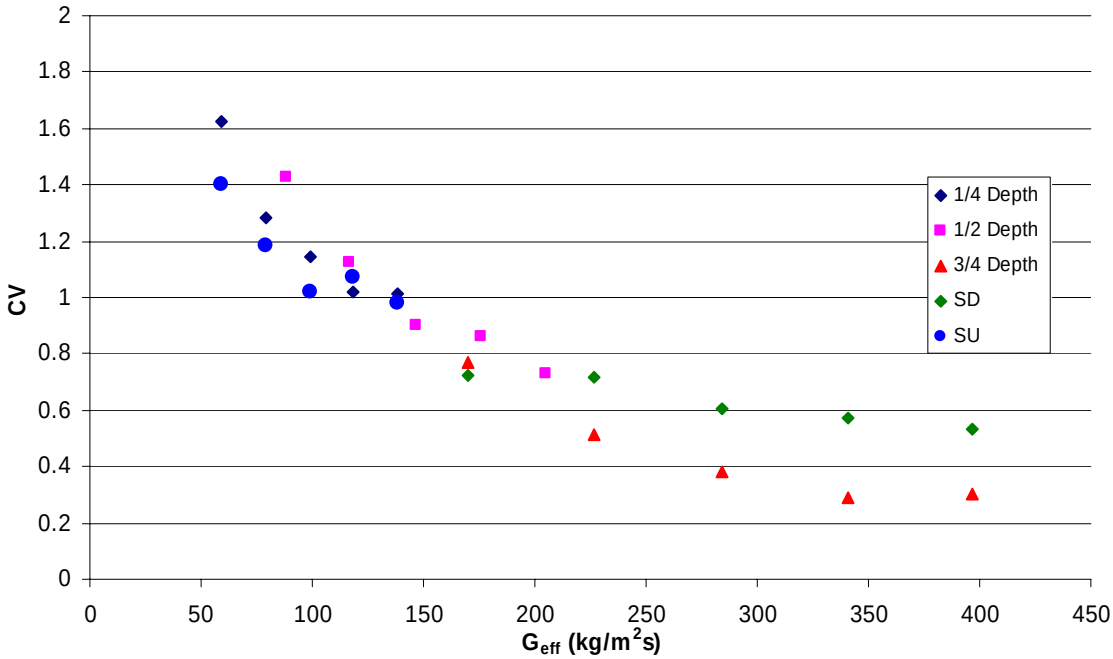

Figure C-130: Effective Mass Flux Effects, Long Entrance, 15% Inlet Quality

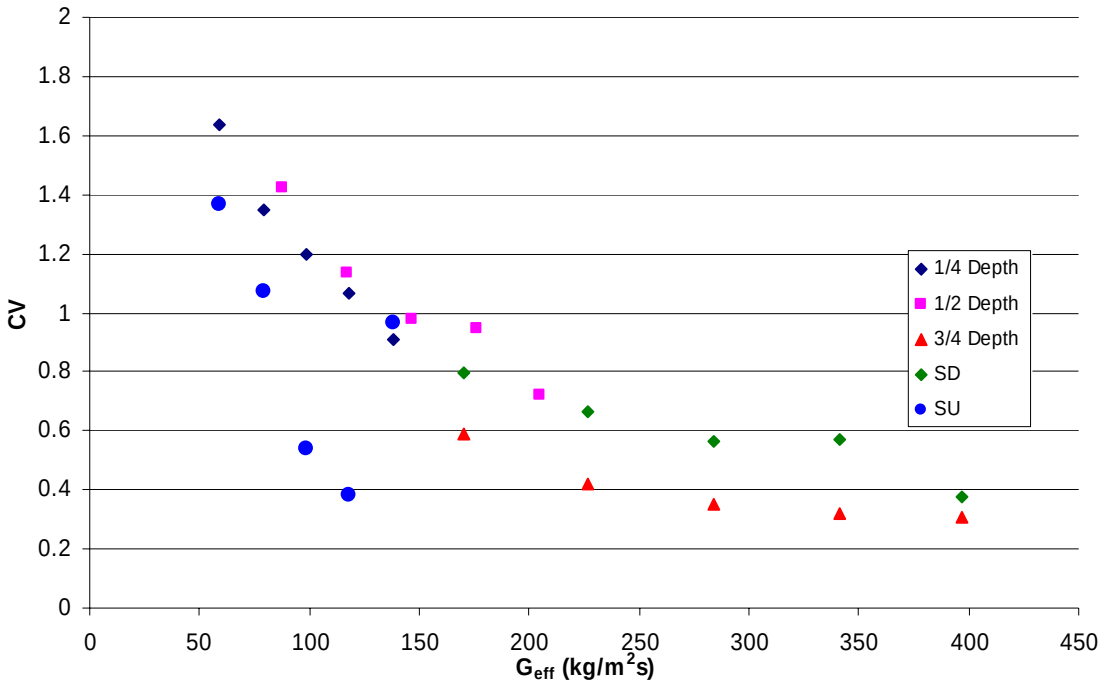

Figure C-131: Effective Mass Flux Effects, Long Entrance, 20% Inlet Quality

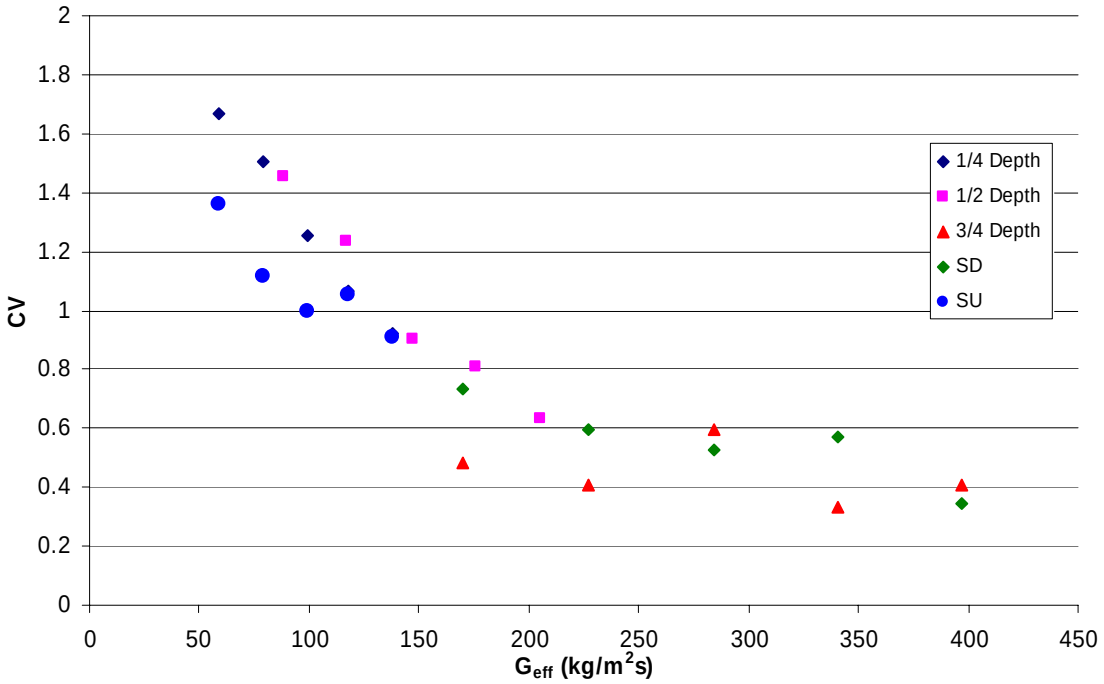

Figure C-132: Effective Mass Flux Effects, Long Entrance, 25% Inlet Quality

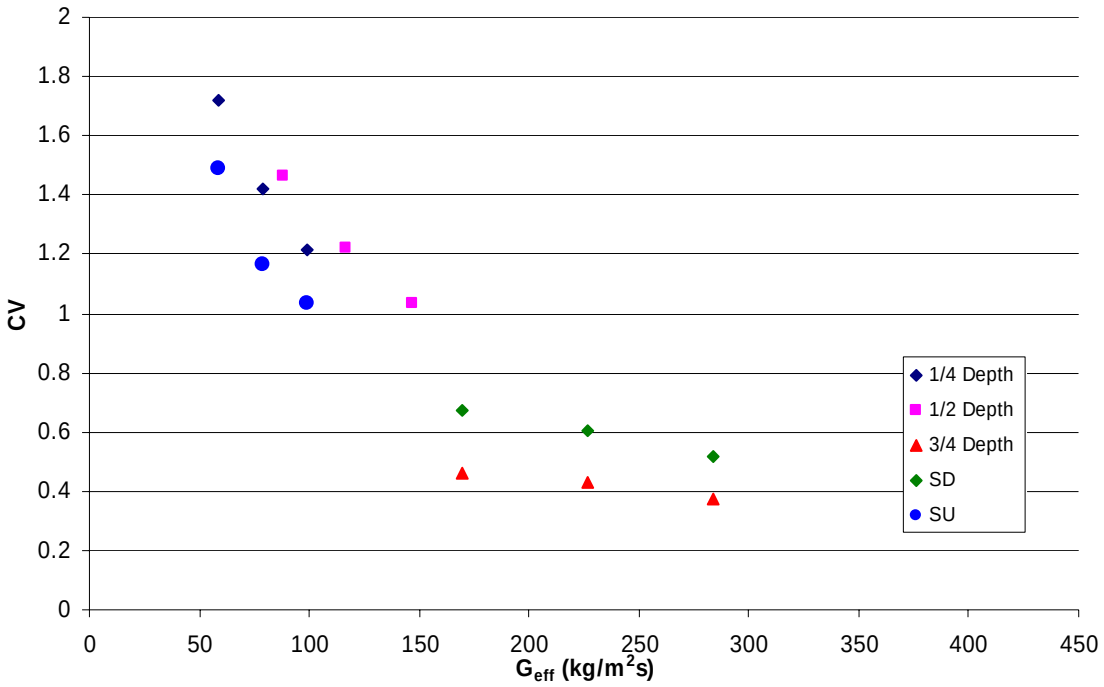

Figure C-133: Effective Mass Flux Effects, Long Entrance, 30% Inlet Quality

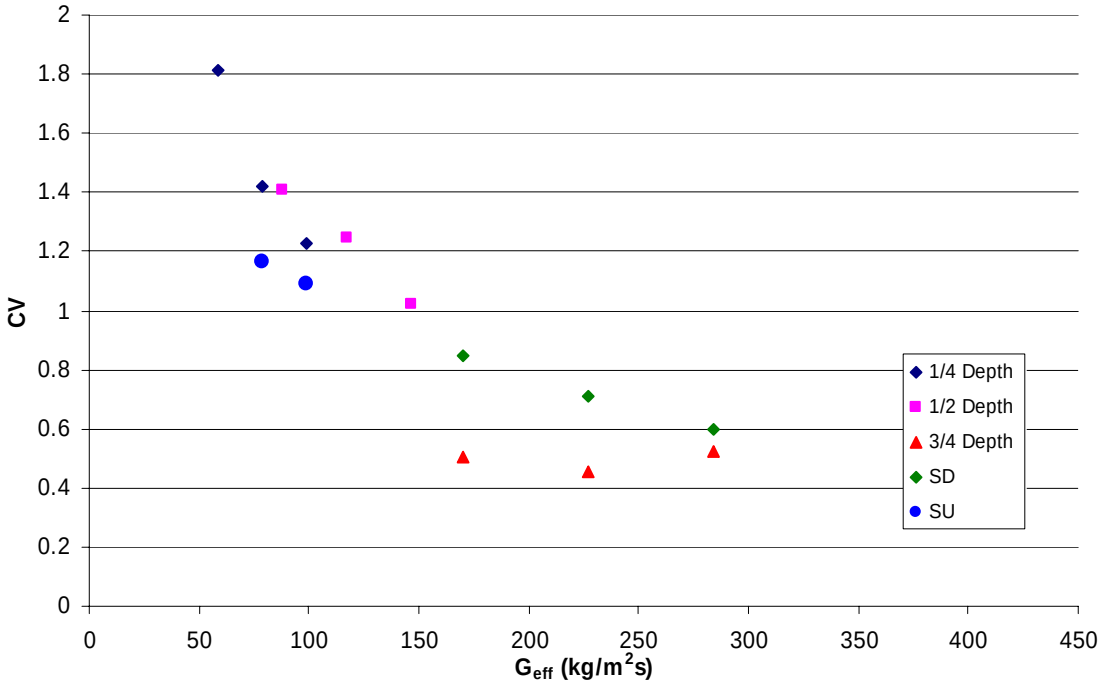

Figure C-134: Effective Mass Flux Effects, Long Entrance, 35% Inlet Quality